Final Report

THERMODYNAMICS OF ORGANIC ATMOSPHERIC AEROSOLS

Prepared for

California Air Resources Board
and the
California Environmental Protection Agency

Contract #98-314

Prepared by

John H. Seinfeld
Robert J. Griffin
California Institute of Technology
Pasadena, CA 91125

Betty K. Pun
Christian Seigneur
Atmospheric and Environmental Research, Inc.

Donald Dabdub
University of California, Irvine

February 2002

Disclaimer

The statements and conclusions of this Report are those of the contractor and not necessarily those of the California Air Resources Board. The mention of commercial products, their source, or their use in connection with material reported herein is not to be construed as actual or implied endorsement of such products.

Acknowledgements

This report was submitted in fulfillment of ARB contract #98-314, "Thermodynamics of Organic Atmospheric Aerosols", by the California Institute of Technology under the partial sponsorship of the California Air Resources Board. Work was completed as of August 1, 2001.

Table of Contents

Figures

Tables

Abstract

Organic species are an important component of atmospheric particles. Particulate organic compounds, suspected to be a possible source of human health effects in inhaled particles, arise from both direct emissions and gas-to-particle conversion in the atmosphere. Those arising from gas-to-particle conversion, so-called secondary organic aerosols, transfer to particles based on equilibrium partitioning between the gas and particle phases. The ability to represent that partitioning is central to atmospheric models that can be used to predict organic aerosol levels. The goal of this project is to develop a general organic gas-particle partitioning model appropriate for use in three-dimensional atmospheric models and apply it to predict organic aerosol levels in the South Coast Air Basin. The partitioning model divides semi-volatile organic species (those with sufficiently low vapor pressure to condense, at least in part, to the aerosol phase) into hydrophobic and hydrophilic categories and then computes the partitioning of those molecules to satisfy thermodynamic equilibrium and total mass conservation.

Executive Summary

The demonstration of attainment of the National Ambient Air Quality Standards (NAAQS) for Particulate Matter (PM) will require the use of three-dimensional atmospheric models (EPA, 2000). It is essential to continue to improve the most promising model(s) to ensure state-of-the-art treatment of all important physic-chemical processes. Atmospheric PM consists of inorganic species, organic compounds, and water. An atmospheric model simulates gas-phase atmospheric chemistry and the processes that lead to gas-to-particle conversion of both inorganic and organic species. The gas-particle distribution of volatile species is governed by thermodynamic equilibrium. Models for the gas-particle distribution of inorganic species, such as nitrate, ammonium, and chloride, including water, are quite well developed (Zhang et al., 2000). The principal goal of the most present contract is to develop a comparable state-of-the-art thermodynamic equilibrium model for organic species and implement it in a three-dimensional model.

A significant challenge in developing an organic aerosol equilibrium model is that, in contrast to the inorganic case in which there are a relatively small number of distinct species, there are literally hundreds of atmospheric organic compounds capable of existing in both gas and aerosol phases. Even if all these compounds could be identified, it is not possible to track each one individually in a three-dimensional atmospheric model. As in the case of gas-phase atmospheric chemistry in highly anthropogenically influenced areas, it is necessary to form a set of surrogate organic species that encompass the classes of molecules capable of partitioning between gas and aerosol phases.

The organic equilibrium module is based on categorizing organic compounds as hydrophilic and hydrophobic. Hydrophilic compounds dissolve in existing particles that contain an aqueous phase of inorganic compounds. In this mixture, organic solutes may be present as molecules or ions (in the case of electrolytes such as organic acids) in the aqueous phase. Organic solutes that partition into the particulate phase are associated with additional water. Hydrophobic surrogate compounds absorb into an organic phase, which contains both primary and secondary components. In its current implementation the module simulates the partition of five hydrophilic and five hydrophobic surrogate compounds that represent 42 condensable organic species.

Two three-dimensional urban-scale atmospheric models were utilized in the present study: the California Institute of Technology (CIT) model and Models-3/CMAQ. The current version of the CIT model is described in this report and references therein the current version of Models-3/CMAQ available from the U.S. Environmental Protection Agency is described by Byun and Ching (1999). Several components of Models-3/CMAQ were modified to include the option of using the new aerosol module, and these are detailed in this report.

The two three-dimensional models were tested individually on two episodes in the South Coast Air Basin: Models-3/CMAQ on the August 27-28, 1987 SCAQS episode and CIT on the Sepmber X-Y, 1993 episode. The two components of secondary organic aerosol, hydrophilic and hydrophobic, were predicted to exhibit quite different behavior. The formation of aqueous-phase SOA was probably limited by partitioning during the day; higher concentrations were predicted at night when RH is high. Primary organic carbon represents the dominant component of organic carbon in the South Coast Air Basin.

Chapter 1

Secondary organic aerosol: I. Atmospheric chemical mechanism for production of molecular constituents

1.1 Introduction

Atmospheric urban and regional scale gas-phase chemical mechanisms describe the formation of oxidants such as ozone (O_3), the hydroxyl radical (OH), and the nitrate radical (NO_3), the consumption of reactive organics, and reactions of the resulting organic peroxy radicals with species such as the oxides of nitrogen (NO_x = NO + NO_2). Mechanisms that have been used in urban and regional atmospheric models include that of *Lurmann et al*. (LCC) [1987], the Carbon Bond IV Mechanism (CB-IV) [*Gery et al*., 1989], the Regional Acid Deposition Model (RADM2) [*Stockwell et al*., 1990], the Regional Atmospheric Chemistry Model (RACM) [*Stockwell et al.,* 1997], and the Statewide Air Pollution Research Center Mechanism (SAPRC-97) [*Carter et al*., 1997]. In addition, *Jenkin et al*. [1997] have presented a master chemical mechanism consisting of 120 parent organic compounds, 2500 chemical species, and approximately 7000 reactions.

Secondary organic aerosol (SOA) is formed in two steps. First, a sufficiently large parent organic is oxidized, resulting in products that have vapor pressures significantly lower than that of the parent. If their vapor pressures are low enough, these products can partition to the aerosol phase via condensation (adsorptive or absorptive) or homogeneous nucleation. Because low-vapor pressure products are needed to form SOA, in general, only those parent organics with 6 or more carbon atoms are capable of producing oxidized products that form SOA [*Odum et al*., 1996]. Existing gas-phase atmospheric chemical mechanisms do not include the detailed organic chemistry necessary for prediction of SOA formation. One reason for this is that much of the chemistry of the larger organics that leads to semi-volatile products is not known.

This paper describes a new chemical mechanism, termed the Caltech Atmospheric Chemistry Mechanism (CACM), that has two goals: (1) to include state-of-the-art treatment of ozone formation chemistry; and (2) to explicitly predict the concentrations of secondary and tertiary semi-volatile oxidation products that have the potential to act as constituents of SOA. In the treatment of O_3 formation chemistry, CACM relies on the recent work of *Stockwell et al*. [1997], *Jenkin et al*. [1997], and *Carter* [1997, 1999]. The mechanism contains a significant expansion of organic product chemistry in order to predict the formation of multi-functional, low vapor pressure products. In addition to the extension of the mechanism to include more detailed organic chemistry, relevant experimental and empirical information on rate constants and product yields (e.g., alkyl nitrate formation versus NO to NO_2 conversion) have been implemented in CACM [*Carter and Atkinson*, 1989; *Atkinson* 1990, 1994, 1997; *Goumri et al*., 1992; *Lay et al*., 1996; *Alvarado et al*., 1998]. While specific organic chemical mechanisms have been developed to model smog chamber SOA data (see, for example, *Barthelmie and Pryor* [1999]), we present here the first detailed atmospheric chemical mechanism that is directed toward explicit prediction of formation of the semi-volatile products that could constitute observed SOA. The product distributions in the mechanism to be presented are based either on limited observed product data or on extrapolation of the behavior of smaller organics. We recognize, of course, that precise product specifications are likely to change as more is learned about the mechanisms of SOA formation.

CACM includes a total of 191 species: (1) 120 fully integrated species (fully integrated species have concentrations that are solved for numerically based on kinetics, emission, and deposition.) [15 inorganic, 71 reactive organic, and 34 unreactive organic]; (2) 67 pseudo-steady state species [2 inorganic and 65 organic]; and (3) 4 species that have fixed concentrations. Table 1.1 shows a complete list of the species that are included in CACM. Table 1.2 gives the reactions included in CACM with appropriate Arrhenius rate constant expressions. The goals of the present paper (Part I) are twofold: (1) to describe the inorganic and organic chemistry in the mechanism; and (2) to evaluate the performance of the mechanism in simulating gas-phase chemistry during a well studied episode in the South Coast Air Basin (SoCAB) of California, August 27-29, 1987. Parts II and III, respectively, will derive a module to predict SOA formation based on thermodynamic equilibrium and present complete gas- and aerosol-phase simulations in the SoCAB for a 1993 episode.

1.2 Inorganic Chemistry

Inorganic chemistry within CACM (Reactions 1-42 in Table 1.2) is derived primarily from the SAPRC-99 mechanism of *Carter* [1999]. Only a brief overview of the inorganic chemistry need be given here. Photolysis rate constants are given in Table 1.3, and rate constants determined by three-body kinetics are listed in Table 1.4. Additional rate constants not falling into one of these categories are shown in Table 1.5.

Tropospheric inorganic chemistry is driven by a few relatively well understood reactions. NO is converted to NO_2 primarily via the reaction of NO with O_3 or the peroxy radicals (RO_2 or HO_2) that are formed by the reaction of OH with a number of species. (Reactions of organic species with O_3 or NO_3 also lead to RO_2 formation.) Photolysis of NO_2 results in the formation of $O(^3P)$, which combines with O_2 to form O_3. Photolysis of O_3 leads to formation of both $O(^3P)$ and $O(^1D)$, the latter of which reacts with water to form OH. $O(^1D)$ can also be collisionally stabilized to form $O(^3P)$. Other reactions that produce OH are the photolysis of HONO, the reaction between O_3 and HO_2, and the photolysis of H_2O_2. HONO is formed by the reactions of OH with NO and NO_2 with H_2O, and H_2O_2 is formed by the self-combination of HO_2.

The nitrate radical, NO_3, is formed primarily by the combination of NO_2 and O_3 but is relatively unimportant during the day because of its high rate of photolysis. Other sources of NO_3 include the reaction of NO_2 with $O(^3P)$ and the oxidation of HNO_3 by OH. HNO_3 is formed in the reaction of NO_2 with OH, by the combination of HO_2 and NO_3, or by the hydrolysis of N_2O_5. (The kinetics of the NO_2-OH reaction [*Dransfield et al*., 1999] have been significantly updated as compared with those in the extended LCC mechanism used by *Harley et al*. [1993].) HNO_4 is formed by the reaction of NO_2 with HO_2. Sinks for HNO_4 include decomposition and reaction with OH. Oxidation of SO_2 by OH forms SO_3, which is rapidly hydrolyzed to form sulfuric acid (H_2SO_4).

1.3 Organic Chemistry

In existing gas-phase urban and regional atmospheric mechanisms, organic chemistry has been focused primarily on predicting the concentrations of peroxy radicals that are generated as a result of hydrocarbon oxidation. In an effort to address the computational demands of gas-phase mechanisms to be used in three-dimensional atmospheric models, parent organics are often lumped into surrogate groups. In CACM, primary organic compounds are lumped in a manner similar to that described by *Stockwell et al*. [1997]. The result is a set of surrogate compounds designed to represent the entire array of gas-phase organic species emitted to the atmosphere.

Oxidation reactions of the surrogate parents are tracked individually, with multiple pathways being represented by the dominant reaction [*Kwok and Atkinson*, 1995; *Atkinson*, 1997]. Reactions of the resulting alkyl peroxy radicals are also included. From the reactions of these alkyl peroxy radicals, it is possible to predict the formation of surrogate oxidation products. If a product is considered reactive, it can go on to form tertiary (and so on) oxidation products. Prediction of specific products is important because gas-particle partitioning, through the link to vapor pressure, is highly dependent on molecular size and degree of functionality [*Yu et al*., 1999; *Pankow et al*., 2001]. Concentrations of the secondary, tertiary, etc. oxidation products then allow for prediction of the partitioning of organic molecules between the gas- and aerosol phases (Part II).

In CACM, the lumped model compound corresponding to a given individual parent hydrocarbon is determined by considering the size of the molecule, its structural characteristics (e.g., branched versus cyclic versus straight chain), its functionality (both location and type), its reactivity, and its experimentally determined potential for forming SOA, if available. Taking the 'average' structure of the compounds within a group (a group being appropriately defined) yields the surrogate for each group. Twenty-three individual groups, either surrogates or those described explicitly, are used (See Table 1.1). Instead of generating an aggregate rate constant for the surrogates as described by *Stockwell et al*. [1997], the rate constant for the model parent is used (either based on experimental data or calculated using structure-reactivity relationships; see Tables 2 and 6).

1.3.1 Alkanes

Alkanes are found in significant quantity in urban atmospheres [*Fraser et al*., 1997; *Schauer*, 1998; *Schauer et al*., 1999a, 1999b]. Methane chemistry is included explicitly in CACM, but because of its large mixing ratio, the concentration of methane remains fixed. The main tropospheric loss process for methane is the well documented oxidation by OH (reaction 43) to form the methyl peroxy radical ($RO_2$1). $RO_2$1 can then react with NO (reaction 110) in the presence of O_2 to form HO_2, formaldehyde (HCHO), and NO_2, with other peroxy radicals (represented henceforth as RO_2T) (reaction 111) to yield HCHO and HO_2, or with HO_2 to form HCHO (reaction 112). Throughout CACM, alkyl peroxy radical reactions with RO_2T are assumed, for simplicity, to form the same products as the NO reaction that results in the conversion of NO to NO_2. In addition, reactions with HO_2 are assumed to form the degradation products of the corresponding intermediate hydroperoxide since hydroperoxides are relatively reactive and often form very similar products upon oxidation [*Seinfeld and Pandis*, 1998]. To account accurately for RO_2T (which is formed along with every individual RO_2i species) concentrations, its reactions with NO, HO_2, and itself are also included in CACM (reactions 94-96).

1.3.2 Short Chain Alkanes

Short chain alkanes (ALKL) are considered as those with 2 to 6 carbon atoms. Based on the structural aggregation, 2-methyl-butane is used to represent these compounds, as shown in Table 1.1. In general, alkanes with more than one carbon atom are oxidized by OH abstraction of an H-atom with the subsequent addition of O_2 to form the alkyl peroxy radical [*Atkinson*, 1997]. As discussed above, the alkyl peroxy radical further reacts with NO, HO_2, or RO_2T. In the case of ALKL, oxidation by OH (reaction 58) results in the formation of $RO_2$5, which is a lumped alkyl peroxy radical formed by other parent hydrocarbons as well. $RO_2$5 is treated as a

primary peroxy radical with three carbon atoms and upon reaction with NO (reaction 122), can form the corresponding alkyl nitrate or NO_2, HO_2, and the corresponding aldehyde. The yield of alkyl nitrate formation versus NO to NO_2 conversion is calculated based on *Carter and Atkinson* [1989]. The HO_2 and RO_2T reactions also form HO_2 and an aldehyde (ALD2) (reactions 123 and 124). In this case, the alkyl nitrate formed in the NO reaction is treated as ALKL. When reactive small chain compounds that are not expected to contribute to SOA (either by dissolving in an aqueous phase or by absorption into an organic phase) are formed, they are reclassified within parent groups according to their size and most reactive functional group.

1.3.3 Medium Chain Alkanes

Medium chain alkanes (ALKM) are taken as those with 7 to 12 carbon atoms and are represented by 3,5-dimethyl-heptane. Initial OH oxidation of this species forms RO_220 (reaction 78). Like the corresponding RO_25, RO_220 is formed by more than one parent species and is represented by a lumped structure, 3-methyl-4-heptyl-peroxy radical. RO_220 reacts similarly to RO_25 (reactions 176-178) including the formation of an alkyl nitrate (AP3). (Alkyl nitrates with the potential to partition to the aerosol phase are labeled as AP*i*.) The alkoxy radical formed in these reactions, however, has sufficient chain length that the dominant mechanism involving this radical proceeds by isomerization through a 1,5-H shift [*Atkinson*, 1997]. The result is RO_218, a hydroxy alkyl peroxy radical, that can react like other peroxy radicals (reactions 170-172) to form a hydroxy alkyl nitrate (AP2), HO_2, and a hydroxy ketone (UR16). (Products that are considered nonreactive or whose oxidation products do not have vapor pressures estimated to be an order of magnitude less than the first product itself are labeled as unreactive, UR*i*; such species are assumed to have a first-order loss coefficient of 10^{-3} min^{-1} in order to prevent excessive build-up of these compounds). In this case, the alkyl nitrate products have sufficiently high carbon number that they or their oxidation products could potentially participate in SOA formation. The oxidation of such alkyl nitrate products proceeds by OH abstraction of the H-atom closest to the nitrooxy group. Subsequent decomposition reactions and reactions with O_2 result in the release of NO_2 and formation of functionalized products. In the case of AP2 (reaction 351), UR16 is assumed to form. In the case of AP3 (reaction 352), a ketone (UR32) is formed.

1.3.4 Long Chain Alkanes

Long chain alkanes (ALKH) are represented by *n*-hexadecane since hexadecane exhibits the approximate average number of carbons of those long chain *n*-alkanes that reside at least partially in the gas phase. Oxidation proceeds as above (reaction 93) and results in the formation of RO_232, which is formed only from the oxidation of ALKH and is represented by 8-hexadecyl peroxy radical. Reaction of RO_232 (reactions 215-217) forms either 8-hexadecyl nitrate (AP11) or RO_241 (8-hydroxy-11-hexadecyl-peroxy radical) via the 1,5-H shift. RO_241 (reactions 218-220) forms either 8-hydroxy-11-hexadecyl nitrate (AP12) or 11-hydroxy-8-hexadecanone (UR20) via a second isomerization and reaction with O_2. Oxidation of AP11 and AP12 (reactions 360 and 361) results in the formation of the corresponding carbonyls (UR34 and UR20, respectively). The chemistry of ALKH is shown in Figure 1.1a.

1.3.5 Non-biogenic Alkenes

1.3.6 Ethene

Despite their high reactivity [*Atkinson*, 1997], alkenes are still found in high concentration in the ambient [*Fraser et al*., 1997], which is indicative of significant emissions [*Schauer*, 1998; *Schauer et al*., 1999a, 1999b]. Given that its atmospheric chemistry is relatively well understood [*Atkinson*, 1997], ethene (ETHE) is treated explicitly. Reaction of alkenes with OH, NO_3, O_3, and $O(^3P)$ (reactions 49-52 respectively for ETHE) are taken into account. In the case of ETHE, addition of OH results in the formation of $RO_2$2, a lumped 2-hydroxy, 4-carbon, primary peroxy radical, that can undergo peroxy radical reactions similar to those described in the alkanes section above (reactions 113-115). However, in the case of the NO reaction, an alkyl nitrate product is not formed because of the small carbon number [*Carter and Atkinson*, 1989]. Products of these reactions are HCHO, ALD2, and HO_2. Reaction of ETHE with NO_3 proceeds similarly with an ONO_2 group replacing the OH group in the radical ($RO_2$3). The reactions of $RO_2$3 (reactions 116-118) create HCHO, ALD2, and HO_2; NO_2 is liberated from $RO_2$3 upon reaction as well. The reaction of ETHE with O_3 is initiated by O_3 attack of the double bond in the well established bridging mechanism. The decomposition of the highly energetic intermediate leads to formation of a short chain *n*-carboxylic acid (ACID), HO_2, CO, OH, HCHO, and H_2O. Yields of these products are shown in Table 1.2 and are derived from *Jenkin et al*. [1997]. The final reaction of ETHE is that with $O(^3P)$, leading to formation of $RO_2$1, CO, HO_2, and $RO_2$4, an aldehydic 2-carbon peroxy radical, with yields shown in Table 1.2 and derived from *Atkinson* [1997]. $RO_2$4 acts like other peroxy radicals (reactions 119-121); however, radicals such as $RO_2$4 that exhibit an α-carbonyl are assumed not to form alkyl nitrate products [*Jenkin et al*., 1997].

1.3.7 Short Chain Alkenes

Short chain alkenes with 3 to 6 carbon atoms (OLEL) are represented by 1-pentene because of the high ambient presence of straight chain α-alkenes. Similar to ETHE, OLEL is consumed by OH, NO_3, O_3, and $O(^3P)$ (reactions 54-57). As with ETHE, OH and NO_3 reaction lead to $RO_2$2 and $RO_2$3, respectively. OLEL reaction with O_3 leads to formation of HCHO, ALD2, ACID, CO, OH, CO_2, HO_2, ALKL (a reclassified reactive product), and $RO_2$5 in yields shown in Table 1.2 and derived from *Jenkin et al*. [1997]. The OLEL reaction with $O(^3P)$ leads to ALKL (a reclassified reactive product), ALD2, $RO_2$4, and $RO_2$5 in yields also shown in Table 1.2 and derived from *Atkinson* [1997].

1.3.8 Long Chain Alkenes

Longer chain alkenes (OLEH) are those with 7 or more carbon atoms and are represented by 4-methyl-1-octene because of the high ambient presence of branched α-alkenes. As before, OH, NO_3, O_3, and $O(^3P)$ can react with OLEH (reactions 74-77 respectively). Reactions with OH and NO_3 lead to $RO_2$18 and $RO_2$19, respectively. The reactions of $RO_2$18, represented by a lumped structure (2-methyl-2-hydroxy-5-heptyl peroxy radical), are described above. $RO_2$19 is formed exclusively by OLEH and is the corresponding radical with the nitrooxy group in the 1-position and the peroxy radical at the 2-position. Its reactions (173-175) result in the formation of HCHO and 3-methyl-heptanal (RPR1) (Reactive products that are capable of participating in SOA formation and that do not exhibit a nitrooxy group are labeled RPR*i* or RP*i*.). The reactions typical of RPR1 (aldehydes) will be discussed in the next section. Oxidation or photolysis of RPR1 (reactions 300-302) leads to formation of $RO_2$20 or the corresponding acyl peroxy radical ($RO_2$55). The corresponding peroxy nitrate compound (PAN7), $RO_2$20, and 3-methyl-heptanoic

acid (UR1) are formed in the reactions of $RO_2$55 (reactions 303-307). Details of acyl peroxy radical reactions will also be given in the next section. The reaction of OLEH with O_3 leads to the formation of HCHO, RPR1, ACID, UR1, CO, OH, HO_2, CO_2, ALKM (a reclassified reactive product), and $RO_2$20 in yields described in Table 1.2 and derived via *Jenkin et al*. [1997]. The OLEH-O(^{3}P) reaction forms ALKM, RPR1, $RO_2$4, and $RO_2$20 in yields described in Table 1.2 and derived via *Atkinson* [1997].

1.3.9 Aldehydes

Aldehydes, emitted in large amounts and formed via atmospheric chemistry, contribute significantly to the overall reactivity of the urban atmosphere [*Grosjean et al*., 1996]. Degradation of formaldehyde (HCHO) occurs by photolysis (reactions 44 and 45) and oxidation by OH (reaction 46) and NO_3 (reaction 47). Higher *n*-aldehydes (ALD2) are represented by *n*-pentanal. Because of the importance of aldehyde reactions (with respect to RPR species leading to UR species capable of forming SOA), a general aldehyde mechanism is discussed here. Like HCHO, higher aldehydes are degraded by OH, NO_3, or photolysis. OH and NO_3 degradation proceed via abstraction of the aldehydic H-atom and result in the formation of water or nitric acid and an acyl radical ($RC(O)O_2$•), after the subsequent addition of O_2. Photolysis is assumed to form a primary alkyl radical, CO, and an H-atom radical. The alkyl radical and the H-atom radical each react immediately with O_2 to form an alkyl peroxy radical and a hydroperoxy radical, respectively.

The acyl peroxy radical can then undergo reaction with NO, NO_2, HO_2, and RO_2T. In the NO reaction, NO is converted to NO_2, resulting in decomposition of the remainder of the original radical to form CO_2 and a primary alkyl radical that immediately forms an alkyl peroxy radical upon addition of O_2. CO_2 and a primary alkyl peroxy radical are also formed in the RO_2T reaction. NO_2 adds to the radical to form a peroxy acyl nitrate species (denoted as PAN*i*) that can thermally decompose back to $RC(O)O_2$• and NO_2. Acyl peroxy radicals are converted to organic acids in the reaction with HO_2. This pathway is less likely to occur relative to the NO or NO_2 reactions under high NO_x conditions typical of urban atmospheres [*Niki et al*., 1985; *Moortgat et al*., 1989] but accounts for one path of secondary formation of the organic acids observed in the atmosphere [*Fraser et al*., 1999; *Nolte et al*., 1999]. At present, the known routes of organic acid formation in the atmosphere cannot account for measured ambient concentrations [*Jacob and Wofsy*, 1988; *Seinfeld and Pandis*, 1998].

The photolysis of ALD2 (reaction 59) leads to the formation of $RO_2$5, CO, and HO_2. Degradation of ALD2 by OH (reaction 60) and NO_3 (reaction 61) results in the corresponding acyl radical ($RO_2$6), which follows the chemistry described above (reactions 125 and 129). Products include NO_2, CO_2, $RO_2$5, ACID, O_3, and PAN1.

1.3.10 Ketones

Atmospheric ketones are less abundant than aldehydes [*Fraser et al*., 1997], but like aldehydes, they have both primary [*Schauer*, 1998; *Schauer et al*., 1999b] and secondary sources. Ketones in CACM are broken down into two groups: short chain ketones with between 3 and 6 carbons (KETL) and long chain ketones with 7 or more carbons (KETH).

Ketones (for example, $R_1CH_2C(O)R_2$) either photolyze or are oxidized by OH [*Atkinson*, 1994]. It is assumed that the OH reaction proceeds via abstraction of the H-atom in the position α- to the carbonyl functionality. After addition of O_2, this results in the formation of $R_1CH(O_2$•$)C(O)R_2$, a keto-alkyl peroxy radical. Photolysis yields cleavage of the carbon-carbon

bond adjacent to the carbonyl. After addition of O_2, the results are $R_1CH_2O_2\bullet$, a simple alkyl peroxy radical, and $R_2C(O)O_2\bullet$, an acyl peroxy radical. The keto-alkyl peroxy radical, of course, reacts with NO, HO_2, and RO_2T to form an alkoxy radical in the position α- to the carbonyl. This radical will decompose to form a higher aldehyde ($R_1C(O)H$) and the acyl peroxy radical described above.

KETL is represented by 2-pentanone because of the frequent occurrence of small chain ketones that have the functional group in the 2-position. Following the mechanism described above, the reaction of KETL with OH (reaction 62) yields RO_27, a keto-alkyl peroxy radical that is represented by a lumped structure with 4 carbons, the keto group in the 2-position, and the peroxy radical in the 3-position. Analogously, the photolysis of KETL (reaction 63) results in RO_25 and a 2-carbon acyl radical, RO_28. Because RO_28 is formed in so many reactions in CACM, it is treated as a fully integrated species. RO_27 follows the reaction patterns (reactions 130-132) discussed earlier for alkyl peroxy radicals with carbonyls in the α-position. RO_28 follows the reaction patterns (reactions 133-137) discussed earlier for acyl peroxy radicals; the resulting products include peroxy acetyl nitrate (PAN2).

Similarly, 2-heptanone represents KETH. Photolysis of KETH (reaction 71) also yields RO_25 and RO_28. Oxidation of KETH by OH (reaction 70) results in the formation of RO_216, 2-keto-3-heptyl peroxy radical, which results in products identical to those of KETL (reactions 164-166). Because the final products formed by KETL and KETH are similar, separating them into two groups is based solely on kinetics.

1.3.11 Alcohols

Alcohols have both anthropogenic and biogenic sources [*Harley et al*., 1992; *Goldan et al*., 1993; *Sharkey*, 1996]. Hydroxyl groups, which characterize alcohols, are also present in multi-functional secondary organic oxidation products [*Yu et al*., 1999].

Methanol (MEOH) and ethanol (ETOH) have well understood atmospheric chemistry [*Atkinson*, 1994]. Degradation of these compounds proceeds via OH abstraction of an H-atom from either a C-H or O-H bond. For MEOH (reaction 48), the resulting intermediates react instantaneously with O_2 to form HCHO and HO_2. For ETOH (reaction 53), the split between C-H and O-H abstraction is determined from the rate constants of each pathway [*Kwok and Atkinson*, 1995]. If the H-atom is abstracted from an O-H bond, the resulting intermediate immediately reacts with O_2 to form ALD2 and HO_2. If the H-atom is abstracted from a C-H bond, the result is either ALD2 or RO_22 depending on the location of the abstraction. 2-Hexanol represents alcohols with three or more carbon (ALCH). Abstraction by OH of an H-atom from the carbon chain is expected to be the dominant sink for ALCH (reaction 69). The resulting radical is RO_22.

1.3.12 MTBE

Because methyl-*tert*-butyl ether (MTBE) is a constituent of reformulated gasoline sold in the region during the period of interest, it is the only ether explicitly tracked in CACM. (Others are included in ALKL or ALKM as in *Stockwell et al*. [1997].) Reaction of MTBE with OH (reaction 68) proceeds via H-atom abstraction and forms RO_215. RO_215 reacts with NO, HO_2, or RO_2T (reactions 161-163) to form ALD2, ALKL, KETL, and HCHO in yields described in Table 1.2 and based on the work of *Japar et al*. [1990] and the estimates of *Harley et al*. [1993].

1.3.13 Aromatics

Aromatic species comprise a significant portion of the hydrocarbon component of motor vehicle emissions [*Harley et al*., 1992] and have been identified as the most likely class of anthropogenic SOA precursors [*Odum et al*., 1996, 1997]. Aromatics are found in relatively high concentrations in the urban atmosphere [*Fraser et al*., 1999] and come from a variety of sources [*Schauer*, 1998; *Schauer et al*., 1999a, 1999b].

Aromatic species are aggregated depending on their reactivity, their degree and nature of substitution, and their potential for SOA formation, as determined by *Odum et al*. [1996, 1997]. Low SOA-yield aromatics (AROL, represented by 1,2,3-trimethylbenzene) are those with two or more methyl side groups and no functional side groups (such as phenols, aldehydes, acids, or nitro groups); high SOA-yield aromatics (AROH, represented by *m*-(*n*-propyl)-toluene) have one or no methyl side groups and no functional side groups. Phenolic species (AROO, represented by 2,6-dimethyl-phenol) may have one or more alkyl side groups and one or more phenolic substituents. Aldehydic aromatics (ARAL, represented by *p*-tolualdehyde) have one aldehydic functional group; acidic aromatics (ARAC, represented by *p*-toluic acid) have one carboxylic functional group. Gas-phase polycyclic aromatic hydrocarbons (PAHs, represented by 1,2-dimethyl-naphthalene) have multiple aromatic rings. Generally, only PAHs with two aromatic rings remain in the gas-phase; those with more partition between the gas- and aerosol-phases [*Fraser et al*., 1999]. The chemistry of aromatics proceeds typically via OH addition to the ring of H-atom abstraction from alkyl side chains. Any deviations are explained appropriately in the sections below.

1.3.14 Low Yield Aromatics

Products of AROL chemistry (reaction 79) include AROO, a cyclohexadienyl radical (RAD3), and $RO_2$21 (formed from H-atom abstraction from a side chain). The yields of these products are described in Table 1.2 and are derived from *Atkinson* [1990, 1994]. $RO_2$21 (reactions 179-181) forms a methyl nitrooxy substituted aromatic (AP4) or an aldehydic aromatic product (ARAL). AP4 is assumed to form ARAL as well (reaction 353). RAD3 can react either with NO_2 (reaction 105) to form nitro-trimethylbenzene (UR12) or predominantly with O_2 (reaction 98) to form a cyclohexadienyl peroxy radical ($RO_2$34), which can then isomerize (reaction 228) to form a bicyclic peroxy radical ($RO_2$43) or react with NO, HO_2, and RO_2T (reactions 229-231) [*Klotz et al*., 1997]. Reaction of $RO_2$34 leads to 4,5-dimethyl-6-keto-2,4-heptadienal, RP11. $RO_2$43 reactions (232-234) form ring cleavage products such as methyl glyoxal (MGLY). The remaining unreactive ring cleavage products in this second pathway do not contribute to SOA formation so they are grouped together for all aromatic parents except PAH. They are represented by 2-methyl-butenalic acid, RP10. In an effort to account for acid formation in aromatic oxidation (and the subsequent formation of SOA), RP11 reacts with OH (reaction 334) to form directly the corresponding acid (UR26) (as in the acyl radical reaction mechanism described in detail above), instead of undergoing the full range of aldehyde reactions. RP10 can either react with OH (reaction 332) to form the corresponding anhydride (UR24) or photolyze (reaction 333) to form the corresponding furan (UR25). MGLY is modeled to behave as an aldehyde, and follows the reaction pattern described earlier (reactions 263-365). Products of MGLY oxidation include $RO_2$8, CO, HO_2, and $RO_2$48, a 3-carbon, keto-acyl radical. $RO_2$48 follows the acyl radical reaction pattern described above (reactions 266-270) and forms NO_2, CO_2, $RO_2$8, keto-peroxy-propionyl nitrate (PAN4), and keto-propanoic acid (UR21), which is

considered capable of forming SOA because of its solubility in the aqueous phase. The chemistry of AROL is shown in Figure 1.1b.

1.3.15 High Yield Aromatics

Because of the degree of substitution of this class of compounds, only ring addition is taken into account in the oxidation of AROH [*Atkinson*, 1994]. The products of this first step are AROO, HO_2, and a cyclohexadienyl (RAD4) radical similar to that formed in AROL oxidation. Yields are given in Table 1.2. Upon reaction with NO_2 (reaction 106), RAD4 forms the nitro-form of AROH (UR13). However, RAD4 predominantly reacts with O_2 (reaction 99) to form another cyclohexadienyl peroxy radical ($RO_2$35) that can isomerize (reaction 235) to form $RO_2$44 or react (reactions 236-238) to form primarily RP11. $RO_2$44 reacts (reactions 239-241) to form MGLY and RP10. The yield of the ring fragmentation products and kinetics are the only differences between the chemistry of AROL and AROH.

1.3.16 Phenolic Species

In contrast to AROL and AROH, both NO_3 and OH can initiate oxidation of AROO. NO_3 abstracts the H-atom from the phenolic functional group (reaction 72) to form RAD1, a dimethyl-benzoxy radical. In an effort to account for observed concentrations of nitro-phenols [*Fraser et al*., 1999], it is assumed that RAD1 reacts only with NO_2 (reaction 103) to form dimethyl-nitro-phenol (RPR4). OH oxidation of AROO (reaction 73) proceeds via side chain abstraction ($RO_2$17) or addition to the ring to reform AROO or another cyclohexadienyl radical (RAD2). Yields for this reaction are presented in Table 1.2. $RO_2$17 reacts similarly to other organic peroxy radicals with the primary products including a nitrooxy derivative of AROO (AP1) and hydroxy-tolualdehyde (RPR2) (reactions 167-169). As before, RAD2 reacts predominantly with O_2 (reaction 97) to form a cyclohexadienyl peroxy radical ($RO_2$33) or can react with NO_2 (reaction 104) to form RPR4. $RO_2$33 can isomerize to $RO_2$42 (reaction 221) or can react (reactions 222-224) to form primarily 4-hydroxy-3,5-dimethyl-2,4-hexadiendial, RPR9. $RO_2$42 (reactions 225-227) yields MGLY and RP10. Upon oxidation (reaction 350), AP1 will yield RPR2. Similarly to RP11, RPR2 reacts with OH (reaction 308) to form directly the corresponding acid (UR2). RPR9 also forms directly the corresponding acid (RP17) (reaction 331), which further reacts to form the corresponding diacid (UR29) (reaction 347).

1.3.17 Aromatic Aldehydes

The degradation of ARAL by NO_3 (reaction 81) proceeds via abstraction of the aldehydic H-atom, resulting in the formation of HNO_3. In an effort to account for ambient concentrations of aromatic acids [*Rogge et al*., 1993; *Fraser et al*., 1999], it is assumed that the resulting acyl radical immediately reacts with HO_2 to form the corresponding aromatic acid (ARAC) and O_3. Degradation of ARAL by OH (reaction 82) can proceed via three distinct pathways: abstraction of the H-atom from the aldehyde group, abstraction of an H-atom from the methyl side group, or ring addition. The split between these is determined kinetically assuming that OH adds directly to the ring to form a phenolic compound in the same yield as discussed previously. As with the NO_3 reaction, abstraction of the aldehydic H-atom leads directly to acid formation. Abstraction of an H-atom from the methyl group leads to the formation of $RO_2$22 which can proceed (reactions 182-184) to form primarily an aromatic compound with either one aldehyde and one nitrooxy-methyl side chain (AP5) or two substituent aldehyde side groups (RPR6). Upon oxidation (reaction 354), AP5 is converted to RPR6. Again in an effort to account for ambient

formation of aromatic acids and diacids [*Rogge et al*., 1993; *Fraser et al*., 1999], the aldehyde groups of RPR6 are converted directly to acids (reactions 320 and 321). RPR7 describes an aromatic ring with one aldehyde and one acid substituent group. ADAC describes the aromatic species with two acid groups. (The UR*i* notation is not used with ADAC, as aromatic diacids are also constituents of primary aerosol.) As with the other aromatic species discussed so far, addition of OH to the aromatic ring in ARAL results in the formation of a cyclohexadienyl radical, RAD5. As before, RAD5 can react with NO_2 (reaction 107) to form the corresponding nitro-tolualdehyde (RPR5) or with O_2 (reaction 100) to form the cyclohexadienyl peroxy radical, $RO_2$36. The aldehyde group of RPR5 can be converted directly to the acid (reaction 319) to form methyl-nitro-benzoic acid (UR14). Similar to the radicals formed from other aromatic species, $RO_2$36 can isomerize (reaction 242) to $RO_2$45 or undergo reaction (reactions 243-245) to form 2-methyl-5-formyl-2,4-hexadiendial, RP12. $RO_2$45 reacts (reactions 246-248) to form MGLY and RP10. The three aldehyde groups of RP12 subsequently can be converted directly to acids forming, in order, RP13, RP18, and UR30 (reactions 335, 336, and 348).

1.3.18 Aromatic Acids

Because the carboxylic acid moieties in CACM are considered unreactive, the degradation of ARAC is driven by reaction with OH (reaction 83) via either side chain H-atom extraction ($RO_2$23) or addition to the ring (UR2 or RAD6). Reactions of $RO_2$23 (reactions 185-187) yield either the methyl-nitrooxy derivative (AP6) or RPR7. When oxidized by OH (reaction 355), AP6 yields RPR7. Similar to other cyclohexadienyl radicals, RAD6 reacts predominantly with O_2 (reaction 101) to form the corresponding cyclohexadienyl peroxy radical ($RO_2$37) but can also react with NO_2 (reaction 108) to form the nitro derivative of ARAC (UR14). Isomerization of $RO_2$37 (reaction 249) leads to the formation of $RO_2$46, which reacts (reactions 253-255) to form RP10 and MGLY. Reaction of $RO_2$37 (reactions 250-252) leads to the formation of RP13.

1.3.19 Polycyclic Aromatic Hydrocarbons

The final lumped aromatic compound considered in CACM is PAH. The sink for PAH is reaction with OH (reaction 92), which can lead to $RO_2$31 (H-atom abstraction from the side chain), UR11 (hydroxy-PAH), or an aromatic cyclohexadienyl radical (RAD7) similar to those formed by monoaromatic compounds. $RO_2$31 reacts (reactions 212-214) as before to form the methyl-nitrooxy derivative (AP10) and the aldehyde derivative (UR19). AP10 forms UR19 upon oxidation by OH (reaction 359). RAD7 reacts with O_2 (reaction 102) to form $RO_2$38 or with NO_2 (reaction 109) to form nitro-PAH (UR15). $RO_2$38 can isomerize (reaction 256) to $RO_2$47 or react (reactions 257-259) to form 2-(dimethyl propenal)-benzaldehyde (RP14). The aldehyde groups in RP14 can be converted successively to acids, RP19 and UR31 (reactions 337 and 349). The reactions of $RO_2$47 (reactions 260-262) lead to MGLY and 2-formyl-acetophenone (RP15). The aldehyde group in RP15 can be converted to acid (reaction 338) resulting in the formation of 2-carboxy-acetophenone (UR27).

1.3.20 Biogenics

Biogenic organics play an important role in atmospheric chemistry [*Lamb et al*., 1993; *Guenther et al*., 1995]. Isoprene (ISOP) and the monoterpenes are considered in CACM; sesquiterpenes are ignored because of their extremely low emission rate relative to those of isoprene and the monoterpenes and since little is known about their oxidation patterns.

1.3.21 Isoprene

The atmospheric behavior of isoprene (ISOP), 2-methyl-1,3-butadiene, has been studied in detail [*Paulson et al*., 1992ab; *Yu et al*., 1995; *Kwok et al*., 1995; *Carter and Atkinson*, 1996]. ISOP does not contribute significantly to SOA formation [*Pandis et al*., 1992] but can contribute to ozone formation if emitted at a high enough rate. Because the mechanism of ISOP oxidation has been presented in detail previously, only an overview is given here.

Like other unsaturated molecules, ISOP is oxidized by OH, NO_3, O_3, and $O(^3P)$ (reactions 64-67). The mechanism in CACM assumes that OH and NO_3 addition to the double bonds occurs only at the two most probable spots, as determined by the stability of the resulting radicals [*Atkinson*, 1997]. The split between these locations is determined kinetically. The most preferred OH attack occurs first (approximately 2/3) in the 1-position and second (approximately 1/3) in the 4-position, resulting in a tertiary peroxy radical, $RO_2$9, and a secondary peroxy radical, $RO_2$10, respectively. The reactions of $RO_2$9 (reactions 138-140) are assumed to result in the formation of methyl-vinyl-ketone (MVK), HCHO, HO_2, and NO_2 (NO_2 in the NO case only). Correspondingly, the reactions of $RO_2$10 (reactions 141-143) result in the formation of methacrolein (MCR), HCHO, HO_2, and NO_2 (NO_2 in the NO case only). The NO_3 oxidation pattern is analogous, with $RO_2$11 and $RO_2$12 having a nitrooxy group instead of an OH group. Upon reaction (reactions 144-149), these species liberate NO_2 and form MCR, MVK, HCHO, HO_2, and NO_2. The ISOP-O_3 reaction forms MVK, MCR, HCHO, OLEL (a reclassified small product), CO_2, ACID, CO, OH, HO_2, $RO_2$13, and $RO_2$14 in yields shown in Table 1.2 and derived from *Jenkin et al*. [1997]. $RO_2$13 is a 4-carbon, unsaturated peroxy radical with a keto group and leads to HCHO and a 3-carbon, unsaturated acyl radical ($RO_2$39) (reactions 150-152). $RO_2$39 follows the previously discussed reaction pattern for acyl radicals (reactions 153-157) and results in the formation of $RO_2$14, CO_2, an unsaturated peroxy nitrate compound (PAN3), OLEL, ACID, and O_3. $RO_2$14 is a 2-carbon, unsaturated peroxy radical that is converted to OLEL or $RO_2$7 upon reaction (reactions 158-160). The ISOP-$O(^3P)$ reaction yields OLEL (reclassified) and ALD2 in yields shown in Table 1.2 and derived from *Atkinson* [1997].

MCR and MVK are major oxidation products of ISOP and are included explicitly. MVK reacts with OH, O_3, and $O(^3P)$ (reactions 271-273); the NO_3 reaction is not considered because of its comparatively small rate constant [*Carter*, 1999]. OH reaction proceeds via addition and leads to the formation of $RO_2$49. Reactions of $RO_2$49 (274-276) lead to MGLY, HCHO, and HO_2 (and NO_2 in the NO reaction). The MVK-O_3 reaction results in the formation of MGLY, HCHO, ACID, UR21, ALD2, CO, CO_2, HO_2, OH, water, and $RO_2$8 in yields shown in Table 1.2 and derived from *Jenkin et al*. [1997]. Reaction between MVK and $O(^3P)$ leads to KETL (reclassified), $RO_2$4, and $RO_2$8 in yields shown in Table 1.2 and derived from *Atkinson* [1997]. MCR can also react with OH, NO_3, O_3, and $O(^3P)$ (reactions 277-280). The OH and NO_3 reactions can proceed via addition to the double bond ($RO_2$51 and $RO_2$52 respectively) or via H-atom abstraction from the aldehyde group ($RO_2$50). $RO_2$50 behaves similarly to the acyl radicals that have been described previously (reactions 281-285). Products include NO_2, CO_2, $RO_2$14, PAN5, ACID, and OLEL. $RO_2$51 and $RO_2$52 (reactions 286-291) lead to the formation of HCHO and MGLY. Reaction between MCR and O_3 leads to HCHO, MGLY, OH, CO, HO_2, ACID, and $RO_2$53 as shown in Table 1.2 with yields derived from *Jenkin et al*. [1997]. $RO_2$53 (reactions 292-294) leads to the formation of $RO_2$54, an aldehydic, 2-carbon acyl radical, which follows the reactions characteristic of acyl radicals (reactions 295-299). Products include NO_2, CO_2, CO, HO_2, glyoxalic acid (RP16), and the corresponding peroxy nitrate compound (PAN6). Degradation of RP16 proceeds via photolysis (reaction 341) or abstraction of the aldehydic H-

atom by OH or NO_3 (reactions 339 and 340). The abstraction pathway leads to the formation of the corresponding acyl radical ($RO_2$58) that will form products that include NO_2, CO_2, CO, OH, the corresponding peroxy nitrate species (PN10), and the corresponding acid (oxalic acid, UR28) (reactions 342-346). The chemistry of ISOP is illustrated in Figure 1.1c.

1.3.22 Monoterpenes

Despite evidence that monoterpenes are not easily aggregated according to SOA formation potentials [*Griffin et al*., 1999], we lump them in this way because the uncertainties associated with monoterpene chemistry preclude representation at any greater level of detail. α-Terpineol, which represents relatively low SOA-yield monoterpenes (BIOL), encompasses the carbon number, structural characteristics, and reactivity of the group members as well. BIOL is oxidized by OH, NO_3, O_3, and $O(^3P)$ (reactions 84-87). OH addition to the double bond leads to $RO_2$24, a dihydroxy, tertiary peroxy radical. (NO_3 addition results in the analogous radical, $RO_2$25, with an ONO_2 group replacing the OH group in the 2-position.) Reactions $RO_2$24 and $RO_2$25 (reactions 188-193) result in the nitrooxy product (AP7) and the keto-aldehyde (2-hydroxy-3-isopropyl-6-keto-heptanal, RPR3) caused by ring cleavage. Upon oxidation (reaction 356), AP7 forms RPR3 as well. Oxidation of BIOL by $O(^3P)$ is assumed to result in two products (epoxide, UR5, and carbonyl, UR6) in yields estimated from *Alvarado et al*. [1998] and shown in Table 1.2. The attack by O_3 and resulting decomposition result in the formation of UR3, UR4, CO, RPR3, HO_2, H_2O_2, OH, and $RO_2$26 in yields shown in Table 1.2 and derived from *Jenkin et al*. [1997]. UR3 and UR4 are the resulting hydroxy-keto-acid and keto-aldehyde respectively. $RO_2$26 is a trisubstituted (hydroxy group, aldehyde, and ketone) organic peroxy radical. The reactions of $RO_2$26 (reactions 194-196) lead primarily to the formation of $RO_2$8 and UR17, a hydroxy dial. Reactions of RPR3 follow the reaction pattern assumed for aldehydes, as it assumed that the aldehyde is the most reactive moiety within RPR3. These reactions (reactions 309-311) result in the formation of the corresponding acyl radical ($RO_2$56) or UR4. The acyl radical reaction pattern followed by $RO_2$56 (reactions 312-316) leads to formation of NO_2, CO_2, UR4, PAN8, UR3, O_3, and UR4.

CACM also incorporates a class (BIOH) for those monoterpenes that have relatively high SOA yield parameters [*Griffin et al*., 1999]. The structure chosen to represent this group is γ-terpinene because of its high reactivity and large SOA formation potential. As with all other unsaturated compounds, BIOH is oxidized by OH, NO_3, O_3, and $O(^3P)$ (reactions 88-91). OH addition is assumed to occur so that the peroxy radical is at the most stable possible location. The result is a cyclic, unsaturated, hydroxy peroxy radical ($RO_2$27). NO_3 oxidation occurs analogously to form the corresponding nitrooxy peroxy radical ($RO_2$28). Reactions of $RO_2$27 and $RO_2$28 (reactions 197-202) result in either the corresponding nitrooxy compound (AP8) or the keto-aldehyde ring cleavage product (UR7). UR7 is also formed by the reaction of AP8 with OH (reaction 357). In the $O(^3P)$ reaction, UR9 (epoxide) and UR10 (ketone) are formed in yields shown in Table 1.2 and derived from *Alvarado et al*. [1998]. The O_3-BIOH reaction leads to UR7, UR8, CO, OH, H_2O_2, $RO_2$29, and $RO_2$30 in yields shown in Table 1.2 and derived from *Jenkin et al*. [1997]. UR8 is the corresponding keto-acid ring cleavage product. $RO_2$29 is a primary peroxy radical with an unsaturated bond and a ketone moiety. Its reactions (203-205) lead to the appropriate nitrooxy product (AP9) or another peroxy radical ($RO_2$40) formed by isomerization. Upon oxidation (reaction 358), AP9 yields the corresponding unsaturated keto-aldehyde (UR33). The reactions of $RO_2$40 (206-208) lead to decomposition and the formation of $RO_2$8 and an unsaturated hydroxy aldehyde (RPR8). The corresponding reactions of $RO_2$30

(209-211), which exhibits an unsaturated bond, a ketone group, and an aldehyde, lead to the formation of UR18 (an unsaturated dial). Two photolysis pathways (reactions 324 and 325) are given for RPR8, one in which CO, HO_2, and $RO_2$9 are formed and another in which the corresponding acyl radical, $RO_2$57, is formed. (This is due to the α-position of the aldehyde relative to the unsaturated bond.) $RO_2$57 is also formed by the OH and NO_3 abstraction of the aldehydic H-atom from RPR8 (reactions 322 and 323 respectively). Following the behavior of other acyl radicals (in reactions 326-330), $RO_2$57 leads to $RO_2$9, CO_2, NO_2, the corresponding peroxy nitrate compound (PAN9), the corresponding acid (UR23), O_3, and $RO_2$9.

1.4 Gas-Phase Simulation of the SCAQS Episode of August 27-29, 1987 in the SoCAB

We have presented a chemical mechanism for urban/regional atmospheric chemistry including SOA precursors. In its ozone formation chemistry, the mechanism builds upon previous work of *Stockwell et al*. [1997], *Jenkin et al*. [1997], and *Carter* [1997,1999]. The mechanism is intended for use in three-dimensional urban/regional atmospheric models, where both ozone formation and SOA production are to be predicted. As a prelude to these comprehensive simulations, it is of importance to establish the performance of the mechanism in ozone prediction. The SoCAB of California, because of the availability of both emissions inventories and comprehensive monitoring, has traditionally served as the benchmark for evaluating the performance of three-dimensional urban/regional atmospheric models. Consequently, we present here a simulation of gas-phase chemistry in the SoCAB of California. We will evaluate ozone predictions of the new mechanism against both observed data and the earlier simulations of *Harley et al*. [1993]. The CIT model serves as the basic three-dimensional model [*Harley et al*., 1993; *Meng et al*., 1998]; it conforms to the three-dimensional model structure embodied in the U.S. Environmental Protection Agency's Models 3 [*United States Environmental Protection Agency,* 1999], so modules presented in the present series of papers can be used in that framework as well.

1.4.1 August 27-29, 1987 SCAQS Episode

During the summer and fall of 1987, an intensive monitoring program known as the Southern California Air Quality Study (SCAQS) took place in the SoCAB [*Lawson*, 1990], which is shown graphically in Figure 1.2. The meteorological and air quality measurements made during this program provide a detailed ambient data set that has been used a number of times to evaluate atmospheric models. Previous simulations of the episode of August 27-29, 1987 include those of *Harley et al*. [1993], *Harley and Cass* [1995], *Jacobson et al*. [1996], and *Meng et al.* [1998]. We will consider this episode as well to evaluate the performance of the gas-phase mechanism presented here. *Harley et al*. [1993] give emissions and boundary and initial conditions information for this episode. Therefore, only summary tables need be given here. Table 1.7 shows a highly aggregated emissions profile for one of the days simulated, and Table 1.8 gives the upwind boundary conditions. *Harley et al*. [1993] also describe the deposition module and meteorology used in CIT.

1.4.2 Ozone Simulation

Predicted (dashed) mixing ratios of O_3 (black) and NO (gray) in Pasadena and Riverside are compared to data observed (solid) at those locations in Figures 3 and 4, respectively. For Pasadena it is seen that O_3 is underpredicted on each day, with a slight shift in the peak predicted O_3 to a later time than that observed on the first day. NO simulations match observed data reasonably well except on the third day, when NO is significantly overpredicted at rush hour

times (even though the third day is a Saturday). In Riverside, O_3 is underpredicted on the first day and matched well on the second and third days. Peak NO is underpredicted, but NO is slightly over predicted at night. These under- and overpredictions are most likely linked to inaccuracies in the NO_x and gas-phase organic emissions inventories and uncertainties in the chemistry. These trends typify the predictions at other locations throughout the SoCAB. Pasadena and Riverside are chosen because they are downwind of major emissions sites and, thus, represent locations that are expected to display secondary species in higher concentrations.

A statistical analysis of simulated results versus observed data has been performed for NO_2 and O_3 (Table 1.9). Statistics considered include bias, normalized bias, standard deviation, gross error, and normalized gross error. The methodology for these calculations is described in *Harley et al*. [1993]. These numbers are comparable to those of *Harley et al*. [1993] and, moreover, are typical of the level of agreement achieved in current three-dimensional modeling studies [*Harley and Cass*, 1995; *Jacobson et al*., 1996; *Meng et al*., 1998]. CACM predictions (dashed) compared to those of *Harley et al*. [1993] (solid) are shown for Pasadena and Riverside in Figures 5 and 6, respectively (using the same color scheme as Figures 3 and 4). In each case, O_3 CACM predictions usually exceed those from *Harley et al*. [1993]. Correspondingly, NO predictions are generally lower. Since the emissions, meteorology, and model structure are identical to those of *Harley et al*. [1993], the differences seen in Figures 5 and 6 can be ascribed solely to changes in the chemical mechanism.

1.4.3 Total Semi-volatile Species

A principal goal of the gas-phase mechanism CACM is to predict concentrations of those surrogate organic products that have the potential to partition to the aerosol phase. Based on available or estimated vapor pressures or solubility, a product is considered to have the potential to partition to the aerosol phase if it meets one or more of the following criteria: (1) it is known to be partially soluble; (2) it is an aromatic acid; (3) it is an aromatic with two functional groups that are not aldehydes; (4) it has 12 or more carbon atoms (excluding primary gas-phase emission of ALKH and PAH); (5) it has at least 10 carbons and two functional groups; (6) it has at least 6 carbon atoms and two functional groups, one of which is an acid; or (7) it is trifunctional. The products considered capable of forming SOA based on these criteria are marked with a plus sign (+) in Table 1.1. The total gas-phase concentration of those products represents the mechanism's prediction of the 'atmospheric reservoir' of potential SOA components and is compared (solid) in Figure 1.7 to observed concentrations of SOA (x) for August 28, 1987 in Claremont [*Turpin and Huntzicker*, 1995]. Figure 1.7 shows that the predicted temporal behavior of the total mass of compounds available to partition to SOA tracks well the pattern observed for ambient SOA. Figure 1.7 also shows that the mechanism predicts sufficient mass to account for the observed SOA concentrations.

Reliable techniques for estimating/measuring ambient concentrations of SOA lag behind those for inorganic aerosol. The data of *Turpin and Huntzicker* [1995] presented here were generated by a technique that delineates primary organic carbon (OC) and elemental carbon (EC) aerosol concentrations under conditions when production of SOA should be low. The assumption made with this technique is that EC and primary OC have the same sources, so that a representative ratio of primary OC to EC for a given region exists. In order to determine this ratio, ambient measurements of the OC/EC ratio are made on days when photochemical activity is expected to be low or an average ratio is obtained by determining the ratio at individual emissions sites. Subsequent ambient measurements are then made during times when

photochemical activity is expected to occur, and it is assumed that if the ambient value of OC/EC is greater than the characteristic primary OC/EC value, the excess OC consists of SOA [*Turpin and Huntzicker*, 1995]. The main advantage of this approach is its simplicity; however, there are associated uncertainties. First, the primary OC/EC ratio varies from source to source and may be dependent on factors such as meteorology, time of day, and season. Also, obtaining an average primary OC/EC ratio is difficult because of problems associated with sampling of semi-volatile organics, and it has been shown that different sample collection and analysis techniques result in different values for this ratio at the same location and time [*McMurry*, 1989; *Turpin and Huntzicker*, 1995]. Finally, even on days when there is little potential for photochemical activity, previously formed SOA may be present from prior days.

1.4.4 Uncertainty Analysis

Historically, among all the uncertainties associated with three-dimensional urban/regional atmospheric simulations, the largest are those associated with the emissions inventory. From a chemical mechanism perspective, uncertainty lies in the rate constants, the product yields, and the mechanisms of degradation of second-, third-, and further generation products. These issues have been discussed in detail previously [*Harley et al*., 1993; *Jacobson et al*., 1996; *Stockwell et al*., 1997]. While there are a number of areas of uncertainty in the chemical mechanism that one might select for analysis, space does not permit a lengthy analysis of such uncertainties, especially with regard to ozone formation. However, it is informative in the present case to investigate aspects of the chemical mechanism to which prediction of semi-volatile products might be especially sensitive.

Because aromatics are known to be an important source of anthropogenic SOA [*Odum et al*., 1996] and because uncertainties in aromatic chemistry have been well documented [*Atkinson*, 1994], an issue that merits evaluation here is the sensitivity of SOA predicted from aromatic precursors to key aspects of aromatic photooxidation. One particular rate constant that has the potential to be especially influential is that which describes the isomerization of radicals formed in aromatic-OH chemistry (reactions 221, 228, 235, 242, 249, and 256) [*Lay et al*., 1996]. This rate constant affects SOA formation because slower isomerization will lead to less MGLY and RP10 formation and more formation of semi-volatile products. Because earlier models generally underpredicted organic aerosol [*Meng et al*., 1997, 1998], we consider here only the effect of halving the isomerization rate constant in an uncertainty analysis. Changes between the two cases are very small for NO, NO_2, and O_3; there is a slight decrease in O_3, a slight increase in NO, and mixed results for NO_2. Figure 1.7 also compares the total amount of organic material available to partition to SOA in Claremont on August 28, 1987 in the base case (solid) and that in which the bridging rate constant is halved (b/2 case, +). It is seen that decreasing the bridging rate constant results in a significant increase in the amount of organic mass with the potential to form SOA, especially in the early morning and early afternoon.

A second source of uncertainty in the chemical mechanism is the direct conversion of aldehydes to acid groups in certain reactive products. Although the exact mechanism of this conversion remains elusive, such a step attempts to account for observed ambient concentrations of semi-volatile organic acids [*Rogge et al*., 1993; *Nolte et al*., 1999]. Since assuming 100% conversion certainly overestimates acid formation, this yield is also halved (reactions 81, 82, 308, 319, 320, 321, 331, 336, 337, 338, 347, 348, and 349). Figure 1.7 also shows the results for this scenario (acid case, dashed) for August 28, 1987 in Claremont. While there are essentially no changes in the simulations for O_3 and NO_x in this case, predictions of total SOA material are

seen to decrease as expected. However, the magnitude of these changes is not as large as that of the b/2 case (+). Figure 1.8 shows the percentage of the total SOA precursor concentration that must partition to account for the observations of *Turpin and Huntzicker* [1995] in the base case (solid), the b/2 case (+), and the acid case (dashed). It is seen that in each case, sufficient concentrations of SOA precursor material are predicted to account for the observations of *Turpin and Huntzicker* [1995].

1.5 Conclusions

Previous gas-phase mechanisms describing urban/regional atmospheric chemistry have focused primarily on describing the formation of ozone. This paper describes a new chemical mechanism, the Caltech Atmospheric Chemistry Mechanism (CACM), that describes explicitly organic chemistry in an effort to predict the concentrations of secondary and tertiary organic oxidation products that can act as constituents of secondary organic aerosol. Parent organics in CACM must be aggregated into lumped surrogate structures. In total, CACM includes 191 species: 120 fully integrated species (15 inorganic, 71 reactive organic, and 34 unreactive organic), 67 pseudo-steady state species (2 inorganic and 65 organic), and 4 species that have fixed concentrations. These species participate in over 360 reactions.

The primary justification for lumping of gas-phase organic compounds into surrogates is the reduction in the number of independent variables and hence computational demands. Detailed analytical and numerical evaluations of lumping are outside the scope of the current research contract. These include use of homogeneous gas-phase reaction systems and comparison to the predictions from the complete chemistry (all species) with those from the corresponding lumped system. This provides estimates of accuracy and clarifies the variables and parameters to which the systems are most sensitive (kinetic parameters, species, choice of surrogates, etc). Such approaches have been presented in the past by Carter and Stockwell in support of the development of lumped mechanisms and are not repeated here.

CACM has been used in the three-dimensional CIT model to predict gas-phase concentrations in the South Coast Air Basin of California for August 27-29, 1987. As part of the Southern California Air Quality Study, ambient measurements were taken during these dates, providing data to which the model results can be compared. As shown in this paper, the predicted mixing ratios of O_3, NO, and NO_2 are statistically comparable to those predicted by the extended mechanism of *Lurmann et al*. [1987], which has been used in the CIT model previously [*Harley et al*., 1993]. Concentrations of secondary and tertiary organic oxidation products capable of forming secondary organic aerosol will be passed to a model designed to predict equilibrium gas-aerosol partitioning of organic oxidation products (Part II). The development of CACM is a first step in allowing for more rigorous treatment of secondary organic aerosol formation in atmospheric models than has been possible previously.

References

Alvarado, A., E.C. Tuazon, S.M. Aschmann, R. Atkinson, and J. Arey, Products of the gas-phase reactions of $O(^3P)$ atoms and O_3 with α-pinene and 1,2-dimethyl-1-cyclohexene, *J. Geophys. Res.*, *103*, 25,541-25,552, 1998.

Atkinson, R., Gas-phase tropospheric chemistry of volatile organic compounds: 1. Alkanes and alkenes, *J. Phys. Chem. Ref. Data*, *26*, 215-290, 1997.

Atkinson, R., Gas-phase tropospheric chemistry of organic compounds, *J. Phys. Chem Ref. Data, Monograph 2*, 1994.

Atkinson, R., Gas-phase tropospheric chemistry of organic compounds: a review, *Atmos. Environ*., *24A*, 1-41, 1990.

Barthelmie, R.J., and S.C Pryor, A model mechanism to describe oxidation of monoterpenes leading to secondary organic aerosol, *J. Geophys. Res.*, *104*, 23,657-23,669, 1999.

Carter, W.P.L., SAPRC-99, available via ftp (http://helium.ucr.edu/~carter/), 1999.

Carter, W.P.L., SAPRC-97, available via ftp (http://helium.ucr.edu/~carter/), 1997.

Carter, W.P.L., and R. Atkinson, Development and evaluation of a detailed mechanism for the atmospheric reactions of isoprene and NO_x, *Intl. J. Chem. Kinetics*, *28*, 497-530, 1996.

Carter, W.P.L., and R. Atkinson, Alkyl nitrate formation from the atmospheric photooxidation of alkanes: a revised estimation method, *J. Atmos. Chem*., *8*, 165-173, 1989.

Countess, R.J., G.T. Wolff, and S.H. Cadle, The Denver winter aerosol: A comprehensive chemical characterization, *J. Air Pollut. Control Assoc.*, *30*, 1194-1200, 1980.

Dransfield, T.J., K.K. Perkins, N. M. Donahue, J.G. Anderson, M.M. Sprengnether, and K.L. Demerjian, Temperature and pressure dependent kinetics of the gas-phase reaction of the hydroxyl radical with nitrogen dioxide, *Geophys. Res. Letters*, *26*, 687-690, 1999.

Fraser, M.P., G.R. Cass, and B.R.T. Simoneit, Particulate organic compounds emitted from motor vehicle exhaust and in the urban atmosphere, *Atmos. Environ*., *33*, 2715-2724, 1999.

Fraser, M.P., G.R. Cass, B.R.T. Simoneit, and R.A. Rasmussen, Air quality model evaluation data for organics 4. C_2-C_{36} aromatic hydrocarbons, *Environ. Sci. Technol*., *31*, 2356-2367, 1997.

Gery, M.W., G.Z. Whitten, J.P. Killus, and M.C. Dodge, A photochemical mechanism for urban and regional scale computer modeling, *J. Geophys. Res.*, *94*, 12,925-12,956, 1989.

Goldan, P.D., W.C. Kuster, F.C. Fehsenfeld, and S.A. Montzka, The observation of a C_5 alcohol emission in a North American pine forest, *Geophys. Res. Lett*., *20*, 1039-1042, 1993.

Goumri, A., L. Elmaimouni, J.-P. Sawyersyn, and P. Devolder, Reaction rates at (297 +/- 3)K of four benzyl-type radicals with O_2, NO, and NO_2 by discharge flow/laser induced fluorescence, *J. Phys. Chem.*, *96*, 5395-5400, 1992.

Griffin, R.J., D.R. Cocker III, R.C. Flagan, and J.H. Seinfeld, Organic aerosol formation from the oxidation of biogenic hydrocarbons, *J. Geophys. Res.*, *104*, 3555-3567, 1999.

Grosjean, E., D. Grosjean, M.P. Fraser, and G.R. Cass, Air quality model evaluation data for organics 2. C_1-C_{14} carbonyls in Los Angeles, *Environ. Sci. Technol*., *30*, 2687-2703, 1996.

Guenther, A., et al., A global model of natural volatile organic compound emissions, *J. Geophys. Res.*, *100*, 8873-8892, 1995.

Harley, R.A., and G.R. Cass, Modeling the atmospheric concentrations of individual volatile organic compounds, *Atmos. Environ*., *29*, 905-922, 1995.

Harley, R.A., A.G. Russell, G.J. McRae, G.R. Cass, and J.H. Seinfeld, Photochemical modeling of the Southern California Air Quality Study, *Environ. Sci. Technol*., *27*, 378-388, 1993.

Harley, R.A., M.P. Hannigan, and G.R. Cass, Respeciation of organic gas emissions and the detection of excess unburned gasoline in the atmosphere, *Environ. Sci. Technol*., *26*, 2395-2408, 1992.

Hoffmann, T., J.R. Odum, F. Bowman, D. Collins, D. Klockow, R.C. Flagan, and J.H. Seinfeld, Formation of organic aerosols from the oxidation of biogenic hydrocarbons, *J. Atmos. Chem.*, *26*, 189-222, 1997.

Jacob, D.J., and S.C. Wofsy, Photochemistry of biogenic emissions over the Amazon forest, *J. Geophys. Res.*, *93*, 1477-1486, 1988.

Jacobson, M.Z., R. Lu, R.P. Turco, and O.B. Toon, Development and application of a new air pollution modeling system 1. Gas-phase simulations, *Atmos. Environ*., *30*, 1939-1963, 1996.

Japar, S.M., T.J. Wallington, J.F.O. Richert, and J.C. Ball, The atmospheric chemistry of oxygenated fuel additives: *tert*-butyl alcohol, dimethyl ether, and methyl-*tert*-butyl ether, *Intl. J. Chem. Kinetics*, *22*, 1257-1269, 1990.

Jenkin, M.E., S.M. Saunders, and M.J. Pilling, The tropospheric degradation of volatile organic compounds: a protocol for mechanism development, *Atmos. Environ*., *31*, 81-104, 1997.

Klotz, B., I. Barnes, K.H. Becker, and B.T. Golding, Atmospheric chemistry of benzene oxide/oxepin, *J. Chem. Soc., Faraday Trans., 93*, 1507-1516, 1997.

Kwok, E.S.C., S.M. Aschmann, J. Arey, and R. Atkinson, Product formation from the reaction of the NO_3 radical with isoprene and rate constants for the reactions of methacrolein and methyl vinyl ketone with the NO_3 radical, *Intl. J. Chem. Kinetics*, *28*, 925-934, 1995.

Kwok, E.S.C., and R. Atkinson, Estimation of hydroxyl radical reaction rate constants for gas-phase organic compounds using a structure-reactivity relationship: an update, *Atmos. Environ*., *29*, 1685-1695, 1995.

Lamb, B., D. Gay, H. Westberg, and T. Pierce, A biogenic hydrocarbon emission inventory for the U.S.A. using a simple forest canopy model, *Atmos. Environ*., *27*, 1673-1690, 1993.

Lawson, D.R., The Southern California Air Quality Study, *J. Air Waste Mgmt. Assoc.*, *40*, 156-165, 1990.

Lay, T.H., J.W. Bozzelli, and J.H. Seinfeld, Atmospheric photochemical oxidation of benzene: benzene + OH and the benzene-OH adduct (hydroxyl-2,4-cyclohexadienyl) + O_2, *J. Phys. Chem*., *100*, 6543-6554, 1996.

Lurmann, F.W., W.P.L. Carter, and L.A. Coyner, A surrogate species chemical reaction mechanism for urban-scale air quality simulation models. Volumes I and II. Report to the U.S. Environmental Protection Agency under Contract 68-02-4104. ERT, Inc., Newbury Park, CA, and Statewide Air Pollution Research Center, University of California, Riverside, CA, 1987.

McMurry, P.H., Final report to the California Air Resources Board under contract A732-075, 1989.

McRae, G.J., *Mathematical modeling of photochemical air pollution*, Ph.D. Thesis, California Institute of Technology, 1981.

Meng Z., D. Dabdub, and J.H. Seinfeld, Size-resolved and chemically resolved model of atmospheric aerosol dynamics, *J. Geophys. Res*., 103, 3419-3435, 1998.

Meng, Z., D. Dabdub, and J.H. Seinfeld, Chemical coupling between atmospheric ozone and particulate matter, *Science*, *277*, 116-119, 1997.

Moortgat, G.K., B. Veyret, and R. Lesclaux, Kinetics of the reaction of HO_2 with $CH_3C(O)O_2$ in the temperature range 253-368K, *Chem. Phys. Lett*., *160*, 443-447, 1989.

Niki, H., P.D. Maker, C.M. Savage, and L.P. Breitenbach, FTIR study of the kinetics and mechanism of Cl-atom-initiated reactions of acetaldehyde, *J. Phys. Chem.*, *89*, 588-591, 1985.

Nolte, C.G., M.P. Fraser, and G.R. Cass, Gas-phase C_2-C_{10} organic acid concentrations in the Los Angeles atmosphere, *Environ. Sci. Technol*., *33*, 540-545, 1999.

Odum, J.R., T.P.W. Jungkamp, R.J. Griffin, R.C. Flagan, and J.H. Seinfeld, The atmospheric aerosol-forming potential of whole gasoline vapor, *Science*, *276*, 96-99, 1997.

Odum, J.R., T. Hoffmann, F. Bowman, D. Collins, R.C. Flagan, and J.H. Seinfeld, Gas/particle partitioning and secondary organic aerosol yields, *Environ. Sci. Technol*., *30*, 2580-2585, 1996.

Pandis S.N., S.E. Paulson, J.H. Seinfeld, and R.C. Flagan, Aerosol formation in the photooxidation of isoprene and β-pinene, *Atmos. Environ*., *25*, 997-1008, 1991.

Pankow, J.F., J.H. Seinfeld, W.E. Asher, and G.B. Erdakos, Modeling the formation of secondary organic aerosol: 1. The application of theoretical principles to measurements obtained in the α-pinene-, β-pinene-, sabinene-, Δ^3-carene-, and cyclohexene-ozone systems, *Environ. Sci. Technol*., *35*, 1164-1172, 2001.

Paulson, S.E., R.C. Flagan, and J.H. Seinfeld, Atmospheric photooxidation of isoprene: 1. The hydroxyl radical and ground-state atomic oxygen reactions, *Intl. J. Chem. Kinetics*, *24*, 79-101, 1992a.

Paulson, S.E., R.C. Flagan, and J.H. Seinfeld, Atmospheric photooxidation of isoprene: 2. The ozone-isoprene reaction, *Intl. J. Chem. Kinetics*, *24*, 103-125, 1992b.

Rogge, W.F., M.A. Mazurek, L.M. Hildemann, G.R. Cass, and B.R.T. Simoneit, Quantification of urban organic aerosols at a molecular-level-identification, abundance and seasonal-variation, *Atmos. Environ*., *27A*, 1309-1330, 1993.

Schauer, J.J., M.J. Kleeman, G.R. Cass, and B.R.T. Simoneit, Measurement of emissions from air pollution sources 1. C_1 through C_{29} organic compounds from meat charbroiling, *Environ. Sci. Technol*., *33*, 1566-1577, 1999a.

Schauer, J.J., M.J. Kleeman, G.R. Cass, and B.R.T. Simoneit, Measurement of emissions from air pollution sources 2. C_1 through C_{30} organic compounds from medium duty diesel trucks, *Environ. Sci. Technol*., *33*, 1578-1587, 1999b.

Schauer, J.J. *Source Contributions to Atmospheric Organic Compound Concentrations: Emissions, Measurements, and Model Predictions*, Ph.D. Thesis, California Institute of Technology, Pasadena, CA, 1998.

Seinfeld, J.H., and S.N. Pandis, *Atmospheric Chemistry and Physics*, Wiley-Interscience, New York, 1998.

Sharkey, T.D., Emission of low-molecular mass hydrocarbons from plants, *Trends Plant Sci*., *1*, 78-82, 1996.

Stockwell, W.R., F. Kirchner, M. Kuhn, and S. Seefeld, A new mechanism for regional atmospheric chemistry modeling, *J. Geophys. Res*., *102*, 25,847-25,879, 1997.

Stockwell, W.R., P. Middleton, J.S. Chang, and X. Tang, The second generation Regional Acid Deposition Model chemical mechanism for regional air quality modeling, *J. Geophys. Res.*, *95*, 16,343-16,367, 1990.

Turpin, B.J., and J.J. Huntzicker, Identification of secondary organic aerosol episodes and quantitation of primary and secondary organic aerosol concentrations during SCAQS, *Atmos. Environ*., *29*, 3527-3544, 1995.

United States Environmental Protection Agency, Web site for Models 3 (http://www.epa.gov/asmdnerl/models3/index.html), 1999

Yu, J., D.R. Cocker III, R.J. Griffin, R.C. Flagan, and J.H. Seinfeld, Gas-phase ozone oxidation of monoterpenes: gaseous and particulate products, *J. Atmos. Chem.*, *34*, 207-258, 1999.

Yu, J., H.E. Jeffries, and R.M. LeLacheur, Identifying airborne carbonyl-compounds in isoprene atmospheric photooxidation products by their PFBHA oximes using gas-chromatography ion-trap mass spectrometry, *Environ. Sci. Technol*., *29*, 1923-1932, 1995.

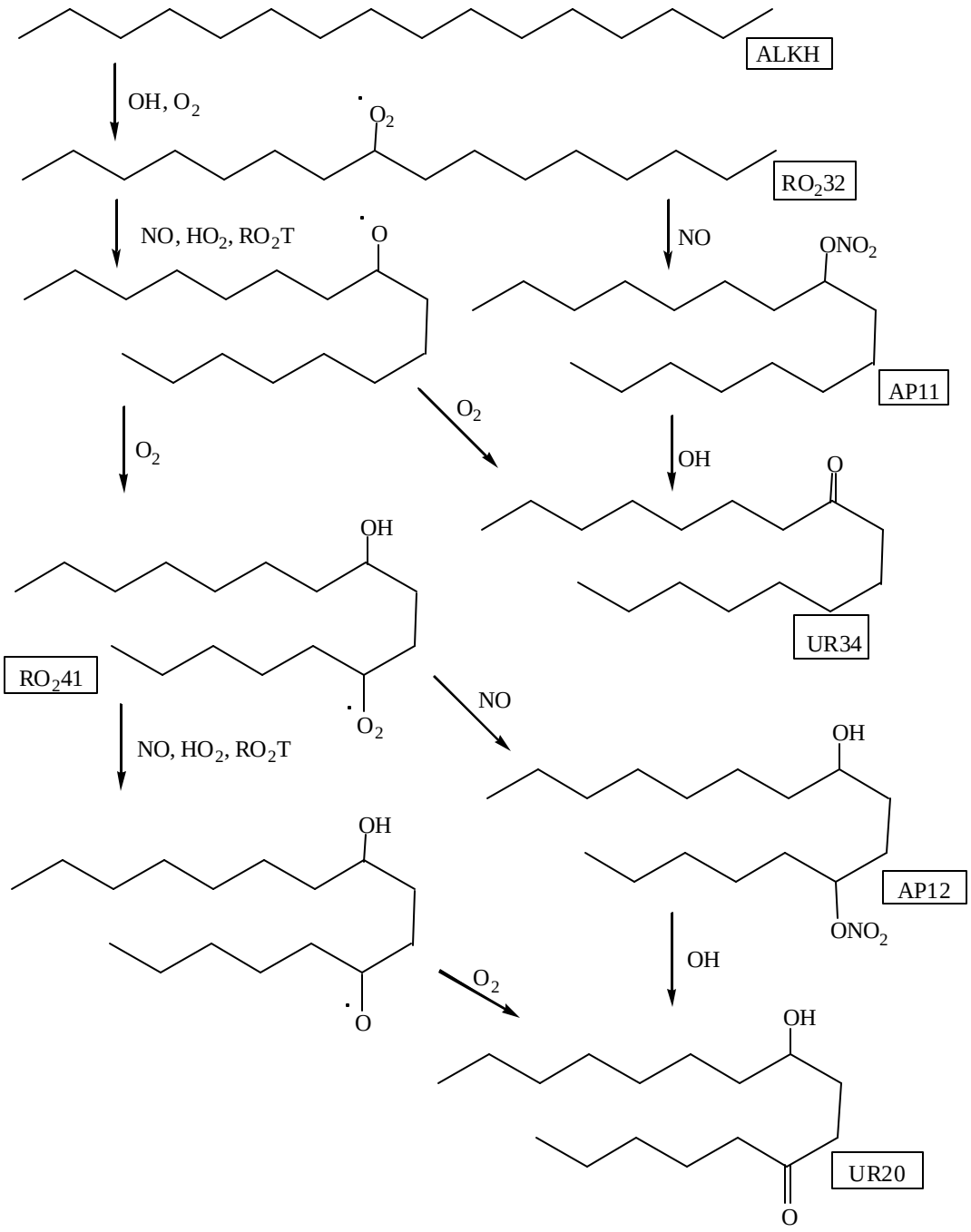

Figure 1.1a. An illustrative example of a degradation mechanism for a parent hydrocarbon: ALKH (see Table 1.1 and text for notation).

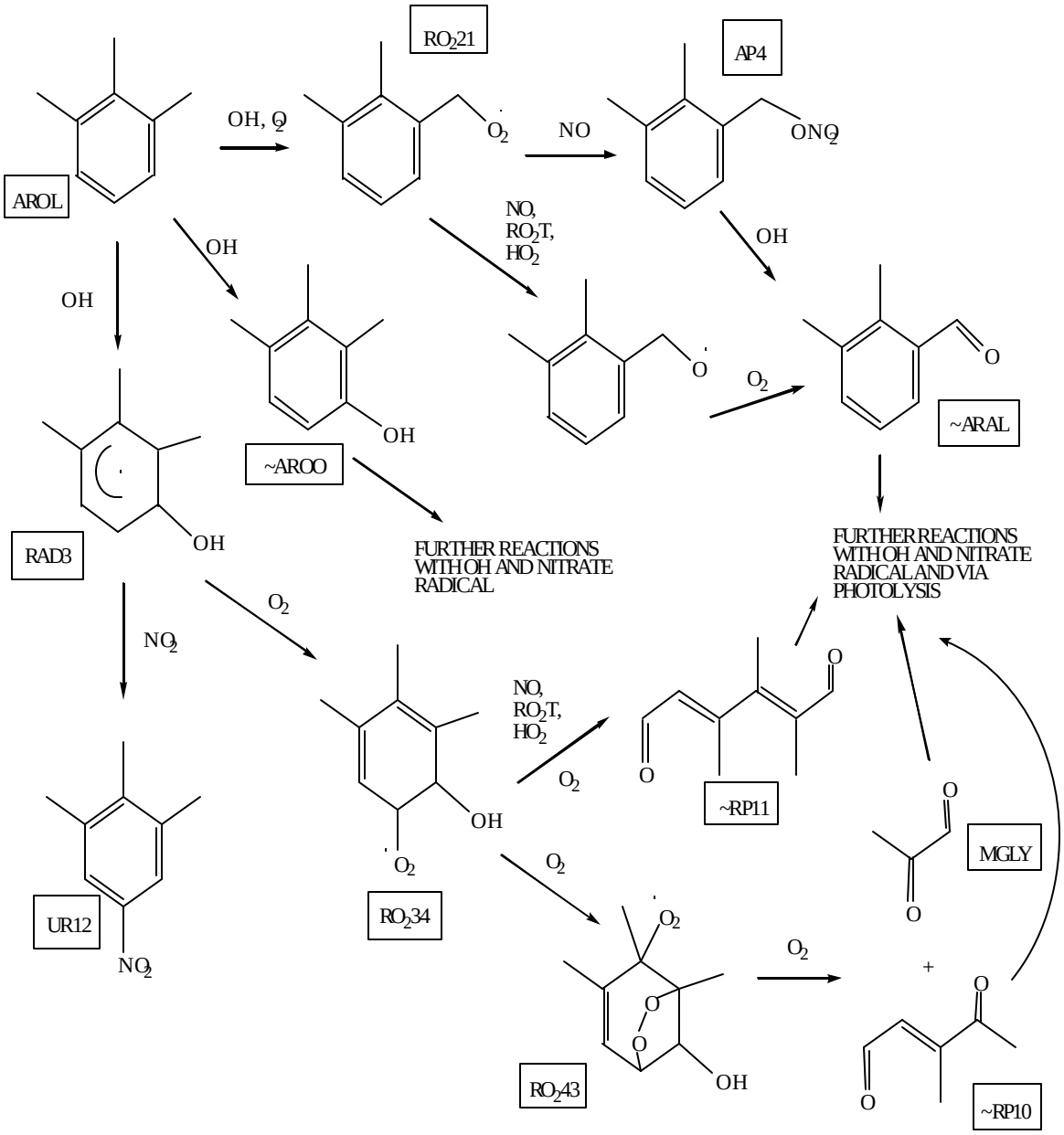

Figure 1.1b. An illustrative example of a degradation mechanism for a parent hydrocarbon: AROL (see Table 1.1 and text for notation).

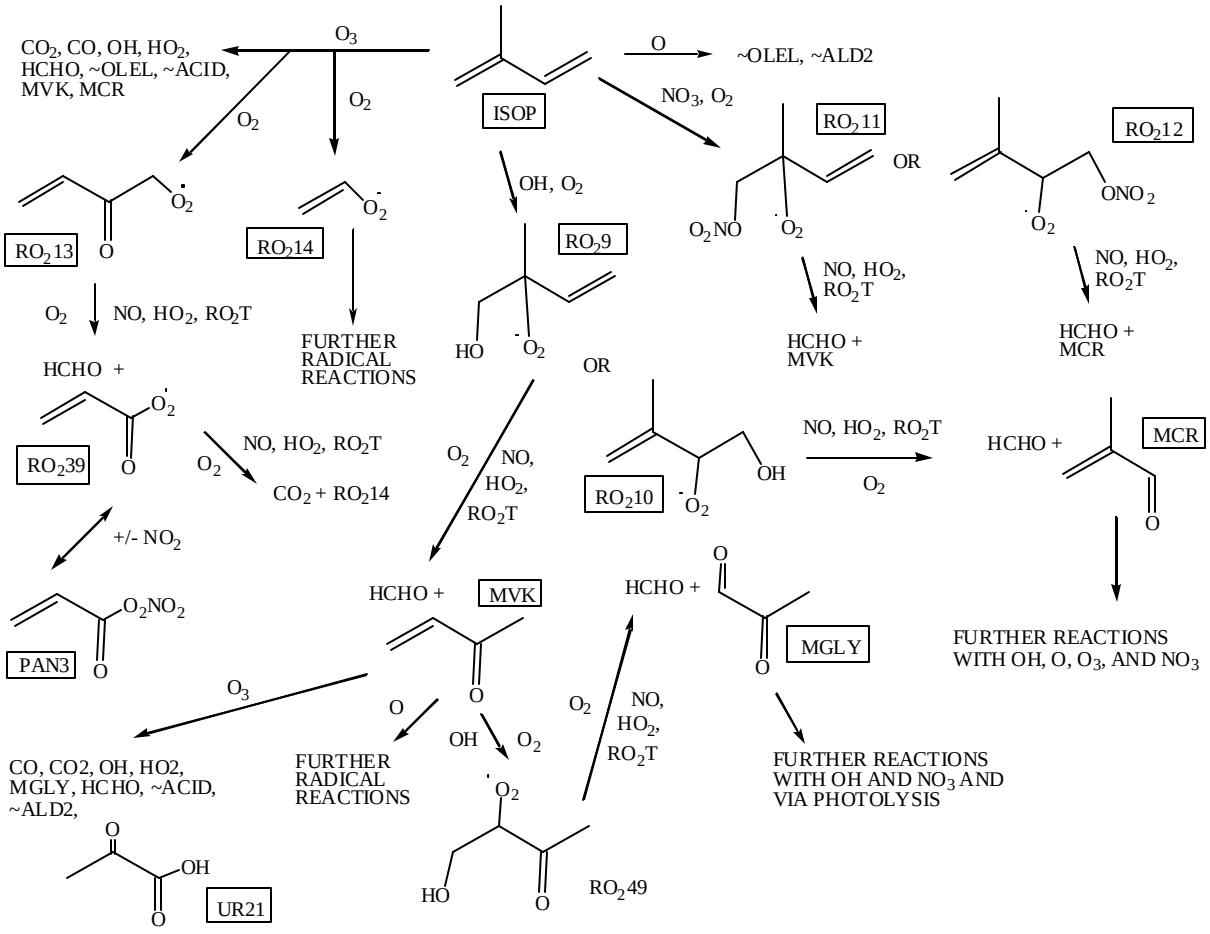

Figure 1.1c. An illustrative example of a degradation mechanism for a parent hydrocarbon: ISOP (see Table 1.1 and text for notation).

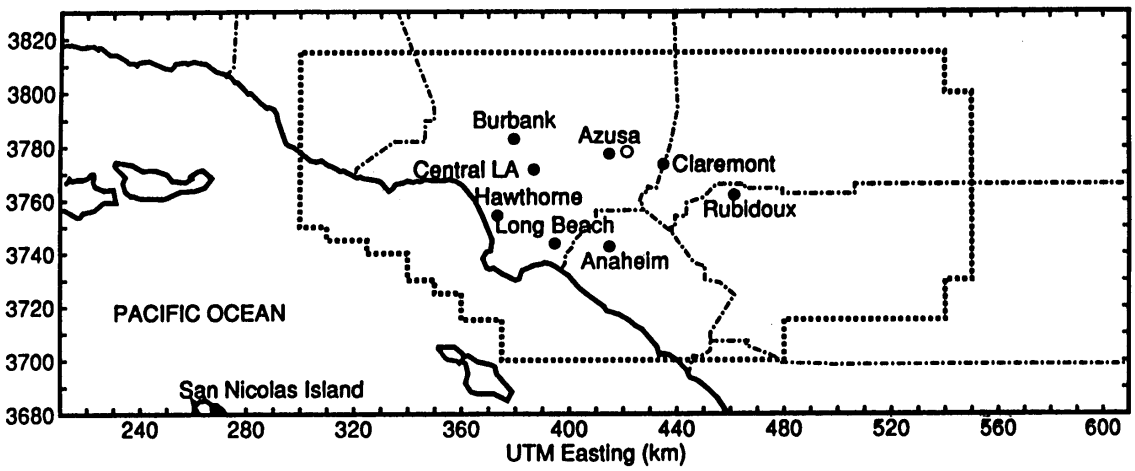

Figure 1.2. A map of the SOCAB. Major suburbs and downtown Los Angeles are indicated for reference.

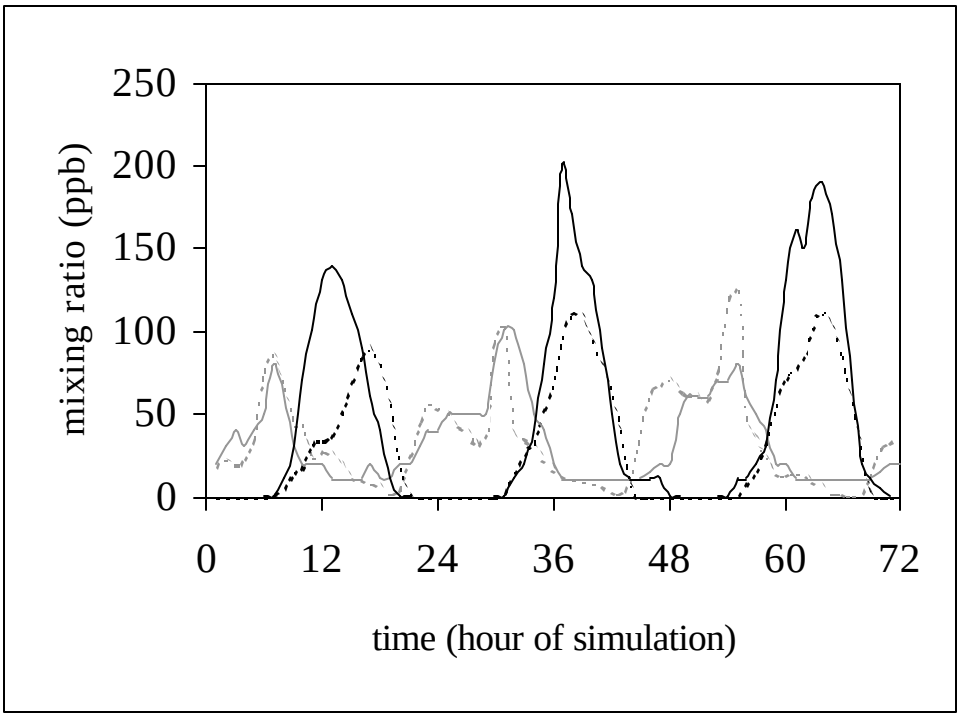

Figure 1.3. Simulated (dashed) versus observed (solid) NO (gray) and O_3 (black) mixing ratios for Pasadena for August 27-29, 1987.

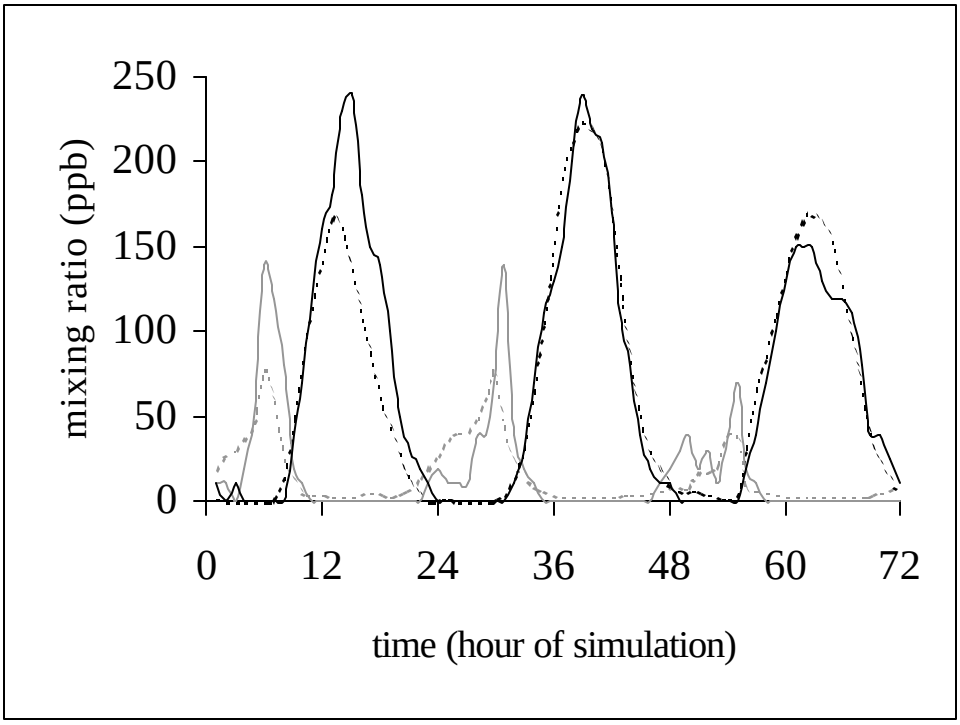

Figure 1.4. Simulated (dashed) versus observed (solid) NO (gray) and O_3 (black) mixing ratios for Riverside for August 27-29, 1987.

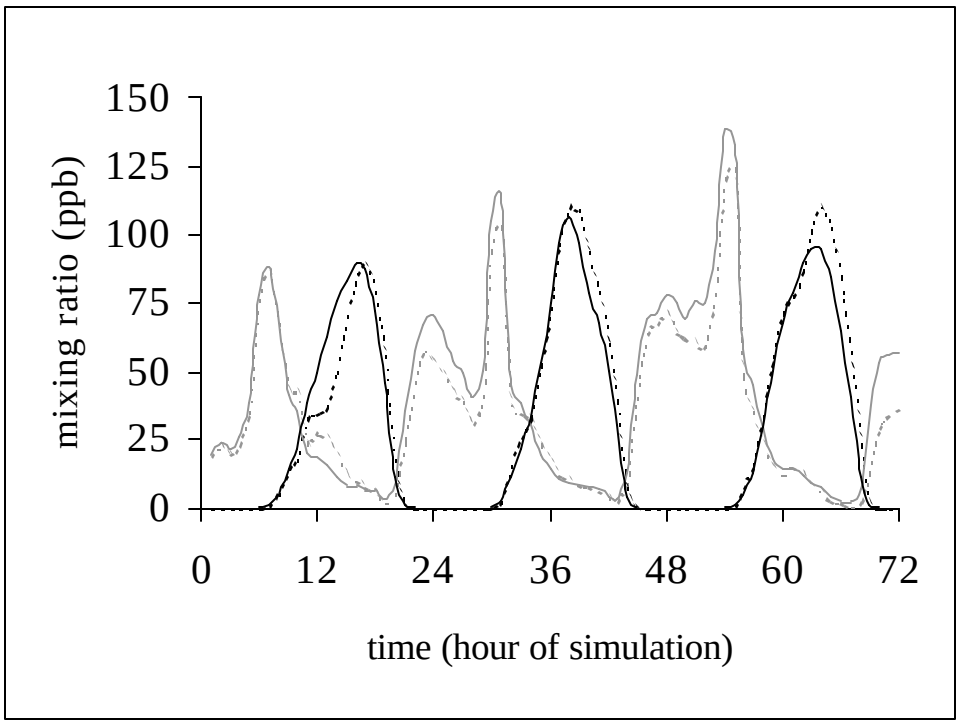

Figure 1.5. Mixing ratios simulated by CACM (dashed) versus those simulated by the extended LCC mechanism (solid) [*Harley et al*., 1993] for Pasadena for August 27-29, 1987. NO is shown in gray; O_3 is shown in black.

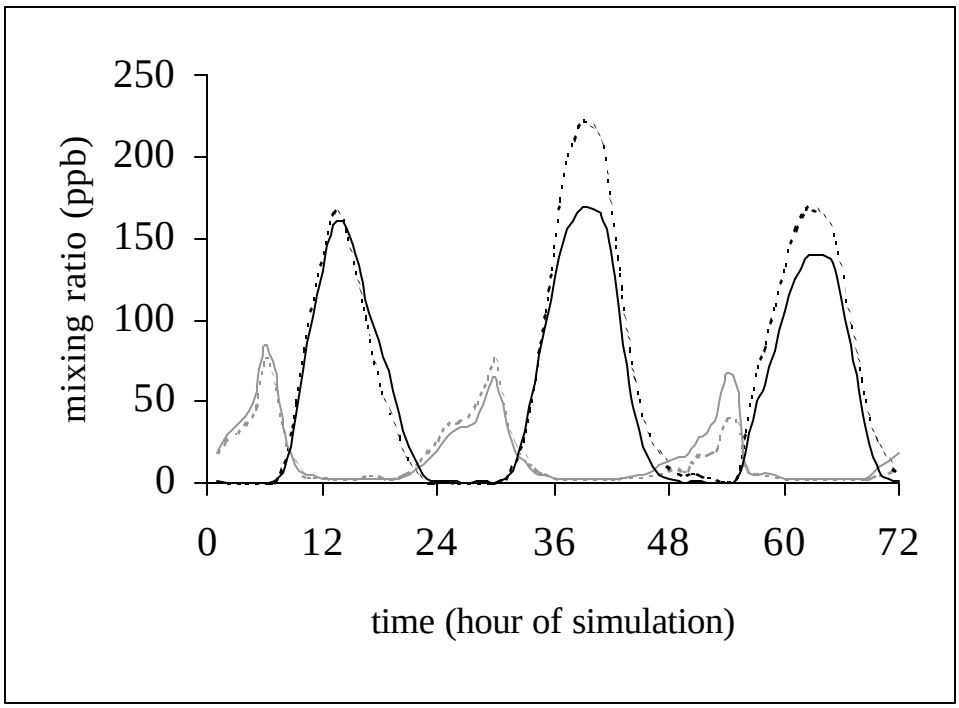

Figure 1.6. Mixing ratios simulated by CACM (dashed) versus those simulated by the extended LCC mechanism (solid) [*Harley et al*., 1993] for Riverside for August 27-29, 1987. NO is shown in gray; O_3 is shown in black.

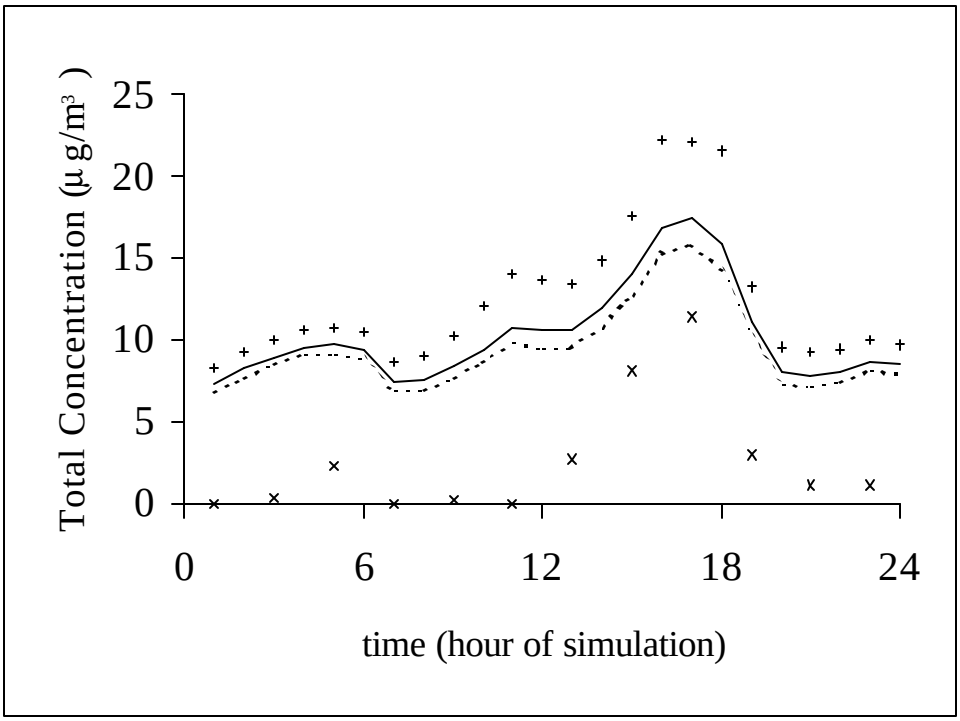

Figure 1.7. Comparison of total predicted SOA precursor concentration in the base case (solid) versus observed SOA data (x) in Claremont on August 28, 1987. The data of *Turpin and Huntzicker* [1995] were converted from µgC/m^3 to µg/m^3 by multiplying by a factor of 1.2 [*Countess et al*., 1980]. Also shown is the sensitivity of the total predicted SOA precursor concentrations to the aromatic radical isomerization rate constant and to the yield of direct conversion of certain aldehydes to acids. b/2 (+) represents the case in which the base case aromatic radical isomerization rate constant is divided by 2; acid (dashed) represents the case in which the yield of direct conversion of certain aldehydes to acids is divided by 2.

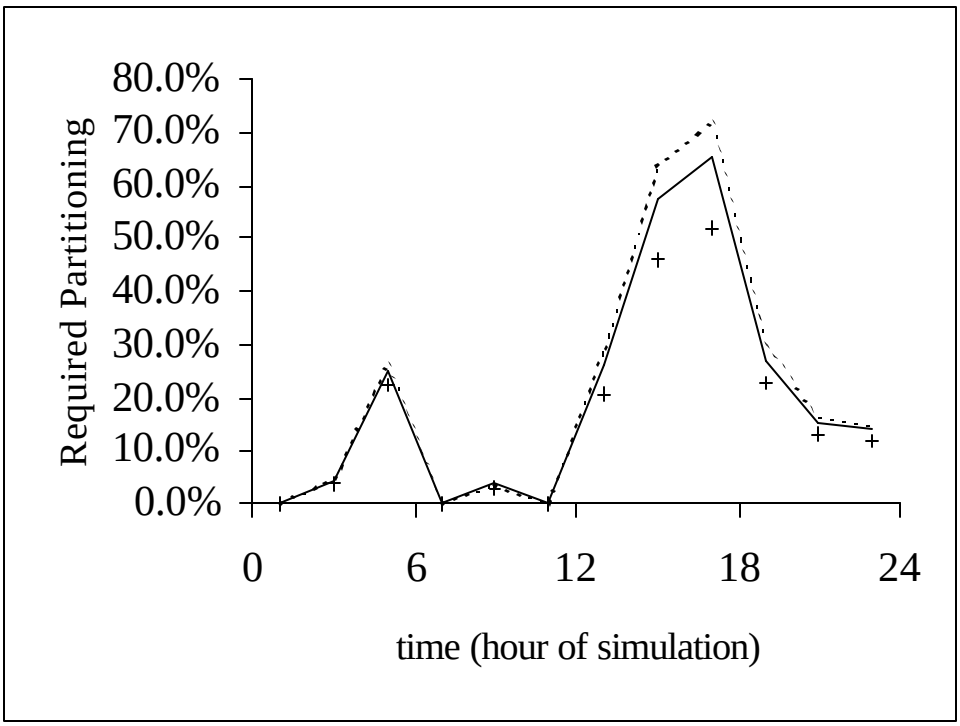

Figure 1.8. Percentage of the total SOA precursor concentration that must partition to account for the observations of *Turpin and Huntzicker* [1995] for the three cases investigated. Solid represents the base case, + represents the b/2 case, and dashed represents the acid case.

Table 1.1 Chemical Species Represented in CACM

Inorganic, Fully Integrated Species

NO	Nitric oxide
NO_2	Nitrogen dio xide
O_3	Ozone
HONO	Nitrous acid
HNO_3	Nitric acid
HNO_4	Pernitric acid
N_2O_5	Nitrogen pentoxide
NO_3	Nitrate radical
HO_2	Hydroperoxy radical
CO	Carbon monoxide
CO_2	Carbon dioxide
H_2O_2	Hydrogen peroxide
SO_2	Sulfur dioxide
SO_3	Sulfur trioxide
OH	Hydroxyl radical

Reactive, Fully Integrated Parent Organic Species (* denotes those that are also formed in CACM)

ETHE	Ethene
OLEL	Lumped alkenes C_3-C_6* (1-pentene)
OLEH	Lumped alkenes >C_6 (4-methyl-1-octene)
ALKL	Lumped alkanes C_2-C_6* (2-methyl-butane)
ALKM	Lumped alkanes C_7-C_{12}* (3,5-dimethyl-heptane)
ALKH	Lumped alkanes >C_{12} (*n*-hexadecane)
AROH	Lumped high SOA yield aromatic species (3-*n*-propyl-toluene)
AROL	Lumped low SOA yield aromatic species (1,2,3-trimethyl-benzene)
AROO	Lumped phenolic species* (2,6-dimethyl-phenol)
ARAL	Lumped aromatic monoaldehydes* (*p*-tolualdehyde)
$ARAC^+$	Lumped aromatic monoacids* (*p*-toluic acid)
PAH	Lumped gas-phase polycyclic aromatic hydrocarbons (1,2-dimethyl-naphthalene)
HCHO	Formaldehyde*
ALD2	Lumped higher aldehydes* (*n*-pentanal)
KETL	Lumped ketones C_3-C_6* (2-pentanone)
KETH	Lumped ketones >C_6 (2-heptanone)
MEOH	Methanol
ETOH	Ethanol
ALCH	Lumped higher alcohols (2-hexanol)
ISOP	Isoprene
BIOL	Lumped low SOA yield monoterpene species (α-terpineol)
BIOH	Lumped high SOA yield monoterpene species (γ-terpinene)
MTBE	Methyl-*tert*-butyl ether

Table 1.1 (cont.) Chemical Species Represented in CACM

Non-reacting, Fully Integrated Organic Species

ADAC$^+$	Lumped aromatic diacids (terephthalic acid)
ACID	Lumped organic acids $<C_6$
UR1	3-Methyl-heptanoic acid
UR2$^+$	3-Hydroxy-4-methyl-benzoic acid
UR3$^+$	2-Hydroxy-3-isopropyl-6-keto-heptanoic acid
UR4	2-Isopropyl-5-keto-hexanal
UR5$^+$	1-Methyl-3-hydroxy-4-isopropyl-1, 2-cyclohexane epoxide
UR6$^+$	2-Hydroxy-3-isopropyl-6-methyl-cyclohexanone
UR7$^+$	3, 7-Dimethyl-6-keto-3-octenal
UR8$^+$	3-Isopropyl-6-keto-3-heptenoic acid
UR9	1-Methyl-4-isopropyl-1, 2-cyclo-4-hexene epoxide
UR10	3-Isopropyl-6-methyl-3-cyclohexenone
UR11$^+$	1, 2-Dimethyl-3-hydroxy-naphthalene
UR12	1, 2, 3-Trimethyl-5-nitro-benzene
UR13	3-*n*-Propyl-4-nitro-toluene
UR14$^+$	2-Nitro-4-methyl-benzoic acid
UR15$^+$	1, 2-Dimethyl-3-nitro-naphthalene
UR16	2-Methyl-2-hydroxy-5-heptanone
UR17$^+$	2-Hydroxy-3-isopropyl-hexadial
UR18	3-Isopropyl-2-pentendial
UR19$^+$	1-Methyl-2-formyl-naphthalene
UR20$^+$	11-Hydroxy-8-hexadecanone
UR21$^+$	Keto-propanoic acid
UR22$^+$	2,6-Dimethyl-3,4-dinitro-phenol
UR23$^+$	3-Isopropyl-4-hydroxy-2-butenoic acid
UR24	Maleic anhydride
UR25	3H-Furan-2-one
UR26$^+$	4, 5-Dimethyl-6-keto-2, 4-heptadienoic acid
UR27$^+$	2-Carboxy-acetophenone
UR28$^+$	Oxalic acid
UR29$^+$	4-Hydroxy-3, 5-dimethyl-2, 4-hexadiendioic acid
UR30$^+$	2-Methyl-5-carboxy-2, 4-hexadiendioic acid
UR31$^+$	2-(Dimethyl-propenoic acid)-benzoic acid
UR32	3-Methyl-4-heptanone
UR33	2-Isopropyl-5-keto-2-hexenal
UR34$^+$	8-Hexadecanone

Table 1.1 (cont.) Chemical Species Represented in CACM

Reactive, Fully Integrated Secondary Organic Species

PAN1	Peroxy pentionyl nitrate
PAN2	Peroxy acetyl nitrate (PAN)
PAN3	Unsaturated peroxy propionyl nitrate (PPN)
PAN4	Keto-PPN
PAN5	Methylene-PPN
PAN6	Peroxy nitrate derived from glyoxal
PAN7	Peroxy 3-methyl-heptionyl nitrate
PAN8$^+$	Peroxy 2-hydroxy-3-isopropyl-6-keto-heptionyl nitrate
PAN9	Peroxy 3-isopropyl-4-hydroxy-2-butenionyl nitrate
PN10	Peroxy n itrate derived from glyoxalic acid
MGLY	Methyl glyoxal
MVK	Methyl-vinyl-ketone
MCR	Methacrolein
RPR1	3-Methyl-heptanal
RPR2	3-Hydroxy-4-methyl-benzaldehyde
RPR3$^+$	2-Hydroxy-3-isopropyl-6-keto-heptanal
RPR4$^+$	2,6-Dimethyl-4-nitro-phenol
RPR5	2-Nitro-4-methyl-benzaldehyde
RPR6	Benzene-1, 4-dialdehyde
RPR7$^+$	4-Formyl-benzoic acid
RPR8	3-Isopropyl-4-hydroxy-2-butenal
RPR9$^+$	4-Hydroxy-3, 5-dimethyl-2, 4-hexadiendial
RP10	2-Methyl-butenalic acid
RP11	4, 5-Dimethyl-6-keto-2, 4-heptadienal
RP12$^+$	2-Methyl-5-formyl-2, 4-hexadiendial
RP13$^+$	2-Carboxyl-5-methyl-2, 4-hexadiendial
RP14$^+$	2-(Dimethyl-propenal)-benzaldehyde
RP15	2-Formyl-acetophenone
RP16	Glyoxalic acid
RP17$^+$	4-Hydroxy-3, 5-dimethyl-2, 4-hexadienalic acid
RP18$^+$	2-Methyl-5-formyl-2, 4-hexadiendioic acid
RP19$^+$	2-(Dimethyl-propenal)-benzoic acid
AP1$^+$	2-Nitrooxymethyl-6-methyl-phenol
AP2	2-Methyl-2-hydroxy-5-heptylnitrate
AP3	3-Methyl-4-heptylnitrate
AP4	1, 2-Dimethyl-3-nitrooxymethyl-benzene
AP5	4-Nitrooxymethyl-benzaldehyde
AP6$^+$	4-Nitrooxymethyl-benzoic acid
AP7$^+$	1-Methyl-1-nitrato-2, 3-dihydroxy-4-isopropyl-cyclohexane
AP8$^+$	1-Methyl-4-nitrato-4-isopropyl-5-hydroxy-cyclohexene
AP9	5-Isopropyl-6-nitrato-4-hexen-2-one
AP10$^+$	1-Methyl-2-nitrooxymethyl-naphthalene
AP11$^+$	8-Hexadecylnitrate
AP12$^+$	8-Hydroxy-11-hexadecylnitrate
RO_2T	Total organic peroxy radical
RO_28	Acetyl peroxy radical

Table 1.1 (cont.) Chemical Species Represented in CACM

Reactive, Inorganic Pseudo-Steady State Species

OSD	$O(^1D)$
O	$O(^3P)$

Reactive, Organic Pseudo-Steady State Species

RO_21	Methyl peroxy radical from oxidation of CH_4
RO_22	Hydroxy alkyl peroxy radical $<C_6$ from oxidation of ETHE, ETOH, OLEL, and ALCH (C_4, 1-peroxy, 2-hydroxy)
RO_23	Nitrato alkyl peroxy radical $<C_6$ from oxidation of ETHE and OLEL (C_4, 1-nitrato, 2-peroxy)
RO_24	Aldehydic alkyl peroxy radical from oxidation of ISOP and ETHE (C_2)
RO_25	Alkyl peroxy radical $<C_6$ from oxidation of KETL, ISOP, ALKL, BIOH, and OLEL (C_3, 1-peroxy)
RO_26	Acyl radical from aldehydic H abstraction of ALD2
RO_27	Keto alkyl peroxy radical $<C_6$ from oxidation of ISOP and KETL (C_4, 2-keto, 3-peroxy)
$0RO_29$	Branched hydroxy alkenyl peroxy radical from oxidation of ISOP (C_4 chain, 1-hydroxy, 2-methyl, 2-peroxy)
RO_210	Branched hydroxy alkenyl peroxy radical from oxidation of ISOP (C_4 chain, 2-methyl, 3-peroxy, 4-hydroxy)
RO_211	Branched nitrato alkenyl peroxy radical from oxidation of ISOP (C_4 chain, 1-nitrato, 2-methyl, 2-peroxy)
RO_212	Branched nitrato alkenyl peroxy radical from oxidation of ISOP (C_4 chain, 2-methyl, 3-peroxy, 4-nitrato)
RO_213	Keto alkenyl peroxy radical from oxidation of ISOP (C_4, 3-keto, 4-peroxy)
RO_214	Alkenyl peroxy radical from oxidation of ISOP (C_2)
RO_215	Ether alkyl peroxy radical from oxidation of MTBE (C_5, accounts for attack on both sides of the ether bond)
RO_216	Keto alkyl peroxy radical from oxidation of KETH (C_7, 2-keto, 3-peroxy)
RO_217	Aromatic peroxy radical from side chain oxidation of AROO
RO_218	Branched hydroxy alkyl peroxy radical $>C_6$ from oxidation of OLEH and ALKM (C_7 chain, 2-methyl, 2-hydroxy, 5-peroxy)
RO_219	Branched nitrato alkyl peroxy radical from oxidation of OLEH (C_8 chain, 4-methyl, 1-nitrato, 2-peroxy)
RO_220	Branched alkyl peroxy radical $>C_6$ from oxidation of OLEH and ALKM (C_7 chain, 3-methyl, 4-peroxy)
RO_221	Aromatic peroxy radical from side chain oxidation of AROL
RO_222	Aromatic peroxy radical from side chain oxidation of ARAL
RO_223	Aromatic peroxy radical from side chain oxidation of ARAC
RO_224	Cyclic dihydroxy alkyl peroxy radical from OH oxidation of BIOL (C_6 cycle, 1-methyl, 1-peroxy, 2, 3-dihydroxy, 4-isopropyl)
RO_225	Cyclic hydroxy nitrato alkyl peroxy radical from NO_3 oxidation of BIOL (C_6 cycle, 1-methyl, 1-peroxy, 2-nitrato, 3-hydroxy, 4-isopropyl)
RO_226	Branched keto hydroxy aldehydic peroxy radical from oxidation of BIOL (C_7 chain, 2-hydroxy, 3-isopropyl, 5-peroxy, 6-keto)
RO_227	Cyclic hydroxy alkenyl peroxy radical from oxidation of BIOH (C_6 cycle, 1-methyl, 1-ene, 4-peroxy, 4-isopropyl, 5-hydroxy)
RO_228	Cyclic nitrato alkenyl peroxy radical from oxidation of BIOH (C_6 cycle, 1-methyl, 1-ene, 4-peroxy, 4-isopropyl, 5-nitrato)
RO_229	Branched keto alkenyl peroxy radical from oxidation of BIOH (C_6 chain, 1-peroxy, 2-isopropyl, 2-ene, 5-keto)
RO_230	Branched keto aldehydic peroxy radical from oxidation of BIOH (C_7 chain, 3-isopropyl, 3-ene, 5-peroxy, 6-keto)

Table 1.1 (cont.) Chemical Species Represented in CACM

$RO_2$31	Aromatic peroxy radical from side chain oxidation of PAH
$RO_2$32	Alkyl peroxy radical from oxidation of ALKH (8-peroxy)
$RO_2$33	Peroxy radical from addition of O_2 to RAD2
$RO_2$34	Peroxy radical from addition of O_2 to RAD3
$RO_2$35	Peroxy radical from addition of O_2 to RAD4
$RO_2$36	Peroxy radical from addition of O_2 to RAD5
$RO_2$37	Peroxy radical from addition of O_2 to RAD6
$RO_2$38	Peroxy radical from addition of O_2 to RAD7
$RO_2$39	Unsaturated acyl peroxy radical from oxidation of ISOP (C_3)
$RO_2$40	Branched hydroxy keto alkenyl peroxy radical from oxidation of BIOH (C_6 chain, 1-hydroxy, 2-isopropyl, 2-ene, 4-peroxy, 5-keto)
$RO_2$41	Hydroxy alkyl peroxy radical from oxidation of ALKH (8-hydroxy, 11-peroxy)
$RO_2$42	Bicyclic peroxy radical from the O_2 bridging in $RO_2$31
$RO_2$43	Bicyclic peroxy radical from the O_2 bridging in $RO_2$32
$RO_2$44	Bicyclic peroxy radical from the O_2 bridging in $RO_2$33
$RO_2$45	Bicyclic peroxy radical from the O_2 bridging in $RO_2$34
$RO_2$46	Bicyclic peroxy radical from the O_2 bridging in $RO_2$35
$RO_2$47	Bicyclic peroxy radical from the O_2 bridging in $RO_2$36
$RO_2$48	Acyl radical from aldehydic H abstraction of MGLY
$RO_2$49	Peroxy radical formed from OH oxidation of MVK
$RO_2$50	Acyl radical from aldehydic H abstraction of MCR
$RO_2$51	Peroxy radical from OH addition to double bond in MCR
$RO_2$52	Peroxy radical from NO_3 addition to double bond in MCR
$RO_2$53	Dicarbonyl peroxy radical from MCR/O_3 reaction (C_3 chain, 1-peroxy, 2-keto, 3-aldehydic)
$RO_2$54	Acyl radical from decomposition of $RO_2$53
$RO_2$55	Acyl radical from aldehydic H abstraction of RPR1
$RO_2$56	Acyl radical from aldehydic H abstraction of RPR3
$RO_2$57	Acyl radical from aldehydic H abstraction of RPR7
$RO_2$58	Acyl acid peroxy radical from aldehydic H abstraction of RP16 (C_2)
RAD1	Radical from NO_3 oxidation of AROO
RAD2	Hexadienyl radical from OH oxidation of AROO
RAD3	Hexadienyl radical from OH oxidation of AROL
RAD4	Hexadienyl radical from OH oxidation of AROH
RAD5	Hexadienyl radical from OH oxidation of ARAL
RAD6	Hexadienyl radical from OH oxidation of ARAC
RAD7	Hexadienyl radical from OH oxidation of PAH
RAD8	Radical from NO_3 oxidation of RPR4

Species with Concentrations not Affected by Reaction

H_2O	Water vapor
O_2	Oxygen
M	Third body
CH_4	Methane

Table 1.2 Reactions contained in the Caltech Atmospheric Chemistry Mechanism

Reaction	Reactants	Products	Rate Constants (cm-molecule-sec units)*	References, Comments
1	$NO_2 + h\nu$	NO + O	See Table 1.3	1
2	$O + O_2 + M$	$O_3 + M$	5.53E+16/TEMP^4.8	2
3	$O + NO_2$	$NO + O_2$	6.5E-12*EXP(119.8/TEMP)	2
4	$O + NO_2 + M$	$NO_3 + M$	See Table 1.4	2
5	$NO + O_3$	$NO_2 + O_2$	1.8E-12*EXP(-1368.9/TEMP)	2
6	$NO_2 + O_3$	$NO_3 + O_2$	1.4E-13*EXP(-2471.1/TEMP)	2
7	$NO + NO_3$	$2\ NO_2$	1.8E-11*EXP(110.7/TEMP)	2
8	$NO + NO + O_2$	$2\ NO_2$	5.09E-18/TEMP*EXP(528.4/TEMP)	2
9	$NO_2 + NO_3 + M$	$N_2O_5 + M$	See Table 1.4	2
10	N_2O_5	$NO_2 + NO_3$	See Table 1.4	2
11	$N_2O_5 + H_2O$	$2\ HNO_3$	2.59E-22	2
12	$NO_2 + NO_3$	$NO + NO_2 + O_2$	4.5E-14*EXP(-1258.2/TEMP)	2
13	$NO_3 + h\nu$	$NO + O_2$	See Table 1.3	1
14	$NO_3 + h\nu$	$NO_2 + O$	See Table 1.3	1
15	$O_3 + h\nu$	$O + O_2$	See Table 1.3	1
16	$O_3 + h\nu$	$OSD + O_2$	See Table 1.3	1
17	$OSD + H_2O$	2 OH	2.2E-10	2
18	OSD + M	O + M	1.53E+11/TEMP*EXP(95.6/TEMP)	2
19	NO + OH + M	HONO + M	See Table 1.4	2
20	$HONO + h\nu$	$0.9\ NO + 0.1\ NO_2 + 0.9\ OH + 0.1\ HO_2$	See Table 1.3	1
21	$NO_2 + H_2O$	$HONO – NO_2 + HNO_3$	4.0E-24	1
22	$NO_2 + OH + M$	$HNO_3 + M$	See Table 1.4	3
23	$HNO_3 + OH$	$NO_3 + H_2O$	See Table 1.5	2
24	CO + OH	$HO_2 + CO_2$	See Table 1.5	2
25	$O_3 + OH$	$HO_2 + O_2$	1.9E-12*EXP(-1001.5/TEMP)	2
26	$NO + HO_2$	$NO_2 + OH$	3.41E-12*EXP(271.8/TEMP)	2
27	$NO_2 + HO_2 + M$	$HNO_4 + M$	See Table 1.4	2
28	HNO_4	$NO_2 + HO_2$	See Table 1.4	2
29	$HNO_4 + OH$	$NO_2 + O_2 + H_2O$	1.5E-12*EXP(362.4/TEMP)	2
30	$O_3 + HO_2$	$OH + 2\ O_2$	1.4E-14*EXP(-598.9/TEMP)	2
31	$HO_2 + HO_2$	H_2O_2	See Table 1.5	2
32	$HO_2 + HO_2 + H_2O$	$H_2O_2 + O_2 + H_2O$	See Table 1.5	2
33	$NO_3 + HO_2$	$0.8\ NO_2 + 0.2\ HNO_3 + 0.8\ OH + O_2$	4.0E-12	2
34	$O + O_3$	$2\ O_2$	8.0E-12*EXP(-2058.4/TEMP)	2
35	SO_2 + OH	H_2SO_4 (via SO_3) + HO_2	See Table 1.4	2
36	$H_2O_2 + h\nu$	2 OH	See Table 1.3	1
37	H_2O_2 + OH	$HO_2 + H_2O$	2.91E-12*EXP(-161/TEMP)	1
38	O + NO +M	NO_2 + M	6.75E-06/TEMP^2.6	2
39	HONO + OH	$NO_2 + H_2O$	2.7E-12*EXP(261.7/TEMP)	2
40	NO_3 + OH	$NO_2 + HO_2$	2.0E-11	2
41	$NO_3 + NO_3$	$2\ NO_2 + O_2$	8.5E-13*EXP(-2450.9/TEMP)	2
42	$OH + HO_2$	$H_2O + O_2$	4.8E-11*EXP(251.6/TEMP)	2
43	CH_4 + OH	$RO_21 + RO_2T + H_2O$	2.66E-12*EXP(-1800.2/TEMP)	2
44	$HCHO + h\nu$	$CO + 2\ HO_2$	See Table 1.3	1
45	$HCHO + h\nu$	CO + H_2	See Table 1.3	1
46	HCHO + OH	$CO + HO_2 + H_2O$	1.2E-14*TEMP*EXP(286.9/TEMP)	4
47	$HCHO + NO_3$	$HNO_3 + CO + HO_2$	2.0E-12*EXP(-2430.8/TEMP)	2
48	MEOH + OH	HO_2 + HCHO + H_2O	6.0E-18*TEMP^2*EXP(170.1/TEMP)	4
49	ETHE + OH	$RO_22 + RO_2T$	1.96E-12*EXP(437.8/TEMP)	5
50	ETHE + NO_3	$RO_23 + RO_2T$	4.89E-18*TEMP^2*EXP(-2282.3/TEMP)	5
51	ETHE + O_3	0.315 CO + 0.06 HO_2 + 0.06 OH + 0.185 ACID + 0.5 HCHO + 0.07 H_2O	9.14E-15*EXP(-2580.3/TEMP)	5
52	ETHE + O	$0.6\ CO + HO_2 + 0.6\ RO_21 + 0.4\ RO_24 + RO_2T$	7.3E-13	5
53	ETOH + OH	CF(1) HO_2 + CF(1) ALD2 + CF(2) RO_22 + CF(2) RO_2T + H_2O	6.18E-18*TEMP^2*EXP(532/TEMP)	4
54	OLEL + OH	$RO_22 + RO_2T$	5.86E-12*EXP(500.3/TEMP)	4
55	OLEL + NO_3	$RO_23 + RO_2T$	1.0E-13*EXP(-800.2/TEMP)	5
56	OLEL + O_3	0.56 CO + 0.2 CO_2 + 0.36 OH + 0.28 HO_2 + 0.5 HCHO + 0.5 ALD2 + 0.24 ACID + 0.1 ALKL + 0.28 RO_25 + 0.28 RO_2T	1.0E-17	5
57	OLEL + O	0.5 ALKL + 0.4 ALD2 + 0.1 RO_24 + 0.1 RO_25 + 0.2 RO_2T	4.66E-12	5

Table 1.2 (cont.) Reactions contained in the Caltech Atmospheric Chemistry Mechanism

Reaction	Reactants	Products	Rate Constants (cm-molecule-sec units)*	References, Comments
58	ALKL + OH	$RO_2$5 + RO_2T + H_2O	3.91E-12	4
59	ALD2 + $h\nu$	CO + HO_2 + $RO_2$5 + RO_2T	See Table 1.3	1
60	ALD2 + OH	$RO_2$6 + RO_2T + H_2O	6.91E-12*EXP(250/TEMP)	1
61	ALD2 + NO_3	HNO_3 + $RO_2$6 + RO_2T	3.0E-13*EXP(-1427/TEMP)	1
62	KETL + OH	$RO_2$7 +RO_2T + H_2O	4.91E-12	6
63	KETL + $h\nu$	$RO_2$5 + $RO_2$8 + 2 RO_2T	See Table 1.3	1
64	ISOP + OH	0.66 $RO_2$9 + 0.34 $RO_2$10 + RO_2T	2.55E-11*EXP(410.2/TEMP)	5
65	ISOP + NO_3	0.66 $RO_2$11 + 0.34 $RO_2$12 + RO_2T	3.02E-12*EXP(-445.9/TEMP)	5
66	ISOP + O_3	0.068 CO_2 + 0.461 CO + 0.5 HCHO + 0.664 OH + 0.366 HO_2 + 0.054 OLEL + 0.121 ACID + 0.389 MVK + 0.17 MCR + 0.271 $RO_2$13 + 0.095 $RO_2$14 + 0.366 RO_2T	7.86E-15*EXP(-1912.9/TEMP)	5
67	ISOP + O	0.925 OLEL + 0.075 ALD2	3.5E-11	5
68	MTBE + OH	$RO_2$15 + RO_2T + H_2O	3.2E-12	7
69	ALCH + OH	$RO_2$2 + RO_2T+ H_2O	See Table 1.6	8
70	KETH + OH	$RO_2$16 + RO_2T + H_2O	See Table 1.6	8
71	KETH + $h\nu$	$RO_2$5 + $RO_2$8 + 2 RO_2T	See Table 1.3	1
72	AROO + NO_3	HNO_3 + RAD1	3.77E-12	2
73	AROO + OH	0.16 HO_2 + 0.16 AROO + 0.1 $RO_2$17 + 0.1 RO_2T + 0.74 RAD2 + 0.1 H_2O	See Table 1.6	8
74	OLEH + OH	$RO_2$18 + RO_2T	See Table 1.6	8
75	OLEH + NO_3	$RO_2$19 + RO_2T	k_{74}*k_{55}/k_{54}	Estimated *k*
76	OLEH + O_3	0.56 CO + 0.2 CO_2 + 0.36 OH + 0.28 HO_2 + 0.5 HCHO + 0.5 RPR1 + 0.12 ACID + 0.12 UR1 + 0.1 ALKM + 0.28 $RO_2$20 + 0.28 RO_2T	k_{74}*k_{56}/k_{54}	Estimated *k*
77	OLEH + O	0.5 ALKM + 0.4 RPR1 + 0.1 $RO_2$4 + 0.1 $RO_2$20 + 0.2 RO_2T	k_{74}*k_{57}/k_{54}	Estimated *k*
78	ALKM + OH	$RO_2$20 + RO_2T + H_2O	See Table 1.6	8
79	AROL + OH	0.16 HO_2 + 0.16 AROO + 0.06 $RO_2$21 + 0.78 RAD3 + 0.06 RO_2T+ 0.06 H_2O	3.27E-11	4
80	AROH + OH	0.16 HO_2 + 0.16 AROO + 0.84 RAD4	See Table 1.6	8
81	ARAL + NO_3	HNO_3 + O_3 – HO_2 + ARAC	1.4E-12*EXP(-1872.2/TEMP)	2
82	ARAL + OH	(0.16-CF(39)) HO_2 + CF(39) O_3 + CF(39) ARAC + CF(45) $RO_2$22 + CF(40) RAD5 + CF(45) RO_2T + (CF(39) + CF(45))H_2O	1.29E-11	2
83	ARAC + OH	0.16 HO_2 + 0.16 UR2 + 0.1 $RO_2$23 + 0.74 RAD6 + 0.1 RO_2T+ 0.1 H_2O	See Table 1.6	8
84	BIOL + OH	$RO_2$24 + RO_2T	1.7E-10	9
85	BIOL + NO_3	$RO_2$25 + RO_2T	1.46E-11	9
86	BIOL + O_3	0.445 CO + 0.055 H_2O_2 + 0.445 HO_2 + 0.89 OH + 0.055 UR3 + 0.445 UR4 + 0.055 RPR3 + 0.445 $RO_2$26 + 0.445 RO_2T	2.5E-16	9
87	BIOL + O	0.75 UR5 + 0.25 UR6	k_{84}*k_{57}/k_{54}	Estimated *k*
88	BIOH + OH	$RO_2$27 + RO_2T	1.77E-10	5
89	BIOH + NO_3	$RO_2$28 + RO_2T	2.91E-11	5
90	BIOH + O_3	0.445 CO + 0.055 H_2O_2 + 0.89 OH + 0.055 UR7 + 0.055 UR8 + 0.445 $RO_2$29 + 0.445 $RO_2$30 + 0.89 RO_2T	1.4E-16	5
91	BIOH + O	0.75 UR9 + 0.25 UR10	8.59E-11	5
92	PAH + OH	0.16 HO_2 + 0.16 UR11 + 0.1 $RO_2$31 + 0.74 RAD7 + 0.1 RO_2T + 0.1 H_2O	7.7E-11	6
93	ALKH + OH	$RO_2$32 + RO_2T + H_2O	See Table 1.6	8
94	RO_2T + HO_2	HO_2	3.41E-13*EXP(800.2/TEMP)	2
95	RO_2T + NO	NO	4.2E-12*EXP(181.2/TEMP)	2
96	RO_2T + RO_2T	RO_2T	1.0E-15	2
97	RAD2 + O_2	$RO_2$33 + RO_2T	7.7E+5/TEMP	10
98	RAD3 + O_2	$RO_2$34 + RO_2T	k_{97}	
99	RAD4 + O_2	$RO_2$35 + RO_2T	k_{97}	
100	RAD5 + O_2	$RO_2$36 + RO_2T	k_{97}	
101	RAD6 + O_2	$RO_2$37 + RO_2T	k_{97}	
102	RAD7 + O_2	$RO_2$38 + RO_2T	k_{97}	

Table 1.2 (cont.) Reactions contained in the Caltech Atmospheric Chemistry Mechanism

Reaction	Reactants	Products	Rate Constants (cm-molecule-sec units)*	References, Comments
103	RAD1 + NO_2	RPR4	3.0E-11	10
104	RAD2 + NO_2	RPR4 + H_2O	k_{103}	
105	RAD3 + NO_2	UR12 + H_2O	k_{103}	
106	RAD4 + NO_2	UR13 + H_2O	k_{103}	
107	RAD5 + NO_2	RPR5 + H_2O	k_{103}	
108	RAD6 + NO_2	UR14 + H_2O	k_{103}	
109	RAD7 + NO_2	UR15 + H_2O	k_{103}	
110	RO_21 + NO	NO_2 + HO_2 + HCHO	4.09E-12*EXP(180.2/TEMP)	11
111	RO_21 + RO_2T	HO_2 + HCHO + RO_2T + O_2	k_{96}	
112	RO_21 + HO_2	HO_2 + OH + HCHO	k_{94}	
113	RO_22 + NO	NO_2 + HO_2 + HCHO + ALD2	2.45E-12*EXP(180.2/TEMP)	11
114	RO_22 + RO_2T	HO_2 + HCHO + ALD2 + RO_2T + O_2	k_{96}	
115	RO_22 + HO_2	OH + HO_2 + HCHO + ALD2	k_{94}	
116	RO_23 + NO	2 NO_2 + HCHO + ALD2	k_{113}	
117	RO_23 + RO_2T	NO_2 + HO_2 + HCHO + ALD2 + C_2+ RO_2T	k_{96}	
118	RO_23 + HO_2	NO_2 + HO_2 + OH + HCHO + ALD2	k_{94}	
119	RO_24 + NO	NO_2 + CO + HO_2 + HCHO	3.45E-12*EXP(180.2/TEMP)	11
120	RO_24 + RO_2T	CO + HO_2 + HCHO + RO_2T + O_2	k_{96}	
121	RO_24 + HO_2	CO + HO_2 + OH + HCHO	k_{94}	
122	RO_25 + NO	CF(3) ALKL + CF(4) NO_2 + CF(4) HO_2 + CF(4) ALD2	2.91E-12*EXP(180.2/TEMP)	11
123	RO_25 + RO_2T	HO_2 + ALD2 + RO_2T + O_2	k_{96}	
124	RO_25 + HO_2	HO_2 + OH + ALD2	k_{94}	
125	RO_26 + NO	NO_2 + CO_2 + RO_25 + RO_2T	1.11E-11*EXP(180.2/TEMP)	11
126	RO_26 + NO_2 + M	PAN1 + M	See Table 1.4	12
127	PAN1	NO_2 + RO_26 + RO_2T	See Table 1.4	12
128	RO_26 + HO_2	O_3 + ACID	k_{94}	
129	RO_26 + RO_2T	CO_2 + RO_25 + 2 RO_2T + O_2	k_{96}	
130	RO_27 + NO	NO_2 + ALD2 + RO_28 + RO_2T	k_{113}	
131	RO_27 + RO_2T	ALD2 + RO_28 + 2 RO_2T + O_2	k_{96}	
132	RO_27 + HO_2	OH + ALD2 + RO_28 + RO_2T	k_{94}	
133	RO_28 + NO	NO_2 + CO_2 + RO_21 + RO_2T	k_{125}	
134	RO_28 + NO_2 + M	PAN2 + M	k_{126}	
135	PAN2	NO_2 + RO_28 + RO_2T	k_{127}	
136	RO_28 + HO_2	O_3 + ACID	k_{94}	
137	RO_28 + RO_2T	CO_2 + RO_21 + 2 RO_2T + O_2	k_{96}	
138	RO_29 + NO	CF(5) OLEL + CF(6) NO_2 + CF(6) HO_2 + CF(6) HCHO + CF(6) MVK	2.08E-12*EXP(180.2/TEMP)	11
139	RO_29 + RO_2T	HO_2 + MVK + HCHO + RO_2T + O_2	k_{96}	
140	RO_29 + HO_2	HO_2 + OH + MVK + HCHO	k_{94}	
141	RO_210 + NO	NO_2 + HO_2 + HCHO + MCR	k_{138}	
142	RO_210 + RO_2T	HO_2 + HCHO + MCR + RO_2T + O_2	k_{96}	
143	RO_210 + HO_2	HO_2 + OH + HCHO + MCR	k_{94}	
144	RO_211 + NO	2 NO_2 + HCHO + MVK	k_{138}	
145	RO_211 + RO_2T	NO_2 + HCHO + MVK + RO_2T + O_2	k_{96}	
146	RO_211 + HO_2	NO_2 + OH + HCHO + MVK	k_{94}	
147	RO_212 + NO	2 NO_2 + HCHO + MCR	k_{138}	
148	RO_212 + RO_2T	NO_2 + HCHO + MCR + RO_2T + O_2	k_{96}	
149	RO_212 + HO_2	NO_2 + OH + HCHO + MCR	k_{94}	
150	RO_213 + NO	NO_2 + HCHO + RO_239 + RO_2T	k_{113}	
151	RO_213 + RO_2T	HCHO + RO_239 + 2 RO_2T + O_2	k_{96}	
152	RO_213 + HO_2	HCHO + OH + RO_239 + RO_2T	k_{94}	
153	RO_239 + NO	NO_2 + CO_2 + RO_214 + RO_2T	k_{125}	
154	RO_239 + NO_2 + M	PAN3 + M	k_{126}	
155	PAN3	NO_2 + RO_239 + RO_2T	k_{127}	
156	RO_239 + HO_2	O_3 + 0.5 OLEL + 0.5 ACID	k_{94}	
157	RO_239 + RO_2T	CO_2 + RO_214 + 2 RO_2T + O_2	k_{96}	
158	RO_214 + NO	CF(7) OLEL + CF(8) NO_2 + CF(8) RO_27 + CF(8) RO_2T	k_{122}	
159	RO_214 + RO_2T	RO_27 + 2 RO_2T + O_2	k_{96}	
160	RO_214 + HO_2	OH + RO_27 + RO_2T	k_{94}	
161	RO_215 + NO	NO_2 + HO_2 + CF(9) ALD2 + CF(10) HCHO + CF(11) KETL + CF(12) ALKL	k_{138}	

Table 1.2 (cont.) Reactions contained in the Caltech Atmospheric Chemistry Mechanism

Reaction	Reactants	Products	Rate Constants (cm-molecule-sec units)*	References, Comments
162	$RO_2$15 + RO_2T	HO_2 + CF(13) ALD2 + CF(14) HCHO + CF(15) KETL + CF(16) ALKL + RO_2T + O_2	k_{96}	
163	$RO_2$15 + HO_2	OH + HO_2 + CF(13) ALD2 + CF(14) HCHO + CF(15) KETL + CF(16) ALKL	k_{94}	
164	$RO_2$16 + NO	NO_2 + ALD2 + $RO_2$8 + RO_2T	1.48E-12*EXP(180.2/TEMP)	11
165	$RO_2$16 + RO_2T	ALD2 + $RO_2$8 + 2 RO_2T +O_2	k_{96}	
166	$RO_2$16 + HO_2	OH + ALD2 + $RO_2$8 + RO_2T	k_{94}	
167	$RO_2$17 + NO	CF(21) AP1 + CF(22) NO_2 + CF(22) HO_2 + CF(22) RPR2	1.25E-12*EXP(180.2/TEMP)	11
168	$RO_2$17 + RO_2T	HO_2 + RPR2 + RO_2T + O_2	k_{96}	
169	$RO_2$17 + HO_2	HO_2 + OH + RPR2	k_{94}	
170	$RO_2$18 + NO	CF(19) AP2 + CF(20) NO_2 + CF(20) HO_2 + CF(20) UR16	k_{167}	
171	$RO_2$18 + RO_2T	HO_2 + UR16 + RO_2T + O_2	k_{96}	
172	$RO_2$18 + HO_2	HO_2 + OH + UR16	k_{94}	
173	$RO_2$19 + NO	2 NO_2 + HCHO + RPR1	1.05E-12*EXP(180.2/TEMP)	11
174	$RO_2$19 + RO_2T	NO_2 + HCHO + RPR1 + RO_2T + O_2	k_{96}	
175	$RO_2$19 + HO_2	NO_2 + OH + HCHO + RPR1	k_{94}	
176	$RO_2$20 + NO	CF(17) AP3 + CF(18) NO_2 + CF(18) $RO_2$18 + CF(18) RO_2T	k_{167}	
177	$RO_2$20 + RO_2T	$RO_2$18 + 2 RO_2T + O_2	k_{96}	
178	$RO_2$20 + HO_2	OH + $RO_2$18 + RO_2T	k_{94}	
179	$RO_2$21 + NO	CF(23) AP4 + CF(24) NO_2 + CF(24) HO_2 + CF(24) ARAL	k_{173}	
180	$RO_2$21 + RO_2T	HO_2 + ARAL + RO_2T + O_2	k_{96}	
181	$RO_2$21 + HO_2	HO_2 + OH + ARAL	k_{94}	
182	$RO_2$22 + NO	CF(41) AP5 + CF(42) NO_2 + CF(42) HO_2 + CF(42) RPR6	k_{167}	
183	$RO_2$22 + RO_2T	HO_2 + RPR6 + RO_2T + O_2	k_{96}	
184	$RO_2$22 + HO_2	HO_2 + OH + RPR6	k_{94}	
185	$RO_2$23 + NO	CF(43) AP6 + CF(44) NO_2 + CF(44) HO_2 + CF(44) RPR7	k_{167}	
186	$RO_2$23 + RO_2T	HO_2 + RPR7 + RO_2T + O_2	k_{96}	
187	$RO_2$23 + HO_2	HO_2 + OH + RPR7	k_{94}	
188	$RO_2$24 + NO	CF(25) AP7 + CF(26) NO_2 + CF(26) HO_2 + CF(26) RPR3	8.89E-13*EXP(180.2/TEMP)	11
189	$RO_2$24 + RO_2T	HO_2 + RPR3 + RO_2T + O_2	k_{96}	
190	$RO_2$24 + HO_2	HO_2 + OH + RPR3	k_{94}	
191	$RO_2$25 + NO	2 NO_2 + RPR3	k_{188}	
192	$RO_2$25 + RO_2T	NO_2 + RPR3 + RO_2T + O_2	k_{96}	
193	$RO_2$25 + HO_2	NO_2 + OH + RPR3	k_{94}	
194	$RO_2$26 + NO	NO_2 + UR17 + $RO_2$8 + RO_2T	k_{188}	
195	$RO_2$26 + RO_2T	UR17 + $RO_2$8 + 2 RO_2T + O_2	k_{96}	
196	$RO_2$26 + HO_2	UR17 + OH + $RO_2$8 + RO_2T	k_{94}	
197	$RO_2$27 + NO	CF(27) AP8 + CF(28) NO_2 + CF(28) HO_2 + CF(28) UR7	k_{188}	
198	$RO_2$27 + RO_2T	HO_2 + UR7 + RO_2T + O_2	k_{96}	
199	$RO_2$27 + HO_2	HO_2 + OH + UR7	k_{94}	
200	$RO_2$28 + NO	2 NO_2 + UR7	k_{188}	
201	$RO_2$28 + RO_2T	NO_2 + UR7 + RO_2T + O_2	k_{96}	
202	$RO_2$28 + HO_2	NO_2 + OH + UR7	k_{94}	
203	$RO_2$29 + NO	CF(29) AP9 + CF(30) NO_2 + CF(30) $RO_2$40 + CF(30) RO_2T	k_{173}	
204	$RO_2$29 + RO_2T	$RO_2$40 + 2 RO_2T + O_2	k_{96}	
205	$RO_2$29 + HO_2	OH + $RO_2$40 + RO_2T	k_{94}	
206	$RO_2$40 + NO	NO_2 + RPR8 + $RO_2$8 + RO_2T	k_{173}	
207	$RO_2$40 + RO_2T	RPR8+ $RO_2$8 + 2 RO_2T + O_2	k_{96}	
208	$RO_2$40 + HO_2	OH + RPR8 + $RO_2$8 + RO_2T	k_{94}	
209	$RO_2$30 + NO	NO_2 + UR18 + $RO_2$8 + RO_2T	k_{188}	
210	$RO_2$30 + RO_2T	UR18 + $RO_2$8 + 2 RO_2T + O_2	k_{96}	
211	$RO_2$30 + HO_2	OH + UR18 + $RO_2$8 + RO_2T	k_{94}	
212	$RO_2$31 + NO	CF(31) AP10 + CF(32) NO_2 + CF(32) HO_2 + CF(32) UR19	6.32E-13*EXP(180.2/TEMP)	11

Table 1.2 (cont.) Reactions contained in the Caltech Atmospheric Chemistry Mechanism

Reaction	Reactants	Products	Rate Constants (cm-molecule-sec units)*	References, Comments
213	$RO_2$31 + RO_2T	HO_2 + UR19 + RO_2T + O_2	k_{96}	
214	$RO_2$31 + HO_2	HO_2 + OH + UR19	k_{94}	
215	$RO_2$32 + NO	CF(33) AP11 + CF(34) NO_2 + CF(34) $RO_2$41 + CF(34) RO_2T	3.2E-13*EXP(180.2/TEMP)	11
216	$RO_2$32 + RO_2T	$RO_2$41 + 2 RO_2T + O_2	k_{96}	
217	$RO_2$32 + HO_2	OH + $RO_2$41 + RO_2T	k_{94}	
218	$RO_2$41 + NO	CF(35) AP12 + CF(36) NO_2 + CF(36) HO_2 + CF(36) UR20	k_{215}	
219	$RO_2$41 + RO_2T	HO_2 + UR20 + RO_2T+ O_2	k_{96}	
220	$RO_2$41 + HO_2	HO_2 + OH + UR20	k_{94}	
221	$RO_2$33	$RO_2$42 + RO_2T	1.64E+42/TEMP^11.4*EXP (-9460/TEMP)	13
222	$RO_2$33 + NO	NO_2 + HO_2 + RPR9	k_{167}	
223	$RO_2$33 + RO_2T	HO_2 + RPR9 + RO_2T + O_2	k_{96}	
224	$RO_2$33 + HO_2	HO_2 + OH + RPR9	k_{94}	
225	$RO_2$42 + NO	NO_2 + HO_2 + RP10 + MGLY	k_{167}	
226	$RO_2$42 + RO_2T	HO_2 + RP10 + MGLY + O_2 + RO_2T	k_{96}	
227	$RO_2$42 + HO_2	HO_2 + OH + RP10 + MGLY	k_{94}	
228	$RO_2$34	$RO_2$43 + RO_2T	k_{221}	
229	$RO_2$34 + NO	NO_2 + HO_2 + RP11	k_{173}	
230	$RO_2$34 + RO_2T	HO_2 + RP11 + RO_2T + O_2	k_{96}	
231	$RO_2$34 + HO_2	HO_2 + OH + RP11	k_{94}	
232	$RO_2$43 + NO	NO_2 + HO_2 + RP10 + MGLY	k_{173}	
233	$RO_2$43 + RO_2T	HO_2 + RP10 + MGLY + O_2 + RO_2T	k_{96}	
234	$RO_2$43 + HO_2	HO_2 + OH + RP10 + MGLY	k_{94}	
235	$RO_2$35	$RO_2$44 + RO_2T	k_{221}	
236	$RO_2$35 + NO	NO_2 + HO_2 + RP11	k_{188}	
237	$RO_2$35 + RO_2T	HO_2 + RP11 + RO_2T + O_2	k_{96}	
238	$RO_2$35 + HO_2	HO_2 + OH + RP11	k_{94}	
239	$RO_2$44 + NO	NO_2 + HO_2 + RP10 + MGLY	k_{188}	
240	$RO_2$44 + RO_2T	HO_2 + RP10 + MGLY + O_2 + RO_2T	k_{96}	
241	$RO_2$44 + HO_2	HO_2 + OH + RP10 + MGLY	k_{94}	
242	$RO_2$36	$RO_2$45 + RO_2T	k_{221}	
243	$RO_2$36 + NO	NO_2 + HO_2 + RP12	k_{167}	
244	$RO_2$36 + RO_2T	HO_2 + RP12 + RO_2T + O_2	k_{96}	
245	$RO_2$36 + HO_2	HO_2 + OH + RP12	k_{94}	
246	$RO_2$45 + NO	NO_2 + HO_2 + RP10 + MGLY	k_{167}	
247	$RO_2$45 + RO_2T	HO_2 + RP10 + MGLY + O_2 + RO_2T	k_{96}	
248	$RO_2$45 + HO_2	HO_2 + OH + RP10 + MGLY	k_{94}	
249	$RO_2$37	$RO_2$46 + RO_2T	k_{221}	
250	$RO_2$37 + NO	NO_2 + HO_2 + RP13	k_{167}	
251	$RO_2$37 + RO_2T	HO_2 + RP13 + RO_2T + O_2	k_{96}	
252	$RO_2$37 + HO_2	HO_2 + OH + RP13	k_{94}	
253	$RO_2$46 + NO	NO_2 + HO_2 + RP10 + MGLY	k_{167}	
254	$RO_2$46 + RO_2T	HO_2 + RP10 + MGLY + O_2 + RO_2T	k_{96}	
255	$RO_2$46 + HO_2	HO_2 + OH + RP10 + MGLY	k_{94}	
256	$RO_2$38	$RO_2$47 + RO_2T	k_{221}	
257	$RO_2$38 + NO	NO_2 + HO_2 + RP14	k_{212}	
258	$RO_2$38 + RO_2T	HO_2 + RP14 + RO_2T + O_2	k_{96}	
259	$RO_2$38 + HO_2	HO_2 + OH + RP14	k_{94}	
260	$RO_2$47 + NO	NO_2 + HO_2 + RP15 + MGLY	k_{212}	
261	$RO_2$47 + RO_2T	HO_2 + RP15 + MGLY + O_2 + RO_2T	k_{96}	
262	$RO_2$47 + HO_2	HO_2 + OH + RP15 + MGLY	k_{94}	
263	MGLY + OH	$RO_2$48 + RO_2T + H_2O	1.72E-11	5
264	MGLY + NO_3	HNO_3 + $RO_2$48 + RO_2T	1.4E-12*EXP(-1897.3/TEMP)	2
265	MGLY + $h\nu$	CO + HO_2 + $RO_2$8 + RO_2T	See Table 1.3	1
266	$RO_2$48 + NO	NO_2 + CO_2 + $RO_2$8 + RO_2T	k_{125}	
267	$RO_2$48 + NO_2 + M	PAN4 + M	k_{126}	
268	PAN4	NO_2 + $RO_2$48 + RO_2T	k_{127}	
269	$RO_2$48 + HO_2	O_3 + UR21	k_{94}	
270	$RO_2$48 + RO_2T	CO_2 + $RO_2$8 + 2 RO_2T + O_2	k_{96}	
271	MVK + OH	$RO_2$49 + RO_2T	4.14E-12*EXP(452.9/TEMP)	2

Table 1.2 (cont.) Reactions contained in the Caltech Atmospheric Chemistry Mechanism

Reaction	Reactants	Products	Rate Constants (cm-molecule-sec units)*	References, Comments
272	MVK + O_3	0.56 CO + 0.2 CO_2 + 0.28 HO_2 + 0.36 OH + 0.5 MGLY + 0.5 HCHO + 0.12 ACID + 0.1 ALD2 + 0.12 UR21 + 0.28 $RO_2$8 + 0.28 RO_2T + 0.2 H_2O	7.5E-16*EXP(-1519.9/TEMP)	2
273	MVK + O	0.85 KETL + 0.15 $RO_2$4 + 0.15 $RO_2$8 + 0.3 RO_2T	4.32E-12	2
274	$RO_2$49 + NO	NO_2 + HO_2 + MGLY + HCHO	k_{113}	
275	$RO_2$49 + RO_2T	HO_2 + MGLY + HCHO + RO_2T + O_2	k_{96}	
276	$RO_2$49 + HO_2	HO_2 + OH + MGLY + HCHO	k_{94}	
277	MCR + OH	CF(46) $RO_2$50 + CF(46) H_2O + CF(47) $RO_2$51 + RO_2T	1.86E-11*EXP(176.1/TEMP)	2
278	MCR + NO_3	CF(46) HNO_3 + CF(46) $RO_2$50 + CF(47) $RO_2$52 + RO_2T	1.5E-12*EXP(-1726.2/TEMP)	2
279	MCR + O_3	0.41 CO + 0.41 HO_2 + 0.82 OH + 0.5 HCHO + 0.59 MGLY + 0.09 ACID + 0.41 $RO_2$53 + 0.41 RO_2T	1.36E-15*EXP(-2113.7/TEMP)	2
280	MCR + O	0.15 CO + 0.15 HO_2 + 0.85 ALD2 + 0.15 $RO_2$7 + 0.15 RO_2T	6.34E-12	2
281	$RO_2$50 + NO	CO_2 + NO_2 + $RO_2$14 + RO_2T	k_{125}	
282	$RO_2$50 + NO_2 + M	PAN5 + M	k_{126}	
283	PAN5	NO_2 + $RO_2$50 + RO_2T	k_{127}	
284	$RO_2$50 + HO_2	O_3 + 0.5 ACID + 0.5 OLEL	k_{94}	
285	$RO_2$50 + RO_2T	CO_2 + $RO_2$14 + 2 RO_2T + O_2	k_{96}	
286	$RO_2$51 + NO	NO_2 + HO_2 + HCHO + MGLY	k_{113}	
287	$RO_2$51 + HO_2	HO_2 + HCHO + MGLY + RO_2T + O_2	k_{94}	
288	$RO_2$51 + RO_2T	HO_2 + OH + MGLY + HCHO	k_{96}	
289	$RO_2$52 + NO	2 NO_2 + MGLY + HCHO	k_{113}	
290	$RO_2$52 + HO_2	NO_2 + MGLY + HCHO + RO_2T + O_2	k_{94}	
291	$RO_2$52 + RO_2T	NO_2 + OH + MGLY + HCHO	k_{96}	
292	$RO_2$53 + NO	NO_2 + HCHO + $RO_2$54 + RO_2T	k_{122}	
293	$RO_2$53 + HO_2	HCHO + $RO_2$54 + 2 RO_2T + O_2	k_{94}	
294	$RO_2$53 + RO_2T	OH + HCHO + $RO_2$54 + RO_2T	k_{96}	
295	$RO_2$54 + NO	CO_2 + CO + NO_2 + HO_2	k_{125}	
296	$RO_2$54 + NO_2 + M	PAN6 + M	k_{126}	
297	PAN6	NO_2 + $RO_2$54 + NO_2	k_{127}	
298	$RO_2$54 + HO_2	O_3 + RP16	k_{94}	
299	$RO_2$54 + RO_2T	CO_2 + CO + HO_2 + RO_2T + O_2	k_{96}	
300	RPR1 + OH	$RO_2$55 + RO_2T + H_2O	See Table 1.6	8
301	RPR1 + NO_3	HNO_3 + $RO_2$55 + RO_2T	k_{61}*k_{300}/k_{60}	Estimated *k*
302	RPR1 + $h\nu$	CO + HO_2 + $RO_2$20 + RO_2T	See Table 1.3	1
303	$RO_2$55 + NO	NO_2 + CO_2 + $RO_2$20 + RO_2T	k_{125}	
304	$RO_2$55 + NO_2 + M	PAN7 + M	k_{126}	
305	PAN7	NO_2 + $RO_2$55 + RO_2T	k_{127}	
306	$RO_2$55 + HO_2	O_3 + UR1	k_{94}	
307	$RO_2$55 + RO_2T	CO_2 + $RO_2$20 + RO_2T + O_2	k_{96}	
308	RPR2 + OH	O_3 – HO_2 + UR2 + H_2O	k_{82}	
309	RPR3 + OH	$RO_2$56 + RO_2T + H_2O	See Table 1.6	8
310	RPR3 + NO_3	HNO_3 + $RO_2$56 + RO_2T	k_{61}*k_{309}/k_{60}	Estimated *k*
311	RPR3 + $h\nu$	CO + 2 HO_2 + UR4	See Table 1.3	1
312	$RO_2$56 + NO	NO_2 + CO_2 + HO_2 + UR4	k_{125}	
313	$RO_2$56 + NO_2 + M	PAN8 + M	k_{126}	
314	PAN8	NO_2 + $RO_2$56 + RO_2T	k_{127}	
315	$RO_2$56 + HO_2	O_3 + UR3	k_{94}	
316	$RO_2$56 + RO_2T	CO_2 + HO_2 + UR4 + RO_2T + O_2	k_{96}	
317	RPR4 + NO_3	HNO_3 + RAD8	3.77E-12	2
318	RAD8 + NO_2	UR22 + H_2O	2.30E-11*EXP(151.0/TEMP)	2
319	RPR5 + OH	O_3 – HO_2 + UR14 + H_2O	k_{82}	
320	RPR6 + OH	O_3 – HO_2 + RPR7 + H_2O	k_{82}	
321	RPR7 + OH	O_3 – HO_2 + ADAC + H_2O	k_{82}	
322	RPR8 + OH	$RO_2$57 + RO_2T + H_2O	See Table 1.6	8
323	RPR8 + NO_3	HNO_3 + $RO_2$57 + RO_2T	k_{61}*k_{322}/k_{60}	Estimated *k*
324	RPR8 + $h\nu$	CO + HO_2 + $RO_2$9 + RO_2T	See Table 1.3	1
325	RPR8 + $h\nu$	HO_2 + $RO_2$57 + RO_2T	See Table 1.3	1
326	$RO_2$57 + NO	NO_2 + CO_2 + $RO_2$9 + RO_2T	k_{125}	

Table 1.2 (cont.) Reactions contained in the Caltech Atmospheric Chemistry Mechanism

Reaction	Reactants	Products	Rate Constants (cm-molecule-sec units)*	References, Comments
327	$RO_2$57 + NO_2	PAN9	k_{126}	
328	PAN9	NO_2 + $RO_2$57 + RO_2T	k_{127}	
329	$RO_2$57+ HO_2	UR23 + O_3	k_{94}	
330	$RO_2$57 + RO_2T	CO_2 + $RO_2$9 + 2 RO_2T + O_2	k_{96}	
331	RPR9 + OH	O_3 – HO_2 + RP17 + H_2O	See Table 1.6	8
332	RP10 + OH	HO_2 + UR24 + H_2O	See Table 1.6	8
333	RP10 + $h\nu$	UR25	See Table 1.3	1
334	RP11 + OH	O_3 – HO_2 + UR26 + H_2O	See Table 1.6	8
335	RP12 + OH	O_3 – HO_2 + RP13 + H_2O	See Table 1.6	8
336	RP13 + OH	O_3 – HO_2 + RP18 + H_2O	See Table 1.6	8
337	RP14 + OH	O_3 – HO_2 + RP19 + H_2O	See Table 1.6	8
338	RP15 + OH	O_3 – HO_2 + UR27 + H_2O	See Table 1.6	8
339	RP16 + OH	$RO_2$58 + RO_2T + H_2O	k_{263}	
340	RP16 + NO_3	HNO_3 + $RO_2$58 + RO_2T	k_{264}	
341	RP16 + $h\nu$	2 CO + OH + HO_2	See Table 1.3	1
342	$RO_2$58 + NO	CO + CO_2 + NO_2 + OH	k_{125}	
343	$RO_2$58 + NO_2 + M	PN10 + M	k_{126}	
344	PN10	NO_2 + $RO_2$58 + RO_2T	k_{127}	
345	$RO_2$58 + HO_2	O_3 + UR28	k_{94}	
346	$RO_2$58 + RO_2T	CO + CO_2 + OH + RO_2T + O_2	k_{96}	
347	RP17 + OH	O_3 – HO_2 + UR29 + H_2O	See Table 1.6	8
348	RP18 + OH	O_3 – HO_2 + UR30 + H_2O	See Table 1.6	8
349	RP19 + OH	O_3 – HO_2 + UR31 + H_2O	See Table 1.6	8
350	AP1 + OH	NO_2 + RPR2 + H_2O	See Table 1.6	8
351	AP2 + OH	NO_2 + UR16 + H_2O	See Table 1.6	8
352	AP3 + OH	NO_2 + UR32 + H_2O	See Table 1.6	8
353	AP4 + OH	NO_2 + ARAL + H_2O	See Table 1.6	8
354	AP5 + OH	NO_2 + RPR6 + H_2O	See Table 1.6	8
355	AP6 + OH	NO_2 + RPR7 + H_2O	See Table 1.6	8
356	AP7 + OH	NO_2 + RPR3 + H_2O	See Table 1.6	8
357	AP8 + OH	NO_2 + UR7 + H_2O	See Table 1.6	8
358	AP9 + OH	NO_2 + UR33 + H_2O	See Table 1.6	8
359	AP10 + OH	NO_2 + UR19 + H_2O	See Table 1.6	8
360	AP11 + OH	NO_2 + UR34 + H_2O	See Table 1.6	8
361	AP12 + OH	NO_2 + UR20 + H_2O	See Table 1.6	8

*If reaction rates depend on concentrations of M or O_2, these rate constants already take this into account by multiplying by the appropriate factor. The host model requires rate constants in ppm-min units. For example, to convert from cm^3 $molecule^{-1}$ s^{-1} to ppm^{-1} min^{-1}, multiply by 4.4E+17/TEMP. The CF(*i*) factors represent product stoichiometric yields estimated or determined kinetically: CF(1), CF(2), CF(39), CF(40), and CF(45)-CF(47) [*Kwok and Atkinson*, 1995]; CF(9)-CF(16) [*Japar et al*, 1990]; and all others [*Carter and Atkinson*, 1989]. Rate constant references: 1. *Harley et al.* [1993]/*Lurmann et al*. [1987]; 2. *Carter* [1997, 1999]; 3. *Dransfield et al.* [1999]; 4. *Atkinson* [1994]; 5. *Atkinson* [1997]; 6. *Atkinson* [1990]; 7. *Japar et al.* [1990]; 8. *Kwok and Atkinson* [1995]; 9. *Hoffmann et al.* [1997]; 10. *Goumri et al*. [1992]; 11. *Jenkin et al.* [1997]; 12. *Stockwell et al.* [1997]; 13. *Lay et al.* [1996].

Table 1.3 Photolysis Rate Constants (shown for 3PM, August 27, 1987 in Los Angeles: 34.058ºN, 118.25ºW) *

Photolyzed Species (Reaction #)	Products	Typical Value of j_i (sec^{-1})	Comments
NO_2 (1)	NO + O	6.68E-3	
NO_3 (13)	NO + O_2	1.65E-2	
NO_3 (14)	NO_2 + O	1.45E-1	
O_3 (15)	O + O_2	3.90E-4	
O_3 (16)	OSD + O_2	1.66E-5	
HONO (20)	0.9 NO + 0.1 NO_2 + 0.1 HO_2 + 0.9 OH	1.30E-3	
H_2O_2 (36)	2 OH	5.07E-6	
HCHO (44)	HO_2 + CO	1.97E-5	
HCHO (45)	CO + H_2	3.38E-5	
ALD2 (59)	CO + HO_2 + $RO_2$5 + RO_2T	4.45E-6	
KETL (63)	$RO_2$5 + $RO_2$8 + 2 RO_2T	9.37E-7	
KETH (71)	$RO_2$5 + $RO_2$8 + 2 RO_2T	9.37E-7	assumed equal to j_{KETL}
MGLY (265)	CO + HO_2 + $RO_2$8 + RO_2T	1.32E-4	
RPR1 (302)	CO + HO_2 + $RO_2$20 + RO_2T	4.45E-6	assumed equal to j_{ALD2}
RPR3 (311)	CO + 2 HO_2 + UR4	4.45E-6	assumed equal to j_{ALD2}
RPR8 (324)	CO + HO_2 + $RO_2$9 + RO_2T	4.45E-6	assumed equal to j_{ALD2}
RPR8 (325)	HO_2 + $RO_2$57 + RO_2T	4.45E-6	assumed equal to j_{ALD2}
RP10 (333)	UR25	4.45E-6	assumed equal to j_{ALD2}
RP16 (341)	CO + OH + HO_2	1.32E-4	assumed equal to j_{MGLY}

*Photolysis rate constants as a function of zenith angle are calculated by integrating over ultraviolet wavelengths the product (actinic irradiance * absorption cross section * quantum yield). Zenith angles are geometrically calculated based on the percentage of daylight that has passed. Cross sections and quantum yields are described in *McRae* [1981] and *Lurmann et al*. [1987].

Table 1.4 Three-Body Kinetics Rate Constant Calculations*

Reaction	k_o^{300}	n	k_{inf}^{300}	m	F
4	9.0E-32	2	2.2E-11	0	0.8
9	2.8E-30	3.5	2.0E-12	0.2	0.45
10	Equilibrium with (9)				
19	7.0E-31	2.6	3.6E-11	0.1	0.6
22†	2.85E-30	2.67	3.13E-11	0	See below
27	1.8E-31	3.2	4.7E-12	0	0.6
28	Equilibrium with (27)				
35	4.1E-31	3.3	2.0E-12	0	0.45
126	9.7E-29	5.6	9.3E-12	1.5	0.6
127	Equilibrium with (126)				

*Three-body rate constants at temperature T (K) and pressure corresponding to [M] (molecule cm^{-3}) are found via the following formulae:

$$k_o(T) = k_o^{300}(T)\left(\frac{T}{300}\right)^{-n} \text{ (cm}^6 \text{ molecule}^{-2} \text{ s}^{-1}\text{)}$$

$$k_{inf}(T) = k_{inf}^{300}(T)\left(\frac{T}{300}\right)^{-m} \text{ (cm}^3 \text{ molecule}^{-1} \text{ s}^{-1}\text{)}$$

$$k(T, z) = \left(\frac{k_o(T)[M]}{1+\left(k_o(T)[M]/k_{inf}(T)\right)}\right) F^{\left(1+\left[\log_{10}\left(k_o(T)[M]/k_{inf}(T)\right)\right]\right)^{-1}} \text{ (cm}^3 \text{ molecule}^{-1} \text{ s}^{-1}\text{)}$$

†The rate constant expression for reaction 22 has small correction factors incorporated into it. It is found as in *Dransfield et al*. [1999].

Table 1.5 Other Rate Constant Calculations

Reaction	Expression*	k_1	k_2	k_3
23	a	7.2E-15*EXP(785.1/TEMP)	4.1E-16*EXP(1439.4/TEMP)	1.9E-33*EXP(724.7/TEMP)
24	b	1.3E-13	3.19E-33	-
31	b	2.2E-13*EXP(598.9/TEMP)	1.85E-33*EXP(981.4/TEMP)	-
32†	b	3.08E-34*EXP(2798.2/TEMP)	2.59E-54*EXP(3180.7/TEMP)	-

*Three-body rate constants at temperature TEMP (K) and pressure corresponding to [*M*] (molecule cm^{-3}) are found via the following formulae:
a) k (cm^3 $molecule^{-1}$ s^{-1}) = $k_1 + k_2[M]$ or b) k (cm^3 $molecule^{-1}$ s^{-1}) = $k_1 + k_3[M](1 + k_3[M]/k_2)$
†Reaction 32 is third order.

Table 1.6 Hydroxyl Radical Rate Constants Calculated Using a Structure-Reactivity Relationship [*Kwok and Atkinson*, 1995]. [*] See below for a simple example calculation.

Reaction	$k*10^{10}$ (cm^3 $molec^{-1}$ s^{-1}) at 300 K	Reaction	$k*10^{10}$ (cm^3 $molec^{-1}$ s^{-1}) at 300 K
69 (ALCH)	0.128	338 (RP15)	0.130
70 (KETH)	0.051	347 (RP17)	2.195
73 (AROO)	2.264	348 (RP18)	1.970
74 (OLEH)	0.347	349 (RP19)	1.336
78 (ALKM)	0.103	350 (AP1)	2.202
80 (AROH)	0.152	351 (AP2)	0.054
83 (ARAC)	0.011	352 (AP3)	0.077
93 (ALKH)	0.197	353 (AP4)	0.331
300 (RPR1)	0.354	354 (AP5)	0.132
309 (RPR3)	0.424	355 (AP6)	0.014
322 (RPR8)	1.145	356 (AP7)	0.305
331 (RPR9)	2.414	357 (AP8)	1.030
332 (RP10)	1.098	358 (AP9)	0.907
334 (RP11)	1.964	359 (AP10)	0.777
335 (RP12)	2.407	360 (AP11)	0.188
336 (RP13)	2.189	361 (AP12)	0.278
337 (RP14)	1.452		

[*] As shown in *Kwok and Atkinson* [1995], the rate constant for OH oxidation of an organic species is dependent on the number and type of structural components and the location of these groups relative to other groups. For example, ALKH is represented by *n*-hexadecane. There are three types of structural components associated with this molecule: $-CH_3$ positioned next to $-CH_2-$ (2), $-CH_2-$ positioned between $-CH_3$ and $-CH_2-$ (2), and $-CH_2-$ positioned between other $-CH_2-$ (14). The rate constant of ALKH is found from $k_{ALKH} = 2k_{CH_3} f_{CH_2} + 2k_{CH_2} f_{CH_3} f_{CH_2} + 14k_{CH_2} f_{CH_2}^2$ where k_i represents a rate constant for group i and f_i represents a temperature dependent substituent factor. In this case, $k_{CH_3} = 4.49 * 10^{-18} T^2 e^{-320/T}$ (cm^3 $molecule^{-1}$ s^{-1}), $k_{CH_2} = 4.50 * 10^{-18} T^2 e^{-253/T}$ (cm^3 $molecule^{-1}$ s^{-1}), $f_i = e^{E_i/T}$ (dimensionless), $E_{CH_3} = 0$ (K), and $E_{CH_2} = 61.69$ (K). The parameters for k_i and f_i for unsaturated bonds and most functional groups also exist.

Table 1.7 Emissions Summary in 10^3 kg/day used in CIT for August 27, 1987

	NMHC	NO_x	CO
On Road Vehicles	1229	678	4743
Other Mobile Sources	601	244	730
Ground-level Point Sources	379	123	139
Biogenic Emissions	110	--	--
Other Elevated Point Sources	6	60	8
Power Plants	1	33	6
Total	2326	1138	5626

Table 1.8 Upwind Boundary Condition Concentrations (ppb)

Species		
CO		200
NO_2		1
NO		1
HCHO		3
ALD2		5
KETL		4
O_3		40
NMHC (ppb C)		100
Speciation*:	ALKL	0.095
	ETHE	0.017
	OLEL	0.018
	AROH	0.015
	AROL	0.016

*Speciation in ppbv per ppb C of NMHC

Table 1.9 Statistical Analysis of CACM performance on August 28 for O_3 and NO_2

Statistical Measure	O_3	NO_2
Bias (ppb)	15.9	-0.4
Normalized Bias (%)	21.7	12.6
σ of Residuals (ppb)	55.3	28.1
Gross Error (ppb)	39.5	21.4
Normalized Gross Error (%)	41.1	51.6

Chapter 2

Secondary organic aerosol: II. Thermodynamic model for gas/particle partitioning of molecular constituents

2.1 Introduction

Organic aerosol (OA) is a significant constituent of particulate matter (PM) [*Stevens et al*., 1984; *White and Macias*, 1989; *Penner*, 1995; *United States Environmental Protection Agency*, 1996; *Murphy et al*., 1998]. For example, in major urban areas such as Philadelphia, Los Angeles, and Chicago, OA has been observed to make up as much as one half of the mass of the measured PM [*United States Environmental Protection Agency*, 1996]. OA can be both primary (POA, emitted as aerosol) and secondary (SOA, formed *in situ* in the atmosphere as condensable vapors). Sources of POA include, among others, combustion processes [*Schauer*, 1998; *Schauer et al*., 1999ab]. SOA is formed as a result of the oxidation of both anthropogenic and biogenic organic species [*Odum et al*., 1996, 1997; *Hoffmann et al*., 1997; *Griffin et al*., 1999]. Oxidation of these species leads to the formation of products that tend to contain a high degree of functionality, including hydroxy, carbonyl, carboxy, nitrooxy, and nitro groups. (See, for example, *Atkinson*, [1994, 1997] and references therein, *Smith et al*. [1999], and *Yu et al*. [1999].) Those products with sufficiently low vapor pressures will partition between the gas and aerosol phases, forming SOA and contributing to the overall PM burden. Some of these products may also partition to the aerosol aqueous phase [*Saxena and Hildemann*, 1996].

Inorganic aerosol thermodynamic equilibrium models are now incorporated in atmospheric aerosol models. (See, for example, *Jacobson et al*. [1997], *Ansari and Pandis* [1999], and *Zhang et al*. [2000] and references therein.) Because of the large number of organic compounds in the atmosphere and because methods to predict their thermodynamic properties in complex organic-water mixtures pose significant theoretical challenges, current gas-aerosol thermodynamic models for organic atmospheric species do not include the same level of detail as those for inorganic species. Experimentally based gas-particle distribution factors for complex mixtures generated by the photooxidation of aromatic and biogenic hydrocarbons are available [*Odum et al*., 1996, 1997; *Hoffmann et al*., 1997; *Griffin et al*., 1999]. The goal is, however, a fundamentally based thermodynamic model that predicts the phase partitioning of individual organic compounds between the gas phase and condensed-phase organic-inorganic-water mixtures. Such a model would afford a first-principles prediction of the amount of OA formed from secondary species in the atmosphere.

This paper presents a module that predicts the equilibrium partitioning of SOA and that is designed for use in a three-dimensional atmospheric model. Concentrations of secondary organic oxidation products predicted by a gas-phase chemical mechanism (Part I, *Griffin et al.* [2001]) are partitioned between the gas and aerosol phases by this module. The equilibrium partitioning module will be incorporated in a comprehensive gas- and particle-phase air quality model for simulations of a 1993 smog episode in the South Coast Air Basin (SoCAB) of California (Part III).

2.2 Review of Previous Techniques to Model SOA

Atmospheric models have been developed that include some treatment of SOA formation [*Jacobson et al*., 1997; *Lurmann et al*., 1997; *Meng et al*., 1998; *Sun and Wexler*, 1998; *Pai et al*., 2000]. The current approaches used to model SOA formation, however, fail to provide a

fundamental treatment of the gas/partitioning processes over a wide range of conditions. Detailed gas-phase mechanisms for SOA formation that have been developed have been limited to chemical systems studied in smog chamber experiments [*Barthelmie and Pryor*, 1999; *Kamens et al*., 1999].

2.2.1 Fractional Aerosol Coefficient

The simplest method that attempts to account for the conversion of a given parent species from the gas phase to oxidation products in the particle phase is based on the fractional aerosol coefficient (FAC). The FAC is defined as the ratio of the SOA formed from a parent organic to the initial amount of that parent species present in a chamber experiment [*Grosjean*, 1992]. The FAC method does not take into account the time needed to form SOA in the atmosphere or the concentrations of available oxidants. Therefore, the amount of the parent species that reacts is not treated explicitly. Because the technique considers no kinetics, SOA can be treated as if it were emitted. As a result, the FAC applies only to conditions for which it was derived; FAC values do not take into account temperature, relative humidity, or initial particle concentrations. Thus, FAC values cannot provide realistic SOA estimates for air quality modeling.

2.2.2 Fixed Aerosol Yield

A second method for estimating SOA formation based on the concentrations of precursors is to assume a fixed SOA yield for a given parent organic. In contrast to the FAC, this approach takes into account the time needed to form SOA, and the yield is defined as the amount of organic aerosol mass that forms per amount of the parent organic mass that reacts [*Pandis et al*., 1992]. Thus, this method takes the reactivity of the parent organic and the availability of oxidants into account. The limitations associated with estimating SOA formation using this method are that there is no dependence of the yield on the existing particle phase, temperature, or relative humidity. Given that yield depends on these variables, it is difficult to determine which experimentally determined yield is the most appropriate to use when modeling conditions vary temporally and spatially and deviate significantly from smog chamber conditions.

2.2.3 Saturation of Oxidation Products

It has been assumed in earlier work that a product formed from the oxidation of a parent organic condenses into the particle phase only when its saturation vapor pressure has been reached [*Pandis et al*., 1992]. The amount of SOA formed is thus defined as the difference between the amount of the product that forms and that product's saturation concentration. Attempts have been made to account for the dependence of saturation vapor pressure on temperature through the Clausius-Clapeyron equation and an estimated heat of vaporization that must be determined experimentally [*Strader et al*., 1999].

2.2.4 Absorptive Partitioning

Recent theoretical derivations and experimental studies have shown that the formation of organic aerosol under dry conditions is best described by a dynamic equilibrium for species that exist in both the gas- and aerosol phases [*Pankow*, 1994ab; *Odum et al*., 1996, 1997; *Hoffmann et al*., 1997; *Griffin et al*., 1999; *Pankow et al*., 2001]. This equilibrium is based on absorptive (incorporation into the bulk) as opposed to adsorptive (adhesion to the aerosol surface) partitioning [*Liang et al*., 1997]. It can be described by a partitioning coefficient that depends on

temperature, the average molecular weight of the absorbing aerosol, the activity coefficient of the partitioning species in the condensed phase, and the vapor pressure of the species. Calculation of partitioning coefficients requires knowledge of the chemical identities and properties of all species in the condensed phase. Because of the equilibrium established between the gas and particle phases, species can partition to the absorbing organic phase at concentrations below their individual saturation vapor pressures. The partitioning of an SOA constituent also is enhanced by the presence of additional POA or SOA species [*Pankow*, 1994ab].

Smog chamber studies have extended the theory of *Pankow* [1994ab] and linked it to the SOA yield [*Odum et al*., 1996, 1997; *Hoffmann et al*., 1997; *Griffin et al*., 1999]. In such studies, multiple products are formed in constant stoichiometric yield from the oxidation of a parent organic and then partition between an absorptive organic aerosol phase and the gas phase. Analysis of a series of experiments with a given parent allow for the estimation of average stoichiometric factors and partitioning coefficients for the resulting product mix. It has been shown that two surrogate products (described by two mass-based stoichiometric parameters and two equilibrium partitioning coefficients) adequately represent observed aerosol formation from the complex mixture of products resulting from oxidation of a given parent organic [*Odum et al*., 1996]. While this technique avoids the necessity of chemical identification and characterization, a limitation of this technique is that these parameters are derived using smog chamber experimental data, which may not be robustly extended to the atmosphere. Smog chamber concentrations usually exceed ambient concentrations, and only minimal information regarding the effects of increased humidity and variable temperature are available [*Cocker et al*., 2001].

2.2.5 Henry's Law

One approach used to approximate the formation of SOA in models describing regional air quality is to assume that the secondary organic compounds associated with PM are absorbed into only the aqueous phase. This absorption is governed by Henry's law [*Jacobson et al*., 1997; *Aumont et al*., 2000], and activity coefficients of organic solutes are typically assumed to be unity. In this manner, only water-soluble organic species are taken into account; those that partition via condensation (absorption into an organic medium or adsorption to aerosol surfaces) are ignored. Once the liquid water content (LWC) of an existing aerosol is assumed or calculated, the amount of OA present in the particle phase is calculated using Henry's law. If the Henry's law coefficient has not been measured, it is assumed that it can be derived using a group contribution method if the structure of the organic compound of interest is known [*Hine and Mookerjee*, 1975; *Suzuki et al*., 1992]. In addition to considering only those organics that are water-soluble, a limitation associated with this technique is that Henry's law, without activity correction, applies only for solutions that are dilute, which is generally an irrelevant condition for ambient aerosols.

2.3 Partitioning Model

The purpose of this work is to develop a thermodynamic model for the phase- and composition distribution of both inorganic and organic aerosol constituents. A major feature of the model is the distinction between those organic oxidation products that are considered hydrophilic (water-soluble organic compounds, WSOC) and those that are considered hydrophobic. This is done for three reasons: to simplify the set of equations that need to be solved simultaneously (thereby reducing computational demand), to avoid unrealistically high activity coefficients that would result if hydrophobic and hydrophilic species were forced to

reside in the same condensed phase, and to more accurately account for dissociation of acidic hydrophilic compounds. Because of the large number of atmospheric organic compounds that fall into each of these categories, for application to three-dimensional atmospheric models it is necessary to choose surrogate compounds to represent each group. These surrogates will be described in Section 4, which describes implementation of the SOA module into three-dimensional models.

In the following module description, the following definitions will be used. POA species are emitted directly to the atmosphere and are considered completely non-volatile. Such species act as partitioning media for hydrophobic SOA species and have no associated particulate water. SOA species are formed only by gas-phase oxidation of volatile organic compounds and are described here as being semi-volatile. There is, of course, the possibility that primary semi-volatile species are emitted in both the particle and gas phases. This fact will be taken into account in emissions inventories when the module described here is incorporated for use in a three-dimensional atmospheric model.

SOA species can be further subdivided (hydrophobic or hydrophilic) based on the predominant partitioning mechanism. Hydrophobic SOA constituents partition via absorption into an organic phase consisting of POA and other SOA species (condensation due to low volatility). Hydrophilic OA constituents interact with inorganic aerosol constituents such as nitrate, sulfate, ammonium, etc.; therefore, the module that has been developed to predict dissolution of WSOC is used in conjunction with an inorganic gas-aerosol equilibrium model such as SCAPE2 [*Kim et al*., 1993; *Meng et al*., 1995] or ISORROPIA [*Nenes et al*., 1998], which predict the equilibrium distribution of inorganic aerosol constituents and the corresponding aerosol LWC and pH. Just as molecular and ion solutes are treated in SCAPE2 or ISORROPIA, the hydrophilic group of organic compounds is divided into two subgroups: electrolytes and molecular solutes. However, because data describing the equilibrium in mixed inorganic/organic/aqueous systems largely do not exist [*Macedo et al*., 1990; *Kikic et al*., 1991; *Clegg et al*., 2001], the inorganic and organic fractions are, at present, treated separately, coupled only through the LWC and pH of the aerosol. At this time, due to the lack of this information, this is deemed the most appropriate approach for the development of a first-generation SOA module. When data on such inorganic/organic/aqueous systems become available, the SOA module will be appropriately updated. Figure 2.1 shows the categorization of ambient constituents, inorganic and organic, modeled in the entire aerosol module.

2.3.1 Hydrophobic Module

The partitioning of compound *i* between the gas- and particle phases can be described by defining a partitioning coefficient, K_i ($m^3\ \mu g^{-1}$) (*Pankow* [1994ab]),

$$K_i = \frac{A_i / \mathrm{TSP}}{G_i} \qquad (1)$$

where A_i ($\mu g\ m^{-3}$ air) is the concentration of the compound in the aerosol phase, G_i ($\mu g\ m^{-3}$ air) is the concentration of the compound in the gas phase, and TSP ($\mu g\ m^{-3}$ air) is the concentration of total suspended PM. This partitioning coefficient describes the equilibrium phase distribution of compound *i* when both adsorptive and absorptive partitioning occur. As stated previously, it has been demonstrated that absorption is the dominant mode of partitioning for organic species in the urban environment [*Liang et al*., 1997]. To derive an expression for an equilibrium

coefficient for absorptive partitioning, only that aerosol mass that is part of an absorptive organic mixture is taken into account,

$$K_{i,om} = \frac{A_{i,om} / M_o}{G_i} \qquad (2)$$

where the subscript *om* represents the absorbing organic phase, and M_o (μg m^{-3} air) is the total concentration of the absorptive material (both POA and SOA) in the *om* phase. M_o is assumed to be equal to the product of f_{om} and TSP, where f_{om} is the absorptive organic fraction of the PM. Because POA species have no associated water and the SOA species that partition to POA are hydrophobic, M_o does not include water in the work discussed here.

To develop a thermodynamic expression for $K_{i,om}$, the concentration variables in equation (2) are converted to molar units, the ideal gas law is applied, Raoult's Law is invoked, and the definition of mole fraction is incorporated. A more detailed derivation can be found in *Pankow* [1994ab]. The resulting expression is

$$K_{i,om} = \frac{760RT}{10^6 \overline{M}_{om} \gamma_i p^o_{L,i}} = \frac{A_{i,om} / f_{om}\,\mathrm{TSP}}{G_i} = f(T, x_i) \qquad (3)$$

where R is the ideal gas constant (0.82 m^3 atm mol^{-1} K^{-1}), T (K) is the absolute temperature, $\overline{M}_{om}$ is the average molecular weight (g mol^{-1}) of the *om* phase, γ_i is the activity coefficient of species i in the *om* phase (pure solvent reference state) and $p^o_{L,i}$ (torr) is its sub-cooled liquid vapor pressure at the temperature of interest.

It is seen in equation (3) that the absorptive partitioning of a compound between an *om* phase and the gas phase is strictly a function of temperature (explicitly and implicitly through vapor pressure) and the composition (through both the average molecular weight and the activity coefficient) of the *om* phase. Assuming vapor pressures are known or can be estimated for a given temperature [*Myrdal and Yalkowsky*, 1997] and that activity coefficients can be estimated, e.g. by a group contribution method such as UNIFAC [*Fredenslund et al*., 1977; *Pankow et al*., 2001], it is possible to predict the fraction of each compound (i = 1 to n, where n is the number of condensable compounds) that resides in each phase. This is done by solving iteratively a set of implicit simultaneous equations that includes equation (2), equation (3), a mass-balance for each compound (the set total concentration of compound i is equal to the sum of its gas- and particle phase concentrations), and the fact that the sum of $A_{i,om}$ values plus all POA concentrations must equal M_o. These constraints make modeling SOA formation via thermodynamic principles feasible as the number of equations reduces to n, with n unknowns (each $A_{i,om}$).

The hydrophobic module is shown schematically in Figure 2.2. Required inputs include the concentration and composition of any non-volatile POA and the total concentrations of the secondary hydrophobic OA constituents. Again, POA species are considered non-volatile, meaning that they reside completely in the particle phase. (In three-dimensional applications it is assumed that a compound does not partition to the gas phase if it is emitted in the particle phase.) POA species, however, do play a key role in this module by contributing to M_o and $\overline{M}_{om}$ and by affecting activity coefficients. (POA species are included in the UNIFAC calculations.)

An initial distribution of the hydrophobic organics is assumed, to obtain a first approximation for the mass concentration (denoted $M_{o,1}$ in Figure 2.2) and composition of the absorbing OA, including POA species. The initial guess for the distribution is determined based on the volatility of the semi-volatile product being absorbed. From this composition, the average molecular weight of the absorbing phase can be calculated. This composition is also used in UNIFAC to calculate the activity coefficients of the POA and the partitioning hydrophobic species. With temperature and a vapor pressure (experimentally determined or estimated using a group contribution method such as that of *Myrdal and Yalkowsky* [1997]) defined, the next step is to calculate an absorptive partitioning coefficient as in equation (3) for each condensing species. Using these partitioning coefficients with $M_{o,1}$ and each individual total concentration (c_i in Figure 2.2), it is possible to calculate a new guess for each G_i based on this equilibrium (from equation (2)). A new $A_{i,om}$ value for each species is then found from a mass balance (c_i – the new guess for G_i). These $A_{i,om}$ values are compared to the initial guesses, and the n $A_{i,om}$ values become the iterated variables. Once the series of $A_{i,om}$ values no longer changes by more than a prescribed small value, the calculations of the hydrophobic module are complete. In these calculations, it is also ensured that the gas-phase concentrations of all compounds do not exceed their saturation vapor pressures.

2.3.2 Hydrophilic Module

Partitioning of WSOC between the gas and aqueous phases is governed by

$$H^{HL}{}_i = \frac{c_{w,i}}{p_i} = \frac{A_i \gamma^{HL}{}_i}{M_i(\mathrm{LWC})p_i} \tag{4}$$

where $H^{HL}{}_i$ (μM atm^{-1}) is the Henry's law constant of species i, determined, for example, by a group contribution method, $c_{w,i}$ is its aqueous phase concentration (μmol l^{-1} of water), and p_i (atm) is the gas phase partial pressure of species i. Here, A_i (μg m^{-3}) still represents the aerosol phase concentration of i, but in this case it refers to the aqueous phase. M_i is the molecular weight of the compound (g mol^{-1}), and $\gamma^{HL}{}_i$ is its activity coefficient in the aqueous mixture (infinite dilution reference state). LWC in this case has units of l of water per m^3 of air. The second half of this expression is a simple unit conversion from the conventional definition of a Henry's law constant (*Schwarzenbach et al*., 1993). For organic acids, solubility is enhanced by the dissociation of molecular solutes into ions, which is governed by equilibrium acid dissociation constants,

$$K_{a,i} = \{\mathrm{H^+}\}\{\text{ORG-Anion}_i\}/\{\mathrm{ORG}_i\} \tag{5}$$

where $K_{a,i}$ is the acid dissociation constant of organic species i (ORG_i) and the {} notation represents the activities of the species of interest. ORG-Anion_i represents the dissociation product. Acid dissociation constants can also be estimated by structure-activity relationships [*Harris and Hayes*, 1982; *Schwarzenbach et al*., 1993].

As shown in equation (4) above, the partitioning of WSOC depends on the activity coefficient of the species in the aqueous mixture. Such activity coefficients measure the deviation from ideality, which is usually significant for highly concentrated ambient aerosols. Various methods can be used to calculate the activity coefficients of ions (See *Kim et al*. [1993] for more detail.), each of which considers only inorganic ion-ion interactions. Limited data for

inorganic-organic ion-ion interactions are available [*Clegg et al*., 2001]. For molecular solutes, UNIFAC can be used to estimate activity coefficients. While UNIFAC was not designed for use with highly polar compounds such as those that are constituents of SOA, it is assumed here that the UNIFAC group contribution parameters for functionalities such as COOH, CHO, CH_2, etc. can be applied to the surrogate molecules. Some parameters are available to treat the interactions between molecular groups and inorganic ions within the UNIFAC framework (e.g., *Kicic et al*. [1991] and *Yan et al*. [1999]). Unfortunately, key inorganic components in the atmosphere, such as ammonium and sulfate, are not included in these studies.

Ideally, the aerosol system would be treated as an interacting mixture of inorganics, organics, and water [*Clegg et al*., 2001]. Because of the lack of experimental data, however, traditional methods of estimating activity coefficients cannot be used for interactions between inorganic and organic ions. Therefore, a number of assumptions must be made. Most importantly, it is assumed that inorganic and organic solutes do not interact. This allows for the decoupling of the organic partitioning of WSOC from the inorganic model (e.g., SCAPE2), in terms of calculating activity coefficients. Also as a result of this assumption, the formation of organic-inorganic salts is not represented. Second, it is assumed that the activity coefficients of organic ions are equivalent to those of the corresponding molecular solute. These are clearly approximations, the validity of which future work must address. At this point, they are deemed appropriate for development of a first-generation inorganic/organic model.

The LWC of the aerosol is also a key parameter in determining the Henry's Law partitioning of WSOC. Because of its simplicity, the Zdanovskii-Stokes-Robinson (ZSR) method is used in three-dimensional atmospheric models to determine the water content of the aerosol solution. (See, for example, *Meng et al*. [1998].) The basic assumption of the ZSR method is that the quantities of water associated with each solute are additive. Therefore, LWC (here, μg water m^{-3} air) is defined by

$$\mathrm{LWC} = \sum_i \frac{m_i}{m_{i0}(a_w)} \tag{6}$$

where m_i is the molar concentration of species i (mol i m^{-3} of air) and $m_{i0}(a_w)$ is the molality of species i (mol i μg^{-1} water) in a binary mixture at the water activity of interest (a_w). Although polynomial fits for inorganic solute concentrations as a function of water activity have been developed by *Kim et al*. [1993] and *Meng et al*. [1995] based on experimental data, this approach is not possible for organic solutes due to lack of activity measurements. An estimation method must be used to determine water activities for binary or multicomponent organic systems. In this regard, UNIFAC can be used to determine the molality of organic solutions at specific water activity, which is equal to the relative humidity at equilibrium [*Saxena and Hildemann*, 1996]. The water associated with the inorganic and organic components is then considered and used in equation (6) to determine the LWC of the aerosol of interest.

The hydrophilic module is shown schematically in Figure 2.3. The required inputs for the hydrophilic module include the SCAPE2 output (LWC and the concentration of hydrogen ions) and the total concentrations of the partitioning secondary hydrophilic organics. The first step in the hydrophilic module is to determine the type of calculation that must be performed. If there is no existing aqueous phase, a calculation using both hydrophilic and hydrophobic species in the hydrophobic module (termed here a saturation calculation) is performed. This is because there is no LWC into which hydrophilic SOA compounds can partition; dissociation cannot be

taken into account in this case. This situation is highly unlikely to occur in the ambient. Subsequent to this saturation calculation, if the relative humidity (RH) is below the deliquescence relative humidity (DRH) of all WSOC species present, the organic phase remains dry. Conversely, if RH is greater than the DRH of any of the hydrophilic species, a new aqueous phase is formed. When a new aqueous phase is formed, the inorganic aerosol remains unaffected since experimental data indicate that the presence of organics does not change the DRH of inorganic aerosol [*Cruz and Pandis*, 2000].

If an aqueous phase does exist at the start of the hydrophilic module calculation, a saturation calculation is performed only if RH is less than the DRH of all of the hydrophilic organic species. In such a case, the hydrophilic SOA compounds will not partition to the aqueous phase. This is again highly unlikely in the ambient. Otherwise, if RH is greater than the DRH of any species, an aqueous equilibrium calculation is performed. The equilibrium calculation involves simultaneously solving mass balance (total concentration, c_i, is equal to the sum of the concentrations in the gas- and aqueous phases), Henry's law (equation (4)), and acid dissociation equations for each species (both ions and molecules) (equation (5)).

Iteration (using a Newton line search method) is required because the activity coefficients are a strong function of the aerosol composition. Once equilibrium values based on the input LWC are reached, an organic-water system is considered to calculate the additional amount of water that is taken up as a result of the presence of the hydrophilic organics. (Recall that RH is greater than at least one DRH in this scenario.) If the change in LWC is significant, the new total LWC and the concentrations of organic ions are passed to SCAPE2 to determine if the distribution of the inorganic aerosol constituents is affected. If this change in LWC is insignificant, the output from the hydrophilic module includes the phase distribution of inorganic aerosol constituents, the phase distribution of hydrophilic organic aerosol constituents, and the LWC of the aerosol. In this regard, LWC is used as an iterative variable that must be consistent between the inorganic and hydrophilic modules.

Similar to the work presented by *Seinfeld et al*. [2001], the hydrophilic module described here will predict an increase in SOA formation as a result of an increase in the LWC of the aerosol through an increase in RH. This is due to the affinity for water exhibited by each of the compounds classified as hydrophilic. There is no interaction between the hydrophobic and hydrophilic fractions of the organic aerosol. Therefore, the partitioning of hydrophobic SOA constituents is not affected by RH as described by *Pankow et al*. [1993]. However, in that study, in contrast to the present one, the authors were investigating the partitioning only of hydrophobic, non-polar compounds.

2.3.3 Case Studies

In order to demonstrate the hydrophobic portion of the model, we define a surrogate SOA compound and a prescribed mixture of POA constituents. These POA species are used only for the evaluation of the hydrophobic module and are only used for illustrative purposes. They will not be used when the SOA module is incorporated into three-dimensional atmospheric models, as described in Section 4.

Representative POA constituents have been reported, for example, based on measurements made in the Los Angeles Basin [*Rogge et al*., 1993] and the San Joaquin Valley of California [*Schauer and Cass*, 1998]. Major classes of organic compounds resolved in the analysis of OA include fatty acids, substituted phenols, aromatic acids, alkanes, and, for the San Joaquin Valley, levoglucosan and other sugar derivatives. Surrogate POA constituents,

excluding those that were shown to have affinity toward the aqueous phase, are chosen from this group based on their observed predominance in the ambient samples described above (Table 2.1). Octadecanoic acid is selected as the surrogate hydrophobic SOA constituent.

The first variable investigated in the evaluation of the hydrophobic module is TSP (with initial f_{om} set to 0.1 for this study in order to match the value used by *Pankow* [1994ab]). For a fixed total amount of octadecanoic acid present (1 $\mu g\ m^{-3}$), increasing initial TSP (from 10 to 100 $\mu g\ m^{-3}$) and, therefore, the mass of each POA constituent (TSP*0.1*mass fraction given in Table 2.1), results in an increase in the amount of octadecanoic acid that partitions to the aerosol phase (A) from approximately 0.35 to 0.8 $\mu g\ m^{-3}$ (Figure 2.4). The resulting changes in average molecular weight and activity coefficients lead to a small decrease in the partitioning coefficient (K) of octadecanoic acid.

Partitioning can also be investigated when the total concentration of octadecanoic acid varies at total fixed TSP (50 $\mu g\ m^{-3}$, yielding 5 $\mu g\ m^{-3}$ of POA with mass fractions defined by Table 2.1). Naturally, increasing the concentration of octadecanoic acid leads to an increase in its amount partitioning to the aerosol phase (A) (Figure 2.5). Changes in the average molecular weight of the absorbing medium and the activity coefficients lead to modest increases in the partitioning coefficient (K) as the total acid concentration is increased.

In order to demonstrate the hydrophilic module, malic ($COOH\text{-}CH_2\text{-}CHOH\text{-}COOH$) and glyoxalic ($CHO\text{-}COOH$) acids are chosen as surrogate WSOC. The properties of these compounds are given in Table 2.2. Malic acid is very soluble; glyoxalic acid is only sparingly so. Table 2.3 shows the input conditions and predictions from the hydrophilic module when acting independent of any inorganic module. Because of its high solubility, virtually all of the malic acid partitions to the aqueous phase, with the ions being the dominant forms. Glyoxalic acid, on the other hand, tends to remain in the gas phase. For what little amount partitions to the aqueous phase, the ion is again the dominant form. The ionic form is prevalent because of the relatively high pH value used in this illustrative example. A change in LWC (ΔLWC) of 0.46 ng m^{-3} is observed due to the aqueous phase concentrations of the two acids and their ions.

If other initial conditions are held constant, the ΔLWC that results due to the dissolution of hydrophilic organics increases as RH increases (Figure 2.6). This is especially important for malic acid, which exhibits deliquescence behavior at approximately 79% RH. Below this humidity, no additional water is associated with the organic aerosol because of the presence of malic acid. Because malic acid is much more soluble, the amount of water associated with malic acid is much greater than that associated with glyoxalic acid, even though both compounds are present at the same total concentrations (gas and aerosol phase combined).

If other initial conditions are again held constant, sensitivity studies also show the overall importance of the aerosol pH (Figure 2.7). A lower aerosol pH affects the dissociation of acids, resulting in molecular solutes being favored over the ionized forms. An increased pH results in a higher effective Henry's law constant for the acids, yielding higher organic concentrations. This increase in the organic concentration also leads to an increase in ΔLWC. These effects are especially evident for glyoxalic acid. Because of the high solubility of malic acid, pH has little effect on the amount of water associated with this species.

The hydrophilic organic module was also evaluated in conjunction with SCAPE2, using both inorganic and WSOC constituents (Table 2.4). In this example, only limited inorganic species are present (ammonia and nitric acid) so that the interactions between inorganics and hydrophilic organics (malic and glyoxalic acids in this case) can be exhibited simply. There are two main effects of the organic solutes. First, the extra water associated with the WSOC induces

additional partitioning of the inorganics to the aqueous phase. Second, the decrease in pH favors the dissolution of basic gases (e.g., ammonia) as opposed to acidic gases (e.g., nitric acid). For example, in the case shown in Table 2.4, the final concentration of NH_4^+ is 0.078 μmol m^{-3}, while in the absence of organics, the concentration of NH_4^+ would be 0.064 μmol m^{-3}.

In each of the modules and in all of the cases tested, the typical number of iterations required was less than 10. While this number depends on the total concentrations of the partitioning compounds, even the most difficult cases converged in less than 20 iterations. The iterative calculations of activity in the aqueous phase are typically the most computationally demanding.

2.4 Implementation in Atmospheric Models

The integration of the aerosol module in an atmospheric model is depicted in Figure 2.8. This figure only describes module implementation needs for three-dimensional atmospheric models; Part III of this series of papers addresses module application. The first set of inputs includes total inorganic concentrations, relative humidity, and temperature. Computationally, this information is passed to the inorganic thermodynamic equilibrium module, the output from which includes the phase and composition distribution of the inorganics and the LWC and pH of the inorganic/water aerosol. If the LWC of the aerosol is zero at this point, a hydrophobic calculation is performed considering all (both hydrophobic and hydrophilic) semi-volatile organic oxidation products. At this point, water uptake of the hydrophilic products only is considered, and the aerosol calculations for the current time step are complete. On the other hand, if the LWC is non-zero after the inorganic calculations (which is the realistic atmospheric condition), its value and that of the pH are passed to the hydrophilic module, along with total concentrations of the hydrophilic organic oxidation products. After these products have been partitioned computationally and the water taken up as a result has been calculated, the total LWC is passed back to inorganic aerosol model to determine if the additional water and the presence of organic ions affect the distribution of the inorganic species. Once the LWC is internally consistent between the inorganic and the hydrophilic organic calculations, the hydrophobic module, which requires total concentrations of the POA constituents and the hydrophobic organic oxidation products, is called. Once the hydrophobic module (which is the last step of the aerosol calculations) determines the appropriate equilibrium distribution for the participating products, predictions include the LWC and the concentrations of all organic oxidation products and inorganic species in each phase.

In its three-dimensional application, the partitioning module is linked to a gas-phase chemical mechanism that predicts the concentrations of semi- or non-volatile organic oxidation products. The Caltech Atmospheric Chemistry Mechanism (CACM) involves over 190 species participating in over 360 reactions [*Griffin et al*., 2001]. As described in Part I, there are over 40 compounds specified in CACM that are considered capable of forming SOA because of their solubility or low vapor pressures. Predicting the partitioning of that number of species is likely to be too computationally demanding, especially in light of the lack of thermodynamic data for multi-functional organic species to support such a detailed speciation. Therefore, these secondary products are further lumped into one of ten groups. The first separation is made on the basis of affinity for water. An organic is considered water-soluble based on the length of the carbon chain ($\leq$ 7 carbons), its solubility (solubility $\geq$ 1g solute/100g water), and its effective Henry's law coefficient ($\geq 1 \times 10^6$ M atm^{-1}). Additionally, those species with 7 or more carbon atoms and three functional groups are considered water-soluble because these compounds exhibit

such a high degree of polarity [*Saxena and Hildemann*, 1996]. Compounds meeting these criteria are defined as hydrophilic and can be further subdivided by size (low or high carbon number), source (anthropogenic or biogenic), and dissociative properties (present only as molecular solutes or as both ions and molecules). This process results in five hydrophilic surrogates. The products from CACM that fall into each group are structurally averaged (number of carbon, number and type of functional groups, etc.) to determine the structure of the five surrogates to be used in the hydrophilic module. Five surrogates for the hydrophobic module were determined similarly. The hydrophobic compounds are divided based on source (anthropogenic versus biogenic), structure (aliphatic versus benzene-based versus naphthalene-based for anthropogenic species), and volatility (for benzene-based anthropogenic species). Reduction of the 42 compounds into 10 (the properties for which are determined using group contribution methods) allows for a substantial reduction in the computational demands of the partitioning module. The 10 resulting compounds and some of their characteristics are described in Table 2.5a. In some cases, the structure of a surrogate was difficult to determine because the averaging technique predicted a fractional number of certain functional groups. This is most important in surrogate B2, in which the aldehyde group could be replaced by either a hydroxy- or a nitro group. Table 2.6 shows the reduction of the CACM species into the ten SOA surrogates listed in Table 2.5a.

Unlike the evaluation studies described in Section 3.3, where the composition of the POA, the value of f_{om}, and the concentration of TSP are set, use within a three-dimensional model require chemically resolved POA emissions. In studies of the air quality in the SoCAB, for example, it has been determined that the organic fraction of aerosol emissions can be classified into 8 categories: *n*-alkanes, polycyclic aromatic hydrocarbons (PAH), oxygenated PAH, diacids, aliphatic acids, substituted monoaromatics, cyclic petroleum biomarkers (e.g., hopanes), and unresolved organic matter (characterized by highly cyclic and branched petroleum biomarkers) [*Schauer*, 1998]. For implementation of the SOA module into a three-dimensional model, the predominant species have been identified and their structures are used as surrogates for these classes. POA structures are needed for the hydrophobic module calculations of activity coefficients. Table 2.5b shows the structure and properties of the 8 compounds chosen for the SoCAB.

The final issue that must be addressed in implementing the module discussed here into three-dimensional models is how the lumping of SOA species for partitioning calculations affects gas-phase reactions. This is important because several of the participating species are reactive in the gas-phase. First, CACM predicts the mixing ratios (ppb) of the species considered capable of contributing to SOA formation. These are then converted to mass concentrations and appropriately summed to give the mass concentration of each surrogate according to the lumping shown in Table 2.6; at the same time, the mass fraction (χ_i) that each CACM product contributes to its surrogate is calculated. With the total summed mass concentration of each surrogate SOA molecule, the SOA partitioning module is called. Upon completion of this module, gas-phase mass concentrations of each lumped surrogate are available. These concentrations are then multiplied by the appropriate χ_i values to calculate the mass concentrations of each of the CACM species that remain in the gas phase. These individual gas-phase mass concentrations are then converted back to the mixing ratios needed in the gas-phase chemical mechanism. In this way, mass is conserved between CACM and the SOA module.

2.5 Discussion

Because experimental data on thermodynamic properties of mixed organic-inorganic aqueous solutions are sparse, many necessary assumptions have been made in the development of the partitioning model. First, if an organic species shows affinity for both the aqueous and organic phases, it is chosen as either hydrophobic or hydrophilic, which may result in the underprediction of its amount in the aerosol phase. If appropriate experimental data become available, compounds that display such behavior can be accounted for explicitly. Second, it is assumed that there is no interaction between aqueous phase inorganics and organics. As thermodynamic data become available, such interactions can be incorporated. Third, the ability of certain hydrophobic organic species to limit water uptake has not been taken into account. Any uncertainties associated with UNIFAC and other group contribution methods for estimating thermodynamic properties add to the uncertainty associated with the partitioning module. Despite these limitations, the current module represents the state-of-the-art for describing SOA formation in a three-dimensional atmospheric model.

References

Ansari, A.S., and S.N. Pandis, An analysis of four model predicting the partitioning of semivolatile inorganic aerosol components, *Aerosol Sci. Technol., 31*, 129-153, 1999.

Atkinson, R., Gas-phase tropospheric chemistry of volatile organic compounds: 1. Alkanes and alkenes, *J. Phys. Chem. Ref. Data, 26*, 215-290, 1997.

Atkinson, R., Gas-phase tropospheric chemistry of organic compounds, *J. Phys. Chem Ref. Data, Monograph 2*, 1994.

Aumont, B., S. Madronich, I. Bey, and G.S. Tyndall, Contribution of secondary VOC to the composition of aqueous atmospheric particles: A modeling approach, *J. Atmos. Chem., 35*, 59-75, 2000.

Barthelmie, R.J., and S.C Pryor, A model mechanism to describe oxidation of monoterpenes leading to secondary organic aerosol, *J. Geophys. Res., 104*, 23,657-23,669, 1999.

Clegg, S.L., J.H. Seinfeld, and P. Brimblecombe, Thermodynamic modeling of aqueous aerosols containing electrolytes and dissolved organic compounds, *J. Aerosol Sci., 32*, 713-738, 2001.

Cocker III, D.R., State-of-the-art chamber facility for studying atmospheric aerosol chemistry, *Environ. Sci. Technol., 35*, 2594-2601, 2001.

Cruz, C.N., and S.N. Pandis, Deliquescence and hygroscopic growth of mixed inorganic-organic atmospheric aerosols, *Environ. Sci. Technol., 34*, 4313-4319, 2000.

CRC Handbook of Physics and Chemistry, 77th edition, ed. by David R. Lide, CRC Press, Boca Raton, FL, 1997.

Fredenslund, A., J. Gmehling, and P. Rasmussen, *Vapor-Liquid Equilibrium Using UNIFAC*, Elsevier, Amsterdam, 1977.

Griffin, R.J., D.R. Cocker III, R.C. Flagan, and J.H. Seinfeld, Organic aerosol formation from the oxidation of biogenic hydrocarbons, *J. Geophys. Res., 104*, 3555-3567, 1999.

Griffin, R.J., D. Dabdub, and J.H. Seinfeld, Secondary organic aerosol: I. Atmospheric chemical mechanism for production of molecular constituents, *J. Geophys. Res.*, this issue, 2001.

Grosjean, D., *In situ* organic aerosol formation during a smog episode: estimated production and chemical functionality, *Atmos Environ., 26A*, 953-963, 1992.

Harris, J.C., and M.J. Hayes, Acid dissociation constant, In Lyman, W.J., W.F. Reehl, and D.H. Rosenblatt, eds., *Handbook of Chemical Property Estimation Methods; Environmental Behavior of Organic Compounds*, McGraw-Hill, New York, 1982.

Hine, J., and P.K. Mookerjee, The intrinsic hydrophilic character of organic compounds: correlations in terms of structural contributions, *J. Org. Chem., 40*, 292-298, 1975.

Hoffmann, T., J.R. Odum, F. Bowman, D. Collins, D. Klockow, R.C. Flagan, and J.H. Seinfeld, Formation of organic aerosols from the oxidation of biogenic hydrocarbons, *J. Atmos. Chem., 26*, 189-222, 1997.

Jacobson, M.Z., Development and application of a new air pollution modeling system 3. Aerosol-phase simulations, *Atmos. Environ., 31*, 587-608, 1997.

Kamens, R., M. Jang, C.-J. Chien, and K. Leach, Aerosol formation from the reaction of α-pinene and ozone using a gas phase kinetics-aerosol partitioning module, *Environ. Sci. Technol., 33*, 1430-1438, 1999.

Kicic, I., M. Femeglia, and P. Rasmussen, UNIFAC prediction of vapor-liquid equilibria in mixed solvent-salt systems, *Chem. Eng. Science, 47*, 2775-2780, 1991.

Kim, Y.P., J.H. Seinfeld, and P. Saxena, Atmospheric gas-aerosol equilibrium I. Thermodynamic model, *Aerosol Sci. Technol., 19*, 157-181, 1993.

Liang, C.K., J.F. Pankow, J.R. Odum, and J.H. Seinfeld, Gas/particle partitioning of semi-volatile organic compounds to model inorganic, organic, and ambient smog aerosols, *Environ. Sci. Technol., 31*, 3086-3092, 1997.

Lurmann, F.W., A.S. Wexler, S.N. Pandis, S. Musarra, N. Kumar, and J.H. Seinfeld, Modeling urban and regional aerosols – II. Application to California's South Coast Air Basin, *Atmos. Environ., 31*, 2695-2715, 1997.

Macedo, E.A., P. Skovborg, and P. Rasmussen, UNIFAC prediction of vapor-liquid equilibria in mixed solvent-salt systems, *Chem. Eng. Sci., 46*, 2775-2780, 1991.

Meng Z., D. Dabdub, and J.H. Seinfeld, Size-resolved and chemically resolved model of atmospheric aerosol dynamics, *J. Geophys. Res.*, 103, 3419-3435, 1998.

Meng, Z., J.H. Seinfeld, P. Saxena, and Y.P. Kim, Atmospheric gas-aerosol equilibrium 4. Thermodynamics of carbonates, *Aerosol Sci. Technol., 23*, 131-154, 1995.

Middlebrook, A.M., D.M. Murphy, and D.S. Thomson, Observations of organic material in individual marine particles at Cape Grim during the First Aerosol Characterization Experiment (ACE-1), *J. Geophys. Res., 103*, 16,475-16,483, 1998.

Murphy, D.M., D.S. Thomson, and T.M.J. Mahoney, *In situ* measurements of organics, meteoritic material, mercury, and other elements in aerosols at 5 to 19 kilometers, *Science*, *282*, 1664-1669, 1998.

Myrdal, P.B., and S.H. Yalkowsky, Estimating pure component vapor pressures of complex organic molecules, *Ind. Eng. Chem. Res*., *36*, 2494-2499, 1997.

Nenes, A., S.N. Pandis, and C. Pilinis, ISORROPIA: A new thermodynamic equilibrium model for multiphase multicomponent inorganic aerosols, *Aquatic Geochem.*, *4*, 123-152, 1998.

Odum, J.R., T.P.W. Jungkamp, R.J. Griffin, R.C. Flagan, and J.H. Seinfeld, The atmospheric aerosol-forming potential of whole gasoline vapor, *Science*, *276*, 96-99, 1997.

Odum, J.R., T. Hoffmann, F. Bowman, D. Collins, R.C. Flagan, and J.H. Seinfeld, Gas/particle partitioning and secondary organic aerosol yields, *Environ. Sci. Technol*., *30*, 2580-2585, 1996.

Pai, P., K. Vijayaraghavan, and C. Seigneur, Particulate matter modeling in the Los Angeles Basin using SAQM-AERO, *J. Air Waste Manage. Assoc*., *50*, 32-42, 2000.

Pandis, S.N., R.H. Harley, G.R. Cass, and J.H. Seinfeld, Secondary organic aerosol formation and transport, *Atmos. Environ*., *26A*, 2269-2282, 1992.

Pankow, J.F., An absorption model of gas-particle partitioning of organic compounds in the atmosphere, *Atmos. Environ*, *28*, 185-188, 1994a.

Pankow, J.F., An absorption model of the gas/aerosol partitioning involved in the formation of secondary organic aerosol, *Atmos. Environ*, *28*, 189-193, 1994b.

Pankow, J.F., J.H. Seinfeld, W.E. Asher, and G.B. Erdakos, Modeling the formation of secondary organic aerosol: 1. The application of theoretical principles to measurements obtained in the α-pinene-, β-pinene-, sabinene-, Δ^3-carene-, and cyclohexene-ozone systems, *Environ. Sci. Technol*., *35*, 1164-1172, 2001.

Pankow, J.F., J.M.E. Storey, and H. Yamasaki, Effects of relative humidity on gas-particle partitioning of semi-volatile organic compounds to urban particulate matter, *Environ. Sci. Technol*., *27*, 2220-2226, 1993.

Penner, J.E., Carbonaceous aerosols influencing atmospheric radiation: Black and organic carbon in *Aerosol Forcing of Climate: Report of the Dahlem Workshop on Aerosol Forcing of Climate, Berlin 1994*, edited by R.J. Charlson and J. Heintzenberg, Wiley, New York, p. 91-108, 1995.

Rogge, W.F., M.A. Mazurek, L.M. Hildemann, and G.R. Cass, Quantification of urban organic aerosols at a molecular level: Identification, abundance, and seasonal variation, *Atmos. Environ*., *27*, 1309-1330, 1993.

Saxena, P., and L.M. Hildemann, Water-soluble organics in atmospheric particles: a critical review of the literature and application of thermodynamics to identify candidate compounds, *J. Atmos. Chem.*, *24*, 57-109, 1996.

Schauer, J.J., M.J. Kleeman, G.R. Cass, and B.R.T. Simoneit, Measurement of emissions from air pollution sources 1. C_1 through C_{29} organic compounds from meat charbroiling, *Environ. Sci. Technol*., *33*, 1566-1577, 1999a.

Schauer, J.J., M.J. Kleeman, G.R. Cass, and B.R.T. Simoneit, Measurement of emissions from air pollution sources 2. C_1 through C_{30} organic compounds from medium duty diesel trucks, *Environ. Sci. Technol*., *33*, 1578-1587, 1999b.

Schauer, J.J. *Source Contributions to Atmospheric Organic Compound Concentrations: Emissions, Measurements, and Model Predictions*, Ph.D. Thesis, California Institute of Technology, Pasadena, CA, 1998.

Schauer, J.J., and G.R. Cass, *Source contributions to airborne particles in the San Joaquin Valley during the IMS95 Study, Contract 97-6PM, Draft Final Report*, California Air Resources Board, Sacramento, CA, 1998.

Schwarzenbach, R.P., P.M. Gschwend, and D.M. Imboden, *Environmental Organic Chemistry*, John Wiley and Sons, Inc., New York, 1993.

Seinfeld, J.H., G.B. Erdakos, W.E. Asher, and J.F. Pankow, Modeling the formation of secondary organic aerosol: 2. The predicted effects of relative humidity on aerosol formation in the α-pinene-, β-pinene-, sabinene-, Δ^3-carene-, and cyclohexene-ozone systems, *Environ. Sci. Technol*., *35*, 1806-1817, 2001.

Smith, D.F., T.E. Kleindienst, and C.D. McIver, Primary product distributions from the reaction of OH with *m*-, *p*-xylene, 1,2,4- and 1,3,5-trimethylbenzene, *J. Atmos. Chem*., *34*, 339-364, 1999.

Stevens, R.K., T.G. Dzubay, C.W. Lewis, and R.W. Shaw, Jr., Source apportionment methods applied to the determination of the origin of ambient aerosols that affected visibility in forested areas, *Atmos. Environ*., *18*, 261-272, 1984.

Strader, R., F. Lurmann, and S.N. Pandis, Evaluation of secondary organic aerosol formation in winter, *Atmos. Environ*, *33*, 4849-4863, 1999.

Sun, Q., and A.S. Wexler, Modeling urban and regional aerosols near acid neutrality – application to the 24-25 June SCAQS episode, *Atmos. Environ*., *32*, 3533-3545, 1998.

Suzuki, T., K. Ohtaguchi, and K. Koide, Application of principal components analysis to calculate Henry's constant from molecular structure, *Computers Chem.*, *16*, 41-52, 1992.

United States Environmental Protection Agency, Web site for Models 3 (http://www.epa.gov/asmdnerl/models3/index.html), 1999

United States Environmental Protection Agency, *Air Quality Criteria for Particulate Matter*, EPA/600/P-95/001, 1996.

White, W.H., and E.S. Macias, Carbonaceous particles and regional haze in the Western United States, *Aerosol. Sci. Technol*., *10*, 106-110, 1989.

Yan, W., M. Toppoff, C. Rose, and J. Gmehling, Prediction of vapor-liquid equilibrium in mixed solvent electrolyte systems using the group contribution concept, *Fluid Phase Equilibria*, *162*, 97-113, 1999.

Yu, J., D.R. Cocker III, R.J. Griffin, R.C. Flagan, and J.H. Seinfeld, Gas-phase ozone oxidation of monoterpenes: gaseous and particulate products, *J. Atmos. Chem.*, *34*, 207-258, 1999.

Zhang, Y., C. Seigneur, J.H. Seinfeld, M. Jacobson, S.L. Clegg, and F.S. Binkowski, A comparative review of inorganic aerosol thermodynamic modules: similarities, differences, and their likely causes, *Atmos. Environ*., *34*, 117-137, 2000.

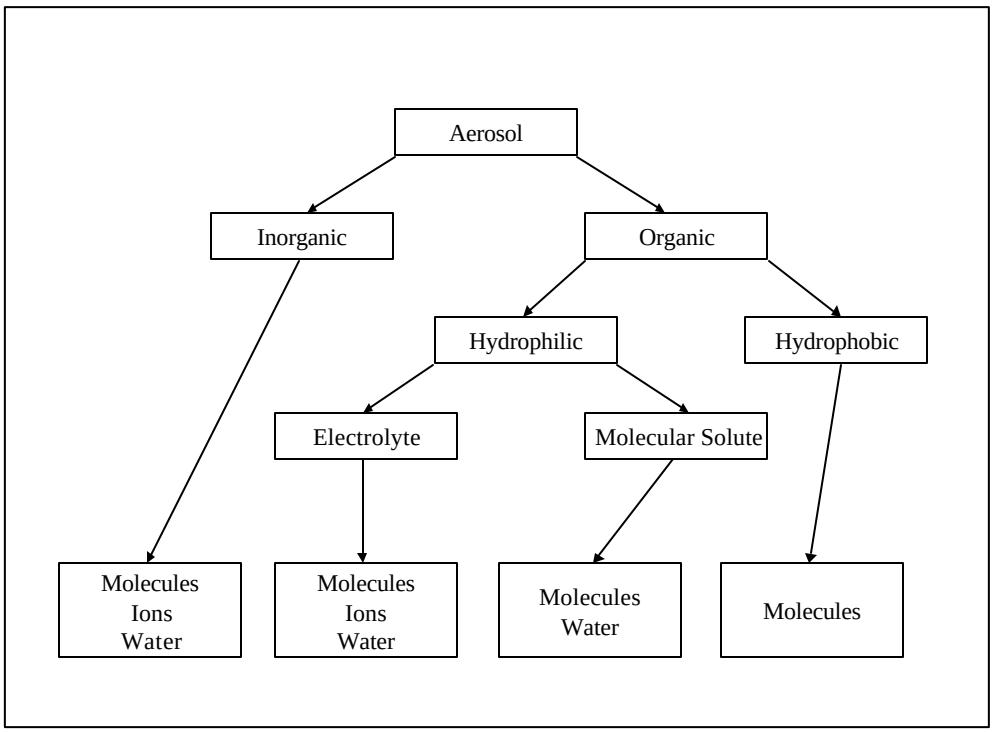

Figure 2.1. Module categorization of aerosol constituents based on their atomic nature (inorganic versus organic), water affinity (hydrophobic versus hydrophilic), and dissociative properties (electrolytic versus molecular).

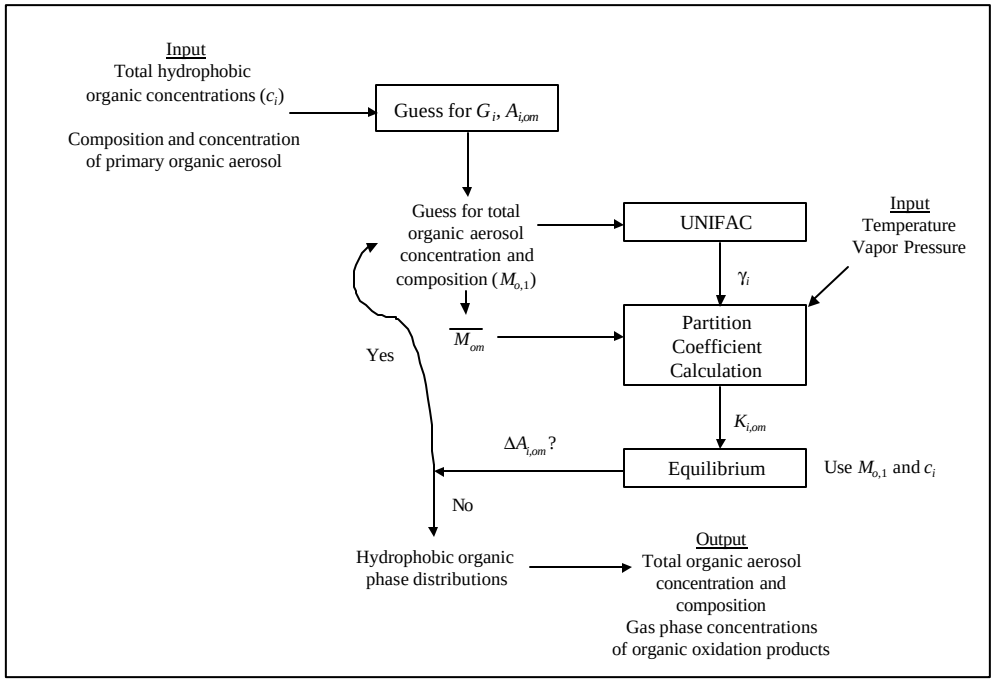

Figure 2.2. Calculation of the partitioning of hydrophobic SOA constituents between the gas and aerosol phases. Steps include an initial guess for the aerosol phase concentrations ($A_{i,om}$), calculation of the average molecular weight of the aerosol phase, use of UNIFAC to determine activity coefficients (for both SOA and POA species), calculation of theoretical partitioning coefficients for each SOA species, and iteration on the vector of $A_{i,om}$ values.

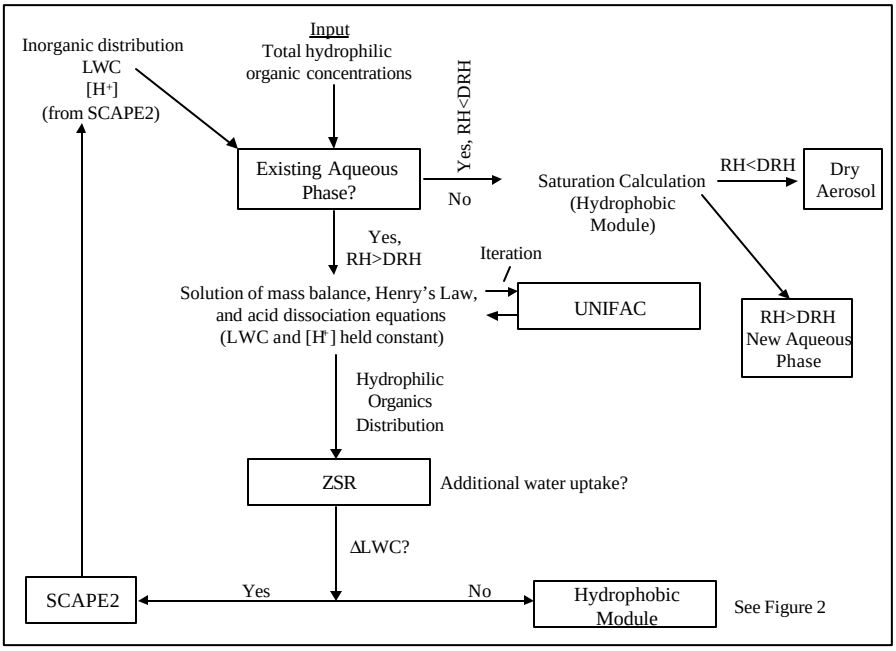

Figure 2.3. Calculation of the partitioning of hydrophilic SOA constituents between the gas and aqueous phases. Steps include determination of the type of calculation to be performed (saturation versus aqueous equilibrium), iterative solution of mass balance, Henry's Law, and acid dissociation constant equations (including iteration in UNIFAC to determine activity coefficients), calculation of water uptake associated with aqueous organics, and iteration on LWC between the hydrophilic module and an inorganic module such as SCAPE2.

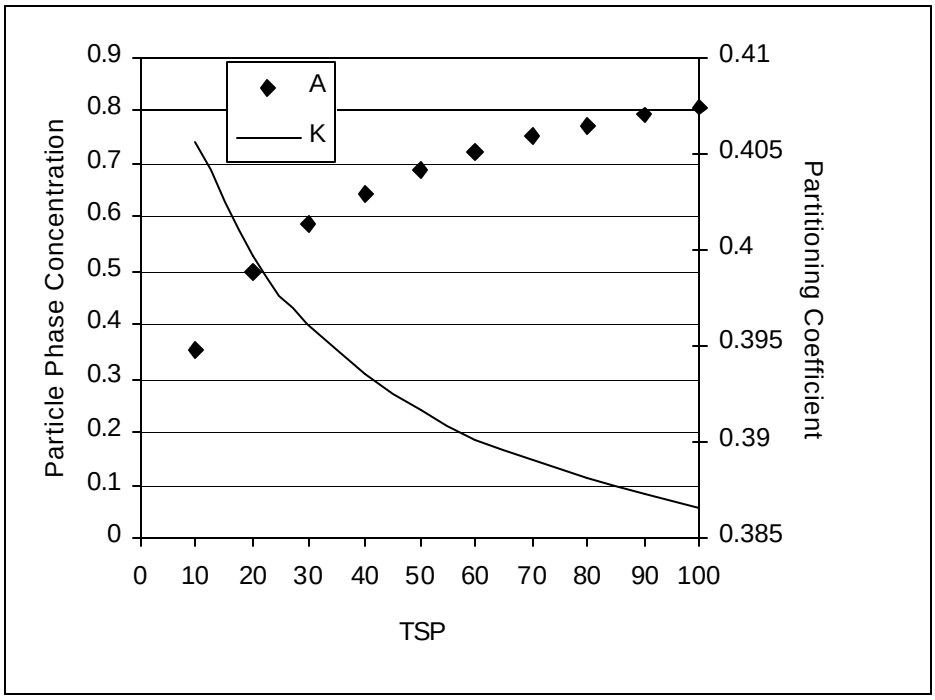

Figure 2.4. Particulate concentrations (A) of octadecanoic acid ($\mu g\ m^{-3}$) and its partitioning coefficient (K) ($m^3\ \mu g^{-1}$) as a function of TSP. TSP is assumed to have an initial organic mass fraction of 0.1, with the speciation of the organic phase described in Table 1. Total concentration of octadecanoic acid = 1 $\mu g\ m^{-3}$.

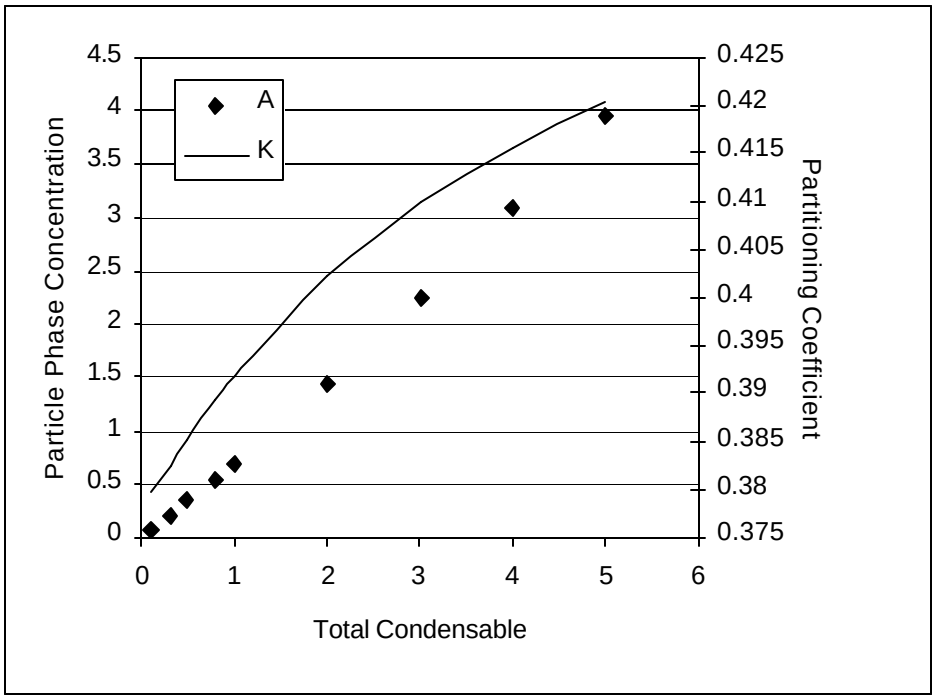

Figure 2.5. Particulate concentrations (A) of octadecanoic acid ($\mu g\ m^{-3}$) and its partitioning coefficient (K) ($m^3\ \mu g^{-1}$) as a function of the total amount of octadecanoic acid (condensable) present. TSP = 50 $\mu g\ m^{-3}$ with 10% being organic material speciated according to Table 2.1.

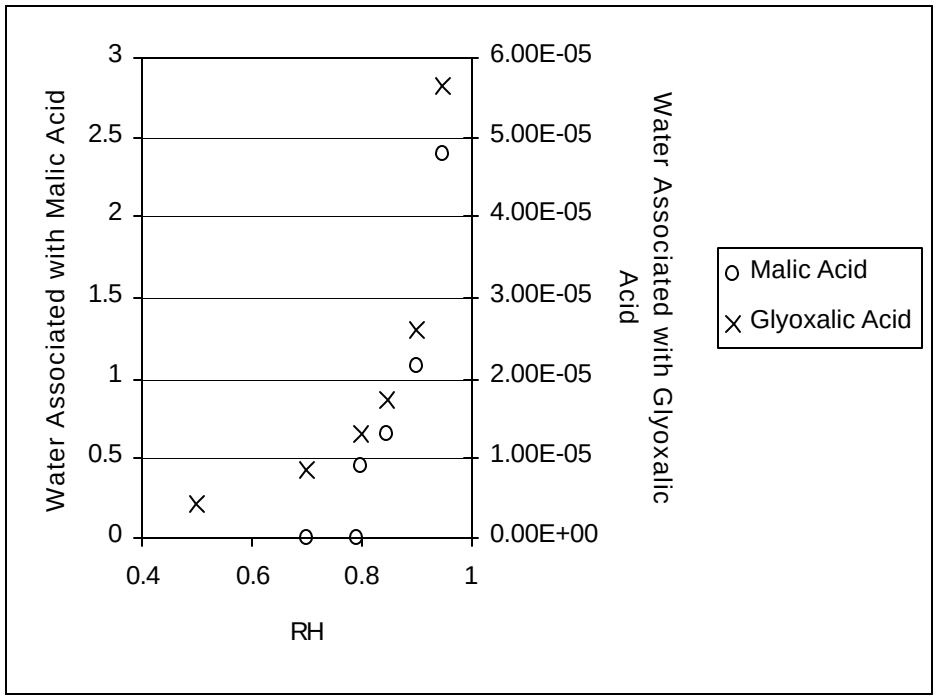

Figure 2.6. Sensitivity of the water associated with malic and glyoxalic acids (ng m^{-3}) to varying RH in the hydrophilic module. Other initial conditions: LWC = 1 µg m^{-3}, pH = 5, total of each solute = 1 ng m^{-3}.

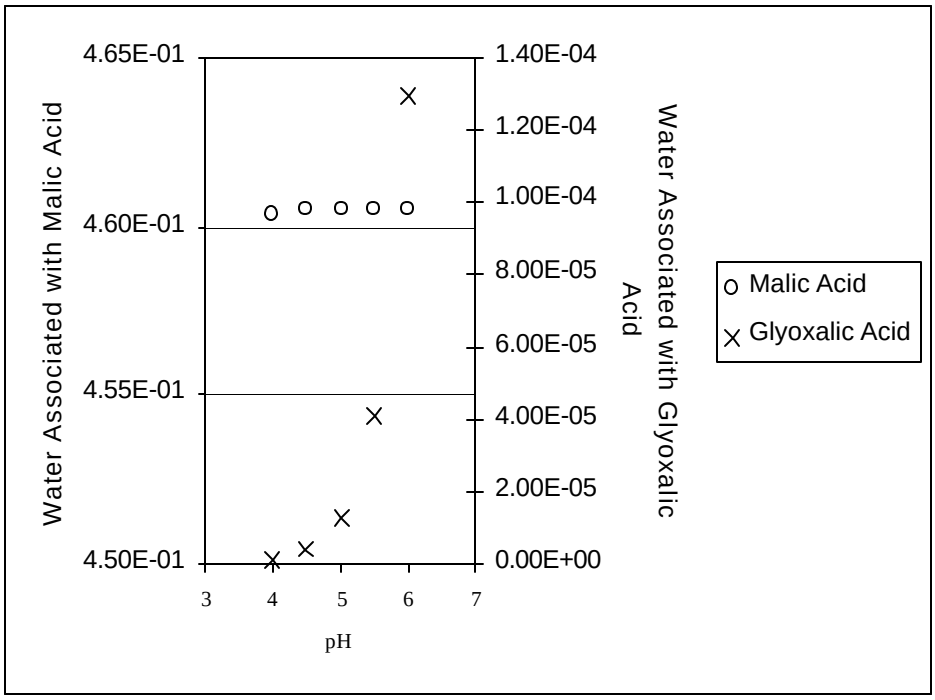

Figure 2.7. Sensitivity of the water associated with malic and glyoxalic acids (ng m^{-3}) to varying pH in the hydrophilic module. Other initial conditions: LWC = 1 µg m^{-3}, RH = 0.8, total of each solute = 1 ng m^{-3}.

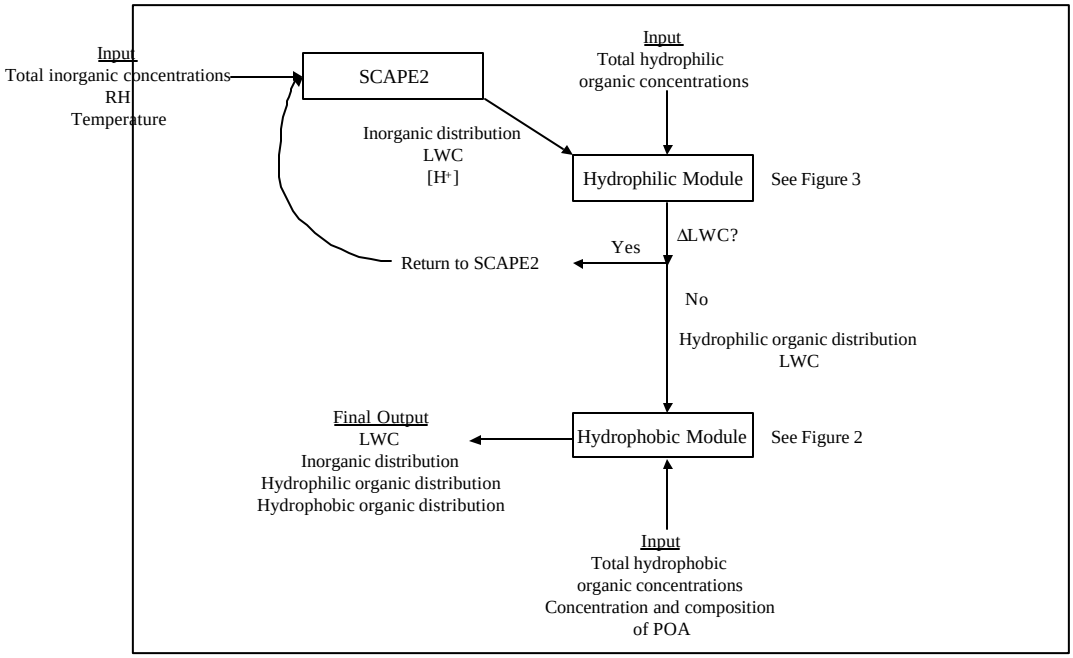

Figure 2.8. Calculation of aerosol water content and the phase distributions of both inorganic and organic aerosol constituents through use of the described module in a three-dimensional atmospheric model. Steps include the use of SCAPE2 to determine inorganic aerosol LWC and pH, calculations using the hydrophilic module (Figure 2.3), iteration on LWC with SCAPE2, and calculations using the hydrophobic module (Figure 2.2).

Table 2.1. Assumed POA composition for evaluation of the hydrophobic module.

	Fatty Acids	Substituted Phenols	Alkanes	Aromatic Acids
Mass Fraction	0.57	0.11	0.17	0.15
Surrogate Structure	Tetracosanoic Acid (C_{24} *n*-acid)	Acetonyl syringol (2,6-dimethoxy-4-acetonyl-phenol)	Nonacosane (C_{29} *n*-alkane)	Phthalic acid (1,2-Benzene-dicarboxylic acid)

Table 2.2. Properties of malic and glyoxalic acids.

	Malic Acid	Glyoxalic Acid
H_i^*	2×10^{13} M atm^{-1}	9×10^{3} M atm^{-1}
K_a^+	3.98×10^{-4} M	6.61×10^{-4} M
K_{a2}^+	7.76×10^{-6} M	--

*Henry's law coefficient, *Saxena and Hildemann* [1996];
+Acid dissociation constants, *CRC Handbook of Physics and Chemistry* [1997]
K_{a2} represents dissociation of the second acid group of malic acid

Table 2.3. Input and output for the evaluation of the hydrophilic module*.

Input		Output	
T	298 K	MA (g)	2.88×10^{-8} μg m^{-3}
RH	0.8	MA (aq)	5.88×10^{-6} μg m^{-3}
LWC	1 μg m^{-3}	MA^- (aq)	5.56×10^{-4} μg m^{-3}
PH	5	MA^{2-} (aq)	4.28×10^{-4} μg m^{-3}
MA (t)	1 ng m^{-3}	GA (g)	1.00×10^{-3} μg m^{-3}
GA (t)	1 ng m^{-3}	GA (aq)	1.24×10^{-10} μg m^{-3}
		GA^- (aq)	1.48×10^{-8} μg m^{-3}
		ΔLWC	0.46 ng m^{-3}

* MA = malic acid, GA = glyoxalic acid
(t) = total available material, (g) = gas-phase concentration
(aq) = aqueous-phase concentration, ORG^- = first dissociation product
ORG^{2-} = second dissociation product
ΔLWC = change in LWC due to the presence of the aqueous organics

Table 2.4. Input and output for the evaluation of the hydrophilic module used in conjunction with SCAPE2.

Input to SCAPE2	
Total NH_3	0.1 μmol m^{-3}
Total HNO_3	0.1 μmol m^{-3}
A. Temperature	298 K
Relative Humidity	0.8
Output of SCAPE2 (Initial Input to the Hydrophilic Module)	
LWC (inorganic)*	15.4 μg m^{-3}
PH	2.28
Additional Input to Hydrophilic Module	
Total Glyoxalic Acid	0.1 μmol m^{-3}
B. Total Malic Acid	0.1 μmol m^{-3}
Output of First Pass of Hydrophilic Module	
LWC (organic)*	14.4 μg m^{-3}
Total organic ions (aq)	0.0071 μmol m^{-3}
C. Total organic molecules (aq)	0.0928 μmol m^{-3}
LWC (total)*	29.8 μg m^{-3}
Output of SCAPE2 and Hydrophilic Module After Iteration on Total LWC	
LWC (inorganic)*	17.5 μg m^{-3}
PH	2.15
D. LWC (organic)*	14.4 μg m^{-3}
Total organic ions (aq)	0.0053 μmol m^{-3}
E. Total organic molecules (aq)	0.0947 μmol m^{-3}
LWC (total)*	31.9 μg m^{-3}

*LWC(inorganic) refers to water associated with inorganics; conversely LWC(organic) refers to water associated with organics. LWC(total) is the sum of the two.
(aq) refers to aqueous phase concentrations

Table 2.5a. Surrogate organic oxidation products to be used in the partitioning module in application in three-dimensional atmospheric models.

Surrogate[§]	Description[*]	#C	COOH	C=O	CHO	OH	ONO_2	NO_2	C=C	$p_{L,i}^{o+}$ (atm)
A1	WSOC, anthropogenic, dissociative, low #C (90)	2	2							7.0E-7
A2	WSOC, anthropogenic, dissociative, high #C (184)	8	2		1				2	1.1E-16
A3	WSOC, anthropogenic, non-dissociative (154)	8			2	1			2	1.3E-6
A4	WSOC, biogenic, dissociative (186)	9	1	1		1			1	2.8E-9
A5	WSOC, biogenic, non-dissociative (186)	10		1	1	1				1.8E-7
B1	Hydrophobic, anthropogenic, benzene-based, low volatility (197)	9	1[a]			1[a]		1[a]		2.4E-9
B2	Hydrophobic, anthropogenic, benzene-based, higher volatility (164)	9	1[a]		1[a]					5.5E-8
B3	Hydrophobic, anthropogenic, naphthalene-based (181)	12					1			1.0E-7
B4	Hydrophobic, anthropogenic, aliphatic (301)	16				1	1			1.8E-8
B5	Hydrophobic, biogenic, aliphatic (170)	10		1		1			1	2.2E-6

F. [§]A refers to hydrophilic surrogates; B refers to hydrophobic surrogates.

[*]Number in parentheses represents the surrogate molecular weight (g mol^{-1})

[+]Values at 298K according to the expressions derived from *Myrdal and Yalkowsky* [1997].

[a]attached to the aromatic ring as opposed to a side chain alkyl substituent

Table 2.5b. Surrogate POA species to be used in the partitioning module in application in three-dimensional atmospheric models.

Species	Description	Chemical Name	Description	Molecular Weight ($g\ mol^{-1}$)
1	*n*-alkanes	*n*-nonacosane	C_{29} *n*-alkane	408
2	Polycyclic aromatic hydrocarbons (PAH)	benzo(ghi)-perylene	PAH consisting of five aromatic rings	276
3	oxygenated PAH	2,6-naphthalene-diacid	PAH with two aromatic rings and two acid substituents	216
4	diacids	butanedioic acid	C_4 *n*-diacid	118
5	aliphatic acids	octadecanoic acid	C_{18} *n*-acid	284
6	substituted monoaromatic compounds	phthalic acid	aromatic ring with two acid substituents	166
7	cyclic petroleum biomarkers	17(α)H-21(β)H-hopane	Five fused aliphatic rings with multiple alkyl substituents	412
8	unresolved organics	branched and highly cyclic material	Four fused aliphatic rings with four branched alkyl substituents	390

Table 2.6a. Hydrophilic CACM Species Reduction into Five SOA Surrogates

Surrogate	Characteristics	Surrogate Species*	Contributing Species
A1	WSOC, anthropogenic, dissociative, low #C	UR28	UR21: Keto-propanoic acid UR28: Oxalic acid
A2	WSOC, anthropogenic, dissociative, high #C	RP18	RP13: 2-Carboxyl-5-methyl-2,4-hexadiendial RP17: 4-Hydroxy-3,5-dimethyl-2,4-hexadienalic acid RP18: 2-Methyl-5-formyl-2,4-hexadiendioic acid UR29: 4-Hydroxy-3,5-dimethyl-2,4-hexadiendioic acid UR30: 2-Methyl-5-carboxy-2,4-hexadiendioic acid
A3	WSOC, anthropogenic, non-dissociative	3-Hydroxy-2,4-dimethyl-2,4-hexadiendial	RPR9: 4-Hydroxy-3,5-dimethyl-2,4-hexadiendial RP12: 2-Methyl-5-formyl-2,4-hexadiendial
A4	WSOC, biogenic, dissociative	2-Hydroxy-3-isopropyl-5-keto-3-hexenoic acid	UR3: 2-Hydroxy-3-isopropyl-6-keto-heptanoic acid UR23: 3-Isopropyl-4-hydroxy-2-butenoic acid
A5	WSOC, biogenic, non-dissociative	RPR3	RPR3: 2-Hydroxy-3-isopropyl-6-keto-heptanal AP7: 1-Methyl-1-nitrato-2,3-dihydroxy-4-isopropyl-cyclohexane UR17: 2-Hydroxy-3-isopropyl-hexadial

* For detailed description of structural components, see Table 2.5a. Notation for contributing species is from *Griffin et al.* (2001).

Table 2.6b. Hydrophobic CACM Species Reduction into Five SOA Surrogates

Surrogate	Characteristics	Surrogate Species*	Contributing Species
B1	Hydrophobic, anthropogenic, benzene-based, low volatility	3,5-Dimethyl-2-nitro-4-hydroxy-benzoic acid	AP1: 2-Nitrooxymethyl-6-methyl-phenol AP6: 4-Nitrooxymethyl-benzoic acid UR22: 2,6-Dimethyl-3,4-dinitro-phenol UR31: 2-(Dimethyl-propenoic acid)-benzoic acid
B2	Hydrophobic, anthropogenic, benzene-based, higher volatility	2,4-Dimethyl-3-formyl-benzoic acid	ADAC: Terephthalic acid RPR4: 2,6-Dimethyl-4-nitro-phenol RPR7: 4-Formyl-benzoic acid RP14: 2-(Dimethyl-propenal)-benzaldehyde RP19: 2-(Dimethyl-propenal)-benzoic acid UR2: 3-Hydroxy-4-methyl-benzoic acid UR14: 2-Nitro-4-methyl-benzoic acid UR27: 2-Carboxy-acetophenone
B3	Hydrophobic, anthropogenic, naphthalene-based	AP10	AP10: 1-Methyl-2-nitrooxymethyl-naphthalene UR11: 1,2-Dimethyl-3-hydroxy-naphthalene UR15: 1,2- Dimethyl-3-nitro-naphthalene
B4	Hydrophobic, anthropogenic, aliphatic	AP12	AP11: 8-Hexadecylnitrate AP12: 8-Hydroxy-11-hexadecylnitrate UR20: 11-Hydroxy-8-hexadecanone UR26: 4,5-Dimethyl-6-keto-2,4-heptadienoic acid UR34: 8-Hexadecanone
B5	Hydrophobic, biogenic, aliphatic	2-Isopropyl-5-methyl-6-hydroxy-2-cyclohexenone	PAN8: Peroxy 2-hydroxy-3-isopropyl-6-keto-heptionyl nitrate AP8: 1-Methyl-4-nitrato-4-isopropyl-5-hydroxy-cyclohexene UR5: 1-Methyl-3-hydroxy-4-isopropyl-1,2-cyclohexane epoxide UR6: 2-Hydroxy-3-isopropyl-6-methyl-cyclohexanone UR7: 3,7-Dimethyl-6-keto-3-octenal UR8: 3-Isopropyl-6-keto-3-heptenoic acid

G. * For detailed description of structural components, see Table 2.5a. Notation for contributing species is from *Griffin et al.* (2001).

Chapter 3

Secondary organic aerosol: III. Urban/regional scale model of size- and composition-resolved aerosols

3.1 Introduction

Comprehensive gas- and aerosol-phase simulations of air quality in the South Coast Air Basin of California (SoCAB) are presented for September 8, 1993, a day on which some of the highest one-hour average ozone concentrations of 1993 in the SoCAB were observed. Simulations were performed using the California Institute of Technology (CIT) three-dimensional urban/regional air quality model. Gas-phase simulations are based on the new atmospheric chemical mechanism developed in Part I [*Griffin et al*., 2001] that includes representation of gas-phase chemistry leading to secondary organic aerosol (SOA) formation. Partitioning of secondary organic oxidation products to either an aqueous or an absorptive organic phase is determined using the new thermodynamic module of Part II [*Pun et al*., 2001]. This work represents the first attempt to simulate organic aerosol formation on a first-principles thermodynamic basis in a three-dimensional atmospheric model.

Previous gas- and aerosol-phase modeling studies performed for the SoCAB using the CIT model focused primarily on the episode of August 27-29, 1987, which was part of the Southern California Air Quality Study (SCAQS). *Meng et al*. [1998] performed a full gas- and aerosol-phase simulation in which particles were both size- and chemically resolved. The major differences between the versions of the CIT model employed by *Meng et al*. [1998] and in the current work are described subsequently. Previous studies using the CIT model have investigated, for example, the link between ozone and particulate matter (PM) [*Meng et al*., 1997] and the contribution of SOA to PM levels in the SoCAB [*Pandis et al*., 1993]. *Jacobson et al*. [1996,1997] have developed a three-dimensional model that has been applied to the 1987 SCAQS episode to simulate gas- and particle-phase air quality. Other simulations of Los Angeles gas and aerosol air quality have been reported for other episodes and using different models. *Lurmann et al*. [1997] used the Urban Airshed Model (UAM) [*Systems Applications International*, 1990a-e] to simulate the SCAQS episode of June 24-25, 1987 while employing the SEQUILIB inorganic thermodynamic model of *Pilinis and Seinfeld* [1987], a precursor to the thermodynamic model used by *Meng et al*. [1998]. The work also included an empirical fog model to account for the effect of fogs on gas-phase photolysis rates; fog processing of aerosols was not considered. SOA modeling work has also been performed in other areas [*Andersson-Sköld and Simpson*, 2001].

In previous studies, ambient aerosols generally have been represented as an internal mixture (in which all particles of a given size have the same composition) using Eulerian grid cells (coordinates that are fixed in space). An assumed internal aerosol mixture does not require that all constituents within a given aerosol particle interact. *Kleeman et al*. [1997], however, recently developed a Lagrangian model (with coordinates that follow the trajectory of an air parcel) that treats airborne particles as an external mixture of different particle classes, defined based on the original emission source of the particle. This model has been applied to both the August 28, 1987 SCAQS episode [*Kleeman et al*., 1997] and to data collected during the summer of 1996 in the SoCAB [*Kleeman and Cass*, 1999]. In the present study we continue to employ the internally mixed assumption, as it is sufficiently accurate for most situations and the

computational demands of a full thermodynamic treatment of inorganic/organic aerosols in a three dimensional model are inordinately large.

3.2 Model Description

The evolution of the host Eulerian CIT model has been described in detail previously [*McRae et al*., 1982; *McRae and Seinfeld*, 1983; *Harley et al*., 1993, *Meng et al*., 1998]. In application to the SoCAB, the horizontal domain of the model is an 80 by 30 grid with a resolution of 5 km; vertical resolution consists of five layers up to 1100 m above the surface. Aerosol concentrations are characterized by mass and are resolved into eight size domains with diameters ranging from 0.04 to 10 μm. Such a sectional approach is the most general and powerful approach for representing aerosol size and composition. It allows for any desired degree of size resolution and chemical speciation and is typically more computationally intensive than a modal approach, such as that used by *Binkowski and Shankar* [1995]. The aerosol is considered to be an internal mixture of elemental carbon, organics, and inorganics including water. Aerosol processes not considered in the present application include coagulation, wet deposition, non-equilibrium chemical reactions that take place on aerosol surfaces, and interactions with fog and clouds.

3.2.1 Aerosol Thermodynamics

The module Simulating Composition of Atmospheric Particles at Equilibrium 2 (SCAPE2) is used to describe the gas-aerosol partitioning of inorganic aerosol constituents [*Kim et al.*, 1993b, *Meng et al*., 1995]. As discussed in Part II [*Pun et al*., 2001], the module has been modified to account for the effect of aqueous phase organic ions on the distribution of inorganic aerosol constituents. SCAPE2 is used to calculate equilibrium surface concentrations of all semi-volatile inorganic species in gas-phase concentration units. These calculations are performed in a size-resolved fashion in which the composition in individual bins is used to determine bin-specific equilibrium gas concentrations. Size-specific condensation or evaporation is then driven by the difference between the calculated equilibrium surface vapor concentration and the bulk gas-phase concentration. Inorganic condensation/evaporation processes are modeled dynamically in this work except for water and carbonates, which are assumed to achieve equilibrium instantaneously. SCAPE2 allows for calculations of multicomponent inorganic activity coefficients by the Bromley, Kusik-Meissner (KM), or Pitzer methods. The KM method is used in the present work, as it has been shown that it gives the most reliable results for simulating concentrated solutions typical of non-ideal ambient aerosols [*Kim et al*., 1993a]. The Zdanovskii-Stokes-Robinson (ZSR) method is used to estimate water activities [*Robinson and Stokes*, 1965]. Temperature dependencies of equilibrium constants and relative humidities of deliquescence are also considered. In addition to water, species considered include sodium, sulfate, ammonium, nitrate, chloride, potassium, calcium, magnesium, and carbonate.

Organic aerosol partitioning is driven by an instantaneous equilibrium between the gas-phase and a condensed aerosol phase (aqueous or organic), as described in Part II [*Pun et al*., 2001]. In the organic aerosol partitioning module, calculations are performed in a bulk mode in which the net composition of the components across all aerosol bins are summed (liquid water content and primary organic aerosol (POA) concentrations). The resulting equilibrium gas and particle concentrations are with respect to bulk properties of the aerosol. Size-resolution of secondary organics that partition between the gas phase and the condensed phase (as opposed to

primary organics that reside completely in the particle phase) is determined based on available surface area within each size bin, as has been done previously [*Meng et al*., 1998].

3.2.2 Homogeneous Nucleation

New particle mass formed via homogeneous nucleation is considered only for the sulfuric acid-water system. Based on binary nucleation of sulfuric acid and water, the threshold sulfuric acid concentration required for new particle formation, C_{crit,H_2SO_4} (μg m^{-3}), is given by

$$C_{crit,H_2SO_4} = 0.16 exp(0.1T - 3.5\mathrm{RH} - 27.7) \quad (1)$$

where temperature (T) is in Kelvin and relative humidity (RH) is between 0 and 1 [*Wexler et al*., 1994; *Meng et al*., 1998]. If the simulated ambient gas-phase concentration exceeds this critical value, the amount in excess is transferred from the gas phase to the aerosol phase in the smallest size bin. The gas-phase concentration is accordingly set to C_{crit,H_2SO_4}. Under typical urban particle loadings, nucleation is generally not expected to occur.

3.2.3 Equations Governing Gas-Phase Dynamics

The spatial and temporal distributions of the concentrations of gas-phase species are governed by the atmospheric convective diffusion equation, as described in *Harley et al.* [1993],

$$\frac{\partial C_i}{\partial t} + \nabla \cdot (\overline{\boldsymbol{V}} C_i) = \nabla \cdot (\boldsymbol{K} \nabla C_i) + R_i + Q_i \quad (2)$$

where C_i is the ensemble mean concentration of species i in the gas phase, $\overline{\boldsymbol{V}}$ is the mean wind velocity vector (later shown as $\overline{\boldsymbol{V}}(\boldsymbol{x},t)$ to indicate its spatial and temporal dependence), $\boldsymbol{K}$ is the turbulent diffusivity tensor (later shown as $\boldsymbol{K}(\boldsymbol{x},t)$), R_i is the rate of formation or removal of species i by reactions in the gas-phase, and Q_i is a source term, such as elevated point emissions. R_i is determined by the chemical mechanism used within the host model. The Caltech Atmospheric Chemistry Mechanism (CACM) described in Part I [*Griffin et al*., 2001] has been developed in order to predict formation of highly oxygenated secondary organic products capable of partitioning to the aerosol phase; this mechanism is used in the present study. CACM includes over 190 chemical species that participate in over 360 reactions. Currently, all emissions are treated as if they occur at ground level, meaning that Q_i is zero in this study. The surface boundary condition for solution of equation (2) sets the upward flux of each species equal to the emissions flux minus that due to dry deposition. A no-flux condition is set at the top of the domain. As described subsequently, lateral boundary conditions and initial conditions are established using measured ambient data. The use of operator splitting allows for the decoupling of the chemistry and the aerosol computations from transport calculations. Therefore, equation (2) is solved to determine C_i as a function of space and time. This vector of concentrations is then used in the inorganic and organic thermodynamic aerosol modules that determine the distribution of each species between the gas and aerosol phases.

3.2.4 Dry Deposition of Gas-Phase Species

As described above, dry deposition of gas-phase species is used to determine surface boundary conditions for solution of the atmospheric diffusion equation. Representation of dry

deposition in the CIT model is described by *Harley et al*. [1993]. A maximum dry deposition velocity, $v_{g\,max}$, is calculated in each grid cell assuming irreversible deposition,

$$v_{g\,max} = \frac{k^2 u(z_r)}{\left[\int_{z_0}^{z_r} \phi_m \left(\frac{z}{L}\right)\frac{dz}{z}\right]\left[2\left(\frac{Sc}{Pr}\right)^{2/3} + \int_{z_0}^{z_r} \phi_p \left(\frac{z}{L}\right)\frac{dz}{z}\right]} \tag{3}$$

where k is von Karman's constant (0.40), $u(z_r)$ is the wind speed at the reference height z_r, z_0 is the surface roughness length, L is the Monin-Obukhov length (indicative of the stability of the boundary layer), Sc is the Schmidt number (the ratio of the momentum diffusivity to the mass diffusivity), and Pr is the Prandtl number (the ratio of the momentum diffusivity to the heat diffusivity). ϕ_m and ϕ_p are functions that describe momentum and heat-flux profiles in the boundary layer [*Businger et al*., 1971]. The dry deposition velocity $v_g^{\,i}$ of each species i is calculated from $v_{g\,max}$ and a surface resistance term

$$v_g^{\,i} = \frac{1}{\left(1/v_{g\,max}\right) + r_s^i} \tag{4}$$

where r^i_s is the surface resistance term for the species of interest in the grid cell of interest. Surface resistance terms vary from grid cell to grid cell because of the 32 different land-use types that exist in the SoCAB. These land-use types include, for example, urban, agricultural, forest, water, and barren land (such as beaches). Resistance terms are also affected by wind speed and atmospheric stability.

3.2.5 Equations Governing Aerosol Dynamics

The number concentration of particles in an incremental volume of air is governed by [*Meng et al*., 1998]

$$\begin{aligned}\frac{\partial n(m,t)}{\partial t} &= -\frac{\partial}{\partial m}\left[I(m,t)n(m,t)\right] + \frac{1}{2}\int_0^m \beta(m', m-m')n(m',t)n(m-m',t)dm' \\ &- n(m,t)\int_0^\infty \beta(m,m')n(m',t)dm' + S(m,t) - L(m,t)n(m,t)\end{aligned} \tag{5}$$

where $n(m,t)$ is the number concentration of particles at time t having total particle mass between m and $m + dm$. The total mass of the particle, m, is given as the sum of the masses (m_i) of each of the individual components. $I(m,t)$ represents the rate of change of the total mass of the particle as a result of condensation or evaporation and is given as the sum of the individual rates of change for each component (sum of dm_i/dt). The rate of coagulation between particles of mass m and those of mass m' is given as $\beta(m, m')$. $S(m,t)$ represents the source term (for example, nucleation) for particles of mass m, and the first-order removal (for example, deposition) of particles of mass m is given by $L(m,t)n(m,t)$.

For most simulations of urban/regional air quality the aerosol mass distribution has been of greater interest than the aerosol number distribution. For species i, the mass concentration

distribution is defined as $q_i(m,t) = m_i n(m,t)$, and the total aerosol mass concentration distribution function, $q(m,t)$, is defined as the sum of all q_i and is equal to the product of m and $n(m,t)$. The normalized growth (or evaporation, if it is negative) rate of species i, H_i, in a particle of given mass m is defined by

$$H_i(m,t) = \frac{1}{m}\frac{dm_i}{dt} \tag{6}$$

where the total growth/evaporation rate (H) of the particle is given by the sum of the individual H_i for all components of the particle.

In most urban and regional modeling applications focusing on aerosol mass concentrations, coagulation can be neglected [*Wexler et al.*, 1994]. Thus, the general equation governing the mass distribution of species i in the aerosol phase becomes

$$\frac{\partial q_i(m,t)}{\partial t} = H_i(m,t)q(m,t) - \frac{\partial}{\partial m}\left[mq_i H\right] + m_i S(m,t) - L(m,t)q_i(m,t) \tag{7}$$

Including the spatial dependence of q_i, incorporating terms for advection and turbulent mixing, and transforming m to a normalized particle diameter ($\mu = \ln(D_p/D_{p0})$, where D_{p0} is the smallest diameter modeled in the size domain) results in the basic governing equation for the aerosol portion of the three-dimensional atmospheric model,

$$\begin{aligned}\frac{\partial p_i(\mu, \boldsymbol{x}, t)}{\partial t} &= -(\overline{\boldsymbol{V}}(\boldsymbol{x},t) - V_s(\mu)\boldsymbol{k})\cdot\nabla p_i + \nabla\cdot\boldsymbol{K}(\boldsymbol{x},t)\nabla p_i \\ &+ H_i(\mu,\boldsymbol{x},t)\,p(\mu,\boldsymbol{x},t) - \frac{1}{3}\frac{\partial}{\partial\mu}\left[Hp_i\right] + S_i(\mu,\boldsymbol{x},t) - L(\mu,\boldsymbol{x},t)p_i\end{aligned} \tag{8}$$

where $p_i(\mu,\boldsymbol{x},t) = (dm/d\mu)q_i$, $\boldsymbol{x}$ is the spatial coordinate vector, $V_s(\mu)$ is the particle settling velocity, and $\boldsymbol{k}$ is the unit vector in the vertical direction.

The growth/evaporation rate of species i is given by [*Wexler et al.*, 1994]

$$H_i(m,t) = \frac{1}{m}\frac{dm_i}{dt} = \frac{2\pi D_p D_i}{m}\frac{C_{\infty,i} - C_{s,i}}{\dfrac{2\lambda}{\alpha_i D_p} + 1} \tag{9}$$

where D_i is the molecular diffusivity of species i in air, λ is the mean free path of air, α_i is the accommodation coefficient for species i on the aerosol, and $C_{\infty,i}$ and $C_{s,i}$ are the concentrations of i in the bulk and at equilibrium at the particle surface, respectively. For inorganic species, surface vapor concentrations are estimated using the thermodynamic routine SCAPE2. Concentrations of organic species in each phase are calculated thermodynamically according to the equilibrium module described in Part II.

At the ground surface, the balance between emission and dry deposition represents a boundary condition for equation (8). This condition is typically expressed with a deposition

velocity, V_d, where $V_d = F/C(z_r)$. F is the downward flux caused by deposition, and $C(z_r)$ is the concentration at reference height z_r (typically 10 m). The flux of species i is given by [*Wesely*, 1989]

$$F_i = [K_{zz}(z) + D_i](dC_i(z)/dz) + V_s C_i(z) \quad (10)$$

where K_{zz} is the zz-component of the eddy diffusivity tensor. Dry deposition of particle-phase species is handled differently than that of gas-phase species because of the need to include deposition due to gravitational settling. The particle deposition velocity, V_d, is then used in a manner similar to $v_{g\ max}$ in equation (4) to calculate overall deposition. Again, deposition to different land-use categories is considered within the CIT model.

3.2.6 Solution of Advection and Condensation/Evaporation Equations

Two new numerical algorithms have been implemented into the CIT model to solve the hyperbolic advection and condensation/evaporation equations in the model. Previously, both of these equations had been solved using Bott's method, as described by *Dhaniyala and Wexler* [1996]. The Quintic Splines Taylor Series Expansion (QSTSE) algorithm, an Eulerian scheme that uses Quintic splines to calculate derivatives in the spatial domain and a Taylor series expansion to progress in time, is used to solve the advection equation [*Nguyen and Dabdub*, 2001a]. Results have shown that the QSTSE algorithm maintains high accuracy while providing significant decreases in computation time over previously used methods. The Partitioned-Flux Integrated Semi-Lagrangian Method (PFISLM) is used to solve both the hyperbolic (redistribution) and growth portions of the condensation/evaporation equation [*Nguyen and Dabdub*, 2001b]. PFISLM was designed specifically to minimize problems associated with the size- and time- discretization of the aerosol operator in atmospheric models. The PFISLM algorithm is positive-definite, peak retentive, and mass conservative and suppresses oscillations in the solution. While still yielding highly accurate results, PFISLM significantly decreases computational demands of the aerosol solver because it is capable of using interpolators of lower order for the solution of the hyperbolic portion of equation (9).

3.3 Required Model Input: Emissions and Meteorology

For the temporally and spatially resolved aerosol emissions inventory, the particle phase is apportioned into eight size sections, and the appropriate mass of each species is placed into the proper size bin at each time and location [*Fraser et al*., 2000]. Aerosol species include elemental carbon, sodium, chloride, ammonium, sulfur (in two oxidation states), nitrate, metals (e.g., calcium, magnesium, and potassium), organics, and unidentified/other material. Organic particle-phase species can be further segregated into seven primary aerosol categories based on chemical analysis of samples from emission sources: *n*-alkanes, polycyclic aromatic hydrocarbons (PAH), diacids, aliphatic acids, substituted PAH, resolved polycyclic species (e.g., hopanes), and substituted monoaromatics. Unresolved organic matter (typically highly cyclic, saturated, and branched petroleum biomarkers) constitutes an eighth POA emissions group [*Rogge et al*., 1993; *Schauer*, 1998; *Schauer et al*., 1999ab, 2001]. Emissions inventories (both particle and gas) were obtained from the South Coast Air Quality Management District (SCAQMD). Summaries of daily particle-phase emissions for September 8, 1993 are given in Table 3.1 by species and size. Initial and boundary conditions for PM are established based on

observed aerosol size and composition distributions obtained in the SCAQS sampling campaign [*John et al*., 1990].

Because the character of the POA species affects the partitioning of the secondary organic oxidation products as described in Part II [*Pun et al*., 2001], representative surrogates must be chosen to represent each POA category listed above (*n*-alkanes, PAH, etc.). The surrogates used are *n*-nonacosane, benzo(ghi)perylene, butanedioic acid, octadecanoic acid, 2,6-naphthalene-diacid, 17(α)H-21(β)H-hopane, phthalic acid (1,2-benzene-diacid), and a polysubstituted decalin compound, respectively. These species are chosen based on their identified prevalence in POA emissions in the SoCAB [*Rogge et al*., 1993; *Schauer*, 1998; *Schauer et al*., 1999ab, 2001]. If an organic species is emitted as aerosol, it is assumed that it remains in the particle phase and is nonreactive.

Species that are included in the other/unidentified category above may include arsenic, bromine, phosphorous, selenium, and silicon, which most likely have crustal sources. The mass of these other/unidentified species is found by the difference between the total gravimetric mass measured during emissions sampling and that mass which can be identified using an array of analytical techniques. Particulate water (not measured analytically) and oxygen or nitrogen associated with organics may also contribute to this category. In the analysis of the emissions, total organic carbon is reported and then converted to total organic mass. In this conversion, the total mass of organics may be underestimated, leading to some organic mass being included in the other/unidentified category. In the current study, the other/unidentified species are treated as nonvolatile components of the aerosol.

A highly aggregated summary for the gas-phase emissions is given in Table 3.2. Hourly gas-phase emissions (point and mobile sources) for each of the model grid cells were supplied by SCAQMD. Mobile source emissions were generated through use of the California Air Resources Board (CARB) emissions model EMFAC-7G [*CARB*, 1998]. Gas-phase emissions are broken down into ammonia, oxides of sulfur (SO_x), oxides of nitrogen (NO_x), CO, and organic species. (Ammonia and SO_x are not shown in the table.) Organic species are lumped according to chemical structure and functionality, reactivity, and experimentally determined SOA forming potential. As discussed in Part I [*Griffin et al*., 2001], the parent organic groups include ethene (ETHE), short-chain alkenes (OLEL), long-chain alkenes (OLEH), short-chain alkanes (ALKL), medium-chain alkanes (ALKM), long-chain alkanes (ALKH), high-SOA yield aromatics (AROH), low-SOA yield aromatics (AROL), phenolic aromatics (AROO), aldehydic aromatics (ARAL), acidic aromatics (ARAC), polycyclic aromatic hydrocarbons (PAH), formaldehyde (HCHO), higher aldehydes (ALD2), short-chain ketones (KETL), long-chain ketones (KETH), methanol (MEOH), ethanol (ETOH), higher alcohols (ALCH), isoprene (ISOP), low-SOA yield monoterpenes (BIOL), high-SOA yield monoterpenes (BIOH), and methyl-*tert*-butyl ether (MTBE). If only total organic emissions are known for a given source, the split among the groups is assumed based on the observed ambient data. These splits are also used to establish boundary and initial conditions (Table 3.3). Previous work has shown that on-road motor vehicle emissions in the SoCAB have been underpredicted significantly by the methodology used to develop spatially and temporally resolved emission patterns from SCAQMD emission inventories [*Pierson et al*., 1990; *Fraser et al*., 1998]. Therefore, hot exhaust emissions of volatile organics and CO from light duty vehicles were increased by a factor of 3 (see, for example, *Harley et al*. [1993] and *Fraser et al.* [2000]). Ammonia emissions are based upon the inventory of *Gharib and Cass* [1984].

Meteorological parameters include relative humidity, temperature, wind, ultraviolet radiation, total solar radiation, and mixing height. Relative humidity is important as it determines, at a given time, the amount of gas-phase water present, which can participate in a number of reactions, including the reaction with $O(^1D)$ to form the hydroxyl radical and with N_2O_5 to form nitric acid, HNO_3. Relative humidity also determines the amount of water that partitions to the aerosol phase at equilibrium. Temperature is a key variable in that it affects the kinetics of gas-phase reactions, the equilibrium constants and relative humidities of deliquescence of the inorganic species, and the partitioning of organic species explicitly and implicitly through its effect on vapor pressure.

Meteorological parameters were obtained from a variety of sources. Hourly observations of surface wind speed and direction were taken at 21 sites by the California Irrigation Management Information Service (CIMIS) and at 32 sites by the SCAQMD. Temperature and relative humidity data were recorded at the 21 CIMIS sites, at 13 of the SCAQMD sites, and at 52 sites operated by the National Climatic Data Center. Total solar radiation was monitored by SCAQMD at six sites and by CIMIS at its 21 sites. Ultraviolet radiation was measured at one site in Central Los Angeles by SCAQMD. Hourly gridded fields for these types of data were made using the methodology described in *Harley et al*. [1993]. Inversion base height and wind aloft were inferred from upper air measurements made daily by SCAQMD in West Los Angeles at 0500 PST and by CARB in Claremont between 0600 and 1400 PST. *Winner and Cass* [1999] demonstrate the method used for creating mixing depth fields from such data.

In this study, it was determined that the traditional method used to calculate vertical eddy diffusivities in the CIT model underpredicts these parameters at the low wind speeds characteristic of this episode, as judged by unrealistically high simulated concentrations at night of both tracer pollutant and secondary species in the majority of locations throughout the SoCAB. The current methodology for calculating vertical eddy diffusivities does not take into account the effects of urban heat islands and mechanical mixing near roadways. Therefore, to achieve more realistic concentrations during the evening hours, vertical eddy diffusivities were increased by enforcing a minimum wind speed and stability class. These changes promote mixing up to the height of the inversion layer but were not propagated to other processes such as advection and deposition.

3.4 Numerical Solution of the Governing Equations

Operator splitting [*McRae et al*., 1982] is used in the CIT model to solve the governing gas and aerosol conservation equations. This is carried out according to the order $T_xT_yT_{z,c}T_aT_yT_x$ where T_x, T_y, $T_{z,c}$, and T_a represent the operators of transport in the x-direction, transport in the y-direction, transport in the z-direction and gas-phase chemistry, and aerosol dynamics, respectively.

The host CIT model is designed to solve numerically for spatial advection and diffusion terms for transport of gas-phase species, and the same techniques are applied for aerosols. Upon completion of a time step for the gas-phase mechanism, the aerosol operator is called and solved as discussed above. The aerosol operator determines the dynamic transport of all species except water, carbonates, and organics between the gas- and aerosol-phases. The excepted species are assumed to achieve equilibrium instantaneously. During these calculations, mass is conserved. The time step for the aerosol operator is determined by calculating the characteristic times for mass transfer of each species in each size section while maintaining the stability of the solution of hyperbolic equations. The smallest of these times is then used if it is less than the maximum

time step chosen during development of SCAPE2. Once the cumulative time of operation for the aerosol operator is equal to a time step of the gas-phase chemical mechanism, the transport calculations are performed.

Aerosols are size-resolved based on a sectional approach; eight discrete size bins are used in the current application. The minimum diameter specified is 0.04 μm, and the maximum is 10 μm. By establishing equidistant spacing on a logarithmic scale in particle diameter, particles are sectioned into 6 bins that are smaller than 2.5 μm in diameter (fine mode) and 2 bins that are larger (coarse mode). If particles grow to sizes larger than 10 μm, their diameters are reduced to 10 μm, and the number concentration in the largest size bin is increased so that aerosol mass concentration is conserved. The opposite is done if particles shrink to sizes below 0.04 μm; the diameters of such particles are increased to 0.04 μm with a corresponding decrease in aerosol number concentration in the smallest size bin. Because aerosol particle number concentrations at the extremes of the size distribution are relatively small, the effect on population dynamics of forcing the particles to remain within the range of 0.04-10 μm while conserving mass is minimal.

3.5 Simulation of the September 8, 1993 Smog Episode in the SoCAB

A specialized monitoring campaign was performed from August 28 to September 13 in the SoCAB during the summer of 1993 [*Fraser et al*., 1996], the goal of which was to identify numerous individual organic species in both the gas and aerosol phases; the current study focuses on September 8. Numerous monitoring sites were operated during the study (Figure 3.1). One site was located on San Nicolas Island, upwind of the Los Angeles basin, observations at which were used to establish upwind boundary conditions. Sites located within the greater Los Angeles area were chosen to represent different characteristic source regions of the SoCAB. Central Los Angeles is the hub of the region's freeway system, experiencing intense primary emissions from automobiles as well as some secondary photochemistry. Downwind locations Azusa and Claremont experience high levels of secondary pollutants. Continuous 4-hour aerosol samples were collected at each of these locations every six hours. Gas-phase species, such as NO, NO_2, O_3, CO, and SO_2, were also monitored hourly by the SCAQMD at 31 monitoring sites located throughout the SoCAB.

During the study, meteorological conditions were controlled by the development of a high-pressure system over the air basin. The episode was characterized by a strong temperature inversion aloft that strongly limited the extent of vertical mixing. Sunny and hot conditions were conducive to intense photooxidation, with peak temperatures in the eastern portion of the basin exceeding 40°C. Slight on-shore winds typically developed in the afternoon, minimally increasing transport of material inland and resulting in slightly foggy conditions in the morning.

Because simulation of gas-phase concentrations has already been addressed in Part I [*Griffin et al*., 2001], only brief consideration will be given here. Temporal profiles of observed (solid) and predicted (open) ozone (triangle) and NO_2 (circle) for Azusa are given in Figure 3.2. As seen in Figure 3.2, CACM and the CIT model predict the temporal behavior of these species at this location with accuracy that is generally consistent with that of previous SoCAB simulations. (See Part I.) The missing NO_x peak in the morning is most likely a result of inaccuracies in the emission inventory and probably contributes to the underprediction of peak ozone. The temporal profiles of the simulated (open) and observed (solid) concentrations of MGLY, which represents dicarbonyls that result from ring-breaking reactions of aromatics, are shown in Figure 3.3 for Azusa and Central Los Angeles. While MGLY is accurately predicted in the morning and evening (generally within 1 ppb), peak mid-day concentrations are

underpredicted by a factor of 2 to 3. However, the temporal peak in MGLY is well represented, as it is in *Fraser et al*. [2000].

Selected aerosol simulations are shown in Figures 4 through 6. While the majority of the results presented here will focus on SOA, Figure 3.4 shows simulated (open) and observed (solid) ammonium (circle) and nitrate (triangle) 4-hour average aerosol mass concentrations for Azusa. It is seen that nitrate levels tend to be underpredicted by a factor of 2-3 in earlier parts of the day and overpredicted by approximately 25% later. Ammonium aerosol concentrations are accurately represented in the morning and afternoon (within 1 $\mu g\ m^{-3}$) but are overpredicted by less than a factor of 2 in the evening. Simulations of the 24-hour average (the basis for ambient air quality standards [*United States Environmental Protection Agency*, 2001]) concentrations for ammonium and nitrate aerosol can also be compared to the observed 24-hour average concentrations. Both the simulated 24-hour average ammonium concentration (by less than a factor of 2) and the simulated 24-hour average nitrate concentration (by approximately 15%) in Azusa are overpredicted.

Figure 3.5 shows simulated (open) total organic aerosol mass concentrations at Central Los Angeles (an upwind site) and Claremont (a downwind site) versus observed concentrations (solid). Total organic aerosol mass is shown because of the inability of field measurements to distinguish between POA and SOA. Figure 3.5 indicates underprediction of the organic aerosol mass in a downwind location in the early part of the day; the most plausible explanation is that the particulate emissions inventory does not accurately reflect emissions of POA that impact this location. Other possible explanations (for example, inadequate initial conditions or gas-phase chemistry) have been eliminated using model diagnostic studies. Conversely, the organic aerosol mass concentration is overpredicted in the upwind location at night; in this location, it is believed that inaccurate simulation of nighttime turbulent mixing is responsible for the overprediction due to the fact that this overprediction at night is not species specific, as discussed earlier. These trends have been observed in simulations of aerosol concentrations in similar locations in the SoCAB. Simulations of the 24-hour average for organic aerosol are within 50% of the observed averages. Observed organic aerosol mass concentrations shown in Figure 3.5 are adapted from organic carbon aerosol data presented by *Fraser et al*. [2000] by multiplying by a factor of 1.4 [*Gray et al*., 1984] to account for non-carbon mass associated with organics.

Figure 3.6 shows the simulated and observed aerosol composition at Central Los Angeles, Azusa, and Claremont at 1400 on September 8, 1993. As seen, total aerosol composition (by mass) is predicted to be mildly dependent on location. In each location, aerosol nitrate is predicted to be the most prevalent species, followed by organics, ammonium or sulfate, other species (which include primary elemental carbon as well as carbonates and metals), and sea salt. Water and other inorganics are not included in this composition distribution. In comparing observed to simulated compositions, it should be pointed out that in all three locations, simulated organic aerosol contributions to mass are less than those observed. Simulated nitrate and ammonium aerosol contributions are both greater than those observed. These trends are consistent with the temporal simulations presented in Figures 4 and 5. Simulated sulfate (within 5%) and sea salt (within 1%) contributions to mass are consistently represented when compared to observations. The contribution of other species is underrepresented in simulations. Given that the role of carbonates is limited and that metals and elementary carbon are primary in nature, the most plausible explanation for this underprediction is an inaccuracy in the emissions inventory.

The simulated contribution of organic aerosol to total particulate levels is greatest in Azusa (45%) and smallest in Claremont (31%). The distribution of organic aerosol between

secondary and primary varies between locations as well, with SOA reaching its peak percentage in Central Los Angeles (62% of total organic aerosol) and minimum percentage in Claremont (45% of total organic aerosol).

Figure 3.7 shows simulated surface-level total organic PM concentrations throughout the SoCAB at 1400 on September 8, 1993, and Figure 3.8 and 3 show the corresponding predictions for SOA at 1200 and 1400 respectively. Concentrations range from 4 to 40 $\mu g\ m^{-3}$ in the total organic aerosol case and from less than 0.5 to 25 $\mu g\ m^{-3}$ and from less than 0.5 to 17 $\mu g\ m^{-3}$, respectively, for the two SOA plots. Figure 3.7 and 2 indicate that SOA is predicted to contribute a significant fraction by mass of the total organic aerosol throughout the SoCAB in this episode. Organic aerosol concentrations are predicted to be highest in areas downwind that experience both secondary aerosol formation and significant transport of aerosol species from upwind locations with large sources of primary aerosol. Comparison of Figure 3.8 and 3 shows the expected movement inland and dilution of the peak of predicted SOA concentrations as the simulation advances in time. The aerosol concentration peaks exhibited in the top left corners of Figure 3.7 through 3 are a result of the very low mixing heights predicted during this episode in the northwest section of the SoCAB.

Table 3.4 shows the contributions to simulated SOA concentrations of anthropogenic and biogenic precursors and the hydrophobic and hydrophilic mechanisms of SOA formation described in Part II [*Pun et al*., 2001] at 1400 on September 8, 1993 in Central Los Angeles, Azusa, and Claremont. Anthropogenic SOA is shown to be the dominant contributor to total SOA in each of these locations (98.3%, 96.9%, and 92.7% by mass, respectively); however, it should be noted that the contribution of anthropogenic species to SOA decreases with downwind location. Biogenically derived SOA is most important in the eastern half of the SoCAB, as plant cover increases in the SoCAB going from upwind to downwind locations. Table 3.4 also exhibits that the dominant formation route for SOA in the SoCAB is via hydrophobic partitioning. SOA formed by this mechanism is estimated to contribute 84.0%, 77.3%, and 64.6% by mass to SOA in Central Los Angeles, Azusa, and Claremont, respectively, indicating that the hydrophilic mechanism becomes more important in the eastern portion of the SoCAB. This is partly due to the fact that biogenically derived SOA in the SoCAB shows more affinity for the aqueous phase than SOA derived from anthropogenic emissions; as discussed above, the eastern half of the SoCAB is more affected by emissions of biogenic SOA precursors. It should also be noted that the contribution of anthropogenically derived SOA formed via the hydrophilic mechanism increases relative to the hydrophobic mechanism going from upwind to downwind locations. Tertiary and quaternary oxidation products formed in higher concentrations in downwind locations are expected to be of a more oxidized nature, increasing their tendency to partition to the aqueous aerosol phase.

3.6 Discussion/Conclusions

This series of three papers is devoted to developing a first-principles approach to the atmospheric modeling of secondary organic aerosol (SOA). The expanded gas-phase chemical mechanism has been formulated to predict the formation of classes of organic compounds that have been identified in or are likely to be constituents of ambient aerosol. The thermodynamic equilibrium module predicts the gas/particle partitioning of organics, inorganics, and water based on dividing the organic species into hydrophobic and hydrophilic fractions. Each of these modules has been integrated into the three-dimensional urban/regional CIT model and applied to simulate the September 8, 1993 smog episode in the South Coast Air Basin of California

(SoCAB). This work presents for the first time atmospheric simulations of the formation of SOA on a molecular basis. As more is learned about the molecular constituency of organic aerosols, the actual classes of surrogate compounds used may change, but the framework presented in these three papers should stand as a foundation for predicting SOA formation.

A system as complex as the gas-particle laden urban atmosphere is characterized by a large number of parameters and inputs, not the least of which are the basic gaseous and particulate emissions that drive the system. Because of uncertainties inherent in these inputs, simulations of this system, even for a relatively well-characterized region like the SoCAB, cannot be expected to, and indeed do not, always match observations one-to-one. What one seeks are simulations that exhibit the correct physics and an understanding of why predictions do not match observations, when such a match does not occur. Detailed sensitivity studies often provide a means to assess these issues; limited diagnostic model runs aimed at eliminating potential causes of mismatches between predictions and observations have been performed over the course of this work, but space does not permit their detailed presentation here. Future work will continue to explore the properties of the thermodynamic partitioning module and the sensitivity of SOA levels to reductions in precursor emissions both in the SoCAB and in other regions.

References

Andersson-Sköld, Y., and D. Simpson, Secondary organic aerosol formation in northern Europe: A model study, *J. Geophys. Res*., *106*, 7357-7374, 2001.

Binkowski, F.S., and U. Shankar, The regional particulate matter model, 1, Model description and preliminary results, *J. Geophys. Res*., *100*, 26,191-26,209, 1995.

Businger, J.A., J.C. Wyngaard, Y. Izumi, and E.F. Bradley, Flux-profile relationships in the atmospheric surface layer, *J. Atmos. Sci*., *28*, 181-189, 1971.

California Air Resources Board, On-road motor vehicle emission inventory models, CARB Web Site (http://www.arb.ca.gov/msei/mvei/mvei.htm), 1998.

Dhaniyala, S., and A.S. Wexler, Numerical schemes to model condensation and evaporation of aerosols, *Atmos. Environ*., *30*, 919-928, 1996.

Fraser, M.P., M.J. Kleeman, J.J. Schauer, and G.R. Cass, Modeling the atmospheric concentrations of individual gas-phase and particle-phase organic compounds, *Environ. Sci. Technol*., *34*, 1302-1312, 2000.

Fraser, M.P., G.R. Cass, and B.R.T. Simoneit, Gas-phase and particle-phase organic compounds emitted from motor vehicle traffic in a Los Angeles roadway tunnel, *Environ. Sci. Technol*., *32*, 2051-2060, 1998.

Fraser, M.P., D. Grosjean, E. Grosjean, and G.R. Cass, Air quality model evaluation data for organics: 1. Bulk chemical composition and gas/particle distribution factors, *Environ. Sci. Technol*., *30*, 1731-1743, 1996.

Gharib, S. and G.R. Cass, Ammonia emissions in the South Coast Air Basin, open file report 84-2, Environmental Quality Laboratory: California Institute of Technology, Pasadena, CA, 1984.

Gray, H.A., G.R. Cass, J.J. Huntzicker, E. Heyerdahl, and J.A. Rau, Characterization of atmospheric organic and elemental carbon particle concentrations in Los Angeles, *Sci. Tot. Environ*., *36*, 17-25, 1984.

Griffin, R.J., D. Dabdub, and J.H. Seinfeld, Secondary organic aerosol: I. Atmospheric chemical mechanism for production of molecular constituents, *J. Geophys. Res*., this issue, 2001.

Harley, R.A., A.G. Russell, G.J. McRae, G.R. Cass, and J.H. Seinfeld, Photochemical modeling of the Southern California Air Quality Study, *Environ. Sci. Technol*., *27*, 378-388, 1993.

Jacobson, M.Z., Development and application of a new air pollution modeling system 3. Aerosol-phase simulations, *Atmos. Environ*., *31*, 587-608, 1997.

Jacobson, M.Z., R. Lu, R.P. Turco, and O.B. Toon, Development and application of a new air pollution modeling system 1. Gas-phase simulations, *Atmos. Environ*., *30*, 1939-1963, 1996.

John, W., S.M. Wall, J.L. Ondo, and W. Winklmayr, *Acidic aerosol size distributions during SCAQS*: Report to the California Air Resources Board under Contract A6-112-39, 1990.

Kim, Y.P., J.H. Seinfeld, and P. Saxena, Atmospheric gas-aerosol equilibrium I. Thermodynamic model, *Aerosol Sci. Technol*., *19*, 157-181, 1993a.

Kim, Y.P., J.H. Seinfeld, and P. Saxena, Atmospheric gas-aerosol equilibrium II. Analysis of common approximations and activity coefficient calculation methods, *Aerosol Sci. Technol*., *19*, 182-198, 1993b.

Kleeman, M.J., and G.R. Cass, Identifying the effect of individual emissions sources on particulate air quality within a photochemical aerosol processes trajectory model, *Atmos. Environ*., *33*, 4597-4613, 1999.

Kleeman, M.J., G. R. Cass, and A. Eldering, Modeling the airborne particulate matter complex as a source-oriented external mixture, *J. Geophys. Res.*, *102*, 21,355-21,372, 1997.

Lurmann, F.W., A.S. Wexler, S.N. Pandis, S. Musarra, N. Kumar, and J.H. Seinfeld, Modeling urban and regional aerosols 2. Application to California's South Coast Air Basin, *Atmos. Environ*., *31*, 2695-2715, 1997.

McRae, G.J., and J.H. Seinfeld, Development of a second-generation mathematical model for urban air pollution 2. Evaluation of model performance, *Atmos. Environ*., *17*, 501-522, 1983.

McRae, G.J., W.R. Goodin, and J.H. Seinfeld, Development of a second-generation mathematical model for urban air pollution 1. Model formulation, *Atmos. Environ*., *16*, 679-696, 1982.

Meng, Z., D. Dabdub, and J.H. Seinfeld, Size-resolved and chemically resolved model of atmospheric aerosol dynamics, *J. Geophys. Res.*, *103*, 3419-3435, 1998.

Meng, Z., D. Dabdub, and J.H. Seinfeld, Chemical coupling between atmospheric ozone and particulate matter, *Science*, *277*, 116-119, 1997.

Meng, Z., J.H. Seinfeld, P. Saxena, and Y.P. Kim, Atmospheric gas-aerosol equilibrium IV Thermodynamics of carbonates, *Aerosol Sci. Technol*., *23*, 131-154, 1995.

Nguyen, K., and D. Dabdub, Two level time marching scheme using splines for solving the advection equation, *Atmos. Environ*., *35*, 1627-1637, 2001a.

Nguyen, K., and D. Dabdub, Semi-lagrangian flux scheme for the solution of the aerosol condensation/evaporation equation, *Aerosol Sci. Technol*., in press, 2001b.

Pandis, S.N., A.S. Wexler, and J.H. Seinfeld, Secondary organic aerosol formation and transport 2. Predicting the ambient secondary organic aerosol size distribution, *Atmos. Environ*., *27A*, 2403-2416, 1993.

Pierson, W.R., A.W. Gertler, and R.L. Bradow, Comparison of the SCAQS tunnel study with other on-road vehicle emission data, *J. Air Waste Manage. Assoc*., *40*, 1495-1504, 1990.

Pilinis, C., and J.H. Seinfeld, Continued development of a general equilibrium model for inorganic multicomponent atmospheric aerosols, *Atmos. Environ*., *22*, 1985-2001, 1987.

Pun, B.K., R.J. Griffin, C. Seigneur, and J.H. Seinfeld, Secondary organic aerosol: II. Thermodynamic model for gas/particle partitioning of molecular constituents, *J. Geophys. Res*., this issue, 2001.

Robinson, R.A., and R.J. Stokes, *Electrolyte Solutions*, 2nd ed., Butterworths, London, 1965.

Rogge, W.F., M.A. Mazurek, L.M. Hildemann, G.R. Cass, and B.R.T. Simoneit, Quantification of urban organic aerosols at a molecular-level-identification, abundance and seasonal-variation, *Atmos. Environ*., *27A*, 1309-1330, 1993.

Schauer, J.J., M.J. Kleeman, G.R. Cass, and B.R.T. Simoneit, Measurement of emissions from air pollution sources 3. C_1 through C_{29} organic compounds from fireplace combustion of wood, *Environ. Sci. Technol*., *35*, 1716-1728, 2001.

Schauer, J.J., M.J. Kleeman, G.R. Cass, and B.R.T. Simoneit, Measurement of emissions from air pollution sources 1. C_1 through C_{29} organic compounds from meat charbroiling, *Environ. Sci. Technol*., *33*, 1566-1577, 1999a.

Schauer, J.J., M.J. Kleeman, G.R. Cass, and B.R.T. Simoneit, Measurement of emissions from air pollution sources 2. C_1 through C_{30} organic compounds from medium duty diesel trucks, *Environ. Sci. Technol*., *33*, 1578-1587, 1999b.

Schauer, J.J. *Source Contributions to Atmospheric Organic Compound Concentrations: Emissions, Measurements, and Model Predictions*, Ph.D. Thesis, California Institute of Technology, Pasadena, CA, 1998.

Systems Applications International (SAI), User's guide for the urban airshed model, I, *Rep. SYSAPP-90/018a*, Syst. Appl. Int., San Rafael, Calif., 1990a.

Systems Applications International (SAI), User's guide for the urban airshed model, II, preprocessors and postprocessors for the UAM modeling system, *Rep. SYSAPP-90/018b*, Syst. Appl. Int., San Rafael, Calif., 1990b.

Systems Applications International (SAI), User's guide for the urban airshed model, III, the diagnostic wind model, *Rep. SYSAPP-90/018c*, Syst. Appl. Int., San Rafael, Calif., 1990c.

Systems Applications International (SAI), User's guide for the urban airshed model, IV, the emissions preprocessor system, *Rep. SYSAPP-90/018d*, Syst. Appl. Int., San Rafael, Calif., 1990d.

Systems Applications International (SAI), User's guide for the urban airshed model, V, description and operation of the ROM-UAM interface program system, *Rep. SYSAPP-90/018e*, Syst. Appl. Int., San Rafael, Calif., 1990e.

United States Environmental Protection Agency, National Ambient Air Quality Standards Web Site (www.epa.gov/airs/criteria.html), 2001.

Wesely, M.L., Parameterizations of surface resistance to gaseous dry deposition in regional-scale numerical models, *Atmos. Environ*., *23*, 1293-1304, 1989.

Wexler, A.S., F.W. Lurmann, and J.H Seinfeld, Modeling urban and regional aerosols, I. Model development, *Atmos. Environ*., *28*, 531-546, 1994.

Winner, D.A., and G.R. Cass, Modeling the long-term frequency distribution of regional ozone concentrations, *Atmos. Environ*., *33*, 431-451, 1999.

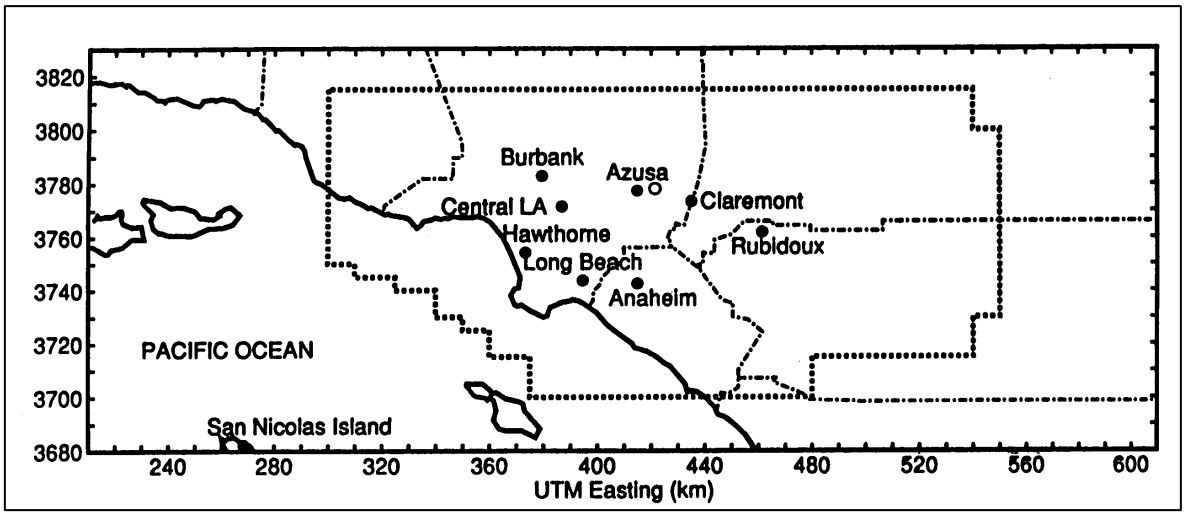

Figure 3.1. The South Coast Air Basin of California showing central Los Angeles, sampling locations during the 1993 smog episode, and other suburbs for reference.

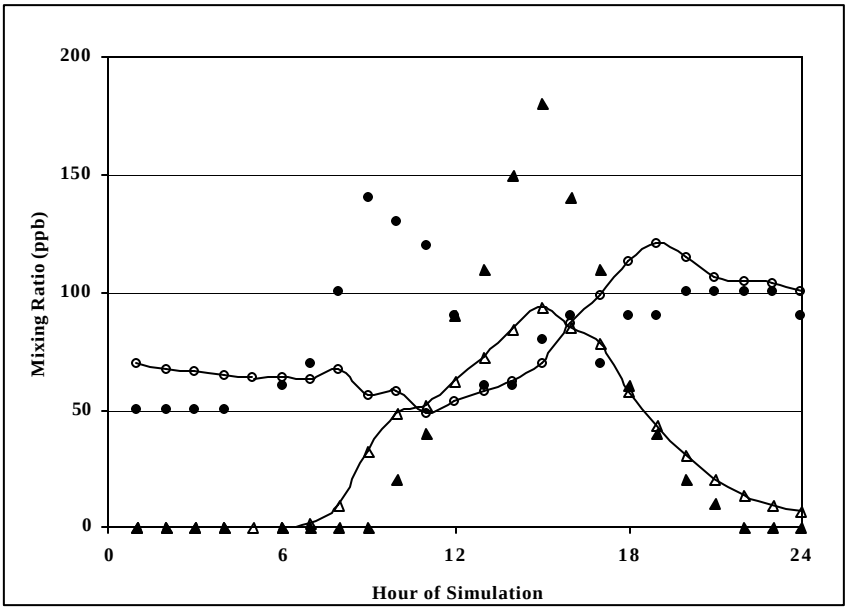

Figure 3.2. Simulated (open) versus observed (solid) NO_2 (circle) and O_3 (triangle) mixing ratios for Azusa for September 8, 1993.

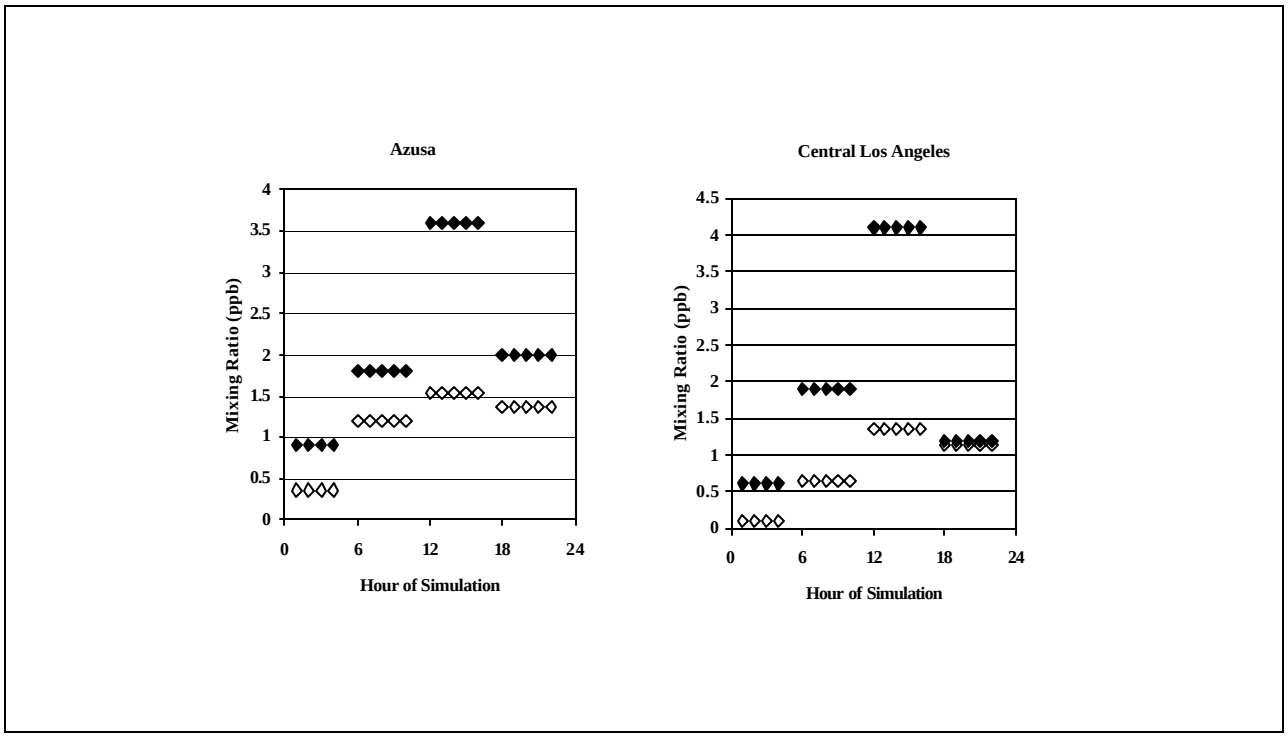

Figure 3.3. Simulated (open) versus observed (solid) MGLY 4-hour average mixing ratios for Azusa (left) and Central Los Angeles (right) for September 8, 1993.

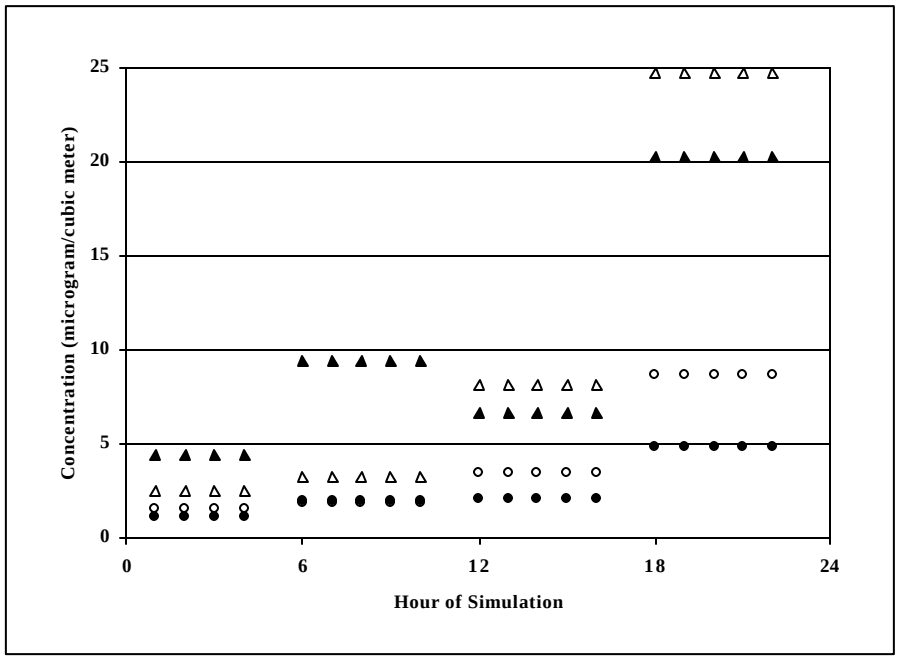

Figure 3.4. Simulated (open) total ammonium (circle) and nitrate (triangle) concentrations (μg m^{-3}) versus observed (solid) concentrations for Azusa for September 8, 1993.

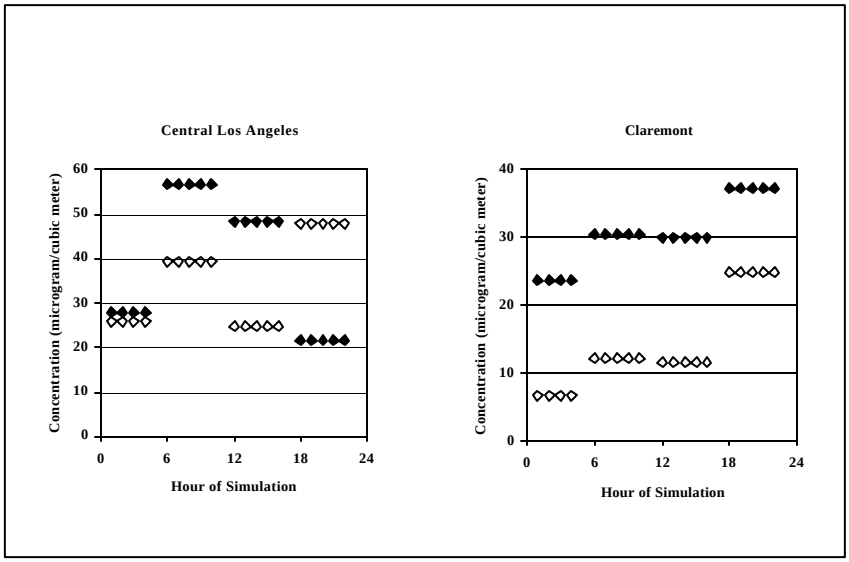

Figure 3.5. Simulated (open) total 4-hour average organic aerosol concentrations ($\mu g\ m^{-3}$) versus observed (solid) concentrations for Central Los Angeles (left) and Claremont (right) for September 8, 1993.

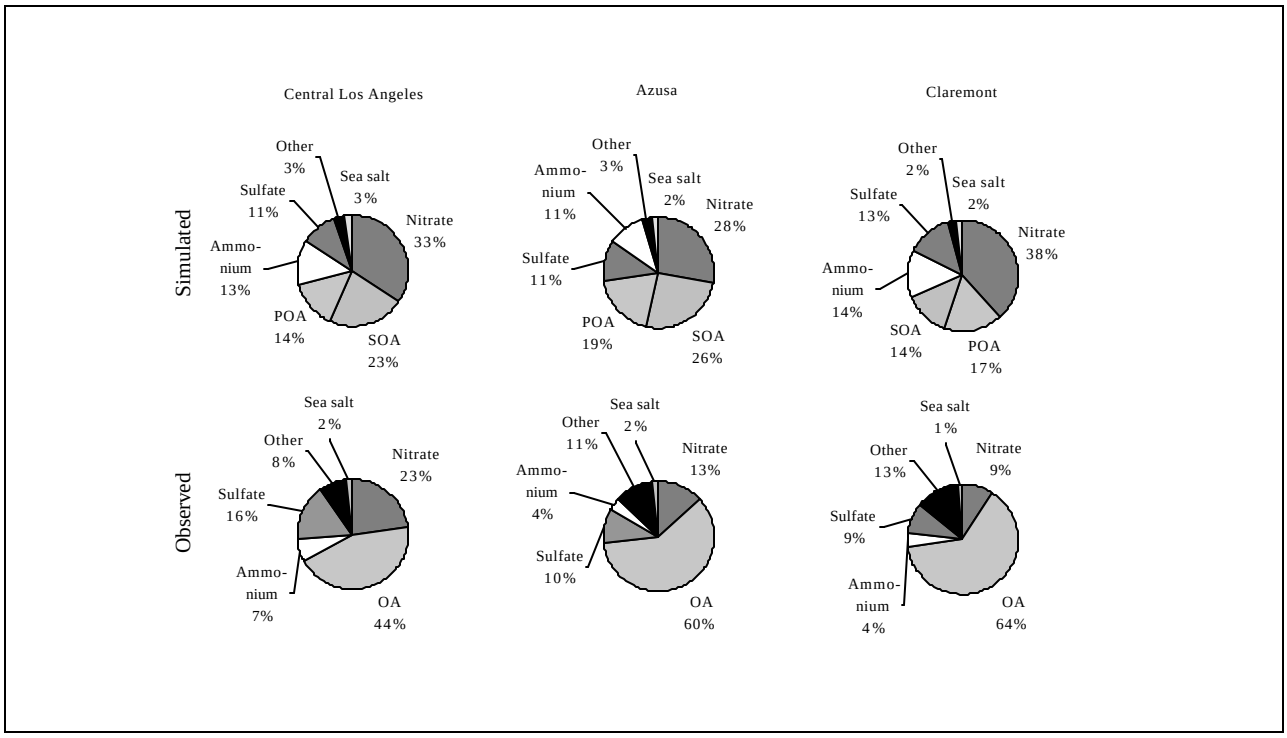

Figure 3.6. Simulated versus observed aerosol mass composition for Central Los Angeles, Azusa, and Claremont at 1400 on September 8, 1993. Other here includes primary elemental carbon, carbonates, and metals; the model categories water and other inorganics are not included.

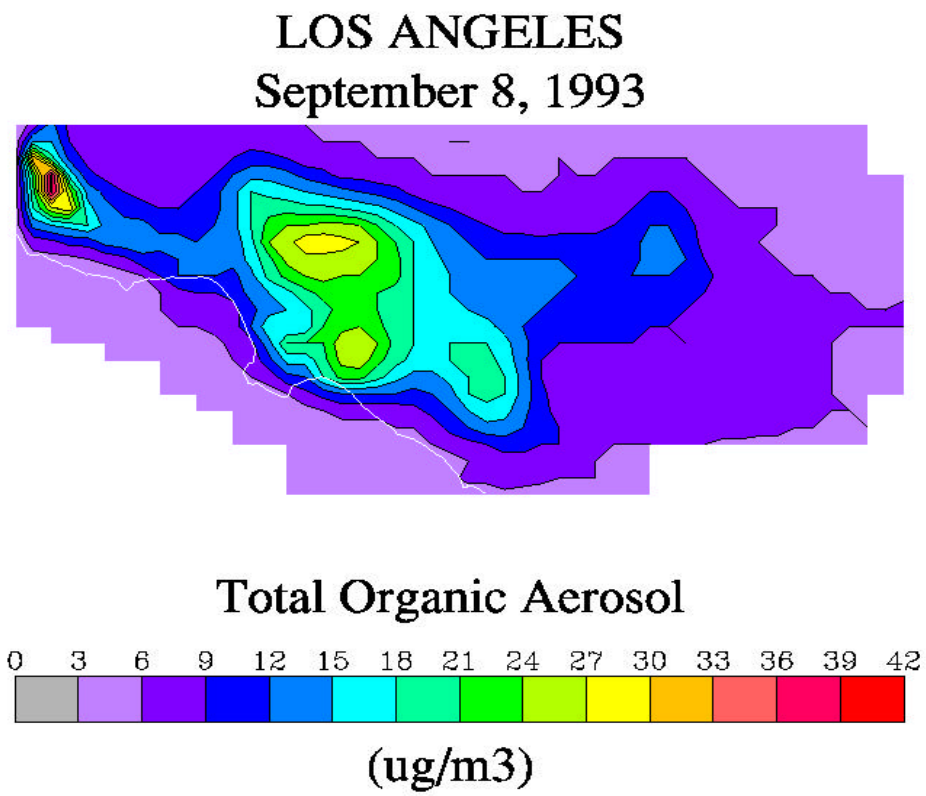

Figure 3.7. Spatial distribution of organic aerosol PM in the SoCAB at 1400, September 8, 1993. (Color versions available from the authors.)

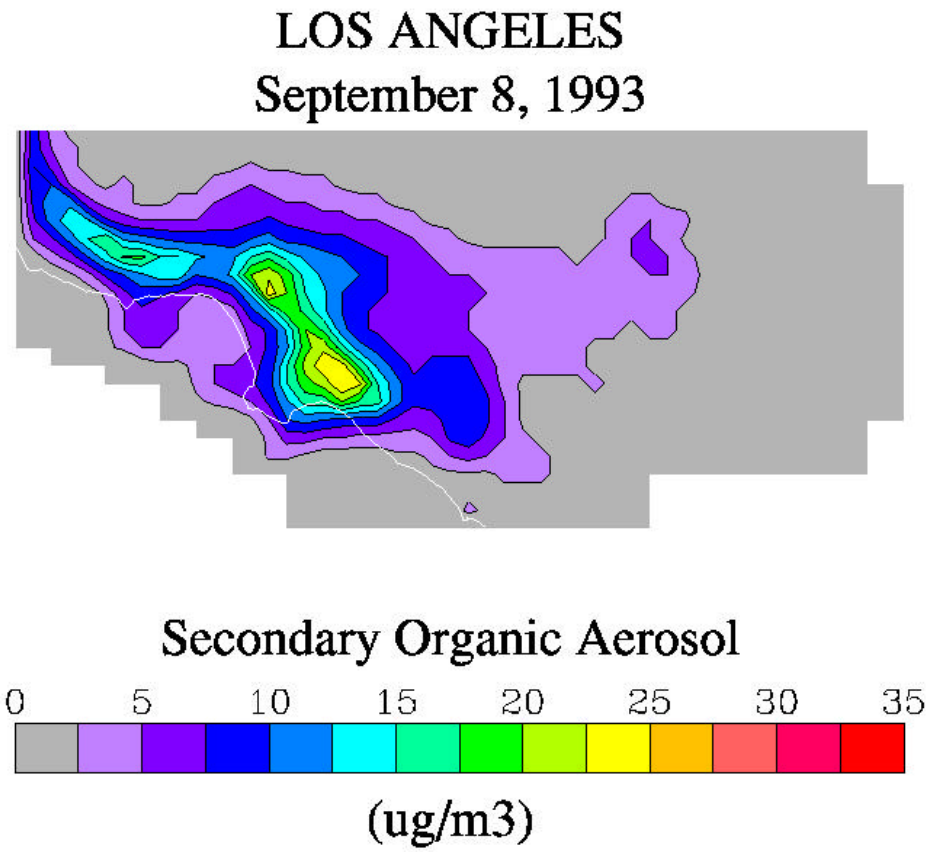

Figure 3.8. Spatial distribution of SOA PM in the SoCAB at 1200, September 8, 1993. (Color versions available from the authors.)

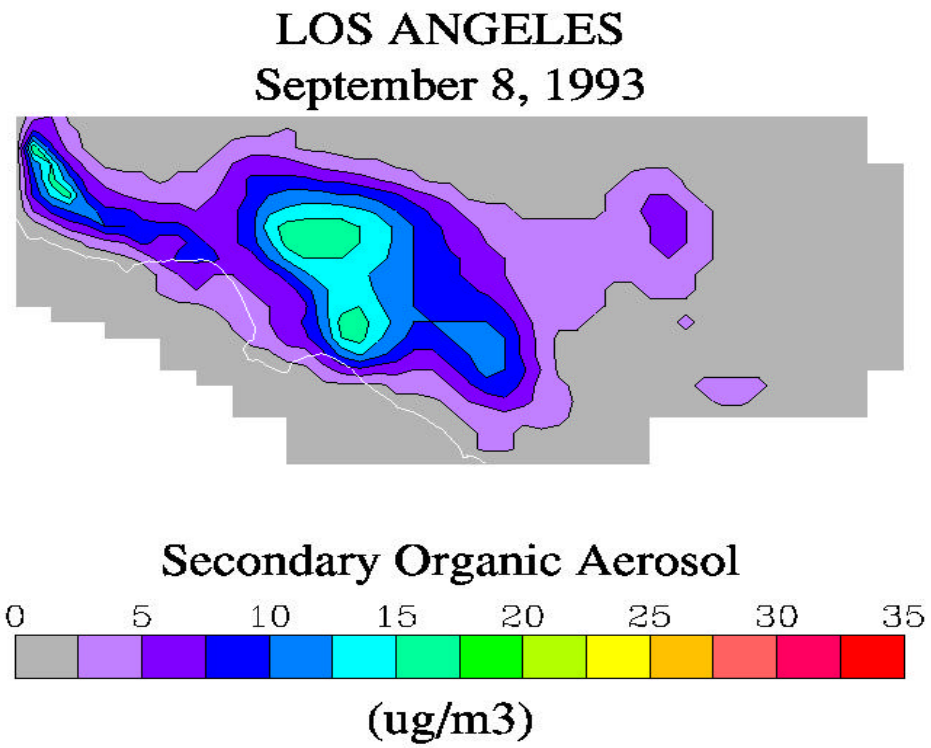

Figure 3.9. Spatial distribution of SOA PM in the SoCAB at 1400, September 8, 1993. (Color versions available from the authors.)

Table 3.1. Particulate emissions by species and size (metric ton day^{-1}) in the SoCAB on September 8, 1993.

Section	1	2	3	4	5	6	7	8	Total
D_p (μm)	0.06	0.11	0.22	0.44	0.88	1.77	3.53	7.07	
EC*	1.2	4.1	4.2	1.1	0.6	0.5	0.9	1.5	14.1
OC*	4.6	6.1	6.9	4.8	3.0	4.2	11.2	20.5	61.3
Sodium Ion	0.1	0.1	0.1	0.05	0.05	0.1	0.2	0.4	1.1
Chloride Ion	0.2	0.2	0.2	0.1	0.1	0.1	0.2	0.3	1.4
Ammonium	0.006	0.022	0.025	0.02	0.013	0.002	0.002	0.002	0.1
Sulfur (VI)	1.2	0.6	0.6	0.6	0.5	0.3	0.7	1.4	5.9
Nitrate	0.2	0.2	0.2	0.1	0.1	0.1	0.2	0.4	1.5
Other	1.8	3.0	9.1	16.6	18.9	35.9	112.5	184.2	382.0
Metals	0	0.1	0.1	0.1	0.1	0.2	1.2	1.2	3.0
Unknown	0.3	2.0	3.2	3.2	3.3	5.5	13.0	25.7	56.2
Sulfur (IV)	0	0.006	0.009	0.009	0.019	0.021	0.034	0.034	0.1
n-Alkanes	0.1	0.023	0.022	0.013	0.012	0.021	0.1	0.1	0.4
Diacids	0.009	0.028	0.02	0.004	0.002	0.001	0.001	0.001	0.1
Oxygenated PAH	0.3	0.015	0.009	0.001	0.001	0	0.001	0.001	0.3
PAH	0.4	0.019	0.019	0.007	0.004	0.006	0.01	0.013	0.5
Cyclics	0.006	0.009	0.007	0.005	0.0004	0.007	0.014	0.024	0.1
Substituted Monoaromatics	0	0	0	0	0	0	0	0	<0.0001
Aliphatic Acids	0.1	0.046	0.1	0.1	0.1	0.1	0.2	0.4	1.1
Total	10.5	16.6	24.8	26.8	26.8	47.1	140.5	236.2	529

*EC = elemental carbon; OC = unresolved organic carbon

Table 3.2. Gas-phase emissions by species and source (metric ton day^{-1}) in the SoCAB on September 8, 1993.

Category	NMOG*	NO_x	CO
Fuel combustion	12.4	105.7	46.9
Waste burning	0.5	1.9	2.8
Solvent use	335.2	0.3	0.2
Petroleum process (storage/transfer)	50.8	0.3	3.7
Industrial processes	21.4	5.5	0.8
Miscellaneous processes	65.9	1.0	9.3
On-road vehicles	1117.6	701.5	9236.9
Other mobile	103.7	250.0	1379.3
Other sources	119.2	0.0	0.3
Total	1826.7	1066.2	10680.1

*non-methane organic gases

Table 3.3. Assumed distribution of non-methane organic gases (NMOGs) when speciation is unknown.

Species *i*	Land factor (ppb_i per ppmC NMOG)	Ocean factor (ppb_i per ppmC NMOG)
ETHE	0.0436	0.0058
ALKL	0.4551	0.1139
ALKM	0.1113	0.0225
ALKH	0.0015	0.0000
OLEL	0.1640	0.0028
OLEH	0.0014	0.0000
AROL	0.1323	0.0000
AROH	0.0999	0.0074
AROO	0.0010	0.0000
PAH	0.0345	0.0000
ISOP	0.0028	0.0000
BIOL	0.0021	0.0000
BIOH	0.0021	0.0000

Table 3.4. Predicted percent contribution to SOA formation of different sources and formation mechanisms in three locations in the SoCAB.

	Central Los Angeles	Azusa	Claremont
Anthropogenic	98.3	96.9	92.7
Biogenic	1.7	3.1	7.3
Hydrophobic	84.0	77.3	64.6
Hydrophilic	16.0	22.7	35.4

Chapter 4

Development of a new aerosol module and incorporation into models-3/Cmaq

4.1 Introduction

The demonstration of attainment of the National Ambient Air Quality Standards (NAAQS) for Particulate Matter (PM) and reasonable progress under the Regional Haze regulations will require the use of three-dimensional (3-D) air quality models (EPA, 2000). A review of the current status of 3-D air quality models for PM (Seigneur et al., 1999) suggested that existing models had several limitations in their treatment of aerosol processes that needed to be addressed before they could be applied in a regulatory context. Therefore, it is essential to improve the most promising model(s) to ensure that they properly treat all the relevant physico-chemical processes. We present in this report the development of a new aerosol module and its incorporation into the EPA Models-3 Community Multiscale Air Quality model (CMAQ). Models-3/CMAQ was selected as the 3-D host air quality model following a review of selected existing 3-D models (Pai et al., 1999; Seigneur et al., 2000).

This aerosol module is referred to as the Model for Aerosol Dynamics, Reaction, Ionization and Dissolution (MADRID). It uses the same algorithms for aerosol dynamics and the thermodynamics of inorganic chemical species as an aerosol module developed earlier under EPRI funding, which is referred to as MADRID 1. The module presented here is referred to as MADRID 2. MADRID 1 and MADRID 2 differ only in their treatment of secondary organic aerosol (SOA) formation. In MADRID 1, SOA formation is simulated using an empirical representation based on experimental data obtained in smog chamber experiments. A new component for SOA formation, that provides a mechanistic representation of SOA formation, was developed and incorporated in MADRID 2.

The organization of the report is as follows. An overview of existing aerosol modules is presented in Section 2. Section 3 describes the new aerosol module, MADRID 2. The implementation of MADRID 2 into Models-3/CMAQ is discussed in Section 4. A test case simulation is presented in Section 5. Concluding remarks are provided in Section 6.

4.2 Overview of Existing Algorithms for Aerosol Modeling

A comprehensive review of the existing algorithms available to simulate gas/particle equilibrium thermodynamics and the dynamics of the particle size distribution was performed by Zhang et al. (1999, 2000). This review is summarized below.

4.2.1 Gas/Particle Thermodynamic Equilibrium

Six modules that simulate the gas/particle partitioning of inorganic species were compared using 40 different case studies. These six modules included MARS-A (Binkowski and Shankar, 1995), SEQUILIB (Pilinis and Seinfeld, 1987), SCAPE2 (Kim and Seinfeld, 1995; Meng et al., 1995), EQUISOLV II (Jacobson, 1999), AIM2 (Clegg et al., 1998a, b) and ISORROPIA (Nenes et al., 1999). All modules treat sulfate, nitrate, ammonium and water. Except for MARS-A, all modules also treat sodium and chloride. In addition, SCAPE2 and EQUISOLV II treat crustal soluble species: calcium, magnesium, potassium and carbonate. The conclusions of this comprehensive review are summarized in Table 4.1.

AIM2 does not simulate alkaline systems and was therefore not considered for incorporation into Models-3/CMAQ. MARS-A is the default model of Models-3/CMAQ. We selected two mew modules for incorporation into Models-3/CMAQ: one that provides treatment of sea salt and is computationally efficient and one that can provide a treatment of all relevant chemical species including sea salt and crustal material. Among the computationally efficient modules, ISORROPIA was judged superior to SEQUILIB (see Table 4.1). For a comprehensive treatment of the aerosol system, both SCAPE2 and EQUISOLV II were considered suitable. Since SCAPE2 was already coupled to the modules that simulate aerosol dynamics (see discussion below), it was selected for incorporation into Models-3/CMAQ.

4.2.2 Aerosol Dynamics

Two major approaches have been used to represent the particle size distribution: the modal approach and the sectional approach. In the modal approach, the particle size distribution is represented by several modes (e.g., Aitken nuclei, accumulation and coarse modes) and an analytical function (typically, a log-normal distribution) is used to represent the particle size distribution of each mode. The aerosol dynamic processes that govern the evolution of the particle size distribution can then be solved analytically. In the sectional approach, the particle size distribution is approximated by a discrete number of size sections. Some properties of the particle size distribution (e.g., mass of individual chemical species) are then assumed to be uniform within each size section and to be conserved as the aerosol general dynamic equation is solved. The modal approach is used in the original Models-3/CMAQ. We selected a sectional approach to represent the particle size distribution of the new aerosol modules being incorporated into Models-3/CMAQ. The processes that govern aerosol dynamics include coagulation, nucleation, growth due to condensation, shrinkage due to volatilization and the mass transfer of chemical species between the bulk gas phase and the particle surface.

Zhang et al. (1999) compared the modal and sectional approaches for coagulation and concluded that the sectional approach (with 8 sections or more) is more accurate than the modal approach. The sectional approach is, however, computationally more demanding. In any case, coagulation can be neglected under most cases for urban/regional 3-D modeling.

A comparison of all algorithms currently used in 3-D air quality models to calculate the absolute rate of particle nucleation showed that all algorithms give highly uncertain results. Consequently, Zhang et al. (1999) recommended the use of a method that calculates the relative rates of new particle formation and condensation on existing particles (McMurry and Friedlander, 1979) instead of calculating the absolute rate of nucleation. This method was selected for the treatment of new particle formation in the new aerosol modules.

The simulation of growth by condensation or shrinkage by volatilization is difficult with a sectional representation because, in 3-D simulations, it leads to numerical diffusion. Three basic approaches have been used to simulate condensational growth:

(1) Semi-Lagrangian techniques that calculate the mass (or number) flux from one section to the next. The basic finite-difference method (e.g., Seigneur, 1982) is the simplest example of a semi-Lagrangian technique. Bott's scheme is a more advanced example of a semi-Lagrangian technique (Bott, 1989).
(2) Lagrangian techniques that calculate the movement of the section boundaries according to the growth law and redistribute the resulting sectional distribution onto the fixed sectional representation. The UAM-AERO scheme (Lurmann et al., 1997)

is an example of a Lagrangian technique where a spline function is used for the redistribution of the sectional representation.

(3) The moving-center technique of Jacobson (Jacobson and Turco, 1995; Jacobson, 1997) where the diameter representative of the section moves according to the growth law (i.e., the equivalent of an Eulerian technique since transfer of mass between sections is minimized).

Among the algorithms tested, the moving center approach appeared to be the most accurate. Bott's algorithm led to significant upstream numerical diffusion under conditions with low PM concentrations. The Quintic Spline Taylor Series Expansion (QSTSE) algorithm of Dabdub (Nguyen and Dabdub, 2001a) was later tested and shown to perform better than Bott's algorithm. Both Bott's algorithm and QSTSE were selected for incorporation into the new aerosol modules.

The transfer of chemical species from the bulk gas phase to large particles is typically slow and, in the case of chemically reactive coarse particles such as sea salt and alkaline dust particles, may prevent the aerosol from reaching thermodynamic equilibrium. There are three major approaches to treat mass transfer between the gas phase and particles:

(1) An explicit treatment of mass transfer that is accurate but computationally demanding.

(2) A full equilibrium approach that is computationally efficient but may be inaccurate in the presence of sea salt or alkaline soil dust, and

(3) An hybrid approach that assumes full equilibrium between the bulk gas phase and the bulk particulate phase but distributes the condensing mass according to a growth law that depends on particle size. This approach offers compromise between accuracy and computational efficiency.

An explicit treatment of mass transfer was found to be important only for cases with significant reactive coarse particle concentrations (i.e., sea salt or soil dust). The hybrid approach where a bulk equilibrium is assumed and the condensing vapor is distributed according to a growth law was found to be a computationally efficient approximation. Accordingly, all three approaches were selected to be incorporated as options in the new aerosol modules.

4.3 Description of the New Aerosol Module

4.3.1 Overview of MADRID 2

Since the existing Caltech aerosol module (Meng et al., 1998) included many components that were considered satisfactory according to that review, it provided the basis for the development of MADRID 2.

Table 4.2 summarizes the components that were selected. Note that there are several options available for gas/particle mass transfer, gas/particle thermodynamics, condensational growth, and nucleation. Coagulation is not treated since it is negligible under most conditions. The formation of new particles can be either simulated using the approach of McMurry and Friedlander (1979) or neglected, which is appropriate under most polluted conditions. The algorithm for new particle formation was developed under the EPRI project and is described in detail in Section 3.3. Two algorithms are available to simulate gas/particle thermodynamic

equilibrium: SCAPE2 and ISORROPIA (version 1.3). SCAPE2 offers the option of a comprehensive treatment (i.e., crustal species are included) whereas ISORROPIA is computationally more efficient.

The treatment for SOA formation is new and was developed under this ARB contract. It is described in detail in Section 3.2.

Three options are available for the simulation of gas/particle mass transfer: A kinetic mass transfer algorithm that is accurate but computationally expensive, a hybrid algorithm and a full equilibrium algorithm. The hybrid algorithm is always used for SOA since organic vapors condense primarily on fine particles and a kinetic mass transfer treatment is, therefore, not necessary.

There are several options for condensational growth. Two growth laws are available. If the hybrid or full equilibrium approach is selected for mass transfer, condensational growth is simulated with a first-order finite difference algorithm. If the kinetic mass transfer option is selected, either Bott's algorithm or the QSTSE algorithm can be selected.

A new formulation was developed under the EPRI project for the treatment of particle dry deposition; it is described in Section 3.4.

The sectional particle size distribution is flexible. The two main options are a two-section representation (i.e., fine and coarse particles) or a multi-section representation where the user can select the number of sections.

It should be noted that some components have limitations. Those are indicated in Table 4.2. The limitations are currently being addressed under EPRI funding and future versions of the aerosol module will include more robust algorithms as those become available.

4.3.2 Treatment of Secondary Organic Aerosol Formation

The SOA module of MADRID 2 is coupled to a gas-phase chemical kinetic mechanism that was developed at the California Institute of Technology (Caltech). This AER/EPRI/Caltech SOA module is hereafter referred to as the AEC module (EPRI, 1999; Pun et al., 1999). The AEC module simulates an external mixture of hydrophilic and hydrophobic organic compounds, as shown in Figure 4.1.

4.3.3 Partitioning of Hydrophilic Compounds

The overall structure of the hydrophilic module is depicted in Figure 4.2. Hydrophilic compounds are miscible with inorganic solutes, such as sulfate and nitrate, at relative humidities above their deliquescence. Therefore, they dissolve in existing particles that contain an aqueous phase of inorganic compounds. In this mixture, organic solutes may be present as molecules or ions (in the case of electrolytes like organic acids) in the aqueous phase. The relationship between gas-phase organic compounds and the dissolved molecules is governed by Henry's law.

$$H_{HA} = \{HA_{(aq)}\} / P_{HA} \qquad (3\text{-}1)$$

where H_{HA} is the Henry's law coefficient, $\{HA_{(aq)}\}$ is the activity of the molecule in the aqueous phase and P_{HA} is the partial pressure of HA in the gas phase. The solubility of organic acids is enhanced by the dissociation of the molecules into ions. Therefore, the acid dissociation equations must also be satisfied.

$$K_A = \frac{\{H^+\}\{A^-\}}{\{HA_{(aq)}\}} \qquad (3\text{-}2)$$

where K_A is the dissociation constant and $\{H^+\}$, $\{A^-\}$ and $\{HA_{(aq)}\}$ are the activities of the proton, the acid anion and acid molecule, respectively.

The activity of a species is calculated as the product of its concentration and the activity coefficient, which characterizes the deviation from ideality. At present, there is no satisfactory way to estimate activity coefficients in a mixed electrolyte/molecular system of organic and inorganic solutes. Therefore, organic-inorganic interactions are not modeled in the activity calculations. Of the methodologies available to calculate activity coefficients of organic compounds, UNIFAC is the most versatile, because it requires only properties of functional groups within the molecule and no molecule-specific experimental data (such data are not available for many of the complex organic compounds present in the atmosphere). We used the UNIFAC method to estimate the activity coefficients of both molecular organic solutes and organic ions in the hydrophilic module. A globally convergent Newton/line search method (Press et al., 1992) is used to solve the system of partition equations.

Organic solutes that partition into the particulate phase are associated with additional water. Two options are provided to calculate the water associated with organic compounds: (1) the ZSR equation can be used to determine the additional water based on UNIFAC-generated data on binary solutions of the solutes in water or (2) UNIFAC can be used to determine the concentration of particulate water such that its activity equals the ambient relative humidity.

When the relative humidity is below the deliquescence point of an organic compound, that compound does not dissolve in the existing aqueous phase and is not associated with additional water.

If no water is associated with inorganic compounds, organic compounds may still partition into the particulate phase if they dissolve into an organic-phase solution. The formation of organic-phase liquid aerosols follows the absorption theory used in the hydrophobic subroutine (discussed below). Additional water may be associated with the hydrophilic compounds that enter the particulate phase through absorption.

Hydrophilic compounds dissolve into an aqueous phase that also contains inorganic species such as sodium, ammonium, sulfate, nitrate, and chloride. Computationally, the aqueous organic aerosol module interacts with the inorganic aerosol module (i.e., SCAPE2 or ISORROPIA) to calculate the pH and liquid water content (LWC) of the aqueous particles (see Figure 4.3). In EPRI (1999), a procedure to link the hydrophilic organic aerosol module with SCAPE2 was presented. Due to its superior computational stability, ISORROPIA was preferred here for the incorporation into a 3-D model. Therefore, we made changes to ISORROPIA (version 1.3), to account for the effect of organic anions in the charge balance equation, the increased liquid water content associated with organic solutes, and the effect of the additional anions on the ionic strength of the solution (a parameter used in calculating the activity coefficient of inorganic ions). These changes were reviewed and approved by A. Nenes, Caltech, the developer of ISORROPIA.

4.3.4 Partitioning of Hydrophobic Compounds

Hydrophobic surrogate compounds are absorbed into an organic phase, which contains both primary and secondary components. The absorption equation is as follows.

$$K_i = \frac{A_i}{\left(M_0 + \sum_j A_j\right) G_i} \tag{3-3}$$

where K_i ($m^3/\mu g$) is the partition coefficient between the gas and particle phases, A_i is the mass concentration in the particle phase ($\mu g/m^3$ air), G_i is the mass concentration in the gas phase ($\mu g/m^3$ air), and M_0 is the mass concentration ($\mu g/m^3$ air) of primary organic compounds that form a part of the absorbing organic medium. The primary organic matter in the absorbing medium is represented by five surrogate compounds, including saturated and unsaturated fatty acids, substituted phenols, long-chain alkanes, and aromatic dicaboxylic acids. K_i depends on the characteristics of the partitioning compound as well as those of the organic mixture in the particulate phase. Pankow (1994) derived the following formula for K_i.

$$K_i = \frac{760RT}{10^6 P_i^{sat} g_i (MW_{om})} \tag{3-4}$$

where R (= 8.2 x 10^{-5} m^3 atm/mol/K) is the gas constant, T (K) is temperature, P_i^{sat} (torr) is the saturation vapor pressure, g_i is the activity coefficient of compound i in the liquid phase, and MW_{om} (g/mol) is the average molecular weight of the organic absorbing medium. A globally convergent Newton/line search method (Press et al., 1992) is used to solve the system of partition equations. The design of the hydrophobic module is shown in Figure 4.4.

4.3.5 Coupling of the AEC Module with CACM

In its current implementation, the AEC module simulates the partition of five hydrophilic and five hydrophobic surrogate compounds that represent 42 organic condensable species produced in the Caltech Atmospheric Chemistry Mechanism (CACM) (R. Griffin, 2000).

The condensable compounds of CACM were first classified as hydrophilic or hydrophobic. Hydrophilic compounds have (1) a short carbon chain ($\leq$ 7 carbons; or $\leq$ 10 carbons with three or more functional groups), (2) high solubility ($\geq$ 1 g solute / 100 g water), and (3) a high effective Henry's law constant ($H^* \geq 1 \times 10^6$ M atm^{-1}). Hydrophobic compounds are identified by their estimated octanol-water partition coefficient (K_{ow}) values. Many of the aromatic acid compounds are associated with sufficiently high H* and solubilities to partition into the aqueous phase, according to the H* and solubility criteria set forth by Saxena and Hildemann (1996). However, K_{ow} estimates indicate that these aromatic compounds are moderately hydrophobic and they are, therefore, assigned to the hydrophobic group.

Next, the 14 hydrophilic and 28 hydrophobic compounds of CACM were grouped into subgroups based on their origins, i.e., whether they are anthropogenic or biogenic. For hydrophilic compounds, we selected three surrogates to represent anthropogenic compounds based on dissociative properties and molecular weight (MW): dissociative and low MW, dissociative and high MW, non-dissociative. There are two surrogates, dissociative and non-dissociative, for biogenic hydrophilic compounds. Anthropogenic hydrophobic compounds are represented by four surrogates, which are benzene-based, nathphalene-based, or aliphatic. The benzene-based category is further divided into high and low vapor pressure compounds. There is only one biogenic hydrophobic surrogate compound and it is aliphatic in nature. In addition to

surrogate secondary compounds, the model is also set up for butanedioic acid, a chemically inert hydrophilic species that may be present as a primary aerosol component.

Each surrogate compound is assigned a molecular structure that represents an "average" structure of the compounds it represents (see Figure 4.5). Thermodynamic properties of the surrogate compounds are defined as follows. Henry's law constants and saturation vapor pressures are estimated for individual condensing compounds using group contribution methods (Drefahl and Reinhard, 1995). The property of the surrogate compound is the mean value of the properties of the individual compounds. Acid dissociation constants and deliquescence relative humidity are assigned by analogy due to the lack of experimental data and estimation methods. Activity coefficients of the surrogate compounds are estimated using UNIFAC based on the surrogate structure.

4.4 Treatment of New Particle Formation

AER implemented the parameterization of McMurry and Friedlander (1979) in the EPRI aerosol module to simulate the formation of new sulfuric acid particles. Unlike other nucleation parameterizations (e.g., Pandis et al., 1994; Kerminen and Wexler, 1994; Fitzgerald et al., 1998; Harrington and Kreidenweis, 1998) in which the absolute nucleation rates of particles are calculated, the approach of McMurry and Friedlander calculates the relative rates of new particle formation and condensation. The rate of change in the number concentration of condensable molecules is calculated as follows.

$$\frac{dN_1}{dt} = R - b_{1,1}N_1^2 - \sum_{j=2}^{k-1} b_{1,j}N_j N_1 - gAN_1 \qquad (3\text{-}5)$$

where R is the production rate of condensable molecules (monomers) by gas-phase chemical reactions; N_1 is the number concentration of monomers; N_j is the number concentration of molecular clusters containing monomers of size j; k is the number of monomers at the minimum detectable particle size; A is the existing particle surface area per volume of gas for particles of size k and larger; g, $b_{1,1}$, and $b_{1,j}$ are collision coefficients for collisions among monomers, between monomers and molecular clusters, and between monomers and existing particles larger than size k-1, respectively. They can be calculated based on kinetic theory. The second term on the right side of Equation (3-5) is the rate at which monomers collide with themselves, and the third term is the rate at which they collide with molecular clusters formed by nucleation. The fourth term is the rate at which monomers are lost by condensation on particles larger than size k-1. Two major assumptions are used to derive the above equation: (1) condensable molecules stick to other condensable molecules, clusters, or particles with which they collide; and (2) reevaporation from clusters and particles is slow compared with the rate of condensational growth. These assumptions are appropriate for sulfuric acid.

The rate of change in the number concentrations of molecular clusters is calculated as follows.

$$\frac{dN_j}{dt} = b_{1,j-1}N_1 N_{j-1} - b_{1,j}N_1 N_j - \frac{gA}{\sqrt{j}}N_j \qquad (3\text{-}6)$$

The first term on the right side of Equation (3-6) is the rate at which monomers collide with molecular clusters of size j-1 to form molecular clusters of size j, the second term is the rate at which molecular clusters of size j collide with monomers. The third term is the rate at which molecular clusters are lost by condensation on particles larger than size k-1. Two major assumptions are used to derive the above equation: (1) the concentrations of molecular clusters are present in quasi-steady state (typically achieved on a time scale of minutes); and (2) collisions between molecular clusters can be ignored (because of their very low rate of collision compare to collision with monomers or large particles). Only the condensation of monomers on clusters and scavenging of clusters by large particles are considered.

The rate of formation of new particles of size k, $G(k)$, is calculated as follows.

$$G(k) = \beta_{1,k-1} N_1 N_{k-1} \tag{3-7}$$

Equation (3-7) can be expressed in the following dimensionless form.

$$\frac{G(k)}{R} = c_{k-1} L \tilde{N}_{k-1} \tilde{N}_1 \tag{3-8}$$

where $c_{k\text{-}1} = \beta_{1,k\text{-}1}/\beta_{1,1}$, and $\tilde{N}_1$ and $\tilde{N}_{k\text{-}1}$ are the dimensionless monomer and cluster concentrations, respectively. They can be calculated from N_1 and N_j, respectively, as follows.

$$\tilde{N}_j = \frac{\beta_{1,1}}{\gamma A} N_j \tag{3-9}$$

L is the product of two ratios at steady state: $\gamma A N_1/R$, which is the ratio of the rate at which monomers collide with pre-existing particles to the rate at which they are produced, and $\gamma A N_1/\beta_{1,1} N_1^2$, which is the ratio of the rate at which monomers collide with pre-existing particles to the rate at which they collide with themselves. The former ratio has a maximum value of 1, which occurs when new particle formation is completely suppressed. When the latter ratio is large compared to 1, heterogeneous condensation dominates. The relative importance of nucleation and condensation can therefore be determined by the magnitude of L. McMurry and Friedlander (1979) reported a value of 0.1 as a threshold value for L, below which new particle formation is important, and above which condensation on pre-existing particles dominates.

The parameter L is a key parameter in the nucleation theory of McMurry and Friedlander (1979) because the dimensionless rate of particle formation depends on L, $\tilde{N}_1$ and $\tilde{N}_{k\text{-}1,}$ and the latter two variables in turn depend only on L. By definition, L can be calculated as follows.

$$L = \frac{\gamma A N_1}{R} \frac{\gamma A N_1}{\beta_{1,1} N_1^2} = \frac{1}{16\sqrt{3}\pi} \left(\frac{4\pi}{3}\right)^{1/6} \frac{(k_b T)^{1/2} A^2}{\upsilon_1^{7/6} \rho^{1/2} R} \tag{3-10}$$

where k_b is the Boltzmann's constant, T is temperature, ρ is the particle density, and υ_1 is the molecular volume of monomers. Assuming that steady state monomer concentrations can be established on a time scale of minutes, L can be derived from Equation (3-5).

$$L = \frac{1}{\tilde{N}_1^2 + \tilde{N}_1 + \sum_{j=2}^{k-1} c_i \tilde{N}_1 \tilde{N}_j} \tag{3-11}$$

Assuming that the cluster concentrations are in a quasi-steady state, a relationship between $\tilde{N}_j$ and $\tilde{N}_1$ can be derived from Equation (3-6).

$$\frac{\tilde{N}_j}{\tilde{N}_1} = \prod_{i=2}^{j} \frac{c_{i-1}\tilde{N}_1}{c_i \tilde{N}_1 + \frac{1}{\sqrt{i}}} \tag{3-12}$$

Substituting (3-12) into (3-11) for cluster concentrations, a relationship between L and $\tilde{N}_1$ can be obtained. However, since L is not an explicit function of $\tilde{N}_1$, numerical iteration is needed to solve Equations (3-10) and (3-11). To implement the theory of McMurry and Friedlander (1979) into the EPRI aerosol module, an initial concentration of N_1 has to be assumed. $\tilde{N}_1$, $\tilde{N}_{k\text{-}1,}$ and the corresponding L are then calculated according to Equations (3-9), (3-12) and (3-11), respectively. This calculated value of L is compared to the value of L calculated based on Equation (3-10). If the difference between the two L values is within the given error tolerance, the assumed N_1 and the calculated $N_{k\text{-}1}$ are used to calculate the rate of new particle formation, $G(k)$. The number concentrations of the newly-formed particles are then converted to the equivalent number concentrations of particles with the lower diameter of the smallest particle size section and added to that section.

The new particle parameterization of McMurry and Friedlander (1979) is computationally demanding because it involves iterating among Equations (3-9) through (3-12). Consequently, a parameterized version that uses a look-up table with precalculated rates for given values of L and k was developed. Figure 4.6 depicts this parameterization where the relative rate of new particle formation (i.e., ratio of new particle formation rate and total gas-to-particle conversion rate) is presented as a function of L (see Equation 3-11) and k. The value of k (number of H_2SO_4 molecules in a new particle) depends on the lowest diameter of the modeled particle size distribution ($d_{p,min}$ and relative humidity (RH)). For example, k=1900 for $d_{p,min}$ =0.01 μm and RH=50%. New particle formation becomes negligible for L>0.1. The parameterized version is the default option in the code. The user can select the detailed calculation by changing a flag parameter in the code. An option for neglecting the calculation of new particle formation is also provided.

4.5 Treatment of Particle Dry Deposition

The treatment used for dry deposition of particles in Models-3/CMAQ is based on the standard resistance approach.

$$V_d = \frac{1}{r_a + r_b + r_a\, r_b\, V_s} + V_s \tag{3-13}$$

where V_d is the total dry deposition velocity of the particle, V_s is the gravitational settling (sedimentation) velocity, r_a is the aerodynamic resistance in the lower atmosphere and r_b is the resistance in the quasi-laminar layer near the surface. Venkatram and Pleim (1999)

demonstrated that this approach does not conserve mass because the resistance component depends on a concentration gradient whereas the sedimentation term does not.
They solved the particle dry deposition flux equation to obtain the following mass-conserving equation.

$$V_d = \frac{V_s}{1 - \exp\left(-(r_a + r_b)V_s\right)} \tag{3-14}$$

We used this expression of the dry deposition velocity for particles in the new aerosol modules. It is calculated for each particle size section and the dry deposition flux is calculated accordingly by size section.

4.6 Incorporation of MADRID 2 Within Models-3/Cmaq

4.6.1 Incorporation of MADRID 2

Models-3/CMAQ was selected as the host model based on a comprehensive review of several 3-D air quality models currently available for application (Pai et al., 1999; Seigneur et al., 2000). Its formulation is described by Byun and Ching (1999). The current version of Models-3/CMAQ available from EPA includes an aerosol module that uses a modal representation of the aerosol size distribution (Binkowski and Shankar, 1995). The new aerosol module MADRID 2 was added as an option within Models-3/CMAQ. We describe below how this incorporation was implemented.

Figure 4.7 depicts the components of Models-3/CMAQ that pertain to the aerosol simulation and, therefore, were modified to incorporate the option of using the new aerosol module.

Three kinds of inputs are specific to the aerosol module: emissions, initial conditions (IC) and boundary conditions (BC) of particulate matter (PM) and gaseous precursors. No changes were needed for PM precursors since they are the same for both aerosol modules. The PM inputs are set up in Models-3/CMAQ using modal characteristics for the size distribution (i.e., mass median diameter, standard deviation and mass of each mode). There is no PM chemical speciation in the emission inputs since Models-3/CMAQ uses fixed fractions of the mass of the modes for chemical speciation (1% and 2% of the mass of the nuclei and accumulation modes for elemental carbon and organic carbon, respectively, and 0% for sulfate, nitrate, ammonium, sodium and chloride). The pre-processors for the emissions, IC and BC inputs were modified to allow the option to use a sectional representation of the particle size distribution. If MADRID 2 is chosen by the user, the modal inputs are used to calculate the corresponding sectional representation according to the number of size sections selected. This calculation is done by integrating each modal distribution (i.e., Aitken nuclei, accumulation and coarse modes) over each section to obtain the modal mass corresponding to each section. For example, the calculation of the mass of the accumulation mode assigned to the first size section, M_{1a}, is as follows.

$$M_{1a} = \int_{d_{p0}}^{d_{p1}} \frac{M_a}{(2p)^{1/2} \log(s_a)} \exp\left[-\frac{1}{2}\left(\frac{\log(d_p / d_{pa}}{\log(s_a)}\right)\right] d\, d_p \tag{4-1}$$

where M_a is the total mass of the accumulation mode, s_a is the standard deviation of the accumulation mode, d_p is the particle diameter, d_{pa} is the geometric mean diameter of the accumulation mode, and d_{po} and d_{p1} are the lower and upper particle diameters of the first size section. Then, the resulting sectional PM size distribution is input into the Chemical Transport Model (CTM) of CMAQ. We elected to perform the conversion from modal to sectional outside of the CTM rather than within the CTM because the former approach keeps the flexibility of using sectional inputs directly (i.e., without converting modal inputs to sectional inputs) if desired. In other words, the user can input the aerosol concentrations with either a modal or sectional format. If the conversion had been incorporated within the CTM, the user would not be able to select a sectional format and would be constrained to a modal format.

In the CTM code, three new modules were created:

- An aerosol module
- A corresponding gas-phase chemistry module
- A corresponding dry deposition module

These modules are filed within the Models-3/CMAQ repository as aero_MADRID2 (in the aero directory), chem_qssa_cacm (an include file used by the gas-phase mechanism solver, see section 4.2), and aero_depv_sec (in the aero_depv directory).

The formulation of MADRID 2 was described in Table 4.2 along with the various options available to the user. A new gas-phase chemistry module, the Caltech Atmospheric Chemistry Mechanism (CACM), was added to provide the reaction products needed for the formation of secondary organic aerosols (SOA). Its incorporation into Models-3/CMAQ is described in Section 4.2. A new dry deposition module was also needed because particle dry deposition depends on particle size. Note that, in the new dry deposition module, the component of the dry deposition velocity that is size-specific needs to be calculated only once since the size sections are fixed within a given simulation. Also, the existing particle dry deposition velocity expression was updated based on the formulation of Venkatram and Pleim (1999).

The model output for the option of the new aerosol module consists of the particulate chemical concentrations by size section and the PM deposition flux by chemical.

4.7 Changes in the Chemical Mechanism

A new gas-phase chemical kinetic mechanism, CACM, was obtained from Dr. Robert Griffin (2000). This mechanism contains 361 reactions of 189 species and provides detailed descriptions of several generations of products from alkanes (3 classes), alkenes (2 classes), aromatics (2 classes), alcohols (3 classes), isoprene, and terpenes (2 classes). This mechanism is uniquely suitable for modeling SOA formation because 42 condensable second- and third-generation products are explicitly represented.

The new mechanism was available to us in the format of a FORTRAN subroutine. In order to implement the mechanism within Models-3/CMAQ, we first reformatted the reactions in the format recognized by the chemistry reader program of Models-3. The graphical user interface (GUI) was used to generate the include files associated with the reactions; such include files contain information about the index of the species involved in each reaction and the stoichiometric coefficients of the reactants and products. Due to a limitation on the maximum number of species processed by the GUI, it was not feasible to use the GUI for the file

containing the names of species and we used the chemistry reader program directly to generate the file.

Several reactions involve variable stoichiometric coefficients to represent competitive pathways and products in a single reaction. Due to the use of include files to store constant stoichiometric coefficients in the original Models-3/CMAQ formulation, a special procedure needed to be devised to treat variable coefficients. These coefficients were entered as 999 in the mechanism reader, as an indication to be reset by a program at the start of the chemistry routine. A separate subroutine was written to calculate the variable stoichiometric coefficients as functions of temperature. The code in the chemistry solver routine was modified accordingly to account for the necessary changes.

Several reactions involve reaction rate constants with complicated functional forms that are not currently defined in the Models-3 chemistry reader. Instead of using the Models-3 chemistry reader to generate automatically the subroutine to calculate reaction rate constants, a separate routine was developed to calculate all reaction rate constants.

The mechanism is described by an include file called RXDT.EXT in the include directory CACM_aqCMU_aeMADRID2_2sec. The codes needed to describe the variable stoichiometric coefficients and rate constants are filed under the chem_qssa_cacm subdirectory of the chemistry solver (chem) directory in the Models-3/CMAQ repository.

4.8 Operational Issues

Secondary organic components are assumed to partition only into the fine mode in the two-section model. This is justified because the predominance of the surface area to which transport occurs resides in the fine mode, although this assumption need not be made. Although the calculations are performed using surrogate species in the AEC aerosol module, gas-phase and particle-phase concentrations of the explicit species are tracked in the model. At the end of the call to the partition module, each explicit condensable species is partitioned between the particle phase and gas phase based on the behavior of the surrogate species, so that the number of moles is conserved between the explicit and surrogate representations.

One operational advantage of the Models-3/CMAQ platform is its flexibility in incorporating modules written in different languages. We have implemented the AEC module in mixed C/Fortran language and incorporated it into the Fortran-based Models-3/CMAQ model as a library of routines.

Multiple iterations are used in the Newton/line search method to solve the simultaneous equations in the AEC routine for aqueous SOA formation, increasing significantly the computational burden for the 3-D model. In the application of the new module in 3-D simulations (see Section 5), we have decreased the frequency for equilibrium partition from every time step (5 to 6 minute) to once every hour. Changing the time step may affect the gas/particle partitioning and the rate of removal of condensing species (e.g., dry deposition of gases instead of particle deposition or vice-versa). In our test simulation, this approximation in the integration time-step for gas/particle partitioning, led to negligible effect on inorganic particulate species (e.g., average error less than 1% for particulate nitrate) and acceptable error on organic particulate species (maximum average error for hydrophobic biogenic SOA of 16%; average error of 12% for total SOA).

4.9 Testing of the New Aerosol Module Within Models-3/Cmaq

4.9.1 Description of the Simulation

Models-3/CMAQ with MADRID 2 was tested with the 27-28 August 1987 SCAQS episode. This episode was used previously to test other 3-D PM models including Models-3/CMAQ, DAQM-V2 and SAQM-AERO (Pai et al., 1999, 2000; Seigneur et al., 2000).

The MADRID 2 simulation was conducted using two aerosol sections, the hybrid approach for gas/particle mass transfer, ISORROPIA for thermodynamics of inorganic components, and no nucleation. MADRID 2 input files were obtained from earlier Models-3/CMAQ simulations (Seigneur et al., 2000) with the exception of the following modifications to treat detailed organic species and PM. CACM contains 19 photolysis reactions, including 7 for inorganic species and 12 for organic species. The photolysis rates were provided by Caltech as a look-up table based on the solar zenith angle. Models-3/CMAQ requires photolysis rates as a look-up table based on hours. Therefore, we calculated the photolysis rates at each hour based on the time of sunrise/sunset. Photolysis rates were scaled based on the NO_2 photolysis rate from our previous SCAQS simulations. Emissions for the volatile organic compounds were obtained from Caltech (R. Griffin, 2000) for 1993 and scaled to 1987 levels for total VOC. Other emissions corresponded to those used by Pai et al. (2000).

The default chemical speciation used by Models-3/CMAQ for fine PM emissions consists of 2% organic carbon (OC), 1% elemental carbon (EC) and 97% other compounds. The chemical speciation of Pai et al. (2000) used here consists of 10.5% OC, 8.2% EC, 3.3% chloride, 0.2% sodium and 77.8% other compounds. The default chemical speciation of Models-3/CMAQ for the initial and boundary conditions is the same as for the emissions. The chemical speciation of Pai et al. (2000) for the initial and boundary conditions of $PM_{2.5}$ is 28.7% sulfate, 12.8% OC, 1.2% EC, 0.4% chloride, 10.9% ammonium, 5.8% nitrate and 40.2% other compounds.

Dry deposition velocities were defined for condensable organic compounds following those of aldehydes, organic nitrates, or organic acids in Models-3/CMAQ. Aromatic compounds were assumed to have zero dry deposition velocities, as prescribed in Models-3/CMAQ.

The 120-hour simulation of the SCAQS episode was completed with MADRID 2 in 72 CPU hours on a Sun Ultra 60 workstation. The relatively long simulation time was due in part to the large number of species simulated in the chemical mechanism, and in part to the SOA module that requires the solution of simultaneous equations.

The MADRID 2 simulation is an operational demonstration of the new aerosol module and no detailed comparison with measurements is presented.

4.9.2 $PM_{2.5}$ Concentrations

Table 4.3 presents the 24-hour average $PM_{2.5}$ concentrations at three locations in the Los Angeles basin: Hawthorne, Central Los Angeles and Riverside (see Figure 4.8). The temporal evolutions of the $PM_{2.5}$ concentrations are similar to those obtained with the original formulation of Models-3/CMAQ and are not presented here (Pai et al., 2000). (As discussed by Pai et al. (2000), the MM5 meteorological simulation led to overpredictions of the mixing height at inland areas which resulted in significant underpredictions of daytime $PM_{2.5}$ concentrations.)

Model predictions overestimate $PM_{2.5}$ concentrations at Hawthorne and Central Los Angeles on August 27. They underestimate $PM_{2.5}$ concentrations at Riverside on August 27 and at Hawthorne, Central Los Angeles and Riverside on August 28. Although predictions of mass of $PM_{2.5}$ are rather poor (e.g. Table 4.3 Riverside prediction 42 versus observation 94), predictions of overall chemical composition (% nitrate, sulfate, OC, EC) of $PM_{2.5}$ are relatively

accurate. Understanding the factors that contribute to this behavior will require further work. Discrepancies between model predictions and observations are likely due to a combination of factors including uncertainties in the meteorological inputs (see above), emissions inventories and model formulation.

4.9.3 $PM_{2.5}$ Chemical Composition

The evolution of the particulate chemical composition is shown in Figure 4.9 for the observations and the new aerosol module MADRID 2 at the three sites: Hawthorne, Central Los Angeles and Riverside. The model predicts an evolution of the aerosol chemical composition that is similar to that observed in the measurements. Nitrate formation is underpredicted by MADRID 2. As a result, the contribution of sulfate (which results in great part from the boundary conditions) is overestimated. The $PM_{2.5}$ contribution of organic compounds (OC) predicted by MADRID 2 (between 12 and 18%) is commensurate with the measurements (between 10 and 15%). Elemental carbon (EC) is underpredicted (e.g., modeled contribution of 4% at Central Los Angeles versus measured value of 7%).

4.9.4 Organic Aerosol Concentrations

Time series plots of SOA concentrations are presented in Figure 4.10 at four sites for MADRID 2. The maximum SOA simulated at these four sites was about 14 $\mu g\ m^{-3}$ in Central Los Angeles. On a domain-wide basis, the average SOA concentration was only about 1.5 $\mu g\ m^{-3}$ on August 28. The maximum simulated one-hour concentration of SOA was about 16 $\mu g\ m^{-3}$, at a location dominated by organic-phase anthropogenic SOA. High SOA concentrations were simulated at Riverside and Claremont at night, whereas high SOA concentrations were simulated during the day at Central Los Angeles and Hawthorne. The overprediction of the daytime mixing heights at Riverside leads to underestimates of $PM_{2.5}$ concentrations (including SOA) during daytime at this location.

The formation of SOA by dissolution (hydrophilic SOA) and by absorption (hydrophobic SOA) resulted in very different behaviors of SOA profiles. Figure 4.11 shows the time series of aqueous-phase and organic-phase SOA and the associated gas-phase condensable compounds at Central Los Angeles. The formation of aqueous-phase SOA was probably limited by daytime relative humidities, as relatively high concentrations of condensable compounds in the gas phase led only to moderate aqueous SOA formation. Higher concentrations of aqueous SOA were observed at night when the relative humidity was high. On the other hand, the time-series plot shows a strong correlation between the concentrations of gas-phase and particle-phase hydrophobic compounds.

Further analyses of the organic carbon fraction of $PM_{2.5}$ are presented in Figure 4.12. At all three locations, primary organic carbon (POC) represented the dominant component of organic carbon. At the Hawthorne and Riverside sites, POC accounted for 43% and 48% of total OC, respectively. POC accounted for 62% of the organic compounds in $PM_{2.5}$ at Central Los Angeles, a POC source area. SOA were grouped into 4 categories, representing aqueous-phase anthropogenic SOA, aqueous-phase biogenic SOA, organic-phase anthropogenic SOA, and organic-phase biogenic SOA. Of the four categories, organic-phase anthropogenic SOA represented the largest fraction of SOA at these sites. On average, the organic-phase SOA was an order of magnitude larger than the aqueous-phase SOA. Low relative humidity in Los Angeles during this episode led to relatively small contributions of aqueous-phase SOA, especially at inland sites. Biogenic SOA were not abundant at the locations studied. Biogenic

SOA were typically more abundant in areas with significant biogenic emissions, and could account for over 50% of total particulate organic carbon in the mountains.

We noted that "elemental carbon is underpredicted.." This is true on a mass basis, but if the percentages were calculated at the 3 sites, the simulation underpredicts EC by 50% (1.3 $\mu g/m^3$ vs. 2.8 at Riverside; 1.6 vs. 3.1 at CELA; 0.7 vs. 1.2 at Hawthorne). These results are for a primary pollutant. Since the problem spans all three sites, it is suggestive of inventory issues rather than faulty meteorology, which leads back to the statement on page 117, lines 23-26, that the "overprediction of the daytime mixing heights at Riverside leads to underestimates of $PM_{2.5}$ concentrations". Interestingly, the underpredictions are significantly less at each site for OC (right on at Hawthorne 4.0 vs. 3.8). There is a need for further justification and clarification of the subject.

4.10 Conclusions

We have implemented and tested a new aerosol module in Models-3/CMAQ. Although this module represents the state of the science in PM modeling, some further refinements appear warranted.

The treatment of mass transfer in the new aerosol module is computationally demanding when using the kinetic option. Using the hybrid or full equilibrium options may lead to inaccuracies for cases with reactive coarse particles such as sea salt or alkaline dust. Implementing the recent hybrid approach of Capaldo et al. (2000) should provide the balance between accuracy and computational efficiency.

The treatment of condensational growth is not satisfactory. The solvers available with the kinetic mass transfer option (Bott's algorithm and QSTSE) have limitations and the first-order finite difference algorithm available with the hybrid and full equilibrium options is highly diffusive numerically. Other numerical approaches should be considered for incorporation into MADRID. Those include the moving center approach (Jacobson and Turco, 1995; Jacobson, 1997), the trajectory-grid (T-G) approach (Chock and Winkler, 2000), the partitioned flux integrated semi-Lagrangian method, PFISLM (Nguyen and Dabdub, 2001b) and the linear interpolation scheme of Koo and Pandis (2000).

We also recommend some updates in the equilibrium modules. At present, SCAPE2 is the only module within the MADRID module that treats crustal elements. However, SCAPE2 is not always numerically robust in 3-D applications. Therefore, it is desirable to incorporate a more robust equilibrium module that can treat the crustal species. EQUISOLV II (Jacobson, 1999) and a newer version of ISORROPIA, are two possible candidates.

The hydrolysis of N_2O_5 in the presence of aqueous aerosols should be incorporated into Models-3/CMAQ. For example, the parameterizations proposed by Jacob (2000) for heterogeneous chemistry could be incorporated into the gas-phase chemical mechanism.

Finally, the effect of biogenic emissions on O_3 and PM formation is likely to become a critical issue as anthropogenic emissions continue to be reduced. CACM represents the state of the science for simulating the formation of condensable organic compounds. However, CACM does not currently model methylbutenol (MBO) and sesquiterpenes, two important components of biogenic emissions. The former is a relative of isoprene; it is emitted from coniferous species and has been found to be important in California. The latter can be a significant precursor for biogenic SOA although sesquiterpene emissions are believed to be less than those of monoterpenes. The addition of these compounds to CACM will enhance its applicability.

The next step will be to evaluate this new version of Models-3/CMAQ with ambient data from special field studies. These data include sulfate, nitrate, ammonium, EC, and OC. In particular, some data on primary vs. secondary OC, as well as molecular composition of OC will be needed to evaluate the new SOA modules. A possible source of such data is the California Regional $PM_{10}/PM_{2.5}$ Air Quality Study (CRPAQS).

References

Binkowski, F.S. and U. Shankar, 1995. The regional particulate matter model. 1: Model description and preliminary results, *J. Geophys. Res.*, **100**, 26191-26209.

Bott, A., 1989. A positive definite advection scheme obtained by nonlinear renormalization of the advective fluxes, *Mon. Wea. Rev.*, **117**, 1006-1015.

Byun, D.W. and J.K.S. Ching, 1999. Science Algorithms of the EPA Models-3 Community Multiscale Air Quality (CMAQ) Modeling System, EPA/600/R-99/030, Office of Research and Development, U.S. Environmental Protection Agency, Washington, D.C.

Capaldo, K.P., C. Pilinis and S.N. Pandis, 2000. A computationally efficient hybrid approach for dynamic gas/aerosol transfer in air quality models, *Atmos. Environ.*, **34**, 3617-3627.

Chock, D.P. and S.L. Winkler, 2000. A trajectory-grid approach for solving the condensation and evaporation equations of aerosols, *Atmos. Environ.*, **34**, 2957-2973.

Clegg, S.L., P. Brimblecombe and A.S. Wexler, 1998a. A thermodynamic model of the system H^+ -NH_4^+ -Na^+ -SO_4^{2-} -NO_3^- -Cl^- -H_2O at 298.15 K, *J. Phys. Chem.*, **102**, 2155-2171.

Clegg, S.L., P. Brimblecombe and A.S. Wexler, 1998b. A thermodynamic model of the system H^+ -NH_4^+ -Na^+ -SO_4^{2-} -NO_3^- -Cl^- -H_2O at tropospheric temperatures, *J. Phys. Chem.*, **102**, 2137-2154.

Drefahl, A. and M. Reinhard, 1995. Handbook of Estimating Physico-Chemical Properties of Organic Compounds, Stanford Bookstore, Stanford, CA.

EPA, 2000. Guidance for Demonstrating Attainment of Air Quality Goals for $PM_{2.5}$ and Regional Haze, Draft 1.1, Office of Air Quality Planning and Standards, U.S. Environmental Protection Agency, Research Triangle Park, NC.

EPRI, 1999. Organic Aerosol Partition Module Documentation, TR-113095, EPRI, Palo Alto, CA.

Fitzgerald, J.W., W.A. Hoppel and F. Gelbard, 1998. A one-dimensional sectional model to simulate multicomponent aerosol dynamics in the marine boundary layer. 1. Modal description, *J. Geophys. Res.*, **103**, 16085-16102.

Griffin, R.J., 2000. Private communication, California Institute of Technology, Pasadena, CA.

Griffin, R.J., D.R. Cocker III, R.C. Flagan and J.H. Seinfeld, 1999. Organic aerosol formation from the oxidation of biogenic hydrocarbons, *J. Geophys. Res.*, **104**, 3555-3567.

Harrington, D. Y. and S. M. Kreidenweis, 1998. Simulation of Sulfate Aerosol Dynamics. I. Model Description. *Atmos. Environ.*, **32**, 1691-1700.

Jacob, D., 2000. Heterogeneous chemistry and tropospheric ozone, *Atmos. Environ.*, **34**, 2131-2159.

Jacobson, M.Z. and R.P. Turco, 1995. Simulating condensational growth, evaporation, and coagulation of aerosols using a combined moving and stationary size grid, *Aerosol Sci. Technol.*, **22**, 29-92.

Jacobson, M.Z., 1997. Development and application of a new air pollution modeling system – II. Aerosol module structure and design, *Atmos. Environ.*, **31**, 131-144.

Jacobson, M.Z., 1999. Studying the effects of calcium and magnesium on size-distributed nitrate and ammonium with EQUISOLV II, *Atmos. Environ.*, **33**, 3635-3649.

Kerminen, V.M. and A.S. Wexler, 1994. Post-Fog Nucleation of H_2SO_4 – H_2O Particle in Smog, *Atmos. Environ.*, **28**, 2399-2406.

Kim, Y.P. and J.H. Seinfeld, 1995. Atmospheric gas-aerosol equilibrium III: thermo-dynamics of crustal elements Ca^{2+}, K^+, and Mg^{2+}, *Aerosol Sci. Technol.*, **22**, 93-110.

Koo, B. and S.N. Pandis, 2000. Evaluation of a one-dimensional trajectory model with equilibrium, dynamic, and hybrid aerosol modules, presentation at the 19th Annual AAAR Conference, St. Louis, Missouri, Nov. 6-10.

Lurmann, F.W., A.S. Wexler, S.N. Pandis, S. Musarra, N. Kumar and J.H. Seinfeld, 1997. Modeling urban and regional aerosols - II. Application to California's south coast air basin, *Atmos. Environ.*, **31**, 2695-2715.

McMurry, P.H. and S.K. Friedlander, 1979. New particle formation in the presence of an aerosol, *Atmos. Environ.*, **13**, 1635-1651.

Meng, Z., J.H. Seinfeld, P. Saxena and Y.P. Kim, 1995. Atmospheric gas-aerosol equilibrium, IV: thermodynamics of carbonates, *Aerosol Sci. Technol.*, **23**, 131-154.

Meng, Z., D. Dabdub and J.H. Seinfeld, 1998. Size- and chemically-resolved model of atmospheric aerosol dynamics, *J. Geophys. Res.*, **103**, 3419-3435.

Nenes, A., C. Pilinis and S.N. Pandis, 1999. Continued development and testing of a new thermodynamic aerosol module for urban and regional air quality models, *Atmos. Environ.*, **33**, 1553-1560.

Nguyen, K. and D. Dabdub, 2001a. Two-level time marching scheme using splines for solving the advection equation, *Atmos. Environ*., in press.

Nguyen, K. and D. Dabdub, 2001b. Semi-Langrangian flux scheme for the solution of the aerosol condensation/evaporation equation, *Aerosol Sci. Technol*., in press.

Odum, J.R., T.P.W. Jungkamp, R.J. Griffin, H.J.L. Forstner, R.C. Flagan and J.H. Seinfeld, 1997. Aromatics, reformulated gasoline, and atmospheric organic aerosol formation, *Environ. Sci. Technol*., **31**, 1890-1897.

Pai, P., S.Y. Wu, K. Vijayaraghavan and C. Seigneur, 1999. Intercomparison of Third-Generation Air Quality Models for Ozone and Particulate Matter, Draft Report (Contract No. WO 8221-01), EPRI, Palo Alto, CA.

Pai, P., K. Vijayaraghavan and C. Seigneur, 2000. Particulate matter modeling in the Los Angeles Basin using SAQM-AERO, *J. Air Waste Manage. Assoc.*, **50**, 32-42.

Pandis, S.N., L.M. Russell and J.H. Seinfeld, 1994. The relationship between DMS flux and CCN concentration in remote marine regions, *J. Geophys. Res.*, **99**, 16945-16957.

Pankow, J.F., 1994. An absorption model of the gas/aerosol partition involved in the formation of secondary organic aerosol, *Atmos. Environ*., **28**, 189-193.

Pilinis, C. and J.H. Seinfeld, 1987. Continued development of a general equilibrium model for inorganic multicomponent atmopsheric aerosols, *Atmos Environ*., **32**, 2453-2466.

Press, W.H., S.A. Teukolsky, W.T. Vetterling and B.P. Flannery, 1992. Numerical recipes in C, Diskette v.2.08, Cambridge University Press, NY, NY, Chapter 9.7.

Pun, B.K., C. Seigneur and P. Saxena, 1999. Modeling Organic Aerosols Using a Surrogate Species Approach, American Association for Aerosol Research Conference, 12 October1999.

Saxena, P. and L. Hildemann, 1996. Water-soluble organics in atmospheric particles: a critical review of the literature and application of thermodynamics to identify candidate compounds, *J. Atmos. Chem*., **24**, 57-109.

Seigneur, C., 1982. A model of sulfate aerosol dynamics in atmospheric plumes, *Atmos. Environ*., **16**, 2207-2228.

Seigneur, C., P. Pai, P. Hopke and D. Grosjean, 1999. Modeling atmospheric particulate matter, *Environ. Sci. Technol*., **33**, 80A-84A.

Segneur, C., P. Karamchandani, P. Pai, K. Vijayaraghavan, K. Lohman and S.Y. Wu, 2000. Model comparisons and application of Models-3/CMAQ APT. First Annual Models-3 Workshop, 12-14 June 2000, Arlington, Virginia.

Venkatram, A. and J. Pleim, 1999. The electrical analogy does not apply to modeling dry deposition of particles, *Atmos. Environ*., **33**, 3075-3076.

Zhang, Y., C. Seigneur, J.H. Seinfeld, M.Z. Jacobson and F.S. Binkowski, 1999. Simulation of aerosol dynamics: A comparative review of algorithms used in air quality models, *Aerosol Sci. Technol*., **31**, 487-514.

Zhang, Y., C. Seigneur, J.H. Seinfeld, M. Jacobson, S.L. Clegg and F.S. Binkowski, 2000. A comparative review of inorganic aerosol thermodynamic equilibrium modules: similarities, differences, and their likely causes, *Atmos. Environ*., **34**, 117-137.

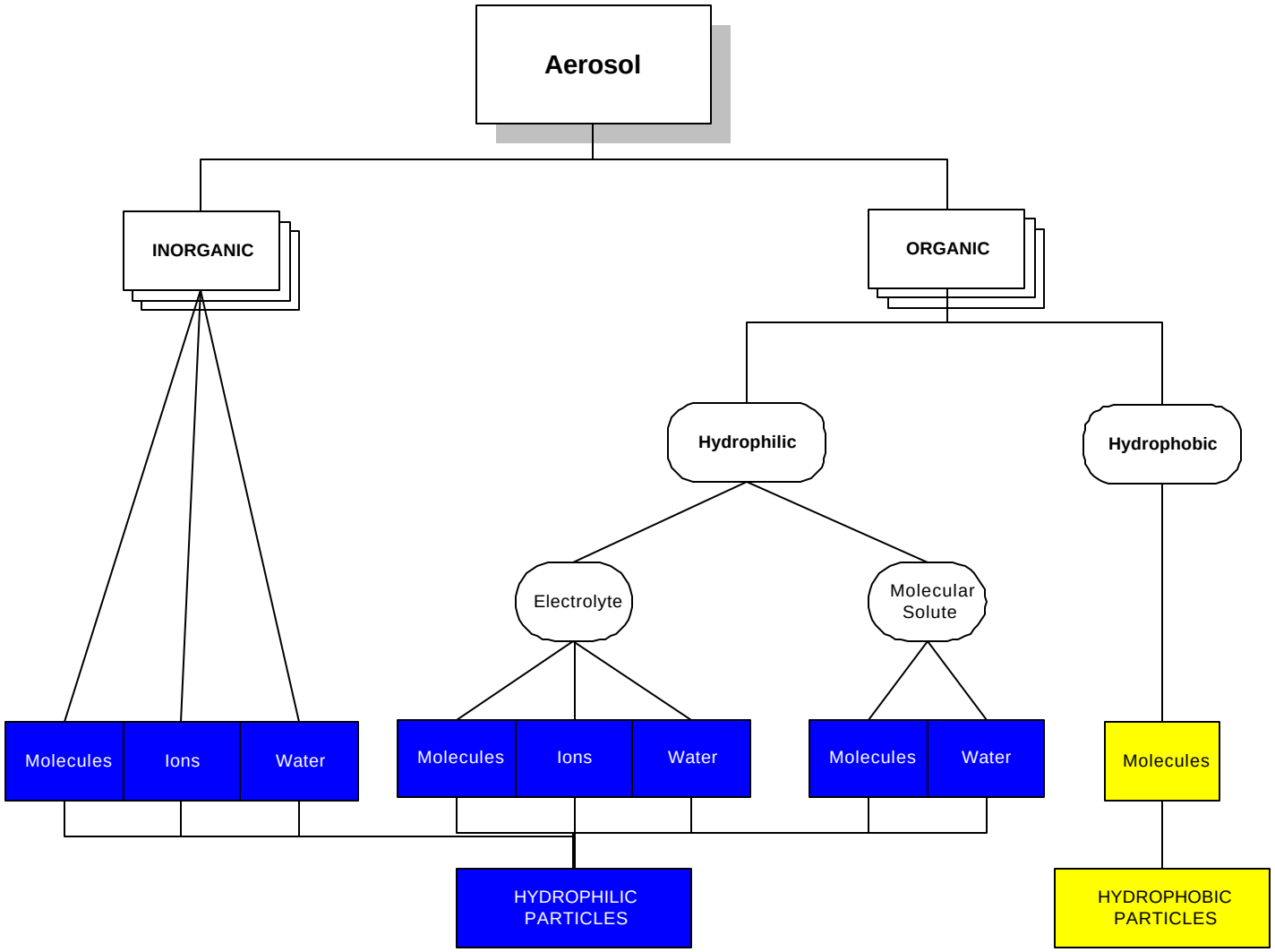

Figure 4.1. The aerosol system modeled in MADRID 2.

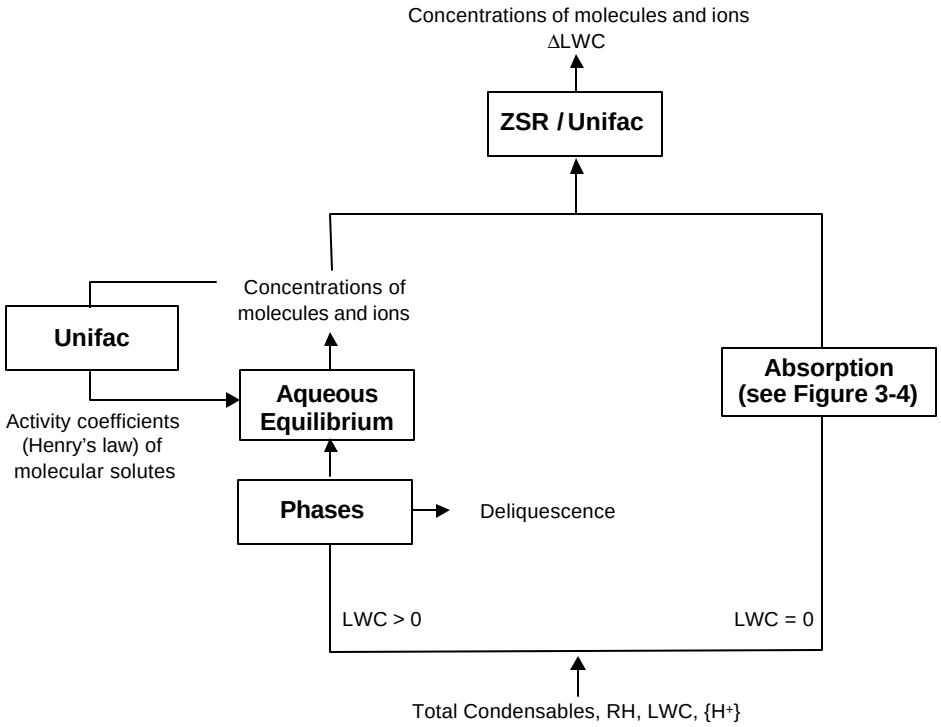

Figure 4.2. Hydrophilic Module Flow Diagram.

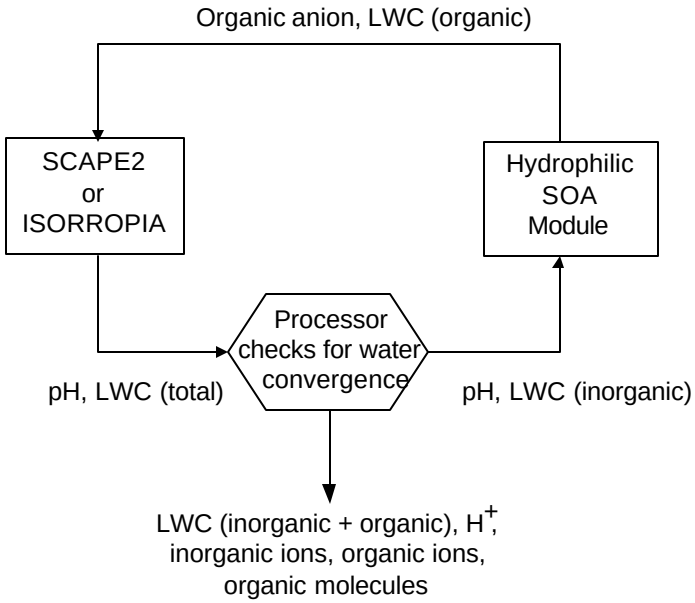

Figure 4.3. Flow chart of the iterative procedure used to solve the hydrophilic SOA-inorganic system.

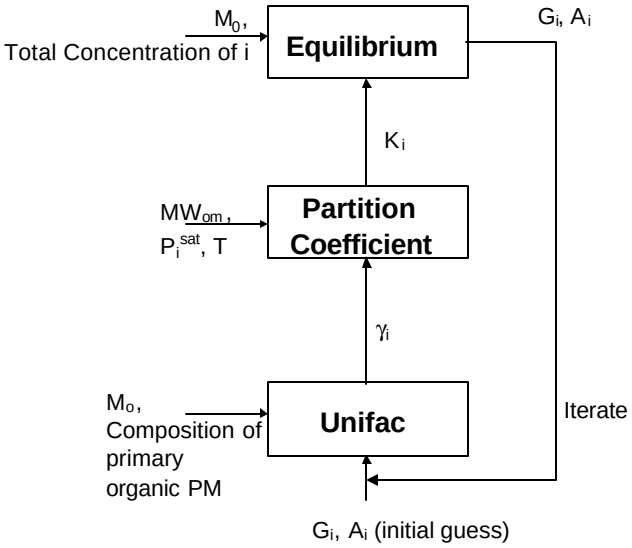

Figure 4.4. Hydrophobic SOA module flow diagram.

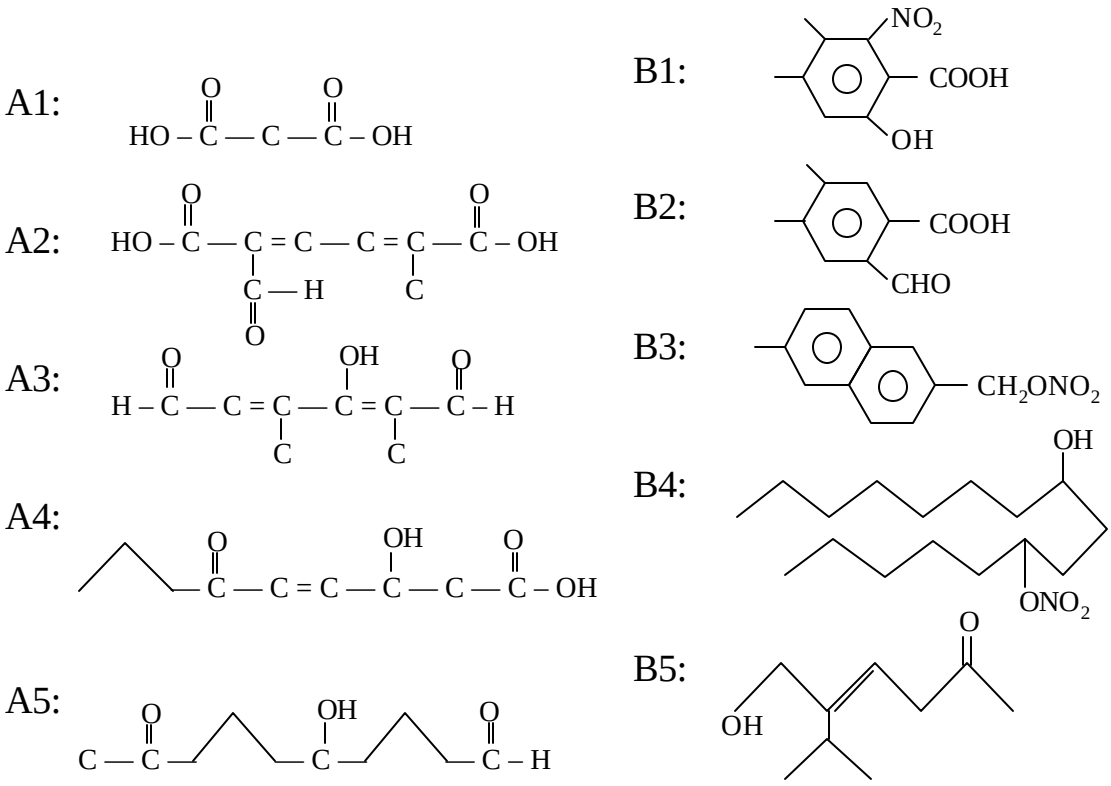

Figure 4.5. Surrogate structures modeled in MADRID 2. Compounds A1 through A5 are hydrophilic; compounds B1 through B5 are hydrophobic. Compounds A1 through A3 and B1 through B4 are of anthropogenic origin. Compounds A4, A5 and B5 are of biogenic origin.

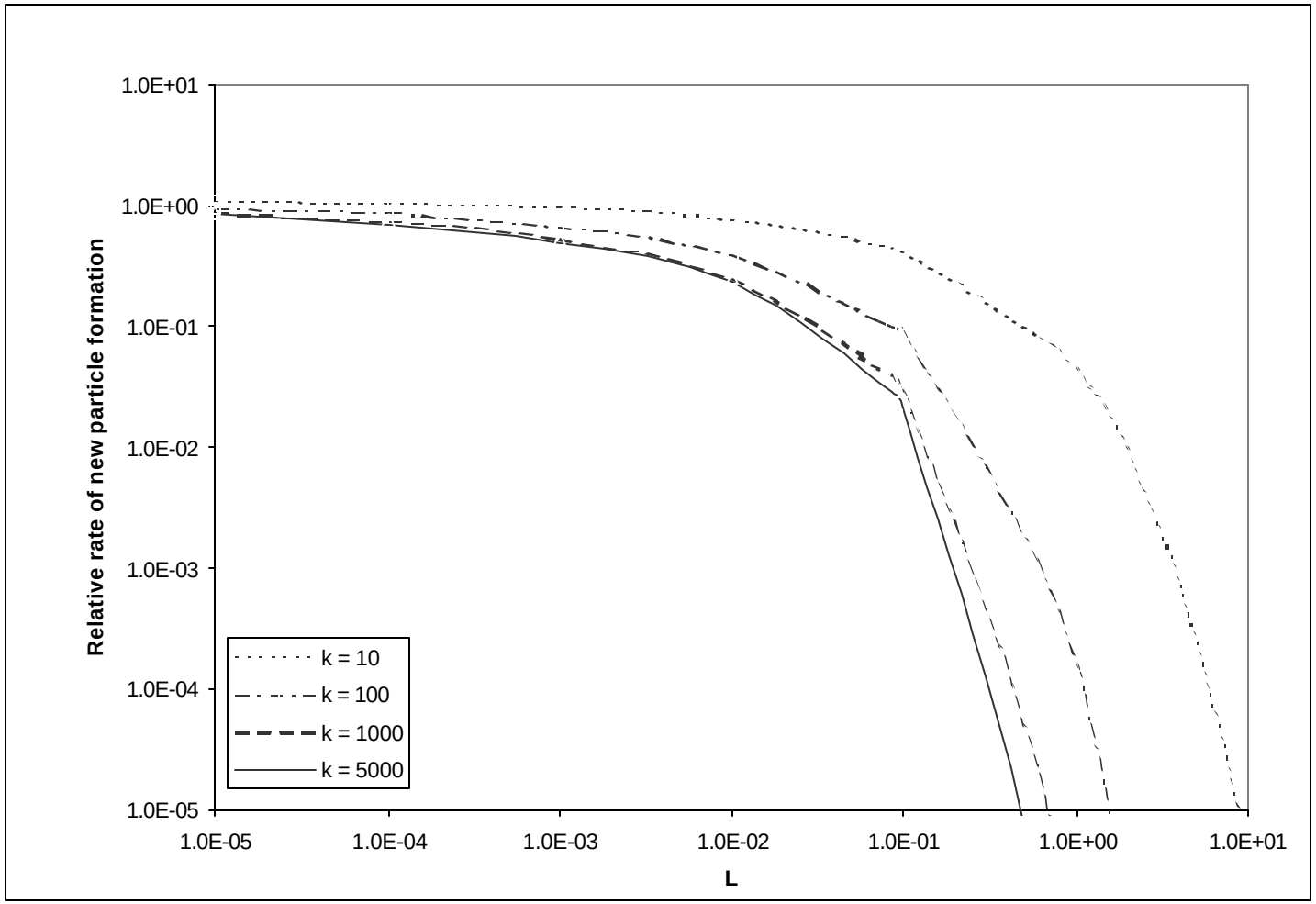

Figure 4.6. Parameterized ratio of new particle formation rate to total gas-to-particle conversion rate as a function of *L* and *k* (see test for details).

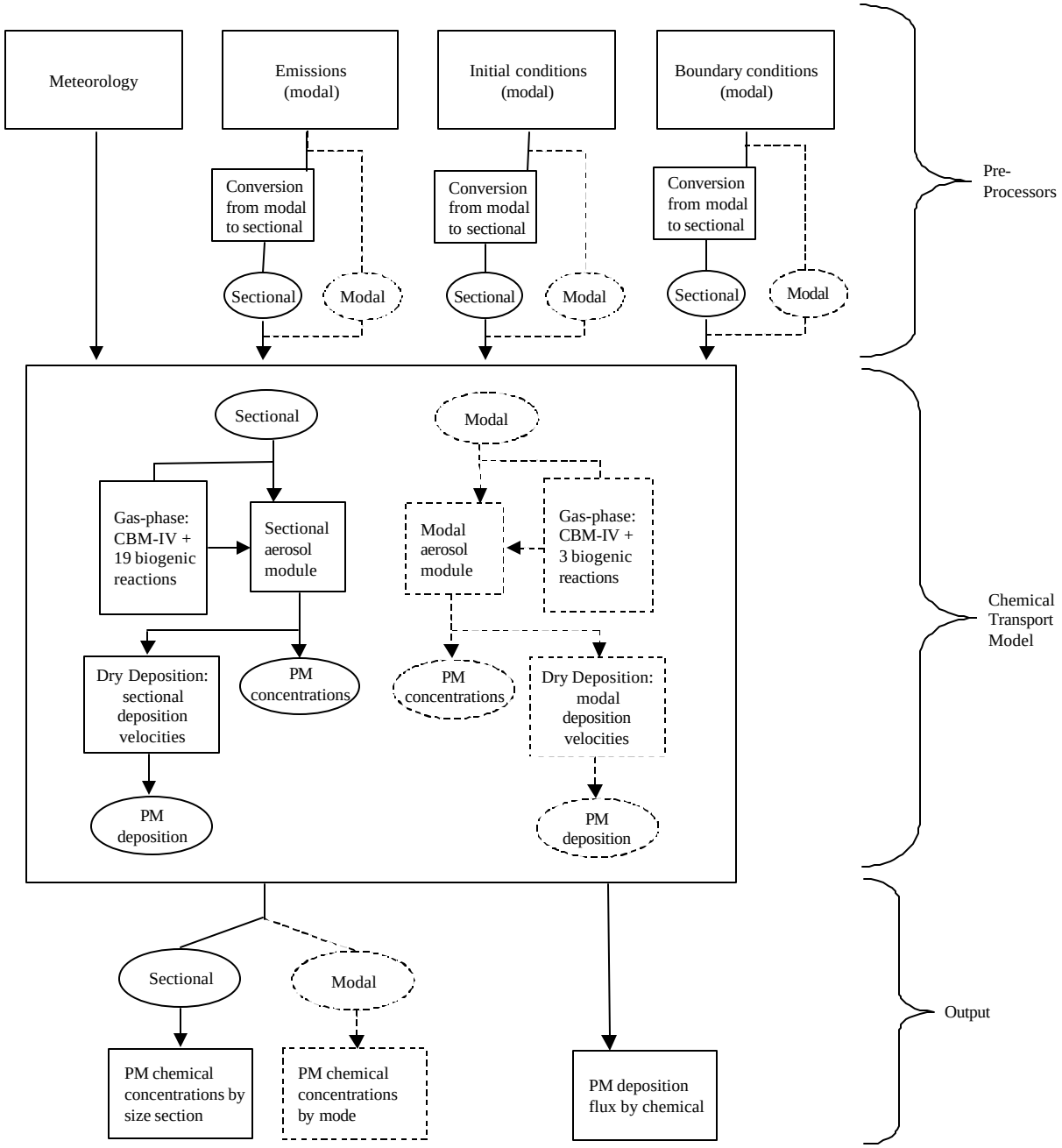

Figure 4.7. Schematic description of the incorporation of the new aerosol module MADRID 2 into Models-3/CMAQ. Only the components pertinent to the aerosol module are shown. The components specific to the modal option are shown in dashed lines.

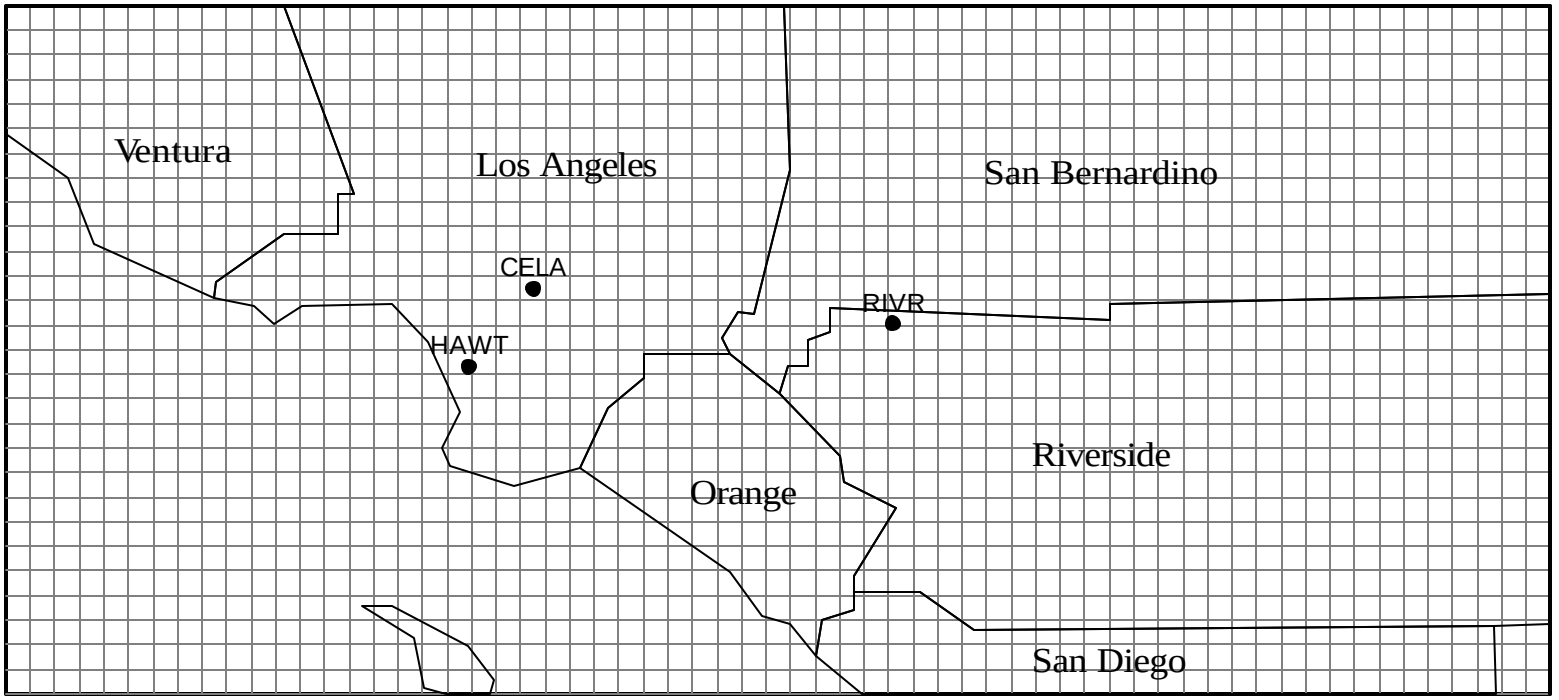

Figure 4.8. Modeling domain with the three regions and three receptor sites.

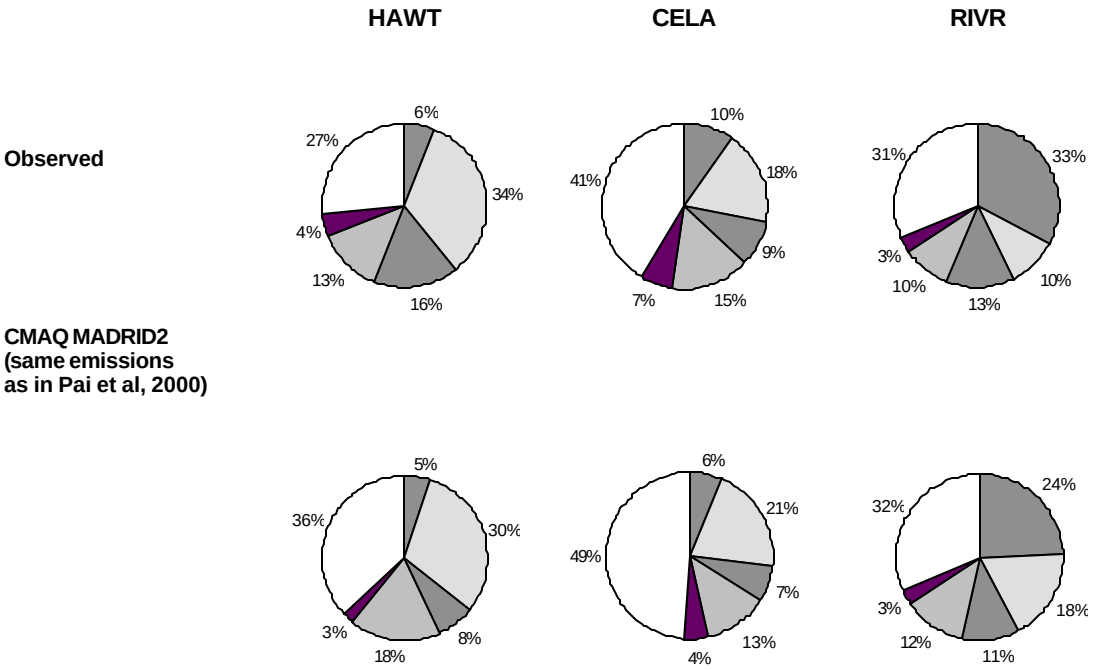

Figure 4.9. Chemical composition of $PM_{2.5}$ observed and simulated by Models-3/CMAQ on 28 August 1987 (24-hour average) at Hawthorne, Central Los Angeles and Riverside, using the sectional aerosol module MADRID 2.

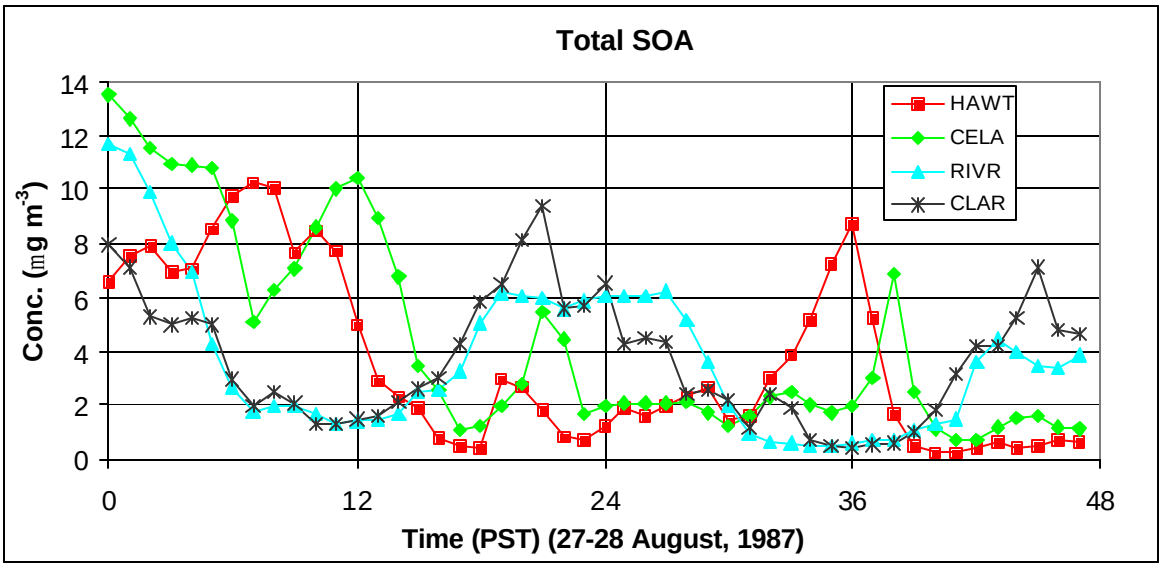

Figure 4.10. SOA concentrations simulated by MADRID 2 at Hawthorne (HAWT), Central Los Angeles (CELA), Riverside (RIVR) and Claremont (CLAR); simulations conducted with emissions of Pai et al. (2000) and two size sections.

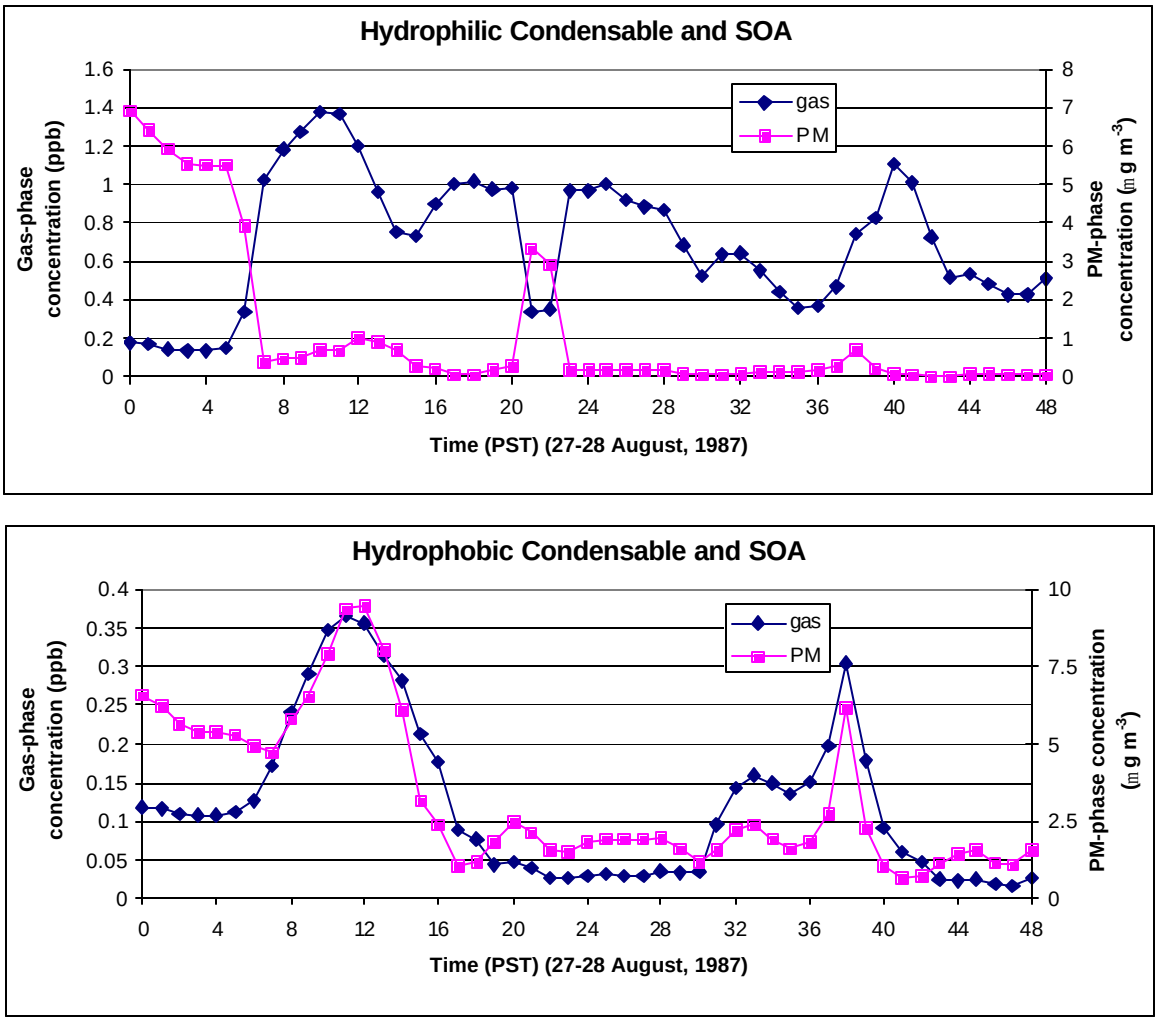

Figure 4.11. Simulations by MADRID 2 of (a) aqueous-phase SOA and hydrophilic gas-phase condensable compounds at Central Los Angeles (CELA), (b) organic-phase SOA and hydrophobic gas-phase condensable compounds at Central Los Angeles.

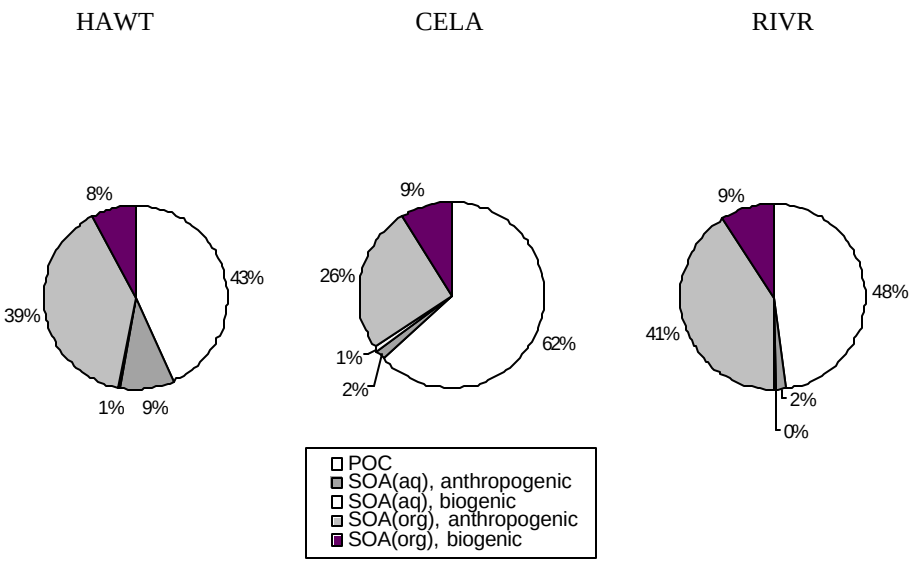

Figure 4.12. Chemical composition of organic carbon $PM_{2.5}$ 24-hour average concentrations simulated by MADRID 2 at Hawthorne (HAWT), Central Los Angeles (CELA), and Riverside (RIVR) on 28 August 1987.

Table 4.1. Comparison of existing modules for gas/particle partitioning of inorganic chemical species.

	MARS-A	**SEQUILIB**	**ISORROPIA**	**SCAPE2**	**EQUISOLV II**	**AIM2**
Performance	Higher H_2O for medium RHs and higher NH_4NO_3 for sulfate-poor cases and low RHs	Poor NO_3^- and H^+ predictions for some sulfate-rich cases; higher NH_4NO_3 for sulfate-poor cases and low RHs	Inaccurate at some high RHs (above 50%) for various conditions including some acidic, neutral and alkaline cases	Higher H^+ for some sulfate-rich cases and low RHs	Higher NH_4Cl for cases with NaCl and low RHs	Not valid for alkaline systems
Stability	Good	Poor for some sulfate-rich/neutral cases and high RHs cases	Good	Non-convergence for some sulfate-rich cases and low RHs	Incomplete convergence for low RHs	Numerical difficulties for very low initial H^+ and NO_3^-
Speed	Fast	Fast	Fast	Moderately fast	Slow for one cell, fast for multiple cells	Relatively slow

Table 4.2. Processes simulated in MADRID 2.

Process	**Module (Options are indicated with numbers)**	**Comments**
Gas-phase chemistry	CACM	Modified to account for additional VOC for SOA formation
Coagulation	None	Coagulation is negligible compared to other processes under most conditions.
Nucleation	1. New particle formation theory of McMurry and Friedlander (1979)[a] 2. None[a]	see Section 3.3
Gas-particle thermodynamic equilibrium for inorganic species	1. SCAPE2 (sulfate, nitrate, ammonium, sodium, magnesium, potassium, calcium, chloride, carbonate, water) 2. ISORROPIA (sulfate, nitrate, ammonium, sodium, chloride, water)[a]	SCAPE2 is currently being revised. The current version fails to converge under some conditions (e.g., low relative humidity). ISORROPIA leads to incorrect predictions of particulate nitrate under some conditions.
Gas-particle equilibrium for organic species	Mechanistic formulation with 10 surrogate species coupled with inorganic aerosol module	see Section 3.2
Gas/particle mass transfer for inorganic species	1. Kinetic algorithm 2. Hybrid algorithm[a] 3. Full equilibrium algorithm	The kinetic algorithm is computationally demanding and may not be suitable for most 3-D simulations. Two condensational growth algorithms are available with the kinetic algorithm (see below).
Gas/particle mass transfer for organic species	Hybrid algorithm	SOA formation occurs primarily on fine particles; therefore, a kinetic approach that allows better treatment for cases with coarse/fine particles mass transfer is not necessary.

Table 4.2. Processes simulated in MADRID 2 (continued).

Process	**Module (Options are indicated with numbers)**	**Comments**
Condensational growth/shrinkage by volatilization	Diffusion-limited condensation/volatilization with options for the advection algorithm and the growth law Finite difference algorithm when hybrid or full equilibrium algorithm is used for mass transfer[a] Advection algorithm when kinetic algorithm is used for mass transfer 1. Bott's algorithm 2. QSTSE algorithm Growth law 1. CIT growth law[a] 2. Fuchs-Sutugin growth law	QSTSE does not apply to the 2-section option. It shows better performance than Bott but fails under some conditions (e.g., 8-section simulation with NaCl).
Dry deposition	Integrated flux approach of Venkatram and Pleim (1999)	see Section 3.4
Aerosol size distribution	Sectional with at least 2 size sections 1. 2-section representation (fine and coarse particles)[a] 2. Multi-section representation[a]	The Stokes diameter is used to define the size section boundaries; note that the $PM_{2.5}$ and PM_{10} definitions are based on the aerodynamic diameter.

(a) Options chosen for testing the 3-D model.

Table 4.3. Observed and simulated 24-hour average $PM_{2.5}$ concentrations ($\mu g/m^3$) in the Los Angeles basin, 27 and 28 August 1987. Simulations were conducted with Models-3/CMAQ. Particulate water is not included in $PM_{2.5}$.

	27 August 1987			28 August 1987		
	Hawthorne	Central Los Angeles	Riverside	Hawthorne	Central Los Angeles	Riverside
Observations	20.8	34.3	68.1	29.2	44.8	94.6
MADRID 2, 2 sections (same emissions as Pai et al., 2000)	34.4	62.0	57.4	22.2	40.6	42.3

APPENDIX
Script used to compile Models-3/CMAQ with aero_MADRID2_2sec.

```
#! /bin/csh -f

setenv M3MODEL /laplace1/models3/aug2000/models
setenv M3TOOLS /laplace1/models3/aug2000/tools

set echo

#:#:#:#:#:#:#:#:#:#:#:#:#:#:#:#:#:#:#:#:#:#:#:#:#:#:#:#:#:#:#:#:#:#:#:#:#:#:#:#:#:#:#:#:#:#:#:#:#:#:#
# user choices: cvs archives
 set Project = $M3MODEL/CCTM
 set GlobInc = $M3MODEL/include/release

# user choices: base directory
 set Base = $cwd

 set APPL  = scaqs_madrid2_nocloud_2sec
 set CFG   = ${APPL}.cfg
 set MODEL = CCTM_$APPL

# user choices: bldmod command
 set Opt = verbose      # show requested commands as they are executed
 set MakeOpt =

# user choices: various modules

 set revision = release       # monocode (>="REL1_4")
# NOTE: m3bld will try to compile with existing code; it will not
#       retrieve new (different release) code. So if your "BLD" directory
#       contains code from a release different than the one you have specified
#       above, m3bld will tell you, but will merrily compile the original code.
#       The workaround is to remove your "BLD" directory and start fresh.

 set ModDriver = ( module ctm_hourlyPM   $revision; )

 set ModPar    = ( module par_noop       $revision; )

 set ModInit   = ( module init_sec       $revision; )

 set ModAdjc   = ( module denrate        $revision; )

 set ModCpl    = ( module gencoor        $revision; )

 set ModHadv   = ( module hbot           $revision; )

 set ModVadv   = ( module vbot           $revision; )

 set ModVdiff  = ( module eddy_sec        $revision; )

 set ModHdiff  = ( module unif           $revision; )

 set ModPhot   = ( module phot           $revision; )

 set ModPing   = ( module ping_noop      $revision; )

 set ModChem   = ( module qssa_CACM      $revision; )
```

```
 set ModAero   = ( module aero_MADRID2_2sec $revision; )

 set ModAdepv  = ( module aero_depv_sec   $revision; )

 set ModCloud  = ( module cloud_noop     $revision; )

 set ModUtil   = ( module util           $revision; )

 set ModPa     = ( module pa             $revision; )

# user choices: emissions processing in vdiff or chem (default)
#set Eopt = chem
#set Eopt =
 set Eopt = vdif

# user choices:  Sun debug compilation
#set Sun_debug = 1
 set Sun_debug =

# user choices: domain and mechanism
 set Reso      = 05
 set Grid      = 63X28
 set Layers    = 15
 set Domain    = d${Reso}_${Layers}
 set Mechanism = CACM_aqCMU_aeMADRID2_2sec
 set Tracer    = trac0               # default: no tracer species
 set PABase    = $GlobInc
 set PAOpt     = pa_noop

 set Decomp    = 1X1

# other user choices set below are:
#    name of the "BLD" directory
#    compiler/link flags
#    library paths
#:#:#:#:#:#:#:#:#:#:#:#:#:#:#:#:#:#:#:#:#:#:#:#:#:#:#:#:#:#:#:#:#:#:#:#:#:#:#:#:#:#:#:#:#:#:#

set Bld = $Base/BLD

#unset echo
 if (! -e "$Bld") then
    mkdir $Bld
    else
    if (! -d "$Bld") then
       echo "   *** target exists, but not a directory ***"
       exit(1)
       endif
    endif
#set echo
 cd $Bld

 set BLD_OS = `uname -s``uname -r | cut -d"." -f1`
 if ($BLD_OS != 'SunOS5') then
    echo "   $BLD_OS -> wrong bldit script for host!"
    exit 1
    endif
 set platf = `uname -i | cut -d"," -f2`

 set xflag0 = "-xtarget=ultra"
 set xflag1 = "-xtarget=ultra2"
 set xflag2 = "-xcache=16/32/1:1024/64/1"
```

```
 if ( $Sun_debug ) then
    set XF_FLAGS  = "-g -C -e -fnonstd"
    set LINK_FLAGS = "-g -C -e -fnonstd -xildoff"
    else
    if ( $platf == "Ultra-30" ) then
       set XF_FLAGS  = "-e -fast -O4 $xflag1 $xflag2"
       set LINK_FLAGS = "-e -fast -O4 $xflag1"
       else if ( $platf == "Ultra-2" ) then
       set XF_FLAGS  = "-e -fast -O4 $xflag0"
       set LINK_FLAGS = "-e -fast -O4 $xflag0"
       else
       set XF_FLAGS  = "-e -fast -g"
       set LINK_FLAGS = "-e -fast -g"
       endif
    endif

 set FC = /opt/6.0/SUNWspro/bin/f90

 set LIB1 = "-L${M3TOOLS}/IOAPI/release/m3io/lib/SunOS5 -lm3iof90"
 set LIB2 = "-L${M3TOOLS}/netCDF/SunOS5 -lnetcdf"
 set LIB3 = "-L${M3TOOLS}/stenex/SunOS5 -lse_noop"
 set LIB4 = "-L${M3MODEL}/CCTM/src/aero/aero_MADRID2_2sec/soa_lib/src2001 -
lsoa"
 set LIBS = "$LIB1 $LIB2 $LIB3 $LIB4"

 set Blder = $M3TOOLS/build/SunOS5/m3bld

 set ICL_BLOCK = $GlobInc
 set ICL_CGRID = $GlobInc
 set ICL_CONST = $GlobInc
 set ICL_FILES = $GlobInc
 set ICL_EMCTL = $GlobInc
 set ICL_IOAPI = $GlobInc
 set ICL_PAR   = $GlobInc
 set ICL_GRID  = $GlobInc/$Domain
 set ICL_MECH  = $GlobInc/$Mechanism
 set ICL_TRAC  = $ICL_MECH
 set ICL_PA    = $PABase/$PAOpt

 if ($Eopt == 'vdif') then
    set CV = -Demis_vdif
    else
    set CV =
    endif

 set PAR =
 set Popt = NOOP
 set STX1 = (-DSUBST_GLOBAL_RMAX=${Popt}_GLOBAL_RMAX\
             -DSUBST_GLOBAL_MIN_DATA=${Popt}_GLOBAL_MIN_DATA\
             -DSUBST_GLOBAL_ISUM=${Popt}_GLOBAL_ISUM\
             -DSUBST_GLOBAL_RSUM=${Popt}_GLOBAL_RSUM\
             -DSUBST_LOOP_INDEX=${Popt}_LOOP_INDEX\
             -DSUBST_PA_INDEX=${Popt}_PA_INDEX\
             -DSUBST_IRR_INDEX=${Popt}_IRR_INDEX\
             -DSUBST_HI_LO_BND_PE=${Popt}_HI_LO_BND_PE\
             -DSUBST_SUM_CHK=${Popt}_SUM_CHK)
 set STX2 = (-DSUBST_PE_COMM1=${Popt}_PE_COMM1\
             -DSUBST_PE_COMM2=${Popt}_PE_COMM2\
             -DSUBST_PE_COMM2E=${Popt}_PE_COMM2E\
             -DSUBST_PE_COMM3=${Popt}_PE_COMM3\
             -DSUBST_PE_COMM3E=${Popt}_PE_COMM3E\
             -DSUBST_3D_DATA_COPY=${Popt}_3D_DATA_COPY\
```

```
              -DSUBST_3DE_DATA_COPY=${Popt}_3DE_DATA_COPY\
              -DSUBST_4D_DATA_COPY=${Popt}_4D_DATA_COPY)
 set STX3 =

 set F_FLAGS = "$XF_FLAGS -I."

 setenv CVSROOT $Project

# make the config file

 cat >! ${CFG} << E+O+X

 model $MODEL;

 cpp_flags  "$CV $PAR $STX1 $STX2";

 def_flags  "$STX3";

 f_compiler $FC;

 f_flags  "$F_FLAGS";

 link_flags "$LINK_FLAGS";

 libraries  "$LIBS";

 global $Opt;

// domain, mechanism and tracer: ${Domain}, ${Mechanism}, ${Tracer}
// project archive: ${Project}

 include SUBST_PE_COMM     $ICL_PAR/PE_COMM.EXT;
 include SUBST_CGRID_DECL  $ICL_CGRID/CGRID_DECL.EXT;
 include SUBST_BLKPRM      $ICL_BLOCK/BLKPRM_500.EXT;
 include SUBST_CONST       $ICL_CONST/CONST.EXT;
 include SUBST_FILES_ID    $ICL_FILES/FILES_CTM.EXT;
 include SUBST_EMPR_VD     $ICL_EMCTL/EMISPRM.vdif.EXT;
 include SUBST_EMPR_CH     $ICL_EMCTL/EMISPRM.chem.EXT;
 include SUBST_IOPARMS     $ICL_IOAPI/PARMS3.EXT;
 include SUBST_IOFDESC     $ICL_IOAPI/FDESC3.EXT;
 include SUBST_IODECL      $ICL_IOAPI/IODECL3.EXT;
 include SUBST_XSTAT       $ICL_IOAPI/XSTAT3.EXT;
 include SUBST_COORD_ID    $ICL_GRID/COORD_${Grid}.EXT;
 include SUBST_HGRD_ID     $ICL_GRID/HGRD_${Grid}_${Decomp}.EXT;
 include SUBST_VGRD_ID     $ICL_GRID/VGRD_${Layers}.EXT;
 include SUBST_RXCMMN      $ICL_MECH/RXCM.EXT;
 include SUBST_RXDATA      $ICL_MECH/RXDT.EXT;
 include SUBST_GC_SPC      $ICL_MECH/GC_SPC.EXT;
 include SUBST_GC_EMIS     $ICL_MECH/GC_EMIS.EXT;
 include SUBST_GC_ICBC     $ICL_MECH/GC_ICBC.EXT;
 include SUBST_GC_DIFF     $ICL_MECH/GC_DIFF.EXT;
 include SUBST_GC_DDEP     $ICL_MECH/GC_DDEP.EXT;
 include SUBST_GC_DEPV     $ICL_MECH/GC_DEPV.EXT;
 include SUBST_GC_ADV      $ICL_MECH/GC_ADV.EXT;
 include SUBST_GC_CONC     $ICL_MECH/GC_CONC.example2.EXT;
 include SUBST_GC_G2AE     $ICL_MECH/GC_G2AE.EXT;
 include SUBST_GC_G2AQ     $ICL_MECH/GC_G2AQ.EXT;
 include SUBST_GC_SCAV     $ICL_MECH/GC_SCAV.EXT;
 include SUBST_GC_WDEP     $ICL_MECH/GC_WDEP.EXT;
 include SUBST_AE_SPC      $ICL_MECH/AE_SPC.EXT;
 include SUBST_AE_EMIS     $ICL_MECH/AE_EMIS.EXT;
 include SUBST_AE_ICBC     $ICL_MECH/AE_ICBC.EXT;
```

```
 include SUBST_AE_DIFF     $ICL_MECH/AE_DIFF.EXT;
 include SUBST_AE_DDEP     $ICL_MECH/AE_DDEP.EXT;
 include SUBST_AE_DEPV     $ICL_MECH/AE_DEPV.EXT;
 include SUBST_AE_ADV      $ICL_MECH/AE_ADV.EXT;
 include SUBST_AE_CONC     $ICL_MECH/AE_CONC.example2.EXT;
 include SUBST_AE_A2AQ     $ICL_MECH/AE_A2AQ.EXT;
 include SUBST_AE_SCAV     $ICL_MECH/AE_SCAV.EXT;
 include SUBST_AE_WDEP     $ICL_MECH/AE_WDEP.EXT;
 include SUBST_NR_SPC      $ICL_MECH/NR_SPC.EXT;
 include SUBST_NR_EMIS     $ICL_MECH/NR_EMIS.EXT;
 include SUBST_NR_ICBC     $ICL_MECH/NR_ICBC.EXT;
 include SUBST_NR_DIFF     $ICL_MECH/NR_DIFF.EXT;
 include SUBST_NR_DDEP     $ICL_MECH/NR_DDEP.EXT;
 include SUBST_NR_DEPV     $ICL_MECH/NR_DEPV.EXT;
 include SUBST_NR_ADV      $ICL_MECH/NR_ADV.EXT;
 include SUBST_NR_N2AE     $ICL_MECH/NR_N2AE.EXT;
 include SUBST_NR_N2AQ     $ICL_MECH/NR_N2AQ.EXT;
 include SUBST_NR_SCAV     $ICL_MECH/NR_SCAV.EXT;
 include SUBST_NR_WDEP     $ICL_MECH/NR_WDEP.EXT;
 include SUBST_TR_SPC      $ICL_TRAC/TR_SPC.EXT;
 include SUBST_TR_EMIS     $ICL_TRAC/TR_EMIS.EXT;
 include SUBST_TR_ICBC     $ICL_TRAC/TR_ICBC.EXT;
 include SUBST_TR_DIFF     $ICL_TRAC/TR_DIFF.EXT;
 include SUBST_TR_DDEP     $ICL_TRAC/TR_DDEP.EXT;
 include SUBST_TR_DEPV     $ICL_TRAC/TR_DEPV.EXT;
 include SUBST_TR_ADV      $ICL_TRAC/TR_ADV.EXT;
 include SUBST_TR_T2AQ     $ICL_TRAC/TR_T2AQ.EXT;
 include SUBST_TR_SCAV     $ICL_TRAC/TR_SCAV.EXT;
 include SUBST_TR_WDEP     $ICL_TRAC/TR_WDEP.EXT;

// Process Analysis / Integrated Reaction Rates processing
 include SUBST_PACTL_ID    $ICL_PA/PA_CTL.EXT;
 include SUBST_PACMN_ID    $ICL_PA/PA_CMN.EXT;
 include SUBST_PADAT_ID    $ICL_PA/PA_DAT.EXT;

 $ModDriver

 $ModPar

 $ModInit

 $ModAdjc

 $ModCpl

 $ModHadv

 $ModVadv

 $ModPhot

 $ModPing

 $ModChem

 $ModAero

 $ModAdepv

 $ModVdiff

 $ModHdiff
```

```
 $ModCloud

 $ModPa

 $ModUtil

E+O+X

# make the model executable

 $Blder $MakeOpt $CFG
 if ($status != 0) then
    echo "   *** failure in $Blder ***"
    exit(1)
    endif

 exit()
```